Modification of Impulse-Radiating Antenna Waveforms to Obtain Damped Sinusoidal waveforms

D. V. Giri
Dept. of ECE, Univ. of New Mexico, Albuquerque, NM
Pro-Tech, 11-C Orchard Court, Alamo, CA 94507, USA
E-mail: Giri@DVGiri.com

F. M. Tesche
EM Consultant (Retired),
Lakeville, CT 06039, USA

Abstract— This paper describes a simple modification that can be applied to the Impulse-Radiating Antenna (IRA) to modify its output waveform to yield damped sinusoidal waveforms, for possible electromagnetic field testing of infrastructure elements. This modification involves placing several metallic screens in front of the antenna, which serves to transform the fast pseudo-impulse from the antenna into a damped sinusoidal waveform. In this presentation, a short parametric study of wire mesh transfer functions is conducted and the transient waveforms produced by several different meshes are described.

 Keywords- Impulse Radiating Antenna, wire mesh, damped sinusoids, infrastructure testing

I   INTRODUCTION

There are many types of threats that can be postulated for a societal infrastructure. These range from natural threats like floods, earthquakes, lightning and the like, to wartime and terrorist threats. In this latter category, one possible threatening environment is a high power electromagnetic (HPEM) field. Occurring in the form of either a transient waveform or a pulsed continuous wave (CW) packet, these electromagnetic waves can have large amplitudes and may cause damage or functional upset in targeted systems. Such HPEM environments can be produced by various methods, including low-tech and low-cost methods using commercially available equipment, as well as high-tech equipment and methods, which are typically available only to governmental organizations or their agents. As an example of such testing in the past, the **Sw**iss **I**mpulse **R**adiating **A**ntenna (SWIRA) has been used in Civil Defense test programs and results have been presented in the open literature. This past work involving the SWIRA has shown that this antenna works well for testing protective facilities by illuminating them with either a broadband transient EM field, or a CW field that is swept in frequency. SWIRA consists of a parabolic reflector of diameter $D = 1.8$ m with a focal length $F = 0.482$ m. The antenna is fed by a four-arm transmission line structure with a pulsed voltage source located at the focal point..

II.   WIRE MESHES IN FRONT OF SWIRA

Figure 1 shows the configuration we are now considering. Three wire meshes having square apertures with dimensions a on the sides are located at a distance R_p from the SWIRA. The conductors comprising the meshes are assumed to have a wire radius of r and are made of highly conducting material with a good electrical bond at the junctions. The mesh planes are assumed to be separated by

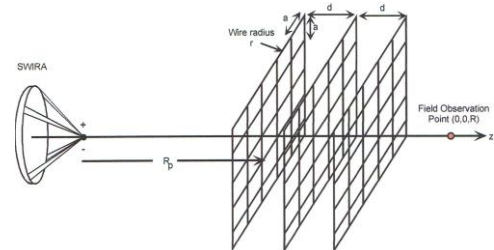a distance d, with free-space serving as the intervening media.

Figure 1. Wire meshes in front of SWIRA

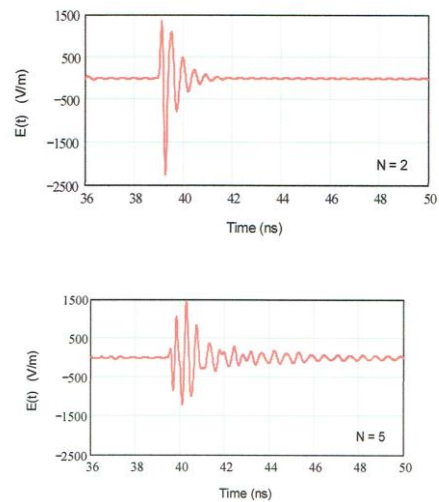Figure 2 shows the radiated e-field at a distance of 10m, for different wire mesh planes.

Figure 2. Evolution of the transmitted SWIRA E-field at a 10 m range for parameters $a = 5$ cm, $r = 2$ mm and $d = 5$cm for the number of wire mesh planes N = 2 and N = 5

From the work reported here, it is clear that the EM field output from the SWIRA can be transformed from a fast, impulse-like signal to one resembling a damped sine wave. By adjusting the wire mesh size and the separation of the mesh sheets, the frequency of oscillation of the damped sine wave can be controlled. We have not performed any measurement and it is suggested that an experiment be performed to validate this concept and the models that have been developed for predicting the responses. Additional details of our modeling can be found in [1].

[1] F. M. Tesche and D. V. Giri, "Modification of Impulse-Radiating Antenna Waveforms for Infrastructure Element Testing", Sensor and Simulation Note 572, 22 October 2015.

Malfunction analysis of CMOS IC according to gate output when HPM occur

J. W. Park, C. S. Huh, C. S. Seo, S. W. Lee
Dept. of Electromagnetic Engneering, INHA Univ.
Nam-gu, Incheon, South Korea
Ginook83@naver.com

Abstract— According to IEC 61000-2-13, many electronic systems are affected by L-band (1-2 GHz) and S-band (2-4 GHz). Therefore, in this study, the malfunction characteristics according to the gate output of the CMOS IC are analyzed, when the HPM (2.45 GHz) occurs. A magnetron was used as an electromagnetic wave source, and a HD74HC was used as a DUT. The malfunction of the IC was confirmed by the gate output voltage and GND current. Experimental results show that the type of malfunction varies depending on the gate output. It is considered that malfunction and failure of the CMOS IC are caused by insulation breakdown of the pn junction inside the IC.

Keywords-HPM, Susceptibility, CMOS IC

I. Introduction

CMOS type devices have the disadvantage that they are easily destroyed by ESD. Therefore, an ESD protection circuit is built in IC. However, ICs may experience malfunction and destruction when intentional electromagnetic inference (IEMI) with a frequency of several GHz to several tens GHz and a peak electric field of several tens of kV/m occurs. According to IEC61000-2-13, many electronic systems have shown significant interference effects in the L-band (1-2 GHz) and S-band (2-4 GHz), and the permanent destruction of the system has been reported. Therefore, in this paper, we analyze GND coupling current of CMOS IC by 2.45GHz HPM. [1]
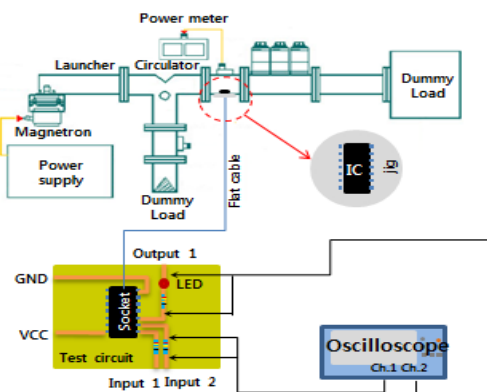
II. Test setup

Figure 1. Test setup

Figure 1 shows the test setup. it consist of an electromagnetic source (magnetron), a DUT (CMOS IC), and a measurement system (Oscilloscope). The electromagnetic waves generated from the magnetron travel along the WR-340 waveguide and are coupled to the semiconductor devices placed on the jig. The HD74HC was used for the DUT. The malfunction of the IC was confirmed by the gate output voltage and GND current.

III. Results

Experimental results show that offset current is 24mA for both ON and OFF state. When gate output was ON state, self-reset and destruction occurred by HPM. When gate output is OFF state, only destruction occurred by HPM. Figure 2 shows the GND coupling current by HPM. When the electromagnetic radiation occurs, the noise is coupled to GND current for both ON and OFF, and there are larger peak current in the IC in the ON state. It is considered that malfunction and destruction of the CMOS IC are caused by pn junction breakdown inside the IC.
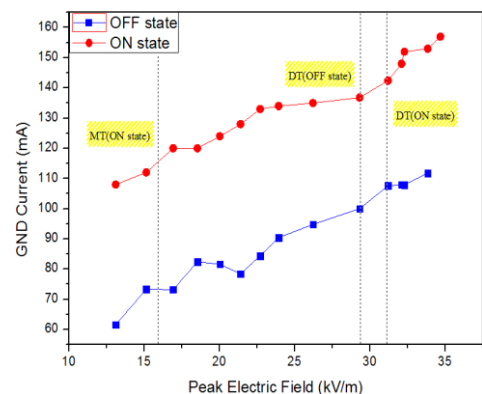

Figure 2. GND coupling current by HPM

REFERENCES

[1] IEC 61000-2-13, Electromagnetic compatibility (EMC) –Part 2-13: Environment –High-power electromagnetic (HPEM) environments –Radiated and conducted

[2] Backstrom, Mats G., and Karl Gunnar Lovstrand. "Susceptibility of electronic systems to high-power microwaves: Summary of test experience." IEEE Transactions on Electromagnetic Compatibility 46.3 (2004): 396-403.

Effect of a Shield Wire on Lightning-Induced Currents on a Buried Cable due to a Direct Strike

H. Tanaka, Y. Tian, Y. Baba
Department of Electrical Engineering
Doshisha University
Kyoto, Japan

C. F. Barbosa
CPqD R&D Centre for
Telecommunications
Campinas, Brazil

T. Tsuboi, S. Okabe
TEPCO Research Institute
Tokyo Electric Power Company
Yokohama, Japan

Abstract— The effect of a shield wire, which is a bare conductor buried above an insulated metallic cable, on lightning-induced currents on the cable sheath has been studied using the finite-difference time-domain (FDTD) method. The lightning strike is just above the shield wire. The FDTD-computed results show that the presence of the shield wire reduces significantly the induced current on the cable sheath and the voltage across the outer insulation layer of the cable. The results also show that the increase of the ground resistivity value increases both the cable and the shield-wire currents.

Keywords- buried cable, FDTD, lightning, shield wire

I. INTRODUCTION

Shield wires are often installed to protect buried telecommunication cables against lightning. This practice consists of burying one or more bare conductors above the cable, along the entire length where the protection is needed. In a previous paper [1], the effects of a shield wire on the lightning-induced currents on a buried cable were studied for a nearby lightning strike (25 m from the cable), using the finite-difference time-domain (FDTD) method [2]. This paper presents a similar study, but for a lightning strike just above the shield wire and the cable.

II. THE FDTD MODEL

Figure 1 shows a 1-km-long cable with a 1-km-long shield wire, each buried at depths 0.7 m and 0.4 m in a homogeneous soil, to be analyzed using the FDTD method. The working volume of 1050 m × 250 m × 1050 m is divided nonuniformly, and surrounded by an absorbing boundary condition. The cable and the shield wire are parallel to the x-axis. The minimum size of cell is 20 mm × 3 mm × 3 mm, which are employed in vicinities of the ends of the shield wire and the cable, and in the vicinity of the lightning channel. The cell size increases gradually as being away from these regions. The total number of the cells is 180 × 130 × 155. The time increment is set to 7.03 ps. The ground resistivity value is set to 850 and 1850 Ωm, and its relative permittivity is 10. The shield wire is modeled by the thin-wire representation proposed by Baba et al. [3]. Using this model, the equivalent radius of the shield wire is 0.69 mm. The cable is modeled as a single solid conductor covered by a dielectric sheath (no internal core conductor or internal insulation layer is considered).

A 1-km-long vertical lightning channel is located above the shield wire and the cable at 500 m from their left ends. It is represented by the modified transmission line model with linear current decay (MTLL), with constant $H = 7000$ m. The return-stroke wave-front speed is set to 130 m/μs, and the channel-base current is adjusted to represent the measured waveform reported in [4].
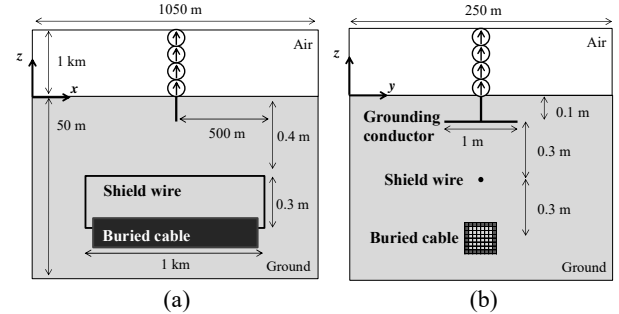

Figure 1. FDTD model for representing the cable, the shield wire, the vertical lightning channel, and the grounding electrode (not to scale): (a) side view, and (b) cross-sectional view.

III. ANALYSIS AND RESULTS

Figure 2 (a) shows FDTD-computed lightning-associated current waveforms on the shield wire for ground-resistivity values of 850 and 1850 Ωm. Figure 2 (b) shows those of the cable-sheath current. Also shown in each figure is the measured waveform. The FDTD-computed waveforms for 850 Ωm agree better with the measured ones provided in [4]. Figure 2 shows that the increase of ground resistivity increases both the cable and the shield-wire currents.
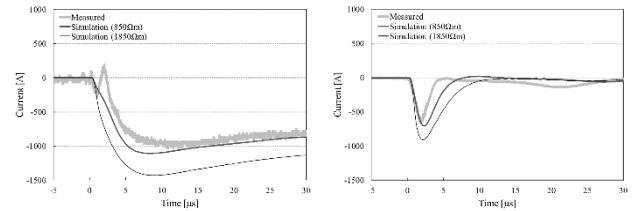

Figure 2. (a) FDTD-computed lightning-associated current waveforms on the shield wire for ground-resistivity values of 850 and 1850 Ωm, and (b) those of cable-sheath current. Also shown are the measured waveforms from [4].

The peak value of the cable-sheath current is reduced by about 40% by the presence of the shield wire and the voltage generated across the outer insulation (between the cable sheath and the soil) of the cable is reduced by about 60%. It follows from the results that both the cable-sheath current and the voltage across cable outer insulation are significantly reduced by the shield wire.

REFERENCES
[1] H. Tanaka, Y. Baba, and C. F. Barbosa, "Effect of shield wires on the lightning-induced currents induced on buried cables", IEEE Trans. EMC, vol. 58, n. 3, pp. 738-746, June 2016.
[2] K. S. Yee, "Numerical solution of initial boundary value problems in solving Maxwell's equations in isotropic media", IEEE Trans. AP, vol. 14, no. 3, pp. 302-307, May 1966.
[3] Y. Baba, N. Nagaoka, and A. Ametani, "Modeling of thin wires in a lossy medium for FDTD simulations," IEEE Trans. EMC, vol. 47, no. 1, pp. 54-60, Feb. 2005.
[4] C. F. Barbosa, A. Zeddam, P. Day, and Y. Burgeois, "Effect of guard wire in protecting a telecommunication buried cable struck by rocket-triggered lightning," ICLP, Uppsala, Jun. 2008.

Software and hardware assessment of FDTD simulations

For very large and complex scenes

L. Labarbe
CEA, DAM, GRAMAT
F-46500 Gramat, France
laurent.labarbe@cea.fr

B. Pecqueux
CEA, DAM, GRAMAT
F-46500 Gramat, France
bernard.pecqueux@cea.fr

Abstract—This paper presents tools recently developed at CEA Gramat to analyze the transient electromagnetic field on large scenes. It focusses on the pre and post processing tools around a FDTD solver: the mesh generation and the result visualization.

Keywords-FDTD; large simulation; mesh generation; result visualization.

I. INTRODUCTION

The Finite-Difference Time-Domain Method (FDTD) is widely used to solve electromagnetic problems. As described in [1], this algorithm can be efficiently implemented on massively parallel computers. An example of such implementation is GORF3D. It has been developed at CEA Gramat for many years ([2]) and is able to use the computation power of the CEA TERA 100 machine described in [3]. While problems of few billions of cells are commonly solved, the generation of such huge meshes can be challenging.

II. METHOD AND TOOLS

A. Mesh generation

The starting point of the example presented here is a generic city part. Different types of buildings compose the entire scene. The CAD model was meshed with triangles. The last step was the conversion of this set of triangles into a Cartesian mesh grid, also called staircase model.

B. Result visualization

An in-house software tool based on VTK [4] has been used to post process the huge amount of data produced by the FDTD simulation of large objects. This tool is able to display the transient electromagnetic field over the entire simulated domain, enabling the user to generate a video for example.

III. EXAMPLE OF RESULTS

A. Study approach

The electromagnetic response calculation of the complete scene is in progress and is organized following this next approach:

- External coupling on house type buildings,
- GORF3D computer evolutions (mesh grid, memory management, solver parallel adaptation, stop and go system, modification of the output files standard for the VTK visualization format),
- Development of the GORFVTK visualization tool for the graphic exploitation of very large scenes because the 2D and 3D classic visualization tools are in default,
- Validation of physic models which are used in the project : reinforced concrete, oblique cables, roof materials,... and research of equivalent material models,
- Comparison of the external electromagnetic response of several buildings alone or included in the urban zone (maximum coupling diagrams, comparison of surface fields for all the configurations).

IV. CONCLUSION

The difficulties linked to the processing of very large structures are shown here:

- Mesh generation doesn't show any difficulty from tools point of view but becomes more and more critical when the number of cells increases. The time to prepare a complete mesh of the entire scene could become preponderant in the most complex cases for the same reason of the results treatment.
- The computation, the storage and the 2D/3D visualization request very large memory resources. Works were undertaken on GORF3D solver and also on GORFVTK visualization tool and will be continued.
- Then, the differences obtained for the case of a building taken alone or placed in the complete scene will be studied and presented in the future paper.

REFERENCES

[1] Allen Taflove, Computational Electrodynamics, The Finite-Difference Time-Domain Method, Artech House, 1995.

[2] L. Morel, B. Pecqueux, R. Vézinet, "Notice d'installation et d'utilisation de la version exportable du code GORF3D", Note interne CEG I94-28, October 1994.

[3] http://www-hpc.cea.fr/en/complexe/pages/29-T100.htm

[4] Visualization Toolkit (VTK): http://www.vtk.org/

The didder

Evaluation of equipment power input susceptibility

L. Labarbe
CEA, DAM, GRAMAT,
F-46500 Gramat, France
laurent.labarbe@cea.fr

J-M. Lopez
CEA, DAM, GRAMAT
F-46500 Gramat, France
jean-marc.lopez@cea.fr

Abstract—This paper presents experimental studies performed in order to evaluate potential destruction of electronic equipment power supplies. These studies are linked with modelization research of power supply stages susceptibility. The experimental devices to test different aggression modes are described, the equipments being tested are presented and then the first results are given.

Keywords-equipment power input susceptibility, modelization.

I.   INTRODUCTION

The knowledge of electronic equipments susceptibility thresholds is mainly based till today on time consuming experimental studies. In this context, the modelization linked to the electronic components susceptibility is crucial. The purpose of this study is to evaluate destruction mechanisms of power supply components. The goal is to build a model for electronic equipments power inputs submitted to conducted electromagnetic aggressions.

II.   PROPAGATION MODES AND INJECTION METHODS

A.   Propagation modes

The injected conducted constraints on the equipment can be of two types: differential mode (DM) or common mode (CM). In practice, these two different modes can coexist. For a same type of equipment, two families can be met: high or low impedance according to the power supply technology. Besides, the equipment behaviour under test is very dependent on the propagation mode of the conducted constraint (DM or CM). The measured susceptibility thresholds are very different between these two following experimental configurations:

- same equipment population for different constraint modes,
- Different equipments for a given constraint mode (DM or CM).

B.   Assembly and injection methods

1)   Off-line electric service description

In order to observe disruption or destruction events, experiments should be performed with supplied equipments. A special electromagnetic installation allows to supply the equipment under test and generates conducted parasites which can be applied in directly or by coupling on the cable.

2)   Injection methods and associated measurements

The used injector delivers pulsed constraints with the following characteristics: few microseconds duration and parametric level. According to the test configuration, the injection will be in DM or CM. Current and voltage are measured very close to the equipment.

3)   Calibration method

This step consists in measuring the constraints on a well-known impedance ($Z_{réf}$) for all injection configurations. For the DM, currents/voltages are measured directly on the electric plug by replacing the equipment (Z_{equi}) by this well-known impedance. A similar phase is performed for CM constraints on the equipment/ground impedance.

III.   CONCLUSION

This abstract presents experiments which are carried out on power supply blocks in order to study their susceptibility according to differential constraint mode.

In particular, a parallel is done between the behavior of low and high impedance equipments families and the results of experiments with disruption or destruction events on the equipments.

The final paper will develop the results in terms of susceptibility according to conducted constraint propagation modes: this part will be based on experiments performed on electronic equipments, and in particular on stand-alone and integrated power supplies.

Radiation of High-Power Ultrawideband Pulses
with Synthesized Spectrum

V.I. Koshelev, A.M. Efremov, V.V. Plisko, E.A. Sevostyanov
Institute of High Current Electronics SB RAS
2/3 Akademichesky Ave., Tomsk 634055, Russia
koshelev@lhfe.hcei.tsc.ru

Abstract – A source of high-power pulses of ultrawideband (UWB) radiation based on the excitation of a 4-element array of combined antennas KA by bipolar voltage pulses of the amplitude up to 80 kV and length 2 and 3 ns has been developed and studied. The antennas optimized to radiate the bipolar pulses of the length 2 and 3 ns were disposed diagonally in the array. A bipolar pulse former had four independent channels. Each channel was connected to one antenna. The time delay between the pulses varied with the length of coaxial cables. Two modes of free-space radiation pulse synthesis have been studied: maximum peak strength of the field and maximum spectrum width.

Keywords – combined antenna; array; ultrawideband radiation

1. INTRODUCTION

High-power sources of UWB radiation based on multielement KA arrays excited by bipolar pulses are developed to study the susceptibility of electronic equipment to treat, to investigate biological effects, and radar with object recognition. At the excitation of the array elements by bipolar pulses of equal length, the frequency bandwidth of the radiated pulse is limited. Previously, to extend the spectrum of UWB radiation, it has been suggested [1] to excite the array elements by bipolar pulses of different length and to synthesize the electromagnetic pulse in the far-field zone. The task of the work presented is to investigate and develop a high-power source of synthesized radiation with the extended frequency band.

II. DESIGN AND RESEARCH DATA

The high-power source of UWB radiation includes a SINUS-160 monopolar pulse generator, a 4-channel former of bipolar pulses of the length 2 and 3 ns, and a 4-element KA array. The bipolar voltage pulses of the amplitude up to 80 kV are rising-edge synchronized at the former output. The time delay between the pulses was changed by the length of the cables. The time delays for synthesis of an

UWB pulse with maximum peak field strength and maximum spectrum width as well as the position of the elements in the array have been found preliminary in numerical calculations. KA excited by equal bipolar pulses should be diagonally disposed. This configuration of the array maintained the direction of the pattern maximum for both operation modes. The spectrum width was evaluated as the ratio of the upper and lower boundary frequencies determined by the level of –10 dB.

The first mode was realized when synchronizing maxima strengths of the fields radiated by KA which were excited by bipolar pulses of the length 2 and 3 ns. The electric field strength has increased by a factor of 4 while the spectrum width has changed insignificantly. The mode of the maximum spectrum width was realized at the optimum time delay of the strength maxima of the fields radiated by KA which were excited by the bipolar pulses of the length 2 and 3 ns. The peak strength of the field was less than in the first mode, and the ratio of the boundary frequencies of the spectrum of synthesized radiation has increased approximately by a factor of 2.

III. CONCLUSION

A high-power source of UWB radiation has been created. Two operation modes have been studied. The optimum structure of the array elements is diagonal providing the position of the pattern maximum perpendicular to the array plane for both modes. The pulses of synthesized radiation with the effective potential of 220 kV have been obtained for the mode with maximum frequency band and 500 kV for the mode with maximum peak field strength at the pulse repetition frequency of 100 Hz.

REFERENCES
[1] Yu. A. Andreev, Yu. I. Buyanov, V. I. Koshelev, V. V. Plisko, and K. N. Sukhushin, "Multichannel antenna system for radiation of high-power ultrawideband pulses," Ultra-Wideband, Short-Pulse Electromagnetics 4, pp. 181–186, 1999.

Dual Polarized Steering Transceiver for Object Detection through the Wall

V.I. Koshelev, E.V. Balzovsky, Yu. I. Buyanov, E.S. Nekrasov
Institute of High Current Electronics SB RAS
2/3 Akademichesky Ave., Tomsk 634055, Russia
koshelev@lhfe.hcei.tsc.ru

Abstract – A dual polarized transceiver for ultrawideband (UWB) radar with discrete pattern steering at radiation and receiving of subnanosecond pulses with central frequency of the spectrum equal to 2 GHz has been developed and tested. The transmitter contains two 4-element linear arrays of combined antennas KA with orthogonal polarizations. The receiver contains a 4-element linear array of the crossed integrated dipole antennas.

Keywords – combined antenna; integrated dipole antenna; array

I. INTRODUCTION

Application of radiation pulses with orthogonal polarizations is a modern trend at development of UWB short-range radar allowing reliably detecting an object. The polarization structure of the reflected pulse increases probability of the steering object recognition. Electronic pattern steering allows searching an object without mechanical transport of the transceiver. In our previous work [1] we have created a dual polarized receiving array with discrete steering. The task of the present work is development of a dual polarized transmitting array with discrete steering and testing of the transceiver in the pattern steering mode.

II. DESIGN AND RESEARCH DATA

The dual polarized transceiver design includes a transmitting and a receiving antenna arrays as well as controlled time delay lines providing horizontal discrete angular pattern steering in the limits of ± 33 degrees in the radiation mode and ± 40 degrees in the receiving mode, respectively. The transmitting KA antennas are horizontally disposed in two lines, four elements in each. The upper line is designed to radiate vertically polarized pulses while the lower one radiates horizontally polarized ones. The distance between the linear arrays was 10 cm at the cross dimension of the antenna equal to 7.5 cm. Each linear array was excited independently by bipolar pulses of the length 0.5 ns through a 4-channel power divider. The receiving array of the crossed integrated dipoles was placed above the transmitting array. Using the controlled time delay lines based on the cable pieces, six directions of the pattern maximum were realized in the transmitting array and seven directions in the receiving array, respectively. Deviation of the prescribed steering angle of the pattern maximum from the measured angle was no more than 3 degrees.

The task of the transceiver testing was to determine the direction angle of the arrival of an UWB pulse reflected from a metal object. A 25-cm thick foamed-concrete wall was used in the experiments, its dielectric permittivity measured before testing being equal to 2. An object of the dimension 20×20×40 cm was disposed at a 190-cm distance from the wall. The transceiver was located closely to the wall. The reflected signal was estimated as the difference of the signals recorded both at the presence and absence of the object. The pulse was recorded by the oscilloscope with the frequency band of 12 GHz and then averaged by 40 measurements. The angular position of the object behind the wall was measured in the limits of ± 33 degrees. The distance between the prescribed angle and the angle estimated by the results of measurements by means of the steering receiving array was approximately equal to one degree provided that it coincided with the discrete steering angle of the receiving array.

III. CONCLUSION

A dual polarized UWB transceiver with the discrete steering in the limits of ± 40 degrees has been created. Different types of antennas were used in the transmitting and receiving arrays. Preliminary tests have shown that under specified conditions the arriving angle of the pulse reflected from the metal object behind the wall is measured with good accuracy.

REFERENCES
[1] E. V. Balzovsky, Yu. I. Buyanov, V. I. Koshelev, and E. S. Nekrasov, "Dual polarized receiving steering antenna array for measurement of ultrawideband pulse polarization structure," Rev. Sci. Instrum., vol. 87, 034703, 2016.

Isotropic Shielding Properties of Loaded Apertures

Numerical and experimental evaluation

Ronny Gunnarsson, Bengt Vallhagen, Mats Bäckström
Saab Aeronautics
Linköping, Sweden

Abstract—It is shown that the aperture transmission cross section can be reduced substantially by surrounding the aperture with thin absorbers. It is further shown that under isotropic conditions, which e.g. prevails inside an overmoded avionic bay, the transmission cross section will not depend on whether the absorber is placed on the front side or the back side of the aperture.

Keywords-shielding; absorber; aperture transmission cross section; isotropic; reverberation chamber

I. INTRODUCTION

For an overmoded cavity the average shielding effectiveness, $\langle SE \rangle$, is given by

$$\langle SE \rangle = \frac{2\pi V}{\sigma_a \lambda Q} \qquad (1)$$

where V is the cavity volume, λ is the wavelength, σ is the aperture transmission cross section and Q is the quality factor. The average shielding effectiveness can, according to (1), be improved by reducing σ. One way of achieving this, while maintaining the open area of the intended aperture, is to surround the aperture with an absorber, see Fig. 1. This was e.g. reported in [1] where transmitted electric fields were presented for the case of normally incident plane waves on resistively loaded apertures. The electromagnetic environment in avionic bays can, from an engineering perspective, generally be regarded as being isotropic, therefore knowledge is needed also of the isotropic transmission cross section, $\langle \sigma \rangle$, which in this case replaces σ in (1).

II. NUMERICAL SIMULATIONS

The transmission cross section of loaded and unloaded apertures, when illuminated by incident plane waves, has been calculated using CST Microwave Studios FIT-solver. Results are presented here for an aperture of size 20×2 mm² in a 2 mm thick and infinitely large perfectly conducting ground plane. Three different absorber configurations have been studied, where the absorber is placed on the front (i.e. illuminated side), the back or on both sides of the aperture. Simulations has been performed for various Eccosorb absorbers and here we present results for a 3.2 mm thick FGM-U-125 absorber frame with width 10 mm. Aperture transmission cross sections were calculated for varying angles of incidence and polarizations, see Fig.1, for each absorber configuration. As will be shown at the conference, whether it is preferential to place the absorber on the front or on the back side of the aperture depends on the angle of incidence of the incident plane wave.
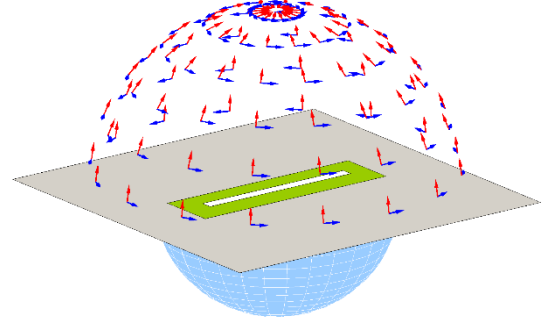

Figure 1. Illustration of electric field vectors for TE (blue) and TM (red) polarized plane waves with varying angles of incidence. Light blue half sphere represents integration surface for the Poynting vector. Absorber (green) on front side of aperture.
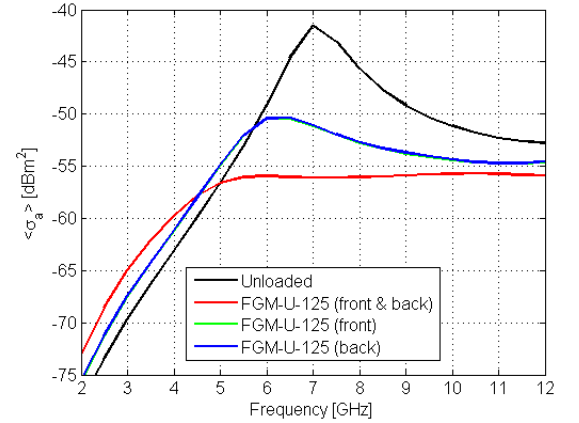

Figure 2. Numerically calculated $\langle \sigma \rangle$ [dBm²] for an unloaded 20×2 mm² aperture as well as the same aperture loaded with Eccosorb FGM-U-125 on the front side, back side or on both sides of the aperture.

The isotropic transmission cross section can be calculated according to [2]:

$$\langle \sigma_a \rangle = \frac{\pi/4}{N_p N_\phi N_\theta} \sum_{p=1}^{N_p} \sum_{f=1}^{N_\phi} \sum_{t=1}^{N_\theta} \sigma_a(p_p, \phi_f, \theta_t) \cdot sin(\theta_t) \qquad (2)$$

where p denote the polarization and θ and ϕ denote the angle of incidence. As shown in Fig. 2, a substantially reduced isotropic aperture transmission cross section is obtained when the absorber is placed on both sides of the aperture. It is further seen that the same isotropic transmission cross section is obtained whether the absorber is placed on the front or on the back of the aperture. At the conference, results from measurements in a nested reverberation chamber will also be presented.

REFERENCES
[1] Omar M. Ramahi and Lin Li, "Analysis and reduction of electromagnetic field leakage through loaded apertures: A numerical study", in , Vol. 25, Issue 7-8, October 2005, pp. 679-693.
[2] R. Gunnarsson and M. Bäckström, "A methodology for the numerical calculation of isotropic aperture transmission cross section", , Jeju, Korea, 2-7 August, 2015.

Innovative Shielding Effectiveness Measurement System

Joly Jean-Christophe[1], Ribière-Tharaud Nicolas[1]
[1] CEA, DAM, Gramat, F-46500 Gramat, France
Jonniau Sylvain[2], Vellas Nicolas[2], Choteau Benjamin[2],
Gaquière Christophe[2], Werquin Mathieu[2]
[2]MC2 Technologies, F-59262 Sainghin en Mélantois, France

Abstract— This paper describes an innovative system to measure the electromagnetic Shielding Effectiveness (SE) for shielded environment such as military shelters or critical infrastructures.
This innovative system avoids the drawbacks of classical double weighting solutions.

Shielding Effectiveness SE

I. INTRODUCTION

In a general point of view, most of the shielding effectiveness systems are based on a double weighting measurement (see figures 1 and 2).
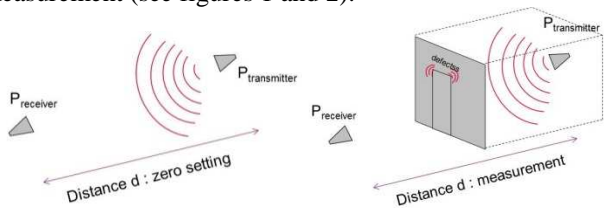

Figure 1: illustration of the zero setting step (on the left), and of the measurement step (on the right)

Then :

$$\text{Shielding Effectiveness} = P_{measurement}/ P_{zero \, setting} \qquad (1)$$

This solution has two main drawbacks and can generate false conclusions:

- between the zero setting step and the measurement step in presence of the shelter, an untimely external electromagnetic source (talkie-walkie, radar emission…) can modify the EM ambiance. In that way, this adverse radiation can be considered as an intrinsic EM leak of the measured enclosure.

- for synchronization reason, receiver and transmitter units often have to communicate with wires, optical fiber or wireless technologies. Those ways of communication can respectively generate mistakes at the enclosure path through or set-up difficulties.

II. PROPOSED SOLUTION

A. *Quadruple weighting*
The transmitted signal has a 50% ratio cycle (see figure 2). The variations (Δ) of the receiving signal are measured (see figure3). Then, shielding effectiveness is expressed with (2) :

$$SE = \Delta \text{ zero setting} - \Delta \text{ measurement} \qquad (2)$$

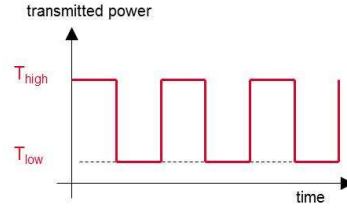This technique eliminates any external adverse EM pollution.

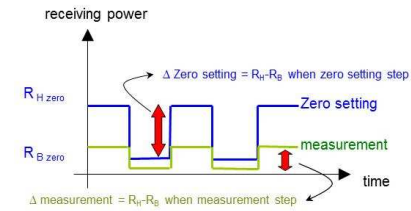Figure 2, representation of the transmitted signal

Figure 3,: representation of the receiving signal

B. *White noise emission*
For continuous frequency measurement and to avoid any link between the units, the solution consists in the emission of a white noise on the bandwidth of interest (for example 1 to 10 GHz).
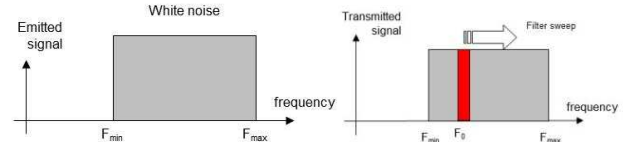A selective band pass filter sweeps along the bandwidth of the receiving signal (see Figure 4).

Figure 4: illustration of the filtering

III. CONCLUSION

The innovative shielding effectiveness system has been realized (see figure 5) in accordance with the quadruple weighting and the white noise emission principles. The expected performances have been verified.
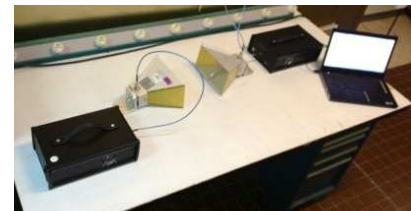

Figure 5: illustration of the system, with the receiving and transmitting units and their associated antennas

REFERENCES
Patent « Mesureur d'atténuation de blindage » , n° FR 15 59888 – 10/16/2015

HEMP Coupling to RF and LAN Cables

Rakesh Kichouliya and Sandeep M satav
EMI-EMC Centre
Research Centre Imarat, P.O. Vigyanakancha
Hyderabad, India

Abstract— This paper presents the experimental HEMP field coupling to RF cables and LAN cables in a utility building. The experiments performed in the worst case coupling scenario. The common mode and differential mode induced terminal voltage and currents are measured. These experimental results can be useful in designing the protection of electrical or electronic systems.

Keywords-HEMP; Field Coupling;

I. INTRODUCTION

The high altitude electromagnetic pulse [1] can be generated by nuclear and non-nuclear means. It poses a serious threat to electronic systems and electronic components [2]. In a typical utility building power cables LAN network cables and RF cables are found for specific purposes. These cables are connected to various electrical and electronic equipments, computer network switches. The HEMP induced voltage and current at the terminals of these cables are required to be computed or experimentally to be measured in order to design the protection of utility building electronic and electrical systems. In this paper the experimental HEMP field coupling to RF cables and LAN cables in a utility building is performed.

II. EXPERIMENTAL SETUP

The experimental studies performed with guided wave NEMP Simulator and 10 m long RG217, Sucoflex-102 and unshielded LAN cable (Schneider Electric ACT ASSI F2). The test setup is shown in figure 1. The simulator generates the 50 kV/m, 10 ns rise time almost double exponential field in the parallel plate section. The cables are laid along the ABCDEF path for maximum coupling condition. The electric field is measured by D dot.
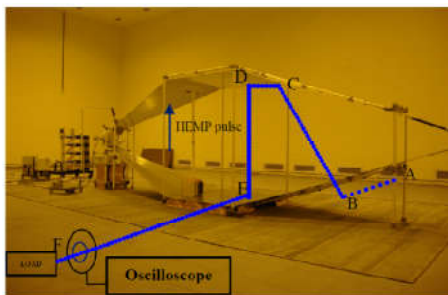

Figure 1.   HEMP Simulator

III. MEASUREMENT RESULTS

All the three cables were laid along the path as shown in figure 1. The measured common mode and differential voltages and current in each cable terminated with load impedance of 50 ohms, are shown in figure 2 to 4.
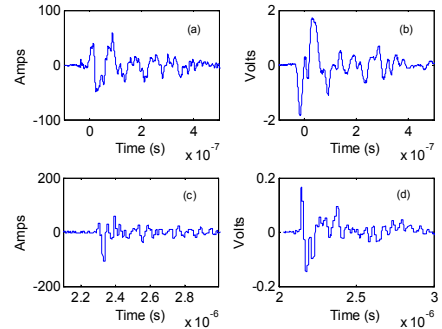

Figure 2.   (a) RG217 induced current (b) RG217 induced terminal voltage (c)Sucoflex-102 induced current and (d)Sucoflex-102 induced terminal voltage.
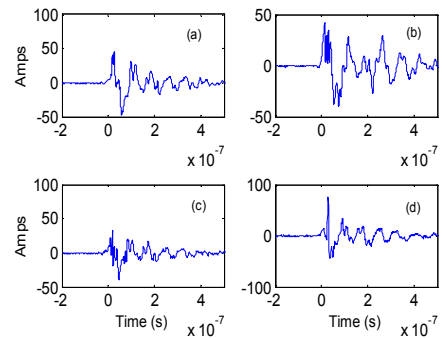

Figure 3.   (a)Blue pair differential current (b Green pair differential current (c) Brown pair differential current and (d)Common mode current on LAN cable
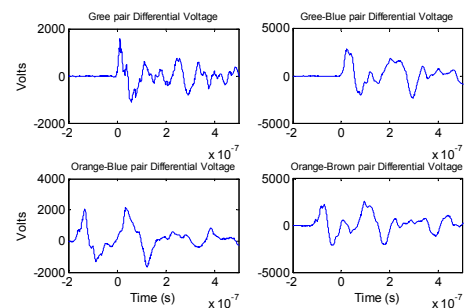
Figure 4.   Differential mode voltages in LAN cable

VI. CONCLUSION

The paper dealt with experimental HEMP (50 kV/m) coupling studies to the RF and LAN cables. The recorded maximum voltage and currents under worst condition, can be utilized for designing the protection circuit for HEMP for the system which employs these cables.

REFERENCES

[1] "Description of HEMP environment-Radiated disturbance, " IEC61000-2-9, 1996.

[2] Michael Camp,Daniel Nitsch, Frank Sabath, Jan-Luiken ter Haseborg and Heyno Garbe, "Susceptibility of Some Electronic Equipment to HPEM Threats",System Design and Assessment Notes, Note 37, 28 February 2004

Laser Induced Microwave Oscillations

Arindum Mukherjee[1], B N Biswas[2], N R Das[3]
[1,2]Dept. of ECE, [3]Institute of Radio Physics & Electronics
[1]CIT, [2]SKFGI, [3]Institute of Radio Physics & Electronics
[1]Assam, [2]Mankundu, [3]Kolkata, [2,3]West Bengal
[1]a.mukherjee@cit.ac.in

Abstract— This short communication audits the sustained microwave oscillation existing inside the OEO. Instantaneous amplitude and phase governing equations are derived using Barkhausen criterion. Their numerical solution shows the growth of RF oscillation in the loop.

Keywords- Opto-electronic oscillator, Barkhausen criterion, amplitude equation.

I. INTRODUCTION

The quality of the signal produced by any oscillator critically depends on the energy storage element in the oscillator circuit. High-Q or low-loss energy storage elements are essential for generating high spectral purity and high stability microwave signals. The Opto-Electronic Oscillator (OEO) represents the first practical microwave oscillator that uses optical energy storage elements to achieve high spectral purity at frequencies ranging from about a hundred MHz to beyond 100 GHz and also with a very high Q. This feature opens a new paradigm for generating high quality microwave signals. In this paper, the Barkhausen criterion for a single loop OEO oscillation is developed, from which the instantaneous amplitude and phase governing equations are derived and numerically solved. The growth of RF oscillation and its FFT is studied using MATHEMATICA 11.0.1.

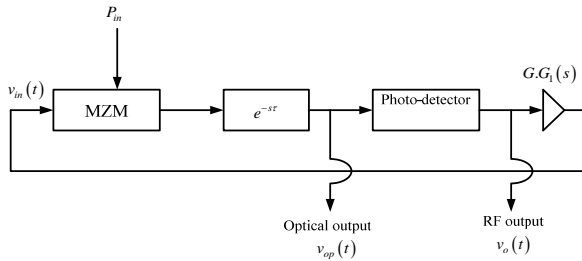## II. MICROWAVE OSCILLATION ENVELOPE USING BARKHAUSEN CRITERION

Figure 1. Simplified model of OEO

Referring to Fig.1, the photo-detector output is [1-2]

$$v_{op}(t) = -2\eta \times V_{ph} \times \cos\left(\frac{\pi V_B}{V_\pi}\right) \times J_1\left[\frac{\pi V(t-\tau)}{V_\pi}\right] \times \sin\left[\omega(t-\tau)\right]$$

$$= \frac{N\left[V(t-\tau)\right]}{V(t)} \times e^{-s\tau} \times v_{in}(t) \quad (1)$$

Again, $v_{in}(t)$ is the input voltage to the modulating grid of the MZM and if '$G_1(s)$' is the normalized transfer function of the RF tuned circuit, one finds that after the first passage of the input $v_{in}(t)$ through the loop, the voltage at the output electrical port will be given by

$$v_{01}(t) = \left[\frac{N\left[V(t-\tau)\right]}{V(t)} \times G_1(s) \times e^{-s\tau}\right] v_{in}(t) = B(s) \times v_{in}(t). \text{ Hence}$$

after the first cyclic passage, the net RF input voltage to the modulating grid of the MZM will be $v_{in1}(t) = G \times B(s) \times v_{in}(t)$, where

$B(s) = \dfrac{N\left[V(t-\tau)\right]}{V(t)} \times G_1(s) \times e^{-s\tau}$ is the feedback factor and '

G ' is the RF amplifier gain. Finally, after a sufficiently large number of cyclic passage through the OEO loop, the net electrical output voltage can be written as $v_0(t) = \dfrac{B(s)}{1-B(s)\times G} v_{in}(t)$, hence, the Barkhausen criterion for sustained oscillation can be expressed as $B(s)\times G = 1$.

Substituting $G_1(s) = \left[1+Q\left(\dfrac{s}{\omega_0}+\dfrac{\omega_0}{s}\right)\right]^{-1}$ in $B(s)$ and equating the real and imaginary parts, one gets

$$\frac{dV}{dt} = \left(\frac{\omega_0}{2Q}\right) \times \left[2\times G\times J_1\left[V(t-\tau)\right]\times\cos(\omega_0\tau) - V(t)\right]$$

$$\frac{d\theta}{dt} = -\left(\frac{\omega_0}{2Q}\right) \times \left[\frac{2G\times J_1\left[V(t-\tau)\right]}{V(t)}\times\sin(\omega_0\tau)\right]. \quad (2)$$

The numerical solution showing the RF oscillation growth and its FFT are shown in Figs. 2-3 respectively.
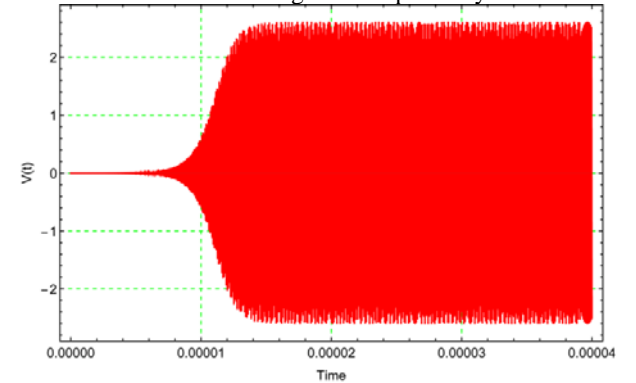
Figure 2. Oscillation growth in OEO
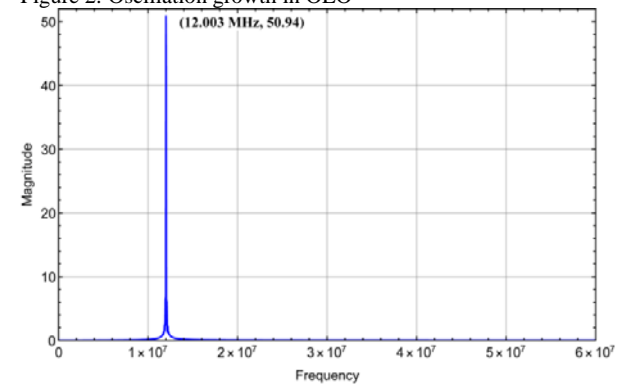
Figure 3. FFT of RF output in OEO

REFERENCES
[1] B.N. Biswas, S. Chatterjee, S. Pal, "Laser induced microwave oscillator," IJECET, vol. 3(1), pp. 211–219, 2012.
[2] A. Mukherjee, B.N. Biswas, N.R. Das, "A study on the effect of synchronization by an angle modulated signal in a single loop optoelectronic oscillator", Optik, vol. 126(19), pp. 1815–1820, 2015.

Design of a broadband 0.22THz 100W Planar Travelling Wave Tube

Vishnu Srivastava
Microwave Tubes Division
CSIR - Central Electronics Engineering Research Institute,
Pilani, Rajasthan, India, 333031.
vsceeri@gmail.com

Abstract—0.22THz TWT of 100W output power, 20dB gain, 40GHz bandwidth is being designed using rectangular sheet electron beam of size 100μm x 650μm, voltage 20kV and current 100mA. A simplified analytical approach is developed for designing of a planar staggered double vane loaded rectangular waveguide slow-wave structure for a broadband 0.22THz TWT. The analytical dispersion and impedance results are found very much comparable with the CST-MWS simulated results over the band of 0.20THz to 0.25THz. Effects of various parameters of a half-period staggered double-vane SWS on dispersion and impedance characteristics are evaluated for achieving a planar TWT of bandwidth more than 40GHz with high interaction impedance. It is shown that pitch and vane height are very significant parameters. In-house developed one- and 2.5-dimensional large signal analysis models (SUNRAY-1D & SUNRAY-2.5D) are being used to analyze RF performance of the planar TWT with input and output waveguide couplers, sever and velocity taper in the circuit.

Keywords- Planar slow-wave structure; THz TWT; Vane loaded rectangular waveguide; Vacuum tubes.

I. INTRODUCTION

A 0.22THz planar TWT of 100W output power, 20dB gain, 40GHz bandwidth and 5-10% efficiency is being designed for high speed data communication, security, radar, and other applications. Various types of periodic slow-wave structures (SWS) for a 0.22THz TWT are comparatively evaluated in terms of bandwidth, interaction impedance, circuit loss, higher order mode, thermal dissipation, and convenience of fabrication. Planar periodic structures are preferred for a 0.22THz TWT because a planar structure provides inherent rectangular beam hole for sheet electron beam operation and it is easier to fabricate using MEMS as well as nano CNC technology. Among various planar structures, staggered double vane loaded rectangular waveguide SWS (SDV-SWS) is found most appropriate in terms of wide bandwidth, high interaction impedance, less circuit loss and less higher-order mode problem. Analytical approach is developed [1] for design of a wideband SDV-SWS of a THz TWT. The analytical design of the planar RF structure for a 0.22THz TWT is evaluated using 3D e.m. field simulator CST-MWS [2014]. Dispersion and impedance results by the developed analytical approach are found very much comparable with the simulated performance. Effects of various parameters of a half-period staggered double-vane SWS on dispersion and impedance

characteristics are evaluated for achieving a planar structure of bandwidth more than 50GHz with high interaction impedance. In-house developed one- and 2.5-dimensional large signal analysis codes of a TWT (SUNRAY-1D and SUNRAY-2.5D) [2] are being used to analyze RF performance of the planar 0.22THz TWT with rectangular sheet electron beam with good accuracy and fast speed.

II. DESIGN OF 0.22THz 100W PLANAR TWT

A. ANALYTICAL DESIGN OF RF SWS
For a TWT of centre frequency (f_C) 0.22 THz and output power 100W, the electron beam of voltage 20kV and current 100mA is selected considering electronic efficiency around 5% (taking account of circuit loss and mismatch at couplers). Staggered double-vane rectangular waveguide SWS, is selected in the present design of a wideband 100W, 0.22THz TWT. There are nine design parameters of a staggered double vane rectangular waveguide SWS for a given beam voltage. These parameters are: pitch of the vanes (p), staggering factor (d), gap between two vanes (g), vane shape (vs), vane thickness (t), vane height (l), beam tunnel height (2a), total height (h), and width (w) of the rectangular waveguide. A simplified analytical approach is developed to determine initial values of these parameters for broadband and high impedance RF circuit.

B. LARGE SIGNAL ANALYSIS
The staggered vane-loaded 0.22THz TWT with input and output waveguide couplers, sever in-between the circuit and velocity taper in the output section is being analysed for its RF performance. One- and 2.5-dimensional large-signal analysis codes (SUNRAY-1D & 2.5D) [2] are being used to achieve output performance of 100W power, 20dB gain and 40GHz bandwidth for centre frequency 0.22THz, with rectangular sheet beam of size 100μm x 650μm, beam voltage 20kV and beam current 100mA. Nano composite Scandate-W dispenser cathode is being developed at CEERI for achieving high current density beam. Design of the planar 0.22-THz TWT using SUNRAY code is checked by comparing the simulated results by SUNRAY code with the simulated performance using CST-PS [2014]. Good agreement is achieved for gain and output power versus frequency over the band of 0.21THz to 0.23THz, but advantage of SUNRAY code is that it is very fast.

REFERENCES
1. [1] V Srivastava, et.al., Design of broadband planar structure for a 0.22-THz TWT, Universal Journal EEE (USA), vol.5, no.1, 2017, pp. 9-19.
[2] V Srivastava, et.al., Analysis of different structures TWTs using SUNRAY-1D and 2.5D codes, IVEC 2015, Beijing.

2017 Update on HEMP and IEMI Standards

R. Hoad
QinetiQ Ltd.,
Cody Technology Park, Farnborough, Hampshire,
GU14 0LX, UK
rhoad@qinetiq.com

W.A. Radsaky,
Metatech Corp.,
358 S. Fairview Ave., Suite E,
Goleta,
CA 93117, USA
wradasky@aol.com

Abstract— Standardisation in the fields of High Altitude Electromagnetic Pulse (HEMP) and Intentional Electromagnetic Interference (IEMI) phenomena has made progress in 2017. Standards pertaining to High Power Electromagnetic (HPEM) environments, protection design and test methods are becoming increasingly important. This paper will provide an overview of some recent developments in HPEM standards.

Keywords-component; *HPEM, IEMI and HEMP*

I. INTRODUCTION

Work on the improvement of standardisation for HPEM phenomena is becoming increasingly important as society begins to rely heavily on electronics-based technologies [1]. HPEM Standards have been developed to provide consistent and often simplified guidance pertaining to three key areas; Environment Definition; Immunity test methods; and Protection Design.

This paper will highlight some recent developments in these areas of HPEM standardisation with particular reference to the work of the International Electrotechnical Commission (IEC), Sub-Committee 77C [2].

II. DISCUSSION

A. Environment Definition

A simplified composite HPEM environment has been produced [3] and recently updated [4], Figure 1.
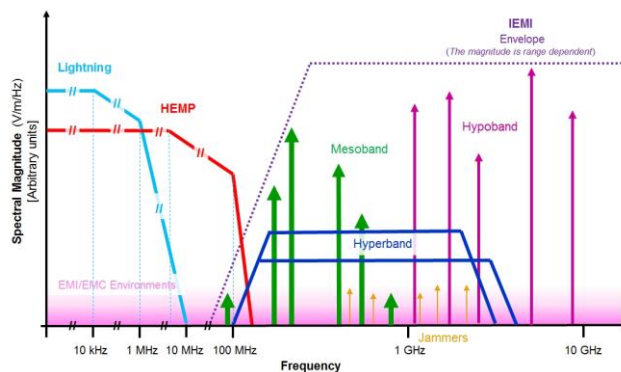

Figure 1. Simplified composite HPEM environment

Standardized descriptions of the HEMP environment have evolved over time.

Recently there has been increased focus on the HEMP E3 environment to understand the similarities and differences between HEMP E3 and Geomagnetic storm type disturbances [5]. IEMI is a relatively new phenomenon however IEC 61000-1-5 [6] provides a mathematically based waveform classification scheme for IEMI.

B. Environment Definition

HEMP and IEMI test standards cover equipment level, system/platform level and fixed installation level test methods. Generating the test environment is often a significant challenge but the IEC has provided standards which act as directories to identify HEMP and IEMI simulators [7 and 8].

Recent developments in HEMP conducted protection testing methods and test levels have introduced a graduated approach in order to allow some flexibility for the performance of protection measures [9] and work is currently underway in IEC SC 77C to produce a test method specifically for Mesoband and Hyperband type disturbances [10].

C. Environment Definition

Recently a guide to the application of HEMP and IEMI protection for a new build or an existing facility has been developed [4].

REFERENCES

[1] H.R. 1073, Critical Infrastructure Protection Act, signed into law on 12/23/16 (P.L. 114-328)

[2] Radasky W. A. and Hoad R., 'Status and Progress of IEC SC 77C High-Power Electromagnetics Publications in 2015', Proceedings of IEEE EMC Europe 2015, Dresden, Germany

[3] Giri, D.V.; Tesche, F.M., 'Classification of intentional electromagnetic environments (IEME)', IEEE Transactions on Electromagnetic Compatibility, Volume: 46, Issue: 3, 2004, Pages: 322 – 328

[4] IEC 61000-5-10 Ed. 1 Guide to the Application of HEMP and IEMI publications' DRAFT

[5] Radasky, W. A., J. Kappenman and R. Pfeffer, "Nuclear and Space Weather Effects on the Electric Power Infrastructure," NBC Report, Fall/Winter 2001, pp. 37-42.

[6] IEC 61000-1-5: High Power Electromagnetic (HPEM) Effects on Civil Systems, PD IEC/TR 61000- 1-5:2004

[7] IEC 61000-4-32: 2002, 'HEMP simulator compendium'

[8] IEC 61000-4-35: 2009, 'HPEM simulator compendium'

[9] IEC 61000-4-25 Ed 2.0, 'HEMP immunity test methods for equipment and systems', 2015

[10] IEC 61000-4-36 Ed. 2.0 'IEMI immunity test methods for equipment and systems', DRAFT

Decades of Evolution in EM Topology

From theory to application for EM coupling on complex systems

J-P. Parmantier*, I. Junqua
ONERA – The French Aerospace Lab, F-31055, Toulouse, France, http://www.onera.fr/en,
*jean-philippe.parmantier@onera.fr

Abstract — This paper starts from the background of EM Topology as it has been formalized by C.E. Baum. Then it reviews how the general theoretical concepts of EM Topology have progressively evolved during the last decades from a guideline for qualitative analysis of EM coupling problems towards dedicated calculation procedures nowadays widely used for quantitative assessment into real complex systems.

Keywords - Electromagnetic Topology, Multiconductor Transmission Line Network, Power Balance

I. GENERAL CONCEPTS

EM Topology is a concept that aims at decomposing a global EM coupling problem into pieces allowing simplification of the EM analysis to local problems in "topological volumes" and EM interaction between those topological volumes. Such an approach can be represented in graphs called "interactions diagram sequences" helping organization of qualitative and quantitative analysis.

First concepts of this approach have been proposed by C.E. Baum and F. Tesche as soon as the 70's (see for example the first edition of the EMP handbook [1]) but the theory has been fully completed by the same authors at the end of the 80's [2]. The general theory proposed by C.E. Baum is seen as an extension of the Multiconductor Transmission Line Network (MTLN) equations for which he developed with F. Tesche and K. Liù the BLT (Baum-Liu-Tesche) equation, which is in fact an original and smart form of a network equation for which the wave formulation allows efficient formulation of propagation equation on tubes (transmission lines) and scattering equation at junctions [3]. The topological network is described as a set of "tubes" on which source waves propagate connected to "junctions". The network equation involves big matrices called "super-matrices" organized in blocks with a subtle organization of labels describing the interdependency between topological volumes. Generalized to any type of volume topology, the Good Shielding Approximation (GSA) is a key approximation in order to introduce mono directional interactions in the interaction diagram sequence that simplifies its management.

II. MTLN

For low frequency concerns (in terms of wavelength of the excitation compared to characteristic dimensions of the object), propagation on cables is a real limitation to the decomposition of a complex structure in volumes as foreseen by EM Topology because cables make totally impossible any efficient application of the GSA. Consequently, without any specific intent to decouple geometrical zones, the number of topological volumes for structures such as automobiles and aircraft are generally limited to 2: one volume for the entire 3D object and one volume for the entire wiring. All the wiring system involves bidirectional branches in the interaction diagram sequence, which implies a network resolution. To this extent, the BLT equation formulation of MTLN matches perfectly the EM topology description requirements (see for example ONERA's CRIPTE code). Besides, the Field-to-Transmission-Line (FTL) model is perfectly suited for the GSA requirements. Indeed, in this model, currents on cables are calculated exactly and the reaction of those currents on the incident field is not strictly required for this analysis. Consequently, this model offers the capability to solve separately (one at a time) the EM scattering by the object (first topological volume) and the response of the wiring (second topological volume).

This model has been widely validated into significantly complex applications [4] and its efficiency for cable design in 3D structures has led to a powerful calculation technique used in industry. Nowadays research work currently focuses on the extension of this approach at low frequencies when common mode coupling brought by the structure becomes relevant (for lightning indirect effect applications on composite structures for example).

III. POWER BALANCE

As far as frequency increases to such a point that volumes become EM cavities, the physics of EM coupling in a complex system totally changes. Whereas lower frequency was dominated by common mode coupling and propagation on cables, such high frequency regimes are dominated by EM coupling localized at the points of application of sources. In addition, the sensitivity to small geometrical changes or positions of observables is such that statistics is the most appropriate approach to obtain reproducible results as it is usually done for tests in Mode Stirring Reverberation Chambers. When various volumes are interconnected, this leads to a global equilibrium of energy for which the Power Balance method [5] allows the description of a full EM problem (including the structures and its wiring) as a single topological network directly laying onto the interaction diagram sequence. In such a network model, junctions become so called "coupling cross-sections" and sources and observables are intended in terms of mean Powers and mean Power Densities. Because of the network model formulation, it has been shown that a specific PWB-BLT equation could be derived and could use the same algorithms as for the MTLN models (see for example ONERA's PWB code).

REFERENCES

[1] K.S.H. Lee: EMP Interaction: Principles, Techniques and Reference Data, a Summa Book, revisited version 1986.

[2] C. E. Baum : The Theory of the Electromagnetic Interference Control. Interaction Note 478, December 1989.

[3] C. E. Baum, T. K. Liù, F. M. Tesche : On the Analysis of General Multiconductor Transmission-Line Networks, Interaction Note 350, November 1978

[4] J. P. Parmantier, V. Gobin, F. Issac, I. Junqua, Y. Daudy, J.M. Lagarde, L. Paletta : ETE III : Application of Electromagnetic Topology on EMPTAC, Interaction Note 527, May 1997.

[5] I. Junqua, J-P. Parmantier, F. Issac, A network formulation of the PWB method for high frequency EM coupling applications, Interactions Note 576, November 2002.

Thermal Simulation of High Power S-Band Tunable Magnetron

S.K. Vyas and T. Tiwari

Center for High Power Microwave Tube and Component Technology, SAMEER,
Technology Complex, IIT Guwahati, Guwahati -781039, INDIA
E-mail: sandeepvyas19@gmail.com, drtntiwari@gmail.com

Abstract— This paper deals with thermal simulation of a high pulse power S-band magnetron operating at spot frequency 2998±5 MHz. The output peak power and average power loss in the magnetron has been calculated by PIC (particle in cell) simulation using CST particle studio which are 3.33 MW and 2.52 kW respectively. The steady state thermal simulation of this magnetron has been carried out using ANSYS workbench. The thermal simulation is done for different values of heat flux and heat transfer coefficient.

Keywords-Magnetron; PIC; Thermal simulation;

I. INTRODUCTION

Magnetron is a cross field vacuum electron device, which is a microwave oscillator, made in the form of a cylindrical diode [1]. Pulsed magnetrons are commercially available in the frequency range 1 GHz to 95 GHz at peak power from 1 kW to 7.5 MW [2]. SAMEER has developed S-band medical LINAC. LINAC system requires a high power RF source for field to beam energy transfer. Magnetron is the most economic and suitable for this work. It has a very complex and compact structure. The efficiency of high power magnetron generally lies between 50 to 60%, there by dissipating remaining power in the form of heat inside the tube. Therefore, thermally efficient design is essential to ensure reliable operation. In this paper, the thermal analysis of pulse power magnetron of 3.33 MW peak and 3.33 kW average powers is presented.

II. Magnetron Simulation

PIC simulation of 12 cavity hole and slot type magnetron with double ring type strapping, output window, and output coupler has been carried out by using CST particle to estimate the output power, anode current, frequency, and efficiency. The operating voltage and magnetic field are 50 kV and 1630 Gauss respectively. The π-mode operating point has been obtained by Hull cut off (1) and Buneman-Hartree (2) equations.

$$V_c = \frac{eB^2 r_a^2}{8m}\left[1-\left(\frac{r_c}{r_a}\right)^2\right]^2 \qquad (1)$$

$$V_T = \frac{\pi c r_a^2}{n\lambda}\left(1-\frac{r_c^2}{r_a^2}\right)B - \left(\frac{2\pi^2\,c^2 r_a^2 m}{e\lambda^2 n^2}\right) \quad (2)$$

PIC simulation results are given in Figs.1 (a-b). Figs. 1(a) and 1 (b) show the electron bunch formation and output power. The output power, current and overall efficiency are found 3.33 MW, 117 A and 57% respectively.
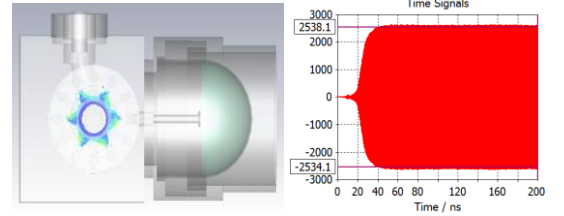

Figure 1: (a) Electron bunch formation, (b) Output power signal at output port

The ANSYS workbench has been used for thermal simulation. Thermal radiation from cathode, electron bombardment, and RF current act as heat source for magnetron. The power loss due to the electron bombardment and RF current can be calculated by using the PIC simulation results which is 2.52 MW. The duty cycle of magnetron is 0.001 so average power loss is 2.52 kW. The cathode requires ≈200 watts power to obtain the emitting temperature. The heat flux is calculated by using these power loss and applied on the area of inner anode circumference. The heat sink is modeled as film coefficient and applied in the cooling channels of magnetron. The values of heat transfer film coefficient are taken in the range of forced liquid cooling [3]. The thermal simulation results of magnetron are given in Table-1. Steady state temperature distribution is shown in Fig. 2.

TABLE-I   THERMAL SIMULATION RESULTS

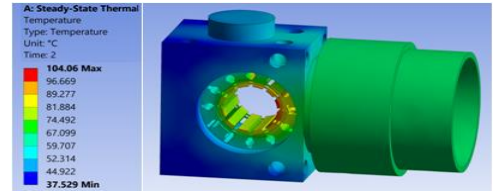| eat fl	eat transfer fil c efficient .	T $_a$	T $_{in}$
7.423×105	1000	196	120
7.423×105	2000	139	67
7.423×105	3000	120	50
7.423×105	4000	110	42
7.423×105	5000	104	37.52

Figure 1: Temperature contour plot for 5000 (W/m^2.K) heat transfer film coefficient

REFERENCES
[1]G. B. Collins, Microwave Magnetrons. New York, NY, USA: McGraw-Hill, 1948.
[2]S.K Vyas, et al, "Review of Magnetron developments", Frequenz, vol 70. issue 9-10,pp 455-462, Sep. 2016.
[3]T L Bergman, et al, "Introduction to heat transfer", John wiley & sons, 2011.

Analyzing HF & LF Radiation Hazard Scenarios with 3D EM Simulation

Rijin Saseendran

CST – Computer Simulation Technology India Private Limited

India

Rijin.Saseendran@cst.com

Abstract— Modern technology means that people are exposed to electromagnetic fields almost everywhere from a variety of sources. While the field strength is typically low in large distance from the source, in close proximity the induced fields and absorbed power may be high enough to harm the body. High-frequency electromagnetic fields, such as from broadcasting systems, mobile communication, Wi-Fi and radar, can all potentially pose radiation hazard (RadHaz) problems, as can low-frequency magnetic fields generated by high currents in applications such as welding guns, trains and electric vehicles. Various standards exist to regulate device design and installation of antennas and high-power components to avoid RadHaz. As the measurement is typically not an option inside the human body, EM simulation is the often only way to analyze the complex field distribution and estimate the resulting hazards in order to ensure a product complies with statutory exposure limits. This presentation shows how complex RadHaz scenarios can be tackled by EM simulation covering an overview of biological EM simulation, discussing human models, material properties, solver technologies and hybrid approaches.

 Keywords- Radiation Hazard, biological EM simulation

Simulation of EMP generation in high power laser facilities

Hanbing Jin1, 2; Cui Meng1, 2
1 Department of Engineering Physics, Tsinghua University
2 Key Laboratory of Particle & Radiation Imaging, Ministry of Education
Beijing, China

Abstract— Based on a 2D particle-in-cell code, the generation of EMP in high power laser facilities is simulated. A time-bias FDTD method is applied to solve Maxwell equations to restrain high frequency noise.

Keywords-electromagnetic pulse; laser target; FDTD

I. INTRODUCTION

An intensive electromagnetic pulse (EMP) can be generated when a high power laser strikes a target. The transient electromagnetic field can have an intensity up to several hundred kilovolt per meter with a broad frequency up to gigahertz, which may affect diagnostics, interfere or even damage electronic equipment. The mechanism of the EMP generation hasn't been understood clearly. However, it is widely accepted that escaping electrons produced in laser-target interaction are the main source of EMP [1]. The work reported here is to simulate the EMP radiated by electrons that escape the target and flow in the chamber. Instead of using a general finite difference time domain (FDTD) method to solve Maxwell equations, a time-bias FDTD method is applied to restrain high frequency noise.

II. Time-bias FDTD method

In the time-bias FDTD method, H field at times $(n-1/2)\Delta t, (n+1/2)\Delta t, (n+3/2)\Delta t$ are used to calculate E field at time $(n+1)\Delta t$. Meanwhile, a low relaxation iteration is applied for filtering. The difference formulas are expressed as:

$$E^{n+1,i} = (1-\tau_i)E^{n+1,i-1} + \tau_i E^n + \tau_i \frac{\Delta t}{\varepsilon}[\nabla \times (\alpha_1 H^{n+3/2,i-1} \\ + \alpha_2 H^{n+1/2,I} + \alpha_3 H^{n-1/2,I}) - J^{n+1/2}] \quad (1)$$

$$H^{n+3/2,i} = H^{n+1/2,I} - \frac{\Delta t}{\mu}\nabla \times E^{n+1,i} \quad (2)$$

Where $E^{n,i}$ represents E field at time $(n+1)\Delta t$ with an iteration count of i. α is time-bias weighting factors and τ_i are a series of relaxation factors.

III. MODLE AND RESULTS

A 2D cylinder chamber model where escaping electrons are ejected from the chamber center is constructed for simulation. A Fourier transform spectrum of EMP generated by 10^{12} electrons is shown in Fig.1, where the result from a general FDTD method is on the upper right corner. Time-bias method get that EMP has a broad frequency extending up to 10 GHz, while results from general method are wrong because of noises.
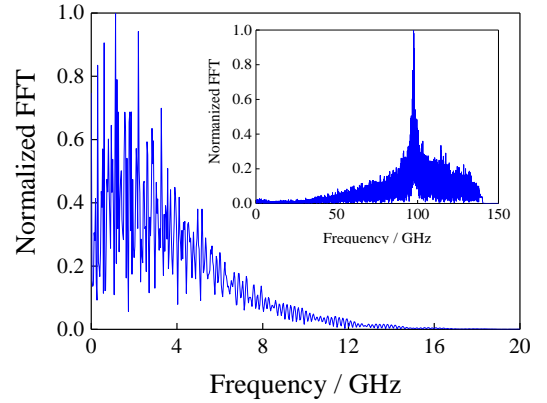

Fig. 1. The spectrum of EMP

The target size effect is explored and compared with the LLNL experiment results [1], as shown in Fig.2. The needed input information of escaping electrons for simulation is calculated according to Ref [2]. The simulation results are in agreement with measurements.
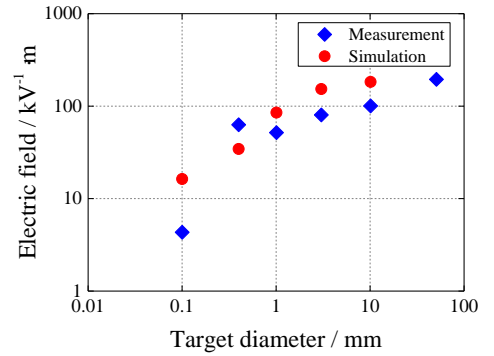

Fig. 2. Dependence of peak electric field as a function of target size

REFERENCES
[1] D.C. Eder, et al., Mitigation of Electromagnetic Pulse (EMP) Effects from Short-Pulse Lasers and Fusion Neutrons, LLNL-TR-411183 Technical Report Lawrence Livermore National Laboratories, March 2009.
[2] Poye, A., et al., Physics of giant electromagnetic pulse generation in short-pulse laser experiments. Phys Rev E Stat Nonlin Soft Matter Phys, 2015. 91(4): p. 043106.I.S.

Probabilistic Assessment of Braid Hardening with Limited Amount of Information

S. Lalléchère, S. Girard, P. Bonnet,
F. Paladian
Université Clermont Auvergne,
CNRS, SIGMA Clermont
Institut Pascal, 4 av Blaise Pascal,
63178 Aubière, France

Chaouki Kasmi
Wireless Security lab,
French Network and Information
Security Agency, ANSSI,
Paris, France

Lars-Ole Fichte
Helmut Schmidt University,
Faculty of Electrical Engineering,
Hamburg, Germany

Abstract—In this proposal, an original stochastic methodology is proposed for the electromagnetic (EM) assessment of metal braids at shielding level. They are mostly characterized by their geometries and electrical properties; modeling transfer impedance may be analytically achieved relying on a diffusive part jointly with magnetic leakage through the braid. Depending on the targeted applications, braided wires are given with a high diversity of input parameters. In this framework, uncertainty propagation methods are used for efficiently extracting statistical characteristics of braid.

Keywords: braided wire; shielding; statistics.

I. INTRODUCTION AND MOTIVATION

Since electromagnetic (EM) hardening of braided cables is still remaining a key issue [1], their shielding effectiveness was widely studied in the literature, especially for EMC experiments. As reminded in [2], (Non) Intentional EM Interferences ((N)IEMI) have been considered as major threats during the last decades, and were massively studied for High Power (HP) sources through European FP7 programs such as STRUCTURES and/or HIRF SE [1]. Indeed, High Intensity Radiated Field (HIRF) certification process is demanding for improved analytical modeling of Transfer Impedance (TI). Due to the intrinsic random nature of EM sources implied (magnitude, appearance, characteristics), severe test procedures have been designed to test systems' failure in laboratory [3]. Because of the inherent complexity of such harsh environments (e.g. when dealing with High Altitude Nuclear Electromagnetic Pulses, HEMP), the probability of failure of systems have to be carefully considered with statistical aims [3]. Additionally to the probabilistic nature of EM Compatibility (EMC) testing processes, input inaccuracies (e.g. precise size of the braid/wire diameters) and drifts between real and computational samples may introduce inaccuracies in the assessment of the EM shielding.

II. PROBLEM STATEMENT

As depicted in [4], the Direct Current (DC) resistance of braid plays a major role in various EMC test benches: triaxial setup, line injection, and direct measurement of the screen [4]. At lower frequencies, TI stands for DC resistance of the screen. It is widely known and is given by

$$R_0 = 4/(\pi * N * C * \sigma * \cos\alpha * d^2), \quad (1)$$

where N is the number of wires, C stands for the number of carriers, σ is the conductivity of wires, and d is their diameter [1]. In the following, the DC conductance G_0 of the braided wire will be considered as the inverse of R_0. From relation (1) and relying on experimental constraints in [1], we will assume d follows a Gaussian distribution with mean $d_0 = 0.202$ mm and coefficient of variation cv=9%. The standard error due to such assumption may be obtained with crude Monte Carlo techniques [5]. This is efficient when dealing with analytical expressions, e.g. relation (1); but unrealistic for classical testing procedures [4]. Smart sampling techniques (e.g. stochastic collocation, SC, [6]) are useful to accurately assess high order statistical moments; re-sampling methods have demonstrated their interest for EMC experiments [5].

III. PROBABILISTIC EXTRACTION OF THE CONDUCTANCE OF BRAIDED SHIELD

Relying on previous assumptions (section II), the aim of this proposal will be to demonstrate the interest of stochastic methods to extract the probability density function of braid DC conductance with a restricted number of measurements. In order to provide a reference solution (analytical one), the simulations are achieved from equa. (1). Fig. 1 both shows the efficiency of metamodeling (two simulations needed with Stochastic Collocation Monte Carlo, SCMC, method) and the high accuracy (fitting) of data obtained from moment generating function based upon efficient assessment of high-order DC conductance statistical moments from SC (less than twenty realizations).
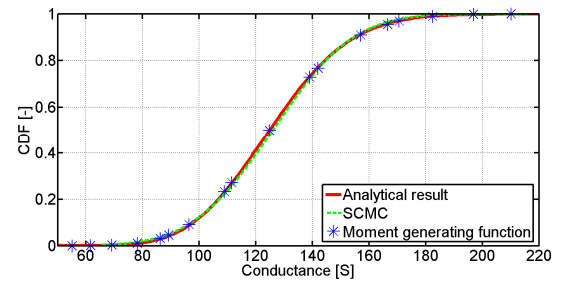

Figure 1. PDF of the conductance (equation (1)) of 1-meter braid.

REFERENCES

[1] H. Schippers and J. Verpoorte, "Uncertainties in TI calculations," ESA workshop on aerospace EMC, Valence, 2016.
[2] C. Kasmi and J. Lopes-Esteves, "Functional Susceptibility of COTS devices to IEMI at local and large-scale levels," in Proc. ICEAA 2016, Cairns, 2016.
[3] L-O. Fichte et al., "Application of Generalized Linear Models to Evaluate NEMP Tests," EMC Europe, Wroclaw, Poland, 2016.
[4] J. Hohloch et al., "Measurement of Transfer Imped. of Compon. for Auto. HVP Networks," EMC Europe, Rome, 2012.
[5] C. Kasmi et al., "Stochastic EMC/EMI experiments optimization using re-sampling techniques," IEEE Trans. EMC, vol. 58, no. 4, 2016.
[6] F. Paladian et al., "Modeling complex systems for EMC applicat. by considering uncertainties," URSI, Istanbul, 2011.

Geomagnetic Sudden Impulse Disturbance Signals Collection and Evaluation

E. B. Savage*, W. A. Radasky[†], J. L.Gilbert

Metatech Corporation, Goleta, California, U.S.A, savagee@cox.net*, wradasky@aol.com[†];

Abstract— One concern for the critical infrastructure is the possible effects of geomagnetic storms. The various types of storms create electric fields along the Earth's surface, which cause high level quasi-DC currents to flow in long power lines – possibly disrupting or damaging the electric power system. It is important to understand the characteristics of such storms. One type of geomagnetic storm is sudden impulse (or sudden storm commencement). This term has a sudden change in the geomagnetic field, and often indicates the beginning of other effects, such as an electrojet. The fast jump in magnetic field generates a spike in electric field. This paper reports on an effort to collect data on typical sudden impulse events.

Keywords – geomagnetic storms, sudden impulse, sudden storm commencement, power infrastructure

1 Introduction

As part of an effort to help define typical geomagnetic storm environments, magnetometer data was collected from 28 stations for 22 sudden impulse events. The data was evaluated to discern any variation with position, such as seen in electrojets having a strong latitude dependence. The magnetic fields were also converted to electric fields, and power line currents calculated for a generic power line.

2 Magnetic (B) Field Measurements

Figure 1 shows a sample measurement, showing the horizontal B field for many locations around the world. It can be seen that there is significant correlation of the signal in terms of signal arrival time, waveshape, and amplitude – which is not true for other types of geomagnetic disturbances. In the plot there are two unusual data lines – these are for high latitude stations (which typically have auroral electrojet starting with the sudden impulse), and show one conclusion: the sudden impulse signal may be uniform throughout the world, except at high latitudes, were there is little correlation with the lower latitude signals.
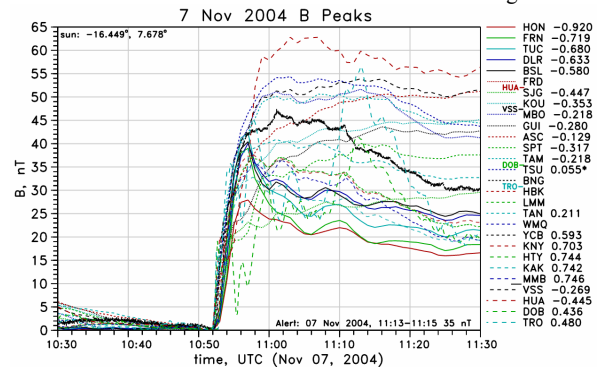

Figure 1. Sample of measured B fields.

3 B Field Variation with Location

Values of horizontal B field peaks for the sudden impulse was extracted for all data sets. Figure 2 shows this data. Here we were trying to see any location dependence. The peaks for each

event were normalized by the simple average peak value for the event, and plot lines drawn for each station (except for the two high latitude stations). With the exception of some data for two stations, there does not seem to be any difference for the various stations – the data seems for be just noise variations around the value 1. Since there was a wide range in latitudes for the stations, this indicates that there is not any latitude dependence. The horizontal axis is sun position (for the time of the event, the angle from the site vertical to the Sun's vertical axis – this is not actual time – it includes the site latitude as well as its longitude). The two exceptions are HUA, in Peru, (red line) and VSS, in Brazil (black line) – for these, if the sun is near over-head, the sudden impulse can be much higher. (HUA is on the geomagnetic equator, but VSS is not.)
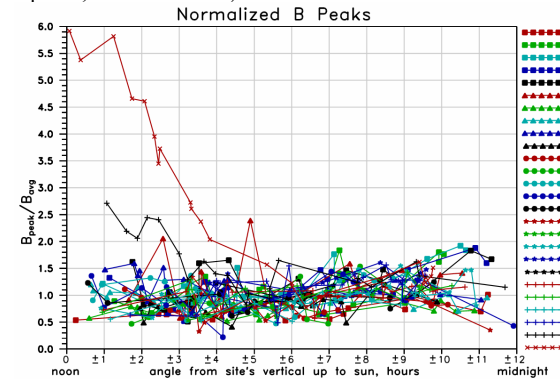

Figure 2. Normalized B field peaks versus Sun position.

4 Prediction of B Field from Satellite Data

An attempt was made to use ACE (Advanced Composition Explorer) satellite measurements to predict sudden impulse B fields on the earth. The particle momentum flux values for 10 events were compared to the corresponding B field measurements, and used to find a constant of proportionality value. Using this value, the particle momentum flux waveform data can be converted to a prediction for the resulting sudden impulse B field. Figure 3 shows an example (red line = satellite prediction, others are measurements of B).
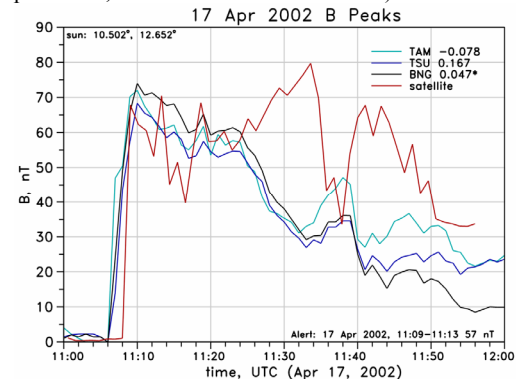

Figure 3. Normalized B field peaks versus Sun position.

5 E Fields and Line Currents

Calculated E fields and GIC (power line currents) will also be shown.

A Performance Compensation Method for Distorted Spaceborne Phased Array Antennas

Congsi Wang
Key Laboratory of Electronic Equipment Structure Design
Ministry of Education, Xidian University,
Xi'an, Shaanxi, China
710071

Yan Wang, Wei Wang
Key Laboratory of Electronic Equipment Structure Design
Ministry of Education, Xidian University,
Xi'an, Shaanxi, China
710071

Abstract—Based on the structural-electromagnetic coupling model, combined with the least squares method, the adjustment quantity of RF phase and amplitude excitation are obtained, which shall be implemented to recover a high quality pattern from a distorted antenna. A linear array of 1×8 elements is analyzed based on this method to compensate the degradation of system performance resulting from mechanical vibrations. Numerical results show this technique permits to restore the steering direction, decrease the side lobes and eventually recover high quality patterns in all directions.

Keywords-Active Phased Array Antenna, Structural-Electromagnetic Coupling, Compensation, Least Squares Method.

I. INTRODUCTION

Aiming at the degradation of electromagnetic performance due to the complex operating environment, this paper analyzes the structural-electromagnetic coupling model of APAA, clarify the influence of structure deformation on electromagnetic property, in addition, transfer phase difference caused by structural deformation to the amplitude and phase of excitation current. Combined with least squares method, we obtain the adjustment of the amplitude and phase to recover high quality patterns in all direction, including main beam direction and side lobe management.

II. STRUCTURAL-ELECTROMAGNETIC COUPLING MODEL

The compensated electric field of APAA is written as

$$E_c = T_c \cdot I_c \tag{9}$$

Finally, the compensation coefficients of excitation are obtained with the following equation.

$$I_c = \frac{T_c^T W T}{T_c^T W T_c} I \tag{10}$$

Where I is the ideally excitation, I_c is the increasing any gravity or structural complexity of excitation after compensation, W is the diagonal weight matrix, T and T_c represent the element pattern and far field distribution with ideal location and the presence of distortions. From the adjusted excitation current we find both the amplitude and phase are modified by least squares method.

III. SIMULATION AND ANALYSIS

A linear array of 1×8 elements is analyzed, based on structural-electromagnetic coupling model and least squares method, to compensate the effect of mechanical vibrations. Then the compensation technique is applied to the deformed linear antenna and the results in Fig.6.
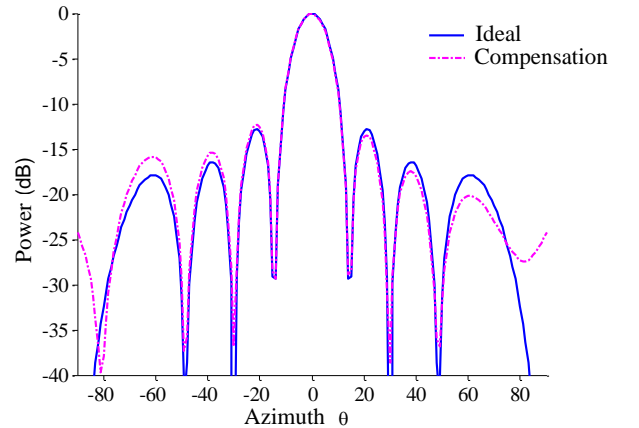

Fig.6 Comparison of ideal and compensated radiating pattern

We can see that the umerical results show that the gain loss is decreased to 0.06 dB from 1.31 dB，fulfilling the requirement of less than 0.5 dB for the engineer use. The SLL improved significantly by falling to -12.32dB from -8.64dB. Furthermore，the pointing accuracy varied from 1 °to 0 °to reshape the main beam direction.

IV. CONCLUSION

The work enables to implement real-time compensation of array antenna. This method performs well in improving the electromagnetic performance and ensures the high quality pattern of the antenna without antenna.

Vulnerability assessment of GNSS antennas to various threats

Ribi re-Tharaud N., Pirotais O., Joly J.-C., Rouquand A.
CEA, DAM, GRAMAT
F-46500 Gramat, France
Gamba G., Dalla Chiara A., Pozzobon O.
QASCOM S.r.l.,
Via O. Marinali 87, 36061 Bassano del Grappa, Italy
Vincent J.-P.
Thales Al nia Space France,
26 Avenue Jean Fran ois Champollion, 31100 Toulouse, France
Crabbe S.
Crabbe Consulting Ltd
Allerheiligenstr. 17, 99084 Erfurt, Germany

Abstract— PROGRESS is a FP7 project focusing on the detection and mitigation of attacks to GNSS infrastructures. This paper presents results obtained in this framework with emphasis on threats to GNSS antennas.

Critical Infrastructure, HPM, Vulnerability, Detection, Protection, GNSS; UAV; Antennas (key words)

I.   INTRODUCTION

PROGRESS project motivation is improving the security and resilience of Global Navigation Satellite Systems (GNSS) with regards to vulnerability from intentional threats. In focus are threats, which are considered to have a low risk of occurrence but potentially very large impacts (physical/explosive attacks, High Power Microwaves attacks, RF spoofing and jamming, Cyber-attacks) [1]. A centralized solution able to automatically detect malicious actions with a built-in reconfiguration capability to ensure the overall system Quality of Service has been developed. The embedded detection system includes hardware dedicated to threats on receiving/emitting facilities for GNSS operations, considering HPM [1], jamming and spoofing attacks [2]. However, a resilient infrastructure requires additional protection means to enhance the protection brought by the detection and reconfiguration solution. Numerical simulations on the infrastructure are used in order to ensure protected by design buildings (assessments of physical safety perimeter, natural electromagnetic shielding of rooms…) [1]. Other specific solutions have also been developed such as a shielding effectiveness measurement system [3].

II.   PHYSICAL ATTACKS ON ANTENNAS

This paper focuses on a scenario involving a civilian UAV carrying an explosive charge close to a dish antenna used for GNSS operations. The aim is to supply a methodology based on numerical simulations in order to assess the physical damage resulting from such an attack and to derive from it the resulting antenna electromagnetic performance losses. The considered targets are dish antennas used in this context: antenna diameter [5- 20m], operating frequency [2-8GHz], able to withstand 125mph winds and 1G seism. The mechanical properties and blast wave effects resulting from the UAV attacks are assessed through the ABAQUS finite element code and its CONWEP module. The electromagnetic antenna properties are assessed through the CST MicroWave Studio in the frequency domain using the integral equations solver (figure 1).
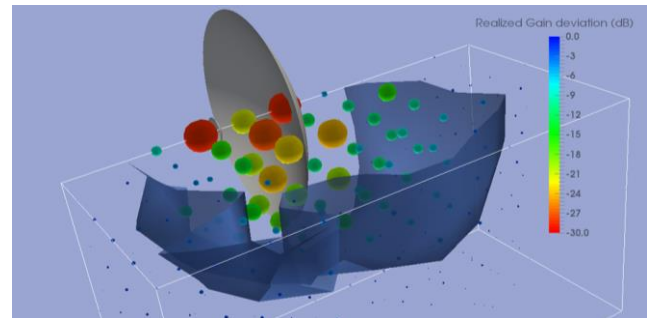

Figure 1.   Explosion impacts on antenna gain

III.   SAFETY PERIMETER ASSESSMENT

For each antenna, 400 UAV positions surrounding the antenna are considered. The physical damages of the explosions are computed as well as the related impact on the antenna electromagnetic properties. A criterion such as a maximum loss of 3dB on the antenna gain is considered in order to define an antenna safety perimeter and thus the relevant physical protection to be applied (figure 2).
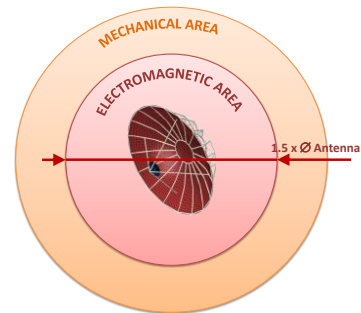

Figure 2.   Rules for antenna safety perimeters

REFERENCES
[1] N Ribi re-Tharaud, J-C Joly, A. Rouquand, S Schopferer, C Michalski, M Schimmerohn, S Crabbe, "PROGRESS project: Vulnerability and protection of GNSS ground-based infrastructures" EuroEM 2016, London, July 2016.
[2] G. Gamba, A. Dalla Chiara, O. Pozzobon, N. Ribi re-Tharaud, J.P. Vincent, "PROGRESS project: jamming and spoofing detection and localization system for protection of GNSS ground-based infrastructures." ION 2016, London, July 2016.
[3] J.-C. Joly, A. N. Ribi re-Tharaud, Jonniau Sylvain, Vellas Nicolas, Choteau Benjamin, Gaqui re Christophe, Werquin Mathieu, "Innovative Shielding Effectiveness measurement system" ASIAEM 2017, July 2017.

Challenges in HPEM-Protection

Armin W. Kaelin
EMProtec AG
Schaubenstrasse 4
CH-8450 Andelfingen / Switzerland
armin.kaelin@emprotec.ch

Abstract — The evolution of HPEM-threats and protection measures are briefly reviewed. Some misconceptions and challenges in actual protection concepts will be addressed.

Keywords: HPEM; EMI; EMC; protection; coordination;

I. INTRODUCTION

Threats of all kind have always inspired mankind to invent appropriate countermeasures. If a threat can't be avoided then countermeasures shall at least minimize the unwanted effects. This paper deals with HPEM-threats (High Power Electromagnetic) and its countermeasures: protection.

The oldest natural HPEM-threat is lightning. Even before man used electricity lightning posed considerable threats by starting forest fires or even killing animals or people. No wonder that in mythology we find many gods of lightning, e.g. Indra in India, Rai-Jin in Japan, Lei Gong in China, Donar or Thor in Germanic mythology, and there are many others.

In the 18th century lightning protection became popular. In Europe the Bohemian priest Prokop Divis installed 1754 a grounded rod next to his house and called it "machina meteorologica". In about the same time in America Benjamin Franklin made his experiments with kites in thunderclouds to prove the electric nature of lightning. He invented the lightning rod to protect houses from lightning induced fire and published a version for household application in 1753.

II. HPEM-Threats

In the meantime electricity and electronics became an important and critical part of our modern infrastructure. No wonder that nowadays lightning is still one of the most powerful and most frequent EM-threats, not only causing fires, but also coupling dangerous surges into our electric infrastructure. With the arrival of electric overhead-lines for power and telephones lightning protection against lightning surges became very important.

One of the earliest documented protection works may that of Sir Preece of the British General Post Office, where he was responsible for the Telegraph system. He investigated the fusing current for wires of different materials and proposed a protection according to Figure 1. Surge currents charge the capacitor and some residual current flows into the cable. In order to keep this current low, the wire was designed to melt like a fuse, a self-sacrificing protection. In 1892 Edison patented the first arrester, which based on a similar self-sacrificing concept like Preece's.

With radio communication Electromagnetic Compatibility (EMC) evolved as a new science to fight EMI (Electromagnetic Interferences) caused not only by lightning but by other electronic equipment. The use of semiconductors and integrated circuits increased the susceptibility of electronics to EMI, also to ESD (ElectroStatic Discharge).
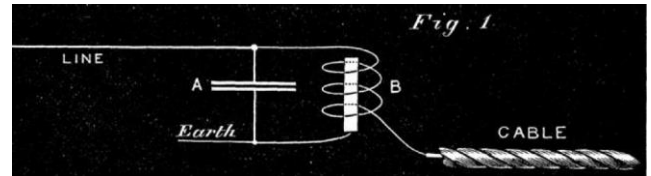

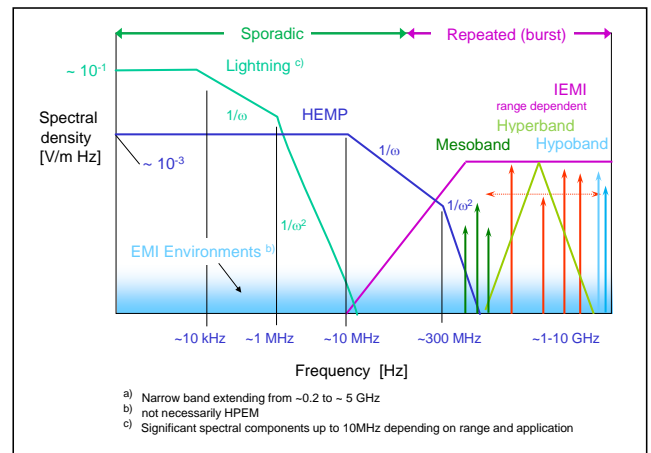Figure 1. Early form of lightning protection by Preece [1]

Figure 2. HPEM-threats spectra (derived from [2]).

During WWII the atomic bomb was developed and Enrico Fermi predicted the "radio flash", which is a new HPEM-threat known as HEMP (High altitude Electromagnetic Pulse). HEMP triggered a lot of protection activities especially for critical infrastructure. IEMI-threats (Intentional Electromagnetic Interference) with range dependent and possibly repeated bursts joined the HPEM-spectrum (see Figure 2).

III. Protection Challenges

HPEM-threats have quite different parameters regarding pulse energy, rate of rise, amplitude etc. This makes protection very demanding. Balanced protection should address both radiated and conducted threats, i.e. shielding and (non-linear) filtering. Conducted threats are typically responsible for 90% of HPEM-energy coupled into a facility, but nearly 90% of the protection costs are spent for shielding. Reliability and cost considerations recommend using filters designed to protect against all threats. This avoids coordination problems between different filters.

Some misconceptions of protection and coordination problems will be addressed in more detail during the presentation.

REFERENCES
[1] Preece W. H., "On the heating effects of electric currents", Proc. Royal Society 36, pp.464-471, 1883
[2] D. V. Giri and A. W. Kaelin, „Many Faces of High-Power Electromagnetics (HPEM) and Associated Problems in Standardization", AMEREM 1996, Albuquerque, N.M.

HEMP/IEMI Filter Design
and Confirmation of Performance

Sergio N. Longoria
Technical Product line Manager, Filters
ETS-Lindgren Inc., Cedar Park, Texas, USA
Sergio.longoria@ets-lindgren.com

Abstract—This paper discusses the design standards used and the testing that should be performed on facility filters for use in HEMP and IEMI protection. While the design and testing of facility filters for EMC is similar to that of filters for HEMP/IEMI there are extra tests designed to confirm the performance of facility filters for HEMP/IEMI protection. We begin by noting the design and safety standards use for the validation of HEMP/IEMI filters. We will then review the various standards that can confirm a filter's attenuation to conducted and radiated threats. This includes a filter's insertion loss performance and its radiated shielding characteristics when attached to an RF shield. A discussion on how Pulse Current Injection (PCI) testing is actually done to confirm HEMP performance will follow and a brief statement on IEMI performance testing. The importance of having the manufacturer's claims verified by a third party will also be addressed.

I. CONSTRUCTION AND SAFETY STANDARDS

A. Design and Test Parameters

In the United States, the de facto standard for guiding the design of filters is found in MIL-PRF-15733 as it provides the basic performance standards to evaluate filters. Everything from how much voltage can the filter withstand to the torque used on the connecting terminals. UL 1283 and IEC 60939 are commercial standards that incorporate and expand on the specifications of the MIL standard as they emphasize electrical safety in the design.

B. Safety Testing and AIC Testing

Filters should be tested for safety according to UL1283 or IEC 60939. The safety testing encompasses such items as DC Dielectric withstand (or Hi-Pot testing), Insulation Resistance, Temperature Rise, Capacitance Discharge (or Bleeder resistance check), Life test. Arc Interrupt Current (AIC) rating testing is a subset of safety, but often neglected by most specifications. In fact, AIC testing is part of UL 1283. In some cases, these tests are to be performed as a validation of design and in other cases, the test is made on 100 % of manufactured products. For example, since Life tests and AIC testing are destructive tests, these are performed typically by a third party on production first articles. As long as production models do not deviate from the first article construction, the test results are considered valid for all subsequent articles produced of that model.

II. PERFORMANCE STANDARDS

A. Insertion Loss

To confirm a filter's conducted attenuation manufacturers typically use MIL-STD-220. It is worth noting that there are other commercial standards available such as CISPR 17 and IEEE 1560. These were written in order to address the perceived shortcomings of the MIL-STD-220 method. Insertion loss testing can be used to indirectly assess a filter's attenuation to conducted IEMI, but it may not be accurate. RF Injection may be more accurate, but typically not done at the factory. A typical test setup for Insertion Loss is shown in figure 1. The measurement of insertion loss is typically not made by a third party, since it is usually a production test. However, on occasion, a third party may be brought in to confirm a manufacturer's claim.
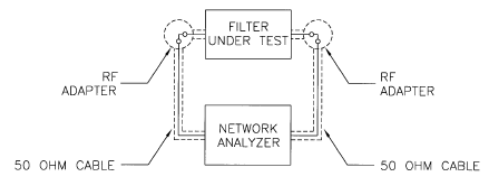

Figure 1. Typical test set up for Insertion Loss testing

B. PCI Testing

For confirmation of HEMP performance, we briefly examine the requirements of military standard MIL-STD-188-125 and commercial standard IEC 6100-4-24. It will be pointed out that the military standard is only concerned with HEMP and not with IEMI. Pulse Current Injection testing is used to verify HEMP performance and filters should be tested for their response during a simulated HEMP event using a double exponential waveform as shown in figure 2. Most of these tests are done as a filter design verification or as an acceptance test in an installation, typically by a third party.
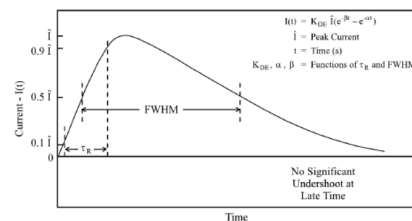
Figure 2. PCI testing waveform

C. Shielding Performance Testing

A shielding effectiveness test can be used to indirectly assess a filter's ability to reduce radiated HEMP/IEMI into a protected area. This test can be performed when the filter is attached to a shield and can be accomplished with well known standards such as MIL-STD-285 or IEEE 299. Other international standards such as IEC 61000-5-10 and IEC 61000-4-36 also provide methods for evaluating immunity to the IEMI threat.

Protection of Points of Entry (PoE) for Defense and Commercial Structures against HPEM

Sergio N. Longoria
Technical Product line Manager, Filters
ETS-Lindgren Inc., Cedar Park, Texas, USA
Sergio.longoria@ets-lindgren.com

Abstract— This paper discusses the use of facility filters for protection of facilities against HPEM within the context of military and commercial standards. The paper will make specific emphasis on the requirements of protection filters both for HEMP and IEMI. But further to this, the paper examines the electrical and mechanical characteristics needed in order to effectively accomplish the task of protecting and also deliver operational reliability and safety.

I. INTRODUCTION

We begin by noting the requirements of military standard MIL-STD-188-125, we then compare this requirement with IEC-61000-4-24. It will be pointed out that the military standard is only concerned with HEMP and not with IEMI. Other standards such as MIL-STD-461 deal with the issue of interference, but not as an act of deliberate and malicious intent. IEC 61000-4-36 is a commercial standard that effectively deals with the IEMI threat. A new standard, IEC 61000-5-10 is a guide for the application of protective measures for HEMP and IEMI.

Filters must handle conducted threats and be constructed in a way that maintain the shielding effectiveness of the protected area they are attached to. As such, the design of these filters should follow established standards and practices. These filters must be designed, validated and tested not only for the required protection, but also as part of an electrical system that must remain operational, reliable, and safe during an attack and during normal operations.

The electrical and mechanical characteristics such as the type of materials used, the filter topology, construction practices, testing, and final installation are of critical importance for an effective mitigation and protection of defense and commercial structures. For example, filters should be built following the requirements of one or more safety standards such as UL 1283 and IEC 60939. A third party may verify performance and ratings in order to validate a manufacturer's claims.

II. THE PROTECTION STANDARDS

A PoE is any place within a shielded structure where there is an opening for passing cables, materials or persons. In this paper, we are concerned only with PoEs that require metallic cables to pass from the unprotected area to the protected area or vice versa. MIL-STD-188-125 establishes that any cables passing through the shield must be treated for an HEMP pulse treat such as E1 and E2. E1 is a fast pulse characteristic of the detonation of a nuclear warhead in space. E2 is a slower pulse usually within the operational frequency of most electrical equipment. In addition, MIL-STD-188-125 establishes that the HEMP protection shield should be 80 dB from 10 MHz to 1 GHz. This does not consider IEMI which can fall on the frequency range above 1 GHz. Fortunately, filters can easily be made to work for IEMI once the filter has been designed to take care of the E1 and E2 pulses. But MIL-STD-188-125 is considered to be the severe protection standard and used mainly for defense structures. IEC 61000-4-24 has come up with different levels of protection depending on the structure to be protected and the type of protection desired. The intent is that extreme protection is costly whereas perhaps in some cases, a short upset of operations may be acceptable in exchange for a more cost effective solution.

III. DESIGN OF PROTECTION FILTERS

A. Electrical Features

All power filters used for HEMP/IEMI protection must have a voltage rating and current rating consistent with the source and load they will be protecting. They should also be rated for the systems' Arc Interrupt Current or AIC. Not doing so could cause catastrophic failure in the event of a system short circuit. In addition, typical designs for HEMP include an input inductor and a fast acting semiconductor device. The input inductor must be sized so that it does not saturate while in normal or abnormal operation. This inductor cannot be made from materials that tend to saturate quickly. In addition, the semiconductor device, typically a Metal Oxide Varistor (MOV) must be selected so as to allow proper voltage operation. The filter must also be equipped with a feedthrough capacitor for high frequency operation. HEMP filters should have independent protected lines and be built to safety standards such as UL 1283 or IEC 60939.

B. Mechanical Features

The filters' enclosure material should be plated steel or stainless steel. This is necessary so that conducted and radiated currents do not pass into the filter and thus into the protected area, but rather get diverted to earth ground or reflected. The proper filter design should have at least one completely sealed compartment on the load side for effective mitigation of HEMP/IEMI of the protected area.

C. Filter Testing

Filters should be tested for safety according to UL1283 or IEC 60939. In addition, the filter expected attenuation (insertion loss), in compliance with the protection requirements should be tested per MIL-STD-220 or CISPR 17. Further, the filters should also be tested for their performance during a simulated HEMP/IEMI event. Most of these are done as design verification stages, typically by a third party, as is also the case with AIC testing.

Computation of Beam-Wave Interaction in Medium Power Gyrotron

N Nayek and T. Tiwari

Center for High Power Microwave Tube and Component Technology, SAMEER,

Technology Complex, IIT Guwahati, Guwahati -781039, INDIA

E-mail: nnayek@gmail.com, drtntiwari@gmail.com

Abstract— This paper deals with computation of beam-wave interaction of a Ka-band CW Gyrotron. The optimized power has been computed which is found to be in excess of 15 kW at operating frequency of 27.918 GHz. The Gyrotron cavity has been designed in TE_{02} operating mode. Start oscillation current(SOC) has been computed on Matlab for TE_{02} operation modes as well as other adjacent competing modes. Particle in cell (PIC) simulation using CST particle studio has been employed to carry out the simulation work where more than 40% electronic efficiency has been achieved.

Keywords-Gyrotron; Material processing; PIC; Cavity design;

I. INTRODUCTION

Gyrotron is cross field device capable of producing megawatts of electromagnetic power in the millimetre and sub-millimetre wave frequencies. It is basically a Cyclotron Resonance Maser (CRM) in which power transfer takes place between Eigen modes of a oversized cavity and the helically moving electron beam. The application of Gyrotron is span over number of areas like communication, strategic or defence, scientific, medical and industrial application. The objective of the present work is to develop a medium power moderately oversized Gyrotron for industrial processing. Industrial processing using mm wave has become popular with the advent of high power mm wave source like Gyrotron. Material processing using mm wave is far more superior, particularly for low loss high end ceramics. Shorter wave length of mm wave gives rise to closely spaced hot spot and consequently more uniform heating inside the material.

II. Design and simulation of Gyrotron Cavity

Being a fast wave device, Gyrotron requires hollow metallic waveguide cavity operating just above cut-off for beam wave interaction. The cavity has three section i.e. down taper, straight section and up taper section. Down taper provides reflection for the operating mode whereas up taper provides weak coupling with the outer section. The combination leads to resonating behavior in the cavity. Initially, eigen mode analysis has been carried out to identify various eigen modes and corresponding frequencies in the cavity. The various dimensions of the cavity have been optimized to increasing spacing between operating mode and competing modes. Beam wave coupling coefficient for desired TE_{02} mode with respect to normalized radius of the cavity has been estimated analytically to obtain electron beam position inside the cavity.
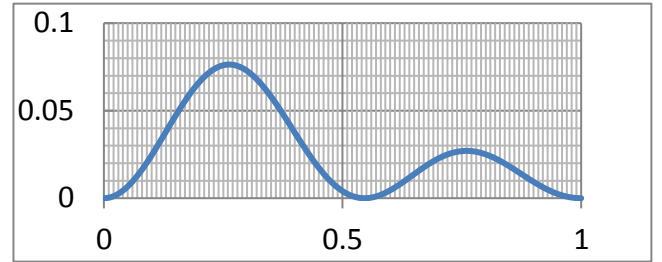

Figure 1: coupling coefficient of operating mode with respect to normalized radius

PIC simulation has been carried out to realize desired mode and frequency of operation in self consistent manner. It also computes output power and efficiency. Start oscillation current (SOC) provides useful information regarding magnetic field required in the cavity for a particular mode. SOC plot, self consistent electric field, electron beam energy spectrum, growth of operating mode and output frequency spectrum has been shown in fig.2, 3, 4, 5& 6, respectively.
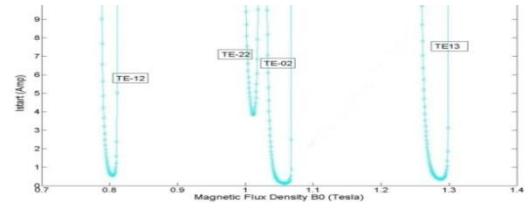

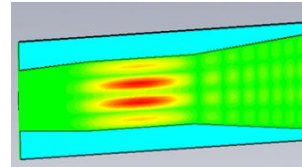Figure 2: SOC with respect to magnetic field
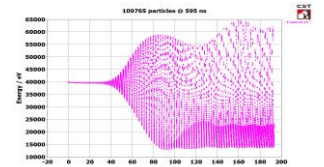

Figure 3: Self consistent mode in the cavity

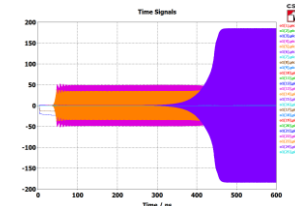
Figure 4: electron beam energy spectrum in cavity

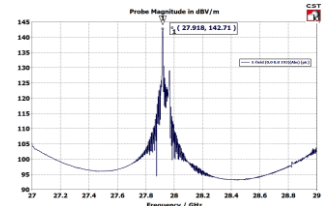Figure 5: Growth of operating mode

Figure 6: Output frequency spectrum

Transient Electric Field Computation on Polymer Insulators Mounted in EHV Lines

Gowrishankar S
Department of Electrical Engineering
National Institute of Technology, Calicut
Calicut, Kerala, India
sgowrishankarhve@gmail.com

Sunitha K
Department of Electrical Engineering
National Institute of Technology, Calicut
Calicut, Kerala, India
sunithak@nitc.ac.in

Abstract— Transient Overvoltages have a greater significance in designing the insulation systems for EHV/UHV transmission systems. Electromagnetic field computation is an effective tool for designing and optimizing the insulation systems. This paper describes the results of electric field computation performed on a 765kV polymer insulator under lightning and switching overvoltages. The results show that the magnitude of electric fields in all critical regions of insulator exceeds the threshold value thus increasing the possibility of flashover and premature ageing of the insulator due to high electric stress during transient conditions.

 Keywords-EHV/UHV lines, Transients, polymer insulators, electric field computation.

I. INTRODUCTION

Nowadays polymer insulators replace the ceramic insulators in high voltage transmission systems due to their superior insulation performance. They are installed with corona rings and grading rings for controlling and leveling the electric field. The dimensioning and positioning of these rings are done by using electric field computations performed with normal operating voltages[1]. In EHV/UHV transmission lines, the switching transients are predominant which decide the insulation level. This demands the importance of E-field analysis under transient overvoltages to be carried out on insulating systems intended for EHV/UHV applications. Electric field computation is carried out on a 765kV polymer insulator under lightning and switching impulse overvoltages.

II. METHOD

The impulse voltages are represented by a double exponential waveform as given in equation (1).

$$V(t) = A [\exp(-\alpha t) – \exp(-\beta t)] \qquad (1)$$

FEM based COMSOL Multiphysics software is used for E-field computation. The insulator with dimensions corresponding to 765kV is modelled as 2D – axi symmetry problem under dry and clean environment. The corona ring and grading ring dimensions and their positions were optimized under AC operating voltage for electric fields in critical regions of insulator to be within the specified level of 2.97kV/mm[2]. For electric field computation, lightning(LI) and switching impulse(SI) voltages specified in equation (1) with peak magnitude of 2100kV and 1550kV respectively are applied with suitable discrete time intervals.

III. RESULTS AND DISCUSSION

The electric field plot w.r.t time in critical regions of insulator during lightning and switching impulses are
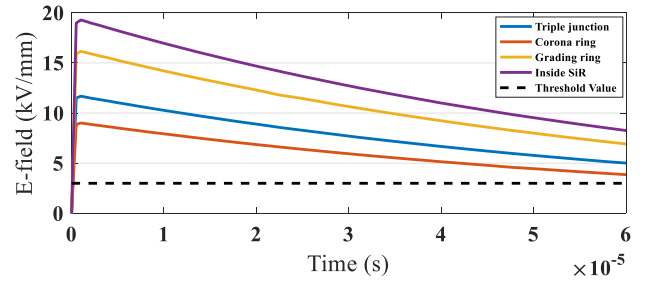

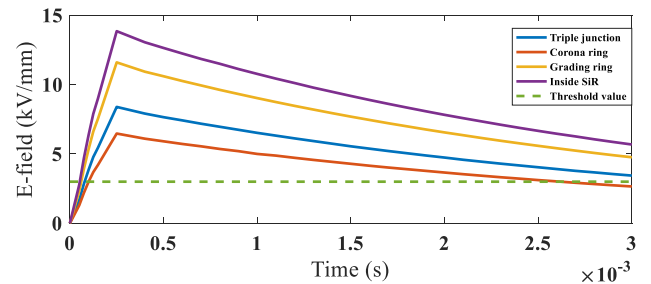Figure 1. Electric field in critical regions during LI

Figure 2. Electric field in critical regions during SI

shown in fig.1 and fig. 2 respectively.

In both cases, the electric field magnitude in critical regions is higher than that of threshold value for the entire duration of impulse voltages. This high electric field will cause the initiation of corona discharges on the surfaces of metal fitting and shed material and may lead to formation of arc and flashover if the transient overvoltage sustains over a period. It also clearly shows that the corona ring and grading ring designed to control AC voltage stress are not efficient during transient conditions. These rings also experience high electric field and become the source of corona discharges. The presence of surface charges, water droplets and contaminants will enhance the electric field and will lead to adverse effects than clean and dry conditions which may cause flashover and premature ageing of EHV/UHV line insulators. This suggests that extra care should be taken regarding transients while designing insulators and field controlling rings intended for EHV/UHV applications.

REFERENCES

[1] T. Doshi and R. S. Gorur, "Electric field computation of composite line insulators up to 1200kV AC", IEEE Trans. Dielectrics and Electrical Insulation, vol. 18, no. 3, pp. 861-867, June 2011.
[2] A. J. Philips, J. kuffel, A. Baker, "Electric fields on AC composite transmission line insulators", IEEE Trans. Power Delivery, vol. 23, no.2, pp. 823-830, April 2008.

Emerging Threats of IEMI for Information Security: recent advances – Plenary Talk

Chaouki Kasmi, José Lopes Esteves
Wireless Security Lab
French Network and Information Security Agency-ANSSI
Paris, France
chaouki.kasmi@ssi.gouv.fr

Abstract—This proposal refers to recent proof-of-concepts published in the literature with a focus on the usability of high power sources as an attack vector against IT and Embedded Systems. The Wireless Security Lab of ANSSI has proposed several proof-of-concepts pointing out how back-door and front-door coupling phenomena can be involved as an attack vector to get access and control smartphones through voice command interfaces and to communicate with air-gapped computers. This contribution is a summary of the today's capabilities to test, detect and exploit effects of IEMI in the cyber security domain.

Keywords: IEMI; Cyber-electromagnetics.

I. CONTEXT

During the last decades, many studies were devoted to the analysis of the susceptibility of electronic devices to intentional electromagnetic interference (IEMI). The detection and the classification of these effects are of fundamental interest, especially for assessing the correlation between effects and a given parasitic exposure. Thus, applying a specific methodology [1], electromagnetic security analysts need the following elements in order to better understand the risks for information security on a tested device:

- Detecting the effects: use of a monitoring tool for hardware and software failure detection;
- Classification of the effects: criticality of effects with regards of the application;
- Correlation and dependence of the effects with a given excitation signal: analysis of a potential correlation between effect and the parameters of the parasitic exposure (e.g. frequency, repetition rate, field amplitude…).

Having in hand these data, it is possible to have a clue on the functional safety [2] based on the application in which the device is used. Our research dedicated to the Electromagnetic Security of IT and embedded systems based on this methodology has led to the design and the demonstration of several proof-of-concepts (PoC) in which IEMI could be involved as an attack vector in the cyber security domain [3-5].

II. EM SUSCEPTIBILITY: A THREAT FOR INFORMATION SECURITY

A. Susceptibility of IT systems and air-gap bridging

Following the methodology mentioned in Section I, it has been observed that some computer failures can be directly correlated with the parasitic waveform parameters. We highlighted in [3] the possibility of modulating the parasitic waveform for encoding binary data that can be decoded by a malicious receiver software running on the targeted computer.

B. Audio interfaces and voice command injection

Later, in the framework of our experimentations, it has been shown that several parts of computers and smartphones react simultaneously to parasitic fields. The parasitic signal envelop was recorded by the audio input interface. It was shown that a continuous wave modulated in amplitude with an audio signal can be automatically demodulated by the audio front-end thus allowing to remotely inject voice commands on embedded systems providing voice command services. By testing smartphones while charging (USB cable connected either to the power network or a computer) or while the headphones were connected, it has been shown that by back-door coupling [4] and front-door coupling [5] we were able to successfully gain access to the target smartphones voice interface.

During the presentation, the methodology will be presented and the proof-of-concepts will be discussed. Ongoing research related to the present topic will be introduced. It will be shown that new applications of high power sources could emerge in a close future especially in the cyber security domain.

REFERENCES

[1] C. Kasmi, J. Lopes Esteves, M. Renard, "Automation of the Immunity testing of COTS computers by the instrumentation of the internal sensors and involving the operating system logs – Technical report ", System Design and Assessment Note SDAN 044, 2014.

[2] K. Armstrong, "How to Do EM Functional Safety – the Latest Guidance From the IET", Special Session on EM Functional Safety, APEMC 2016, Shenzhen, China, May 18-21 2016.

[3] C. Kasmi, J. Lopes Esteves, P. Valembois, "Air-gap Limitations and Bypass Techniques: "Command and Control" using Smart Electromagnetic Interferences", The 3rd Botnet Fighting Conference, Paris, France, 2015.

[4] C. Kasmi and J. Lopes Esteves, "Whisper in the Wire: Voice Command Injection Reloaded", Hack In Paris 2016.

[5] C. Kasmi and J. Lopes Esteves, "IEMI Threats for Information Security: Remote Command Injection on Modern Smartphones," in IEEE Transactions on Electromagnetic Compatibility, vol. 57, no. 6, pp. 1752-1755, Dec. 2015.

Effect Analysis of an EMP at NPPs

Song Hae Ye
KHNP Central Research Institute
KHNP (Korea Hydro & Nuclear Power Co, Ltd.)
Daejeon, Chungcheongnam-do KOREA
songhae.ye@khnp.co.kr

Ho Sun Ryu
KHNP Central Research Institute
KHNP (Korea Hydro & Nuclear Power Co., Ltd.)
Daejeon, Chungcheongnam-do KOREA

Abstract— An electromagnetic pulse (EMP) is an instantaneous, intense energy field that can overload and disrupt at a distance numerous electrical systems and high-technology microcircuits, which are especially sensitive to power surges. A large-scale EMP effect can be produced by a single nuclear explosion detonated high in the atmosphere. All EMP events have three common components: a source, a coupling path, and a receptor. The electromagnetic pulse travels through wires, pipes, and antennas. It can also travel across power grids, destroying electronics as it passes in less than a second. In fact, it is difficult and inefficient to conduct an analysis of the effects of an EMP with the equipment and systems available in nuclear power plants (NPPs) [1]. Thus far, no technical standards or requirements have been developed regarding an effect analysis of an EMP at nuclear power plants. To ensure the safety of operating nuclear power plants under these conditions, the emissions of an EMP must be known before an effect analysis can be done and to devise safety measures in the event of an EMP. Therefore, this paper presents effective methods by which to conduct an effect analysis of an EMP at operating NPPs.

Keywords: HEMP (high-altitude electromagnetic pulse), NPPs (nuclear power plants); POE (point of entry)

I. THE PROPAGATION PATHWAYS OF an EMP

The propagation pathway of EMP can be roughly considered to have two possible routes: radioactivity and conductivity. The radioactive effect refers to an impact transmitted to the ground from high-altitude electromagnetic pulses (HEMP). Such an impact may affect equipment through the point of entry (POE) of the building structure of an NPP. The conductive effect refers to induced voltage or current coupled with exposed cables. The induced voltage and current may affect the equipment and system via connected cables. All of these factors must be considered when conducting an EMP effect analysis for a NPP.

II. EMP EFFECT ANALYSIS APPROACHES

A. The Selection of the Main Objects

Domestic NPPs have critical safety function design concepts that prevent core damage and the escape of radiation. The priority of the critical safety functions is to maintain the safety status of the NPP, as show in Table 1. If an EMP occurs, a reactor shutdown occurs to ensure the safety of the plant. Systems related to a cold shutdown should operate properly after an EMP accident. In other words, it is not necessary to ensure the continuing operation of the plant in intense multiple EMP environments.

B. Simulation of EMP

Generally, an EMP is able to penetrate through the POE and the building wall of NPP concrete structures. It can also adversely affect equipment and systems that are coupled to internal circuits and electronic boards. It is not possible directly to evaluate the impact of an EMP on operating NPPs. We are considering the use of simulation tools to evaluate the electromagnetic shielding ability and conductivity of cables through vulnerable points in NPPs.

C. EMP Field Tests

The corresponding EMP tests will be performed and evaluated in relation to technical requirements such as MIL-STD-188-125-1[2]. The shielding performance test serves to verify the EMP effect with regard to radioactivity. When considering EMP protection at nuclear power plants, it is important to ensure the safety of the public and the plant. The most probable effect of an EMP on a modern nuclear power plant is an unscheduled shutdown. In general, an EMP can be considered a nuisance at nuclear plants, but this event is not considered to be a serious threat to plant safety.

Table 1: The Priority of the Critical Safety Function at NPPs

1	Reactivity Control	5	Core Heat Removal
2	Secure essential power	6	RCS Heat Removal
3	RCS Inventory Control	7	Containment Bldg. Isolation
4	Reactor Coolant System(RCS) Pressure Control	8	Containment Bldg. Temperature, Pressure, Flammable Gas Control

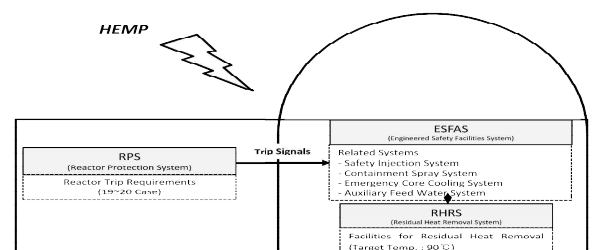Figure1. The main systems used for an EMP affect analysis in a NPP

REFERENCES
[1] Song Hae Ye, Ho Sun Ryu, Min Yi Kim, Eui Jong Lee, The Establishment of Object Selection Criteria for the Effect Analysis of EMP in Operating Nuclear Power Plants
[2] MIL-STD-188-125-1, High-Altitude Electromagnetic Pulse (HEMP) Protection for Ground-Based C4I Facilities Performing Critical, Time-Urgent Missions, 7 Apr 2005.

Distribution of the Electric Field in Small Reverberation Chambers

Lars Ole Fichte
Helmut Schmidt University
Hamburg, Germany
mailto: lo.fichte@hsu-hh.de

Keywords-Electromagnetic Reverberation Chamber, numerical simulation, statistical evaluation

Abstract— Focus of this paper is the fundamental principle of an Electromagnetic Reverberation Chamber. The field properties are discussed, and data obtained from numerical simulation is evaluate to investigate its statistical properties.

I. INTRODUCTION

Electromagnetic reverberations chambers (or mode stirred chambers, MSC) are used for various electromagnetic compatibility (EMC) test procedures, e.g. immunity test, radiated emissions or screening effectiveness tests. MSCs consist of a electromagnetic cavity resonator fed by an RF source; inside the resonator is an asymmetric metal piece, called stirrer, which can be turned to modify the boundary conditions fort he electric field. A DUT placed inside the working volume of a functioning chamber is exposed to an electromagnetic field with constant magnitude and normally distributed angle of incidence and polarization plane.

Tests utilizing MSCs are cost-effective when compared to other methods (semi-anechoic chambers, OATS or GTEM cells), since all relevant parameters can be recorded with fewer measurands: By varying the chamber geometry by means of a mode stirrer, an set of (complex) electric field vectors with Cartesian components is recorded. The real and imaginary parts of those vectors can be treated as random variables. If these agree with theoretical considerations and are normally distributed with zero expectancy and spatially constant chamber-specific variance, reproducible tests are possible which cover all relevant exposure parameters. Under these conditions, single field magnitudes can not be reproduced, and the characteristics of the set of field magnitudes are determined by the distribution. However, it is unclear whether the field distribution of a given chamber satisfies this normal distribution assumption, even if it has been calibrated according to [1].

II. SMALL REVERBERATION CHAMBER

Particularly in the case of a small chamber (i.e. small when compared to the chamber size advised by [1]), valid statements about the field distribution and homogeneity in the test volume are still missing. Such statements would be desirable from the technological point of view, since an application for calibration (miniaturized) antennas becomes possible. The aim of this work is therefore

- to generate a large data base through numerical simulation,
- to evaluate these statistically and thereby
- to evaluate the influence of various parameters on the efficiency of the chamber.

First we define quantities that allow the validation of the efficiency of an MSC. These meet the demands of the industrial standard IEC 61000-4-21, and additionally allow us to compare different chamber concepts with regard to their quality. E.g., the spatial variance of the averaged electric field in the test volume is considered for different numbers of stirrer positions. Another quantity under consideration is the chamber quality, which governs the maximum electric field magnitude E_{max} (P_0) which is excited inside the chamber by feeding it with a specific input power P_0. Implementing the methods to calculate these characteristics allows the analysis of large amounts of data and can be used to analyze both simulation and experimental data.

III. NUMERICAL SIMULATION

Both finite element formulation based on Nédélec edge elements and edge method (EFIE) are used and compared in terms of their advantages and disadvantages. Initially, the analysis is focused on unloaded chambers, but both approaches can easily be extended to chambers loaded with a DUT. Finally, the influence of different parameters on the parameters defined above is analyzed. Specifically, we try to answer the following questions:

- Can the real and imaginary part of each Cartesian component of the electric field be interpreted as realizations of a normally distributed random variable with zero expectancy in a small MVK by favorable adjustment of all parameters (conductivity, stirrer shape and position, antenna characteristics, etc.)?
- Which ist he optimal conductivity of the material the MSC is built of? What is the best "trade-off" between chamber quality and field distribution in the test volume for the respective purpose of the chamber?
- Can the Least Usable Frequency (LUF) be identified by the decline of cumulative spatial variances?

We also discuss the importance of these questions for the functioning of an MSC and examine the connection to ergodic systems. The effect of additional noise is also to be discussed. As a next step, the data obtained by simulation will be compared with experimental data.

REFERENCES
[1] IEC 61000-4-21

NASCAP/GEO CHARGING ANALYSIS OF GSAT-11

Anju Damodaran, Gomathi D., Manvi Gupta, Vivek R. Srivastava,V. Lakshminarayana, P.K. Poddar, V. K. Hariharan, M. Nageswara Rao

Electrical Integration Division-2, Systems Integration Group, ISRO Satellite Centre, Bangalore

Abstract— NASCAP/GEO analyzer program has been used for prediction of charge built up on the surface of GSAT-11 Spacecraft. GSAT-11 is ISRO's first spacecraft in I-6K series of spacecraft. It is a high power (14kW) satellite with mission life of 15 years. It has a combination of several new technologies which include system to generate high DC power, its distribution, Ka-band and Ku-band payloads and all of them accommodated in a new modular structure.

Spacecraft surface charging is the build-up of electrostatic potentials on the exposed surfaces of spacecraft in plasma environment. The GSAT-11 spacecraft is a complicated object consisting of more than one material on surfaces and of bigger dimension in comparison to I2K and I3K class spacecraft. The spacecraft charges differently for different surface materials. This non-uniform charging of surfaces lead to differential charging. Differential charging can cause electrostatic discharges, which may interfere with electronic signals and can be damaging to the spacecraft.

NASCAP/GEO analyzer program has been used for analyzing the on-board absolute surface charging and differential charging of GSAT-11 spacecraft under sunlit / shadow and eclipse conditions. The GSAT-11 is modeled by specifying the geometry considering NASCAP's limitations and the exposed surface materials. The plasma environment is represented in terms of a mathematical function called the Maxwellian distribution function. The worst-case representations for Single Maxwellian distribution in GEO plasma environments have been simulated for estimating the potential build up. The exposed surface materials are shown in Fig.1 as generated by NASCAP. Fig.2 shows the absolute charge built upon the surfaces respectively.

This paper details the surface charging predicted using NASCAP/GEO analyzer program on GSAT-11 S/C for sunlit-eclipse-sunlit, sunlit/shadow and eclipse passage under worst-case environmental conditions. Also the ESD control methodologies adopted are described in the paper.

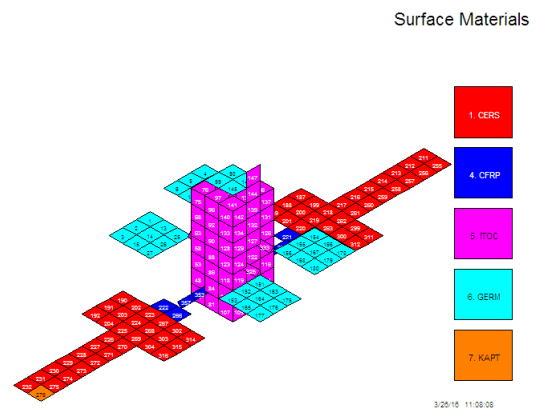**Keywords- NASA Charging Analyzer Program (NASCAP), Spacecraft surface charging, Maxwellian Plasma.**

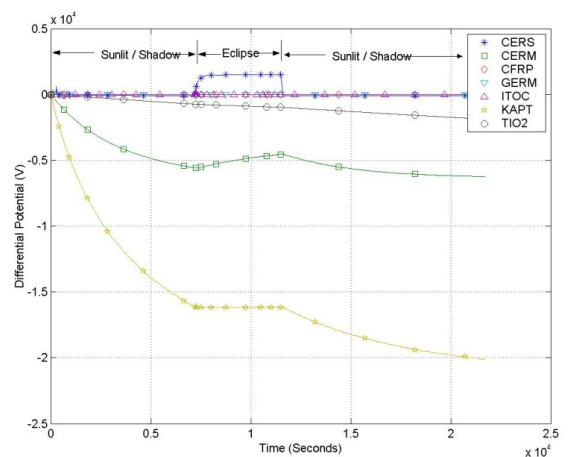Figure 1. Exposed surfaces of GSAT-11 Spacecraft as generated by NASCAP

Figure 2. Differential potential

REFERENCES

[1.] De Forest, S.E. and Mc Ilwain, C.E., "Plasma clouds in the magnetosphere", Joul. Of Geophys. Res., Vol.76, No.16, pp.3587-3611, June 1971.

[2.] De Forest, S.E., "Spacecraft charging at synchronous altitudes", Joul. Of Geophys. Res., Vol.77, pp.651-659, Feb 1972.

Control Theory and Cyber-Physical Systems Defeat

Robert L. Gardner
Dr. Robert L. Gardner, Consultant
Alexandria, VA 22310, USA
Robert.L.Gardner@verizon.net

Abstract—Control theory is used throughout the electronic systems industry. Control theory is also the basis for many other human activities: sports, communications and military operations. Col John Boyd applied the basics of control theory in 1976 to the concept of air combat operations. The fundamentals were then extended to litigation, business and law enforcement. This paper carries those ideas forward to demonstrate defeat (upset) of some simple feedback circuits, then hybrid circuits. Finally, multiple domain (electrical, mechanical, electronic, hydraulic, etc.) cyber physical models are used to demonstrate the same concepts in defeating electronic systems.

Keywords-component; control theory; cyber physical systems; electromagnetic interference

I. INTRODUCTION

This paper was motivated by a paper by Dr. Mary Shaw [1] on the applications of control theory to the design of elements of the Internet of Things. That analogy, combined with the elements of military strategy, as described by the OODA (observe, orient, decide act) loop of Col Boyd [2] suggested a means of understanding electronic upset. The OODA control loop repeats the OODA process with anticipation of the adversary's next action. Winning an engagement with the OODA loop process requires anticipation of the adversary's similar process and acting on that information more quickly than the adversary. Applying the OODA loop process to electronic systems is analogous to cognitive jamming. In IEMI (intentional electromagnetic interference) terms, we need to know the operating waveforms of the target's control processes and how to interfere with those processes.

II. OODA LOOP

The OODA loop consists of the following steps:

Note all surroundings, outside input, unfolding interaction with the environment to include electronic system state and environment.

Shape the observations through experience, system knowledge or physics

Figure out what do – illuminate with most effective waveform.

Completes the loop and repeats the cycle with closure and success.

Getting inside the control loop faster than the adversary is the way to defeat the adversary or system.

III. SYSTEM SIMULATION

Many elements of the Internet of Things as well as other more direct control units such as automotive electronic control units operate on similar principles. Various analog and digital sensors output signals that are read and converted to digital signals. Those digital signals are processed by a microcontroller into digital and pulse width modulated signals that, in turn, drive actuators. The sensors might be as simple as a thermometer or a depth gauge. The actuators might be a valve, a heat source, a laser or a fuel injector. Simulations of failure mechanisms might seem complex but there are only a few architectures like, for example, the CAN-Bus. The Arduino family [3] of systems, sensors and actuators represent a simple, but accessible example of these architectures. In the more complex simulations, we will use a combination of an Arduino Uno, Wolfram SystemModeler and the Modelica language to provide a hardware-in-the-loop simulation [4]. Many different incident waveforms will be used to demonstrate their effects on the system output. Expected system failures might be something like a fuel injector or spark plug firing at the wrong time or not firing. Such misfiring would, in turn, cause an engine failure – the desired effect.

REFERENCES
[1] M. Shaw, "What Can Control Theory Teach Us About Designing Cyber Physical Systems?"
, Reston VA, Dec 2016.
[2] R. Coram,   d The Fighter Pil t   h   hanged the   rt
 f   ar, Hatchett Book Group, New York, 2010.
[3] https://www.arduino.cc
[4] R. L. Gardner, "Pulse Injection of Electromechanical Systems",
, Cairns, Australia, 2016.

High-Power Microwave Sources – Quo Vadis?

Edl Schamiloglu
University of New Mexico
Albuquerque, NM 87131-0001
edls@unm.edu

Abstract— The field of high power microwaves [1] was founded nearly 50 years ago. Its founding was a direct consequence of the availability of new electron beam accelerators that were capable of generating high currents in addition to high voltages – a consequence of the development of modern pulsed power [2]. This presentation will take an historical look at the advances made in high power microwaves, and will look forward to consider where this discipline might go to in the future.

Keywords- high power microwave, relativistic microwave electronics, vacuum electron devices.

I.   INTRODUCTION

The field of high power microwaves (HPMs) had its beginnings in the late 1960s following the availability of pulsed power accelerators capable of generating high current, high voltage pulses. In the beginning there were only two players, scientists from the United States (USA) and the Soviet Union (USSR). The first experiments in the USA were performed at Cornell University [3] and the first experiments in the USSR were a collaboration between the Lebedev Institute in Moscow and the Institute of Applied Physics in Gorky (present day Nizhny Novgorod) [4]. Table 1 summarizes the parameters of pulsed power generators used in a variety of research areas.

TABLE I.   SUMMARY OF TYPICAL VARIOUS PULSED POWER REQUIREMENTS FOR GIVEN APPLICATIONS [2]

Application	Electrical Energy	Pulse Length	Peak Power/Pulse	Burst Avg. Power
High Energy Density Plasma Physics	20 MJ	100 ns	>10's TW	N/A
Intense Electron Beam Radiography	200 kJ	70 ns	< 1 TW	N/A
High Power Microwave (Narrowband)	10 kJ	100 ns	100 GW	100 kW
High Power Microwave (Ultra-Wideband)	10 J	1 ns	10 GW	10 kW
Ion Beam Modification of Materials	< 10 kJ	100 ns	30 GW	Small
Bioelectrics	0.1 mJ – few J	10 – 100's ns	10 kW – 100 MW	< mW - few W

Today research in HPM sources is also taking place widely in Western European countries such as the United Kingdom, France, Germany, and Sweden, as well as in a broad, robust program in China. Many other nations are participating, including Israel, Japan, India, Taiwan, South Korea, and Singapore.

II. FROM EXPERIMENTS TO VIRTUAL PROTOTYPING

For the first 25 years of HPM research the experimentalists led the charge. Then in the mid-1990s, through a combination of careful experiments and particle-in-cell (PIC) simulations [5], the once poor agreement between experimental results and simulations transformed into the today's tremendous confidence in, and reliance on, PIC codes. Today we refer to this as *virtual prototyping* [6]. No experimental prototype will be constructed without virtual prototyping results suggesting outstanding performance.

III. QUO VADIS?

Fig. 1 shows an historical plot of Pf^2 for HPM sources. What can we expect in the coming decades?
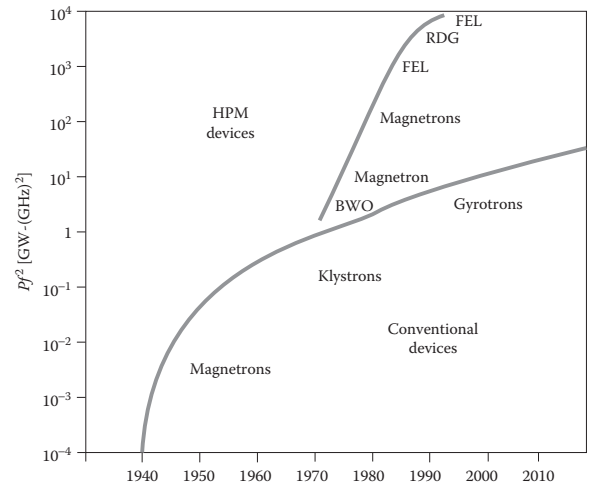

Figure 1. Growth of microwave devices in terms of the figure-of-merit Pf^2 for output power P at frequency f. The points denote the year when the plotted value of Pf^2 was first achieved [1].

REFERENCES

[1] J. Benford, J. Swegle, and E. Schamiloglu, *High Power Microwaves, 3rd Ed.* (Taylor and Francis, Boca Raton, FL, 2016).

[2] E. Schamiloglu, R.J. Barker, M. Gundersen, and A.A. Neuber, "Modern Pulsed Power: Charlie Martin and Beyond," (Invited Paper), Proceedings of the IEEE, vol. 92, 1014-1020, 2004.

[3] J.A. Nation, "On the Coupling of a High-Current Relativistic Electron Beam to a Slow Wave Structure," Appl. Phys. Lett., vol. 17, 491, 1970.

[4] N.F. Kovalev et al., "Generation of Powerful Electromagnetic Pulses by a Beam of Relativistic Electrons," JETP Lett., vol. 18, 138, 1973; ZhETF Pis. Red., vol. 18, 232, 1973.

[5] L.D. Moreland, E. Schamiloglu et al., "Enhanced Frequency Agility of High Power Relativistic Backward Wave Oscillators," IEEE Trans. Plasma Sci., vol. 24, 852, 1996.

[6] R.E. Peterkin and J.W. Luginsland, "A Virtual Prototyping Environment for Directed-Energy Concepts," Comput. Sci. Eng., vol. 4, 42, 2002.

Experimental Hot Tests of a Metamaterial SWS High Power Microwave Source

Edl Schamiloglu, Sarita Prasad, Sabahattin Yurt, and Mikhail Fuks
University of New Mexico
Albuquerque, NM 87131-0001
edls@unm.edu

Abstract— There has been recent interest in the use of metamaterials as slow wave structures (SWSs) in high power microwave (HPM) sources. This was motivated by the ability to engineer novel dispersion relations for beam-wave interaction that could not be achieved using conventional materials. This presentation describes hot tests of a metamaterial SWS that has yielded the highest output power for a metamaterial HPM source to-date.

Keywords- high power microwaves, relativistic microwave electronics, vacuum electron devices, metamaterial slow wave structures.

I. INTRODUCTION

The taxonomy of a metamaterial [1] is challenging. Without getting into the many nuances of this topic, suffice it for us to consider a metamaterial as a subwavelength periodic structure that, for the purposes of this presentation, exhibits double negative behavior, namely both permittivity and permeability are less than zero, $\varepsilon < 0$ and $\mu < 0$. Such a metamaterial SWS (MSWS) allows for the engineering of dispersion relations [2] for novel beam-wave interactions that would not be possible using conventional periodic structures.

The University of New Mexico's (UNM's) MSWS is based on a unit cell comprising a pair of oppositely-oriented broadside-coupled split ring resonators (SRRs). Fig. 1 shows a cross-sectional schematic of the MSWS and with the parameters used in MAGIC particle-in-cell (PIC) simulations. Details on the design of this MSWS can be found in [3]. The SRRs provide for $\mu < 0$ and inserting this into a below-cutoff waveguide provides for $\varepsilon < 0$.

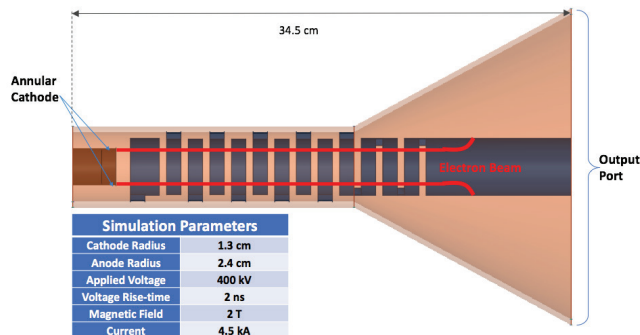| Simulation Parameters	
Cathode Radius	1.3 cm
Anode Radius	2.4 cm
Applied Voltage	400 kV
Voltage Rise-time	2 ns
Magnetic Field	2 T
Current	4.5 kA

Figure 1. Schematic of the UNM MSWS and PIC simulation input parameters.

II. FROM VIRTUAL PROTOTYPING TO EXPERIMENT

Cold test experiments were performed with a crudely-constructed MSWS. HFSS simulations and experimental measurements were in excellent agreement. A constitutive parameter extraction technique proposed by Tretyakov et al. [4] was used on the cold test calculations and measurements, and confirmed the double negative behavior of the MSWS in below-cutoff waveguide.

Fig. 2 shows the experimental setup. UNM's SINUS-6 accelerator was used for the hot tests.
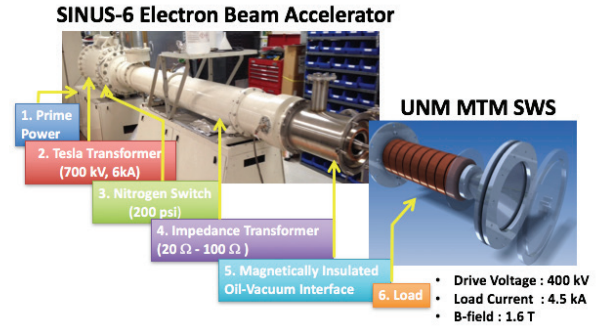

Figure 2. Experimental set-up for hot tests with parameters indicated.

III. RESULTS

MAGIC simulations based on the experimental parameters used in the hot tests predicted 95 MW output at 1.43 GHz when a 340 kV, 5.5 kA electron beam was used. The experimental measurements were 90 MW (estimated) at 1.425 GHz (measured). These results are the highest power generated to-date using a MSWS. This topic is poised to garner tremendous interest in the future [5].

REFERENCES
[1] E. Schamiloglu and M. Fuks, "What's the Meta? (Invited)," Bull. Am. Phys. Soc. vol. 55, No. 15, 2010, Abstract: CM10.00004.
[2] E. Schamiloglu, "Dispersion Engineering for High Power Microwave Amplifiers," *Proc. 4th EuroAsian Pulsed Power Conference/BEAMS Conference* (Karlsruhe, Germany, October 1-4, 2012), p. O5B1-1-6.
[3] S.C. Yurt, M.I. Fuks, S. Prasad, and E. Schamiloglu, "Design of a Metamaterial Slow Wave Structure for an O-type High Power Microwave Generator," Phys. Plasmas, vol. 23, 123115-1-7, 2016.
[4] O. Luukkonen, S.I. Maslovski, and S.A. Tretyakov, "A Stepwise Nicolson–Ross–Weir-Based Material Parameter Extraction Method," IEEE Antennas and Wireless Propag. Lett., vol. 10, pp. 1295-1298, 2011.
[5] J. Luginsland, J. Marshall, A. Nachman, and E. Schamiloglu, *High Power Microwave Sources and Technologies using Metamaterials* (IEEE Press/John Wiley and Sons, New York, NY, in preparation for 2018 publication).

Characterization and Analysis of sensitivity parameters for IEMI effects

Yong Li

School of Electronic and Information Engineering, Xi'an Jiaotong University Xi'an, China

Abstract—Effects of intentionally electromagnetic interference (IEMI) such as high power microwave (HPM) and electromagnetic pulse (EMP) on front end device and circuits are analyzed.The method of analysis is to use a semiconductor simulator based on drift-diffusion model (DDM) and SPICE models are also used in the simulator for device-circuit mix simulations while circuits IEMI effects are studied. In this approach the more susceptive device as PIN diode in limiter circuit, BJTs in low-noise amplifier (LNA) circuit are numerically analyzed by semiconductor simulation, meanwhile, the response of other less damageable device as inductances, capacitances, resistances are numerically studied by SPICE models.In this paper the parameters of external signals such as amplitude, rise time of wave, and the pulse width or duration of signal are presented, and the sensitivity parameters are related to interference and failure mechanisms.Our research deals with relatively simple examples to demonstrate a method for analyze the impact of external electromagnetic power on electronic devices and circuits, and could be used in system level effect analysis in future. The characterizations and analysis of this work can be used in equivalence research.

Keywords—semiconductor device; IEMI; EMP; numerical simulation.

Re isiting the alc lati n f the Earl Ti e E P nd cted En ir n ent

ra† r c rra rt t r a t† ac

†

§

—

stract

This a er re isits the calc lati ns f the e ected c nd cted en ir n ent d e t the c ling f earl ti e high altit de electr agnetic lses t l ng trans issi n lines. e disc ss the c rrent test a ef r s sed at s r i a ilit test la rat ries c nsidering the res lts tained ith a trans issi n line c de that has een i r ed incl ding the e ected radiati n d e t the disc ntin ities at the line ter inati ns.

e rds HEMP Conducted Environment

ntr d cti n

Protection of military and civilian infrastructure against high altitude electromagnetic pulses (HEMP) require the installation of protection devices at the points-of-entry of conducted coupling paths. These devices are usually surge arresters that are designed to short out the induced perturbations generated along long lines after a nuclear burst at several kilometers from the ground. Because of the complexity of experimentally simulating the illumination of long lines with a HEMP radiated environment, the expected perturbations are usually calculated with the use of transmission line theory, e.g. [1, 2].

The specification of the so-called HEMP conducted environment consists in defining the expected waveform and impedance of the Norton/Thévenin equivalent that will reproduce the observed short-circuit current/open-circuit voltage at the points-of-entry, namely, the long line terminations. Several studies performed during the late 1980's and early 1990's to calculate the response of overhead lines have been documented, e.g. [3-5]. A very extensive and thorough work was performed by IEC SC77 committee to define the HEMP conducted environment in [5, 6], and a methodology for a statistical estimation of the short-circuit current parameters was proposed.

This paper revisits the calculations of the expected conducted environment due to the coupling of early-time HEMP to long transmission lines. The methodology in [5] is used to calculate the probability of the short-circuit current parameters due to different exciting waveforms from previous published civilian and military radiated environments [7].

We discuss the current test waveforms that are specified for typical campaigns performed at survivability test laboratories by considering the results obtained with a transmission line code that has been improved by including the expected high-frequency radiation effects due to the discontinuities at the line terminations [8]. This model is supposed to provide more accurate results for overhead lines at several meters from the ground because it accounts for the high frequency phenomena that are not considered in the classical transmission line theory. Also, the frequency dependence of the soil dielectric parameters is also included in the analysis.

To estimate the conducted environment, an overhead line above a lossy ground line is illuminated with a plane wave, and the induced short circuit current is calculated with transmission line theory with an improved model for the vertical risers that provides accurate results at frequencies beyond the upper limit of the classical TL theory [8]. The plane wave polarization is the same adopted in [2] and the elevation, azimuth and polarization angles probability are the same proposed in [5]. The probability of the short-circuit current rise time, duration, peak amplitude and peak derivative are addressed with respect to the conductivity, height, and dip angle.

References

[1]   A. K. Agrawal, H. J. Price, and S. H. Gurbaxani, "Transient Response of Multiconductor Transmission Lines Excited by a Nonuniform Electromagnetic Field," vol. EMC-22, pp. 119-129, 1980.

[2]   F. M. Tesche, M. V. Ianoz, and T. Karlsson, . New York: Wiley, 1997.

[3]   P. Degauque and A. Zeddam, "Remarks on the transmission-line approach to determining the current induced on above-ground cables," vol. 30, pp. 77-80, 1988.

[4]   F. M. Tesche and P. R. Barnes, "A multiconductor model for determining the response of power transmission and distribution lines to a high altitude electromagnetic pulse (HEMP)," vol. 4, pp. 1955-1964, 1989.

[5]   M. Ianoz, B. I. C. Nicoara, and W. A. Radasky, "Modeling of an EMP conducted environment," vol. 38, pp. 400-413, 1996.

[6]   IEC, "61000-2-10: Electromagnetic compatibility (EMC) - Part 2-10: Environment - Description of HEMP environment - Conducted disturbance," ed: IEC, 1998.

[7]   D. V. Giri and W. D. Prather, "High-Altitude Electromagnetic Pulse (HEMP) Risetime Evolution of Technology and Standards Exclusively for E1 Environment," vol. 55, pp. 484-491, 2013.

[8]   G. Lugrin, N. Mora, F. Rachidi, and S. Tkachenko, "Electromagnetic field coupling to transmission lines: A model for the risers," in , 2016, pp. 174-176.

Denoising Video Signals by Reducing EMI/EMC Noise from Video Interfaces

Himanshu Makkar
(PhD Scholar)
Dept of Electronics & Communication
Suresh Gyan Vihar University Jaipur, Rajasthan
himanshu.makkar@mygyanvihar.com

Dr. O.S. Lamba
(Professor)
Dept of Electronics & Communication
Suresh Gyan Vihar University Jaipur, Rajasthan
onkar.lamba@mygyanvihar.com

Abstract - Earlier, the huge external filters and protected cables were the traditional ways to deal with EMI/EMC (electromagnetic interference and electromagnetic compatibility) in video signals. These technique added additional cost, unfavorably affected presentation, and increased the size of, the end product. As these products have, the decreased in size and it may evolved into the modern video players, the solutions have, also had to decrease in the size whereas maintaining or else even the enhancement of the performance. To attain this, the parts in the vein of the MAX9511 graphics video interface have been developed to distribute EMI performance while reducing solution size. To illustrate how this was done we will seem at the display interfaces of a typical PC, and the EMI performances achievable with these devices even though their miniature size. This paper investigates the unlike EMI problems ,that must be the solved for video interface design and the techniques existing to do so. This paper shows the denoising of the video signals,

Keywords: shielding, filtering, EMI, EMC, emissions, radiated, radiator, susceptibility, immunity, conduction, radiation, video, mean square error (MSE), peak signal to noise ratio (PSNR), video denoising, video discrepancy alteration.

I. INTRODUCTION

EMI/EMC testing is partitioned into two common categories:
Emissions This confines what amplitude and the frequency a product that can radiate or conduct to the device does not interfere with the other devices.
Susceptibility (also called Immunity) This testing category, compliments the Emissions requirement in restrictive the amplitude and frequency of the radiated and, conducted signals which can interfere with a product.
The two ways EMI, that can be emitted by a device which are conduction and radiation. These are linked as all radiated EMI is due to current flow.
EMI/EMC failures arise at the weakest point, in a product's design; in this case, a signal and interference enters or leaves a protected and filtered structure. inside the video interface, these are the cables to join devices and perform as an antenna. specially, the cabling that attaches the display, to a PC are mostly vulnerable and frequently cause EMI/EMC troubles.

II. VIDEO AND EMI

D-subminiature kind to connects the display to a PC (**Figure 1**).even though this incorporates the shielding (coax) of the video signals and the common-mode choke (CMC) to decrease radiated and conducted EMI, further filtering is desired to make sure that the EMI requirements are met.
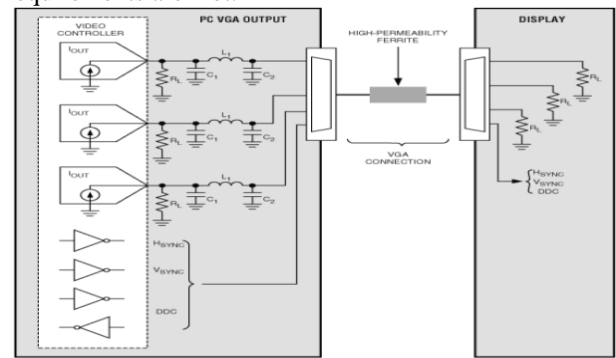

Figure 1. A VGA link is shown with video signals that cause radiated EMI.

III. PROPOSED EMI SOLUTION (MAX9511)

The MAX9511 graphics video interface, offers a matched, triple-channel, and tunable EMI filter for the RGB video over the range of VGA to UXGA resolution among channel-to-channel skew fault of < 0.5ns. Tuning is proficient by the changing of a single resistor (Rx). There are only three to four levels are required, in most of the applications. This allows the modification of a product's EMI profile without making any mechanical or electrical changes.

REFERENCES
[1] "Design of Analog Filters," Schaumann and Van Valkenburg, Oxford University Press.

t d and Para etric nal sis f igh Fre enc Radiati ns in   nicati n et   r in an   r an En ir n ent

Antim Bala Sharma
Research Scholar Department of ECE
SGVU, Jaipur
Jaipur (Rajasthan) India
Email : antimbsharma@gmail.com

Dr. O. S. Lamba
Professor (ECE)
SGVU, Jaipur
Jaipur (Rajasthan) India
Email :onkar.lamba@mygyanvihar.com

Abstract High frequency radiation exists in free space around us from an increasing number of sources and covers a wide range of the EM spectrum. By for the most important and rapidly expanding source are the mobile phone base stations. Radio-frequency electromagnetic fields (RF-EMF) of mobile communication systems are widespread in the living environment; frequent utilization of such devices is unsafe. When a human body is exposed to the electromagnetic radiation, it absorbs radiation. Continuous exposure to low intensity microwave radiations cause serious health problems over the years. This paper investigates the implications of EMR from the mobile cellular Base Station (BS) transmitter to the human body. We have discussed Effects of Mobile Tower Radiations and case studies of different location of urban environment to address the issue.

Keywords— Electromagnetic, Radio-Frequency Electromagnetic fields, Mobile Tower Radiations, Electromagnetic Radiations, Base Station.

I.   INTRODUCTION

Presently, at global level there are more than 6.57 billion mobile phone Subscribers. There has been an exponential growth of mobile telephony in India and all over the globe. The data indicates that 78% of India's population is using mobile phones. To provide better coverage for mobile signals or connectivity more than 70 million towers are erected in India. Cell phones communicate with nearby cell towers mainly through radiofrequency (RF) waves, a form of energy in the electromagnetic spectrum between FM radio waves and microwaves; they are forms of non-ionizing radiation. Cell phone towers (Base Stations) have electronic equipment with antennas that receive and transmit radiofrequency (RF) signals. Cell phone base stations may be free-standing towers or mounted on existing structures, such as trees, water tanks, or tall buildings in dense urban areas. The antennas need to be high enough to adequately cover the area. Typical heights for cell towers are 50–200 feet. Sector antennas for 2G and 3G transmission, broader sector antennas for 4G transmission, and parabolic microwave antennas for point-to-point communications are used in urban and suburban areas. This paper investigates the implications of EMR from the mobile cellular Base Station (BS) transmitter to the human body.

II.   RADIATION EFFECT ON HUMAN BODY FROM THE CELL TOWER

When a human body is exposed to the electromagnetic radiation, it absorbs radiation, because human body contains 70% of liquid. The human height is much greater than the wavelength of the cell tower transmitting frequencies, so there will be multiple resonances in the body, which creates localized heating inside the body. Continuous exposure to low intensity microwave radiations cause serious health problems over the years. This results in boils, drying up the fluids around eyes, brain, joints, heart, abdomen, etc. Electromagnetic Radiation (EMR) is a form of energy emitted and absorbed by charged particles which can be harmful to human body depending upon the radiated power density and the distance from the transmitter. So, in this paper, we have discussed Effects of Mobile Tower Radiations on human health and case studies of different location of urban environment and address the issue.

III.   ANALYSIS OF CELL TOWER RADIATIONS

Cell tower radiation measurement methods can be classified in three categories:-
1. Calculation method

- Prediction of RF fields
- Calculation to determine $EIRP_{th}$

2. Software simulation
3. Field measurement

Field measurement approach was chosen to analyze cell tower radiations in various regions.

Race Track Coil Based Deperming Protocol using Cage System

Sonal Jain, Ratan Singh, Rizwan Ahmed, Faruk Kazi
Veermata Jijabai Technological Institute
Mumbai, Maharashtra, India
sonaljain21691@gmail.com

Abstract— Naval vessels acquire permanent magnetism when they are aligned in a particular direction under the influence of the Earth's magnetic field (EMF) [1]. In deperming, naval vessels are subjected to strong alternating decreasing magnetic field using solenoid coil systems which is constrained with geometrical impediments [2]. In this paper, a deperming protocol with optimized double race track Merritt coil system is proposed. The finite element analysis having trajectory following hysteretic model is done using OPERA FEM DEMAG solver which shows 99.91% homogeneity with greater accessibility of object and lesser number of windings as compared to wrapping based solenoid coil system.

Keywords-Deperming; Uniform magnetic field; Square coil system

I. INTRODUCTION

The deperming protocol consists of multiple stages; a time varying transient half sinusoidal EMF of $120\mu T$ (95A/m) is applied as increasing fields and then reversing its direction to get deperming signature. A simplified hollow cylindrical submarine model with length 25m, thickness 0.02m and 4m diameter is placed inside two cage systems and their simulation results are compared in this paper.

II. METHODOLOGY: CAGE SYSTEMS

A. Solenoid cage system

A cage is designed with length 50m, 6m diameter and 10 turns per meter such that complete model is under the homogenous region of 95.9% homogeneity of solenoid coil. The relation of H_z and I is investigated using Biot-Savart's law given by equation (1). The current supplied to the cage for $1 \mu T$ is found to be 83mA using equation (2) for considered specifications.

$$B_z = \left(\frac{\mu_0 In}{2}\right)\left[\frac{\frac{l}{2}-z}{\sqrt{\left(z-\frac{l}{2}\right)^2+r^2}} + \frac{\frac{l}{2}+z}{\sqrt{\left(z+\frac{l}{2}\right)^2+r^2}}\right] \qquad (1)$$

$$\frac{B_z}{\mu_0} = H_z = 9.7961 * I \qquad (2)$$

B. Four square merritt coil cage system

Race track coil system generates magnetic field with the same degree of homogeneity but has greater access to the space inside the coil system. Therefore we designed semi analytical based Merritt coil by optimizing the coefficient of axial magnetic field generated by square coil using McLaurian series [2]. The flux density-current relation is given by equation (3).Table I summarises the optimized design parameters of four race track Merritt coil.

$$B_z = \frac{4.239*10^{-6}\, nI}{d} \qquad (3)$$

TABLE I.   DESIGN PARAMETERS OF RACE TRACK COIL

Parameter	Values
Side length of the square coil d(m)	30
Positioning of each coil (m)	-15.165,-3.8430,3.8430,15.165
Ampere turn of inner two coil(nI)	167
Ampere turn of outer two coils	395
magnetic field at the centre (μT)	1
Uniformity in region (%)	99.91

III. RESULTS AND ANALYSIS

The alternatively reducing deperming current in coil is scaled up by 80 for generating equal and opposite remanent field for nullifying the permanent signature effect as shown in Fig 1. We observed that the permanent longitudinal signature 2m below the object is 73nT. The signature gradually reduces after every current shot and final signature diminishes to 0.6nT as shown in Fig. 2. This paper eventually showed more degrees of freedom in design which in turn makes implementation of race track coil easier as compared to solenoid based system for deperming of naval vessels.
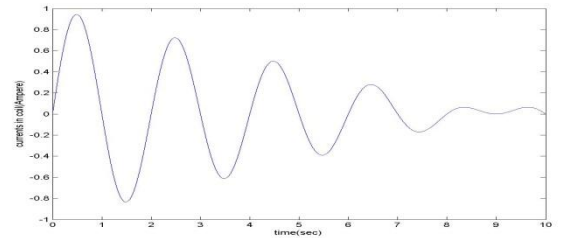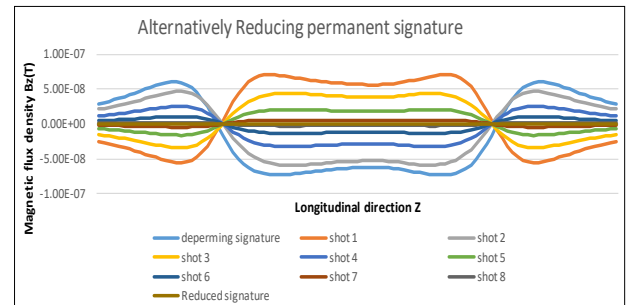

Figure 1.   Current pattern for coil system.

Figure 2.   Deperming signatures after every current shot.

REFERENCES

[1] J.J.Holmes,"Reduction of a ship's magnetic field signatures". *Synthesis Lectures on Computational Electromagnetics*, *3*(1), pp.1-68, 2008,

[2] M.A. Azpurua, "A semi-analytical method for the design of coil-systems for homogeneous magnetostatic field generation". *Progress In Electromagnetics Research B*, *37*, pp.171-189, 2012,

Experimental Characterization of the Grounding Impedance of Wind Turbines

D. Gazzana [1], A. Smorgonskiy [1], N. Mora [2], M. Rubinstein [3], F. Rachidi [1]

[1] Swiss Federal Institute of Technology (EPFL), Lausanne, Switzerland

[2] Montena Technology, Rossens, Switzerland

[3] University of Applied Sciences of Western Switzerland, Yverdon-les-Bains, Switzerland

daniel.dasilvagazzana@epfl.ch, alexander.smorgonskiy@epfl.ch, nicolas.mora@epfl.ch, marcos.rubinstein@heig-vd.ch, farhad.rachidi@epfl.ch

Abstract— In this paper, we present a study of the grounding impedance of wind turbines based on measurements. Two scenarios were considered: In the first one, the measurements were carried out only in the grounding system before the assembly of the wind turbine; in the second one, the complete wind turbine (tower, nacelle and blades) was considered. Preliminary results show that the evaluated grounding impedance is affected by the presence of the complete wind turbine, especially at higher frequencies.

Keywords-Grounding impedance, measurements, numerical simulation, wind turbine.

I. INTRODUCTION

Electric power generation based on wind energy is a fast growing sector of renewable energy production. Lightning is the major cause of damage to wind turbines, causing transient surges and overvoltages in the power grid, inducing interference in control systems. Moreover, direct lightning strikes may cause significant damage to the blades and other wind turbine components. The consequences of these events can be very costly, due to energy production losses, extra maintenance costs or even loss of operating equipment [1].

The grounding system of a wind turbine is essential for dissipating the current originating from a lightning discharge to the earth, functioning as an important component for protection and safety. Thus, proper grounding plays an important role and the evaluation of the grounding impedance can be a valuable practice contributing to a better protection against lightning [2]-[4].

In this context, the goal of this paper is to present a study based on measurements on a wind turbine located in the Mont-Crosin wind park, Switzerland. Specifically, the aim of the study is to evaluate the impact of the presence of the wind turbine (tower, nacelle and blades) on the measurement of the grounding impedance.

II. PRELIMINARY RESULTS

In 2016, several grounding transient measurements were carried out in four new units of the Mont-Crosin wind park, located in the Jura mountains in Switzerland (see Fig. 1). In the experiments, different surge wave-shapes were injected in the grounding system considering two scenarios: In the first one, the measurements were performed only on the grounding system embedded in the turbine foundation; the second one took into account the complete WT, including the tower, the nacelle and the blades [5].

The obtained results suggest that at frequencies beyond 150 kHz or so, the presence of the complete wind turbine affects the measurements of the grounding impedance. Full-wave numerical simulations, assuming the system is linear, are used to support the experimental observations.

Fig 1. Mont-Crosin wind park in Switzerland.

REFERENCES

[1] F. Rachidi, M. Rubinstein, and A. Smorgonskiy, "Lightning protection of large wind-turbine blades," in _____, S. M. Muyeen, Ed. London: Springer, 2012, pp. 227–241.

[2] A. Elmghairbi, M. Ahmeda, N. Harid, H. Griffiths, and A. Haddad, "A technique to increase the effective length of horizontal earth electrodes and its application to a practical earth electrode system," in _____, pp. 690–693, Chengdu, China, Nov. 1-4.

[3] K. Yamamoto, S. Yanagawa, K. Yamabuki, S. Sekioka, and S. Yokoyama, "Analytical surveys of transient and frequency-dependent grounding characteristics of a wind turbine generator system on the basis of field tests," _____, vol. 25, no. 4, pp. 3035–3043, 2010.

[4] A. Smorgonskiy, N. Mora, F. Rachidi, M. Rubinstein, K. Sheshyekani, N. Korovkin, "Measurements of transient grounding impedance of a wind turbine at Mont-Crosin wind park", _____, Taipei, Taiwan, May 26-29.

[5] A. Smorgonskiy, D. Gazzana, N. Mora, M. Rubinstein, F. Rachidi, "On the measurement of the grounding impedance of tall wind turbines," in _____, Seoul, Republic of Korea, June. 26-29.

Behavior Of Gas Discharge Tubes Under Mesoband and Narrowband HPEM Signal Conditions

Matthias Kreitlow
WIS
D-29633 Munster, Germany
matthiaskreitlow@bundeswehr.org

Armin Kaelin
EMProtec AG
CH-8450 Andelfingen, Switzerland
armin.kaelin@emprotec.ch

Markus Nyffeler, Pierre Bertholet
armasuisse
CH-3003 Bern, Switzerland
markus.nyffeler@armasuisse.ch

Abstract—Gas Discharge Tubes (GDT) are widely available as protection elements for the use in rough electromagnetic environments. While GDTs have been proved to work very well for transient events like electromagnetic impulses caused by lightning strikes or nuclear events, there is only little information available about their reaction for typical High-Power Electromagnetic (HPEM) waveforms. In this work, an experimental set-up for testing the suitability of GDTs as protection devices for narrowband high-power microwaves (HPM) and damped sinusoidal (DS) waveforms is presented. The results for nine different GDTs show that these devices do not offer sufficient protection against the mentioned waveforms. The response of the GDTs is largely independent over a variety different manufacturers or types.

Keywords: HPEM, HPM DS, GDT, high-power electromagnetics, protection elements

I. INTRODUCTION

For protecting electronic devices against destruction due to unwanted high voltages Gas Discharge Tubes are often used in special protection circuits. GDTs are known to work very well for transient signals resulting from a lightning electromagnetic pulse (LEMP) or a nuclear electromagnetic pulse (NEMP). As GDTs have a very small parasitic capacitance they are well suited for a wide variety of applications like power lines or data links. Although they are very small GDTs can handle currents of several kilo-amperes.

Typical for GDTs is their highly dynamic behavior. While the static spark-over voltage for DC or very slow rises (<100 V/s) is well defined, this threshold can be much higher for very fast transients. This can lead to a complete loss of the protection features as shown for ultra-wide band signals in [1]. But especially oscillating narrowband and mesoband HPEM waveforms have not been investigated before. These signals with frequencies in the range of GHz change their polarity in a sub-nanosecond time-scale. It is questionable whether GDTs will show an avalanche-breakthrough even when the signal duration and amplitude seem to be sufficiently high.

Thus, real HPEM signals with amplitudes of several kilo-volts have been used in this work.

II. MEASUREMENTS

A. Experimental test set-up

The test set-up shown in Fig. 1 was used to generate the desired HPM and DS waveforms on a 50 Ω coaxial high-voltage cable. A simple λ/4-monopole which was placed in the focus point of a parabolic reflector received the HPEM wave. A PicoTEM-cell helped to determine the incident signal. Afterwards a series of optional attenuators allowed for varying the signal amplitude at the GDTs. After the GTD the signal was further attenuated to protect the oscilloscope. Both the signal from the PicoTEM-cell and the output of the GTD mount are measured by an oscilloscope.
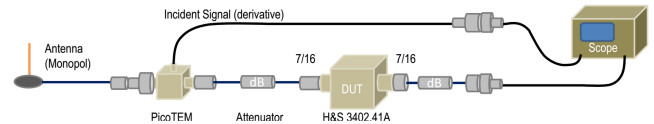

Figure 1.   Schematic view of the measurement set-up

B. Test parameters and GTD types

The narrowband HPM signals were generated using the HPM simulator SUPRA at WIS, Munster. The waveform can be described by an idealized Gauß-modulated sine wave. The test frequencies were chosen to be 1.12 GHz and 2.1 GHz. The signal duration was at least 300 ns.

The DIEHL HPEMcase Lab was used to produce the mesoband DS signals that can be described as an exponential damped sine wave. The center frequency was fixed to 244 MHz and the signal was measurable for at least 7 periods (30 ns).

A selection of nine different GTDs from various manufacturers was inserted into the mount. The static spark-over voltage varied from 75 V to 1500 V whereas the maximum current was rated form 20 kA down to 5 kA.

III. RESULTS

The experiments showed that all types of GTDs at least reacted to HPM and DS signals. The threshold varied along the manufacturers, but in general the GTDs with a higher static spark-over voltage needed higher signal amplitude. However, the breakthrough did never occur at the very beginning of the narrowband HPM signal. In each case the protection effect started only after several periods of the HPM signal. Until this point the signal passes the protection device without any attenuation. In some cases, the GTD fell back into an insulating or high-impedance state after some more periods and limited the voltage to about 1 kV.

The behavior of the GTDs during slower DS pulses was slightly different. In some cases, the breakthrough occurred already at the first period of the signal, but nevertheless voltages of several kV passed the protection device up to that point. Sometimes no reaction could be observed.

It can be concluded that GTDs are not suitable for HPM protection. Especially for high frequency signals they take a relatively long time for a reaction and only limit the signal to voltages in the range of kilo-volts. The test set-up can be seen as a model of a typical front-door coupling scenario. Thus, the signals we applied to the GTDs are a realistic threat. All in all HPM protection seems to be quite difficult as long as the threatening frequencies are in-band. Maybe PIN-diodes could be an effective measure for HPM protection as long as they are combined with the LEMP and NEMP protection in are careful design.

REFERENCES

[1]   A. W. Kälin, M. Nyffeler, "UWB-IEMI laboratory test of single-stage and multi-stage lightning and HEMP-protection devices", EUROEM 2016, London, 2016

Study of GW Range L-band Relativistic Magnetron using PIC

Srinivas Nekkanti
Microwave Tube R&D Centre,
DRDO, BE Complex, Jalahalli,
Bangalore, India
srinivas.nekkanti@outlook.com

M. Joy Thomas
Pulsed Power and EMC Lab,
Department of Electrical Engineering,
Indian Institute of Science, Bangalore, India,
jtm@ee.iisc.ernet.in

Abstract—This paper presents the results of the work on PIC simulation of an L-band relativistic magnetron [1] [2] with axial extraction of the RF power using the CST Particle Studio tool. A magnetron with diffraction output (MDO) configuration [3] has been used for the study. Both solid as well as transparent cathodes [4] have been tried in the analysis so as to know the maximum power, maximum efficiency, cathode current and the RF startup delay time. The maximum power, impedance and efficiencies are 6.8 GW, 47.4 Ω and 50% respectively with the transparent cathode. The maximum efficiency is obtained at a magnetic field of B=0.5T. The radiated power is in the TE_{21} mode.

Keywords- Relativistic magnetron; PIC; L-band;

I. INTRODUCTION

Relativistic magnetrons are good sources for GW Class microwave radiation which has wide applications in the defence as well as in the civilian sector. In the recent past several authors have reported the improvement in efficiency of the relativistic magnetrons using several techniques like modified MDO design and cathode priming techniques. These techniques are applied on well-known MIT A6 magnetron which operates in S-band. The work discussed in this paper is the application of different techniques discussed in the literature to an L-band magnetron. The selection of the frequency band is based on the effectiveness of coupling of radiated RF coupling into electronic circuits and also to get more output power for the same input power.

II. PIC MODEL OF THE MAGNETRON

L-band magnetron has a six vane design. The cathode, anode and vane radii chosen are 12.7 mm, 31.75 mm and 82.55 mm respectively. The vane angle considered is 20°.The vanes are smoothly tapered onto radius that is greater than the cut-off radius of the cylindrical waveguide of radius which is calculated as 150 mm. The taper angles of modified MDO are $\alpha = 17.5^O$ and $\beta = 32^O$. It was tried with other angles, but the output power has been observed maximum only at these angles as in A6 magnetron.

III. SIMULATION AND RESULTS

The voltage applied to the magnetron is 815 kV. The magnetic field is varied between 0.46T to 0.64T for both solid as well as transparent cathodes.

A. With solid cathode

The maximum RF power obtained at a magnetic field of B=0.5T. Fig. 1(a) shows the upstream cathode current which is of 21kA, Fig. 1(b) and (c) show the normalized voltage at the output port of the cylindrical waveguide and its FFT. Fig. 1(d) shows the radiation pattern (TE_{21}) of RF.
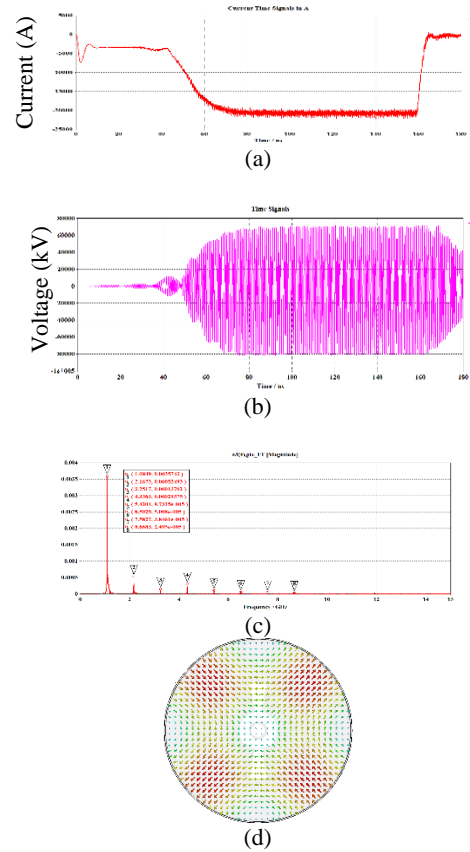

Figure 1. (a) Upstream cathode current (b) Normalized voltage (c) FFT of the RF power (d) TE_{21} mode pattern

REFERENCES
[1] R. R. Smith, J. Benford, B. Harteneck, and H. M. Sze, "Development and Test of an L-band Magnetron," IEEE Trans. Plasma Sci., Vol. 19, pp. 628–631, Aug. 1991.
[2] A. Palevsky and G. Bekefi, "Microwave Emission from Pulsed, Relativistic e-beam Diodes, II: The Multi-resonator Magnetron," Phys. Fluids, Vol. 22, No. 5, pp. 986–996, May 1979.
[3] M. I. Fuks and E. Schamiloglu, "70% Efficient Relativistic Magnetron with Axial Extraction of Radiation through a Horn Antenna," IEEE Trans. Plasma Sci., Vol. 38, No. 6, pp. 1302–1312, Jun. 2010
[4] M. Fuks and E. Schamiloglu, "Rapid start of oscillations in a magnetronwith a 'transparent' cathode," Phys. Rev. Lett., vol. 95, no. 20, p. 205 101, Nov. 2005.

Comparison of Target discrimination using E-pulse in time and frequency domain

Naveena M
Dept.of ECE, Dayananda Sagar College of Engineering
Bangalore, Karnataka, India
naveena.mohan@gmail.com

Dhiraj Kumar Singh
Scientist 'E', LRDE-DRDO
Bangalore, Karnataka, India
dhiraj.lrde@gmail.com

Abstract— Target Discrimination from RADAR A-scan data has been a big challenge. Singularity Expansion Methods have been successfully used in many applications in recent times. E-pulse is one of the most popular SEM based technique for radar target discrimination. In this paper, the target discrimination process using Extinction pulse in time domain and in frequency domain in terms of noise sensitivity has been compared.
 Keywords: E-pulse, AR, EDN, TDN

I. INTRODUCTION

Radar Targets are characterized by their natural frequencies which depend on their size, shape and electrical properties. These natural frequencies are extracted from the late time electromagnetic transient response of the target. As the late time response of a target can be expressed as sum of damped sinusoids, singularity expansion method(SEM) methods are used to find the natural frequencies. One of the popular methods of Radar target discrimination schemes is the E-pulse which uses impulse response of target in time domain. So it overcomes the limitation of waveform generator to sweep through a wide range of frequencies to get the frequency response.

II. Target Discrimination Methods

The E-pulse waveform of a target is an electromagnetic waveform when irradiated on the target will produce a zero output in the late time part of the response. So the convolution of an E-pulse waveform e(t) with the late time measured response waveform of the target $r_l(t)$ is:

$$c(t) = e(t) * r_l(t) = 0 \qquad (1)$$

There are two ways of creating E-pulse and accordingly two ways of discriminating the target; one using SEM method and other using AR(Auto-Regressive) method. The algorithm used in [1] is used to find the start of the late time response in both cases.

A. E-pulse using SEM method

In E-pulse created using SEM method, discrimination of the unknown target involves, dominant pole extraction from the late time response of the unknown target and the Target Discrimination Number TDN(dB) [2]calculation for the set of E-pulses in library to discriminate the target. In this, the generation of E-pulse, involves the extraction of poles (z) and residues from the late time response for which SEM methods like prony method or Matrix Pencil Method are used. The use of SEM method reduces the E-pulse sensitivity to noise and restricts the length of the E-pulse to the number of dominant poles.

The discrimination involves calculation of R=αz of unknown target and TDN(dB) (2) for E-pulses in the library and the expected target E-pulse has the minimum TDN(dB).

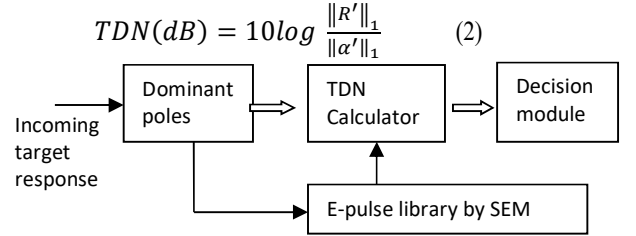$$TDN(dB) = 10log \frac{\|R'\|_1}{\|\alpha'\|_1} \qquad (2)$$

Figure 1. Block Diagram of target discrimination using TDN

B. E-pulse using AR method

In E-pulse created using AR method, discrimination of the unknown target involves, convolution of the unknown target the set of E-pulses in library and finding out the E-pulse Discrimination Number EDN(dB)[1]to discriminate the target. Here, the generation of E-pulse, involves the solution of the linear equations formed by(1) using Yule walker algorithm in AR method. This method increases the E-pulse sensitivity to noise and the length of E-pulse depends on the samples of the late time response with or without interpolation.
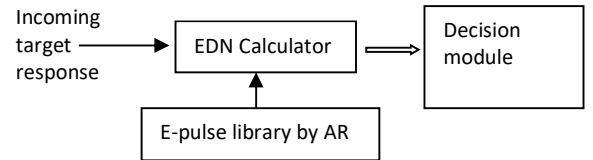

Figure 2. Block Diagram of target discrimination using EDN.

The discrimination involves calculation of EDN(dB) (3) for E-pulses in the library and the expected target E-pulse has the minimum EDN(dB).

$$EDN(dB) = 10log \frac{\int_{T_L}^{T_L+W} c^2(t)dt}{\int_{T_L}^{T_L+W} e^2(t)dt} \qquad (3)$$

These two methods are applied on simulated data which are impulse response of canonical scatterer and the noise sensitivity in these methods is compared in the paper.

REFERENCES
[1] Serguei L. Primak, JoeoVetri,ZsuzsannaDamjanschitz, and SatishKashyap, "Auto-Regressive Filter-Based E-Pulse Discriminating Scheme", IEEE Trans. On Antennas and Propagation, Vol.47, No.1,January 1999
[2]Dhiraj K. Singh; Naveena Mohan ; D. C. Pande ; A. Bhattacharya A Hybrid E-pulse Method for Discrimination of Conducting Scatterers in Resonance Region, IEEE Trans. On Antennas and Propagation, VOL. 62, NO. 8, August 2014

ACHIEVING ELECTROMAGNETIC COMPATIBILITY IN INSAT-3DR SPACECRAFT

Anju Damodaran, C. Anitha, Goutam Kumar Gupta, Bhooma G., NandishS.T.,
MohammedAli A., V.K. Hariharan, M. Nageswara Rao
Electrical Integration Division-2, Systems Integration Group,
ISRO Satellite Centre, Bangalore

Abstract— This paper details the EMI control measures followed in INSAT-3DR spacecraft based on the assessment of the EMI environment of the spacecraft and the implementation of the EMI control measures in EDS to achieve Electromagnetic compatibility of the various systems. The spacecraft served as the platform for the Imager and Sounder payloads with DRT and SAS&R communication payloads. It portrays the complexity of the EMI environment to which the various spacecraft subsystems are subjected, the measures taken to achieve EMC in the Electrical distribution system which interconnects the various subsystems, system level grounding scheme adopted in spacecraft, EMI control techniques in intra system and EMC test conducted at system level. The bonding, grounding, shielding and filtering measures taken to minimize EMI and implementation of ESD mitigation techniques are addressed.

Keywords-EDS, Imager, Sounder and COM payload

I. INTRODUCTION

The INSAT-3DR Spacecraft is a geostationary satellite configured with the proven I-2K bus. The bus is built to meet the payload requirements and it is an exclusive mission for enhanced meteorological observations and monitoring of land and ocean surfaces for weather forecasting and disaster warning. The spacecraft houses the state of art Meteorological payload and communication payload Viz. the Imager and Sounder payloads that generate the meteorological data, MET transmitters that transmit the data to ground , DRT which supports the global collection and distribution of meteorological data and SAS&R communication payload which aid in Search and Rescue operations.

The Six channel Imager payload generates images of the Earth and it's environment in six spectral channels of meteorological importance - Visible, SWIR, MIR, WV, TIR-1 and TIR-2 channels. The Nineteen Channel Sounder provides the vertical profiling of meteorological parameters spread across the visible and IR bands. The MET transmitters are used to transmit the data from camera electronics in Ext C-band. The Data Relay Transponder (DRT) receives globally meteorological, hydrological and oceanographic data from automatic collection platforms and relay back as downlink in Ext. C-band. The Satellite aided Search and Rescue (SAS&R) system detects a distress signal alert for search and rescue operations globally in UHF band and downlink the data in Ext. C-band. The configuration view is shown in the Fig-1.

II. EMC CONSIDERATIONS

The EMC control is aimed to realize best performance of the spacecraft in terms of electromagnetic compatibility. Establishing the Electromagnetic compatibility requirement in such a complex spacecraft system is a challenging due to presence of more sensitive systems, RF near fields and densely packed electronic systems operating in various frequency ranges.

The steps taken to ensure Electromagnetic Compatibility of INSAT-3DR Spacecraft includes analysis for the spacecraft system EMI environment and the control technique, identification of EMI sources like DC-DC converters of various subsystems, identification of EMI susceptors like low level analog signal sensor, Identification of EMI coupling paths like harness, RF leakage joints and application of differential signal systems to increase the noise immunity.

Considering the complexity of electromagnetic environment an appropriate spacecraft layout was evolved in terms of Package placement and identification of harness corridors for harness routing to minimize intersystem coupling. To achieve intra system compatibility various control techniques are applied in the areas of PCB layout, Filtering, Shielding, Electrical Distribution System design, Layout management, EMI Analysis and Prediction, Grounding Scheme and EMC Test Plan
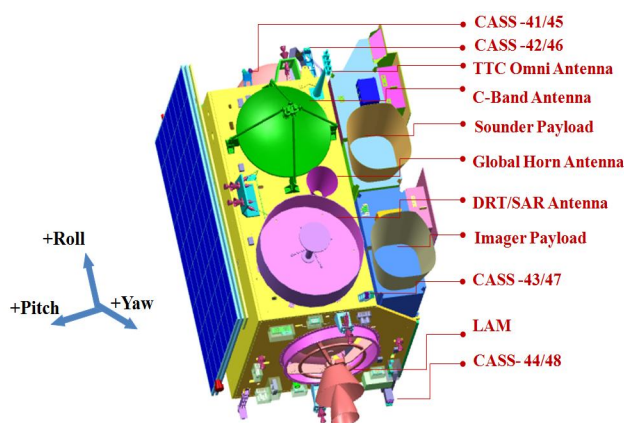

Figure 1. INSAT-3DR Solar panel stowed configuration.

REFERENCES
[1] Comprehensive Design Review document,ISRO-ISAC-INSAT-3DR/3DS-RR-1105,June 2014
[2]Grounding Scheme for INSAT-3DR,ISRO-ISAC-INSAT-3DR-PR-2354,Dec 2013

Issues for Power Grid Substation High-Level EM Protection

E. B. Savage*, W. A. Radasky[†]

Metatech Corporation, Goleta, California, U.S.A, savagee@cox.net*, wradasky@aol.com[†];

Abstract— It is well known that modern society is very dependent on a reliable electric power system (Ref. 1). However, that system can be compromised by electromagnetic threats. One threat is the effect of E1 HEMP or IEMI on the control systems, housed in substation buildings. To address this concern, the EM vulnerability of substations should be evaluated, and hardening applied if necessary. The paper will enumerate and discuss various issues that affect the EM response of substations, and its hardening.

Keywords – power grid, substations, HEMP, IEMI

1. Introduction

Substation hardness evaluation and hardening can be handled as for any building. A known hardening approach is the U.S. standard MIL-STD-188-125-1 (Ref 2), used for HEMP protection of critical communications facilities. The overall concept of this complex specification is to develop a very good Faraday shield for the building, limit external penetration such as cables, and have protectors on any metallic penetrations that cannot be avoided. Properly implemented, the internal electronic equipment does not need any additional special protection. While this approach could be used for a substation building, it would be costly and difficult, especially for existing buildings. Another approach, which the military specification was created to avoid, is to specifically consider all aspects of the vulnerability process, and to address each in terms of optimizing hardness.

It would be useful to know what features are important for substation hardness, and as much as possible, have quantitative hardness values assigned to each feature. Assigning these values is not the purpose of this talk – it is believed that such a database of all aspects of a substation does not currently exist. Instead, this talk intends to encourage research that would help create such a database. Performing and collecting together all the necessary research would provide, for example, the means to evaluate and estimate, within limits, the vulnerability of an existing substation by visual inspections, to suggest corrective hardening steps, and also provide help in designing new substations.

Parts of the necessary research have already been performed, but the work is not complete. In fact the IEC has a new project (IEC 61000-5-10) to develop a basic approach to harden both existing and new buildings to the threats of E1 HEMP and IEMI. This publication emphasizes the overall shielding of the building itself and the grounding of the external cabling, but there are also other issues to be considered. Some general aspects of substation hardness are mentioned below.

2. Substation Building

The building could provide EM shielding to attenuate EM fields, and metal building are preferred. However there are many types of building construction used for substations. Many details are important, including the roof material and its attachment to the walls, doors, and windows.

3. External Cabling

Substations have many cables that run into the control building. This is a significant vulnerability issue. There are many aspects of this that are important, including: cable coupling, shielded cables, signal attenuation at high frequencies, and options for cable troughs. Very important is the cable entry into the building, including current "wipe-off" from shielded cables.

4. Internal Cabling

Fields that get into the building, either through the walls or roof or through external penetrations that then re-radiate inside, are important. They can couple onto internal cabling that leads to critical electronic equipment. The best approach is to enclose the cables within metal conduit, but also running cables close to metal helps.

5. Internal Equipment

It can be very difficult to determine accurate susceptibility levels for the control equipment. The best approach is keeping induced conducted pulses that get to the equipment very low so that any harmful effects would be very unlikely. IEC EMC standards are useful in establishing the immunity of electronic equipment.

6. External Equipment

Critical external equipment should be considered in the same way as the equipment in the substation building itself – it should be within a Faraday shield with external cabling controlled. Coupling to this equipment could send high-level signals down cables toward the substation equipment.

7. Substation Yard

There are issues associated with the bigger picture of the substation, such as large coupling structures (i.e., antenna masts) that are electrically connected to the building.

8. Conclusions

Basically this talk will suggest issues that could use more research – to characterize hardness critical features to help in evaluating and protecting power substations.

REFERENCES

[1] "Report of the Commission to Assess the Threat to the United States from Electromagnetic Pulse (EMP) Attack, Critical National Infrastructures," April 2008, http://www.empcommission.org/docs/A2473-EMP_Commission-7MB.pdf.

[2] MIL-STD-188-125-1, "Department of Defense Interface Standard. High-Altitude Electromagnetic Pulse (HEMP) Protection for Ground-Based C4I Facilities Performing Critical, Time-Urgent Missions, Part 1 Fixed Facilities," 17 July 1998.

and   tics f r   atching   ea s ith stig atis   and Tilt   T

Dr. Sameer D. Hemmady
XL Scientific LLC
6100 Uptown Blvd NE Suite 260
Albuquerque, New Mexico, 87110
USA

Dr. Brad W. Hoff
Air Force Research Laboratories- Directed
Energy Directorate
Kirtland Air Force Base
Albuquerque, New Mexico, 87117, USA

Abstract— **This paper delineates AFRL's ongoing   r in the re r sing f the   and   cti e Denial   ste   D   f r researching   igh P   er icr a e P   ased   er ea ing f energ   t high fl ing aircraft and r c ets in the   st hase f flight t enhance la nch efficienc . salient feat re f   r re r sed s ste   is the se f   a e   atching   tics f r s ita l c rrecting the astig atis   and tilt   anifested the   er ite   a ssian ea e anating fr   the   D   g r tr n s rce and f c sing the energ at the l cati n f the target heat e changer cera ic sa   les nder test.   e refer t this set f   a e   atching   tics as the   T s s ste .   ere   e   resent the   design   eth d l g   f r   r   T s s ste thr gh high fidelit   deling and si lati n   anal sis as   ell as the   antici ated erf r ance f the s ste t   eet   r research re ire ents. Fa ricati n f the   T s s ste is c rrentl nder a at FR RD and is antici ated t   e   erati nal in   .**

e   rds High Power Microwaves, mm-wave, matching optics, power beaming, gyrotron, corrugated waveguide

.   TR D T

Power beaming of microwave energy from terrestrial HPM sources to high flying aircraft and rockets in their boost phase of flight has been identified as an intriguing application of HPM   . Millimeter-wave HPM systems with high Effective Radiated Power transmissions windows in the 95GHz to 200GHz band. To facilitate the use of mm-wave HPM systems for power beaming applications, AFRL is currently repurposing the ADS system to study the behavior of specialized ceramics which can serve as heat-exchangers when integrated onto aerial assets. (ERP), such as AFRL's Active Denial System operating at 95GHz, are ideally suited for this application due to the presence of atmospheric. To support this study, the 100kW, 95GHz, Hermite Gaussian mm-wave beam generated by the ADS source gyrotron in transportainer-1 must be suitably routed and focused from the source gyrotron output window to the ceramic samples, located within an annex test chamber (transportainer-2). The schematic for the physical setup is shown in Fig. 1.
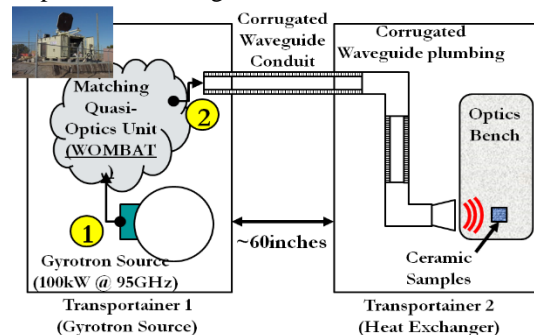

Figure 1: Physical setup for heat-exchanger studies. Inset: Picture of the current ADS system at AFRL.

.   TE   DE   R PT

Cold test beam imaging has revealed that the mm-wave emanating from the 95GHz gyrotron has significant astigmatism and tilt, which is corrected for using a sequence of specially shaped metalized mirrors to maximize the power transfer efficiency from the source to the target samples. This sequence of mirrors, comprising the WOMBAT subsystem is shown in Fig. 2 and the design methodology will be the focus of the presentation. The WOMBAT subsystem is estimated to yield a theoretical maximum of 99.07% power transfer coupling efficiency, resulting in an effective power density on target of ~5kW/sq.cm.
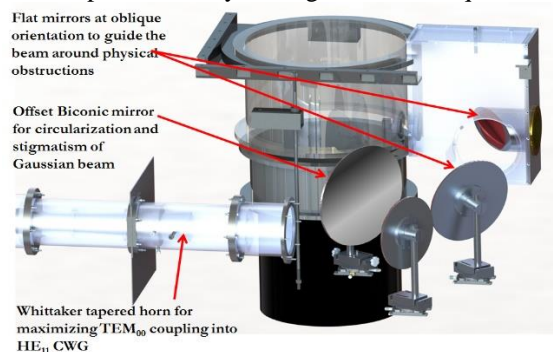

Figure 2. Rendering of the WOMBAT system with salient features highlighted

REFERE   E
[1] J. Benford, "Space propulsion & power beaming using mm systems", Space Energy & Transportation,1,211(1996)

Developing Predictive Scaling Laws for Large Signal RF Response of Elemental MOSFET Devices

Desmond Awungayi, Nishay Sule, Payman Zarkesh-Ha, Edl Schamiloglu, Sameer Hemmady
Department of Electrical and Computer Engineering
University of New Mexico
Albuquerque, NM 87131-0001
dawungayi@unm.edu, nishchay@unm.edu, pzarkesh@unm.edu, edls@unm.edu,
shemmady@unm.edu

Abstract— Predicting the behavior of electronic systems subjected to extreme electromagnetic interference is a growing concern for military and civilian systems operating in ever denser ambient electromagnetic environments. In this research effort, we are developing physics-based predictive scaling laws which describe the behavior of elemental Metal Oxide Semiconductor Field Effect Transistor (MOSFET) devices when subjected to large signal Radio Frequency (RF) injection. We will validate these predictive models with experimental data. These predictive scaling law models will help EMI/EMC engineers develop quick assessment tools for modeling the behavior of higher complexity electronic components and systems exposed to extreme electromagnetic environments.

Keywords- electromagnetic interference and compatibility, RF CMOS, MOSFET, RF injection, Large signal RF modeling.

I. INTRODUCTION

The insistent demand for more powerful computing resources with faster clock speeds has led to the development of smaller, sub-micron MOSFET devices operating with very tightening timing and voltage margins [1]. As the device scale and operating voltages reduces, even moderate levels of injected RF interference can lead to erroneous functional behavior for the elements MOSFET devices. In this research effort, we are developing physics-based predictive scaling laws that describe the nonlinear phenomenology within elemental MOSFET devices subjected to RF injection.

II. EXPERIMENTAL SETUP

Fig. 1 shows a layout schematic of the elemental devices fabricated on a single wafer. The layout comprises the following circuits – 1X NMOS; 1X PMOS; 10X NMOS; 10X PMOS; 1X Inverter; 10X Inverter; 10X inverter +ESD; 4-stage buffer; ring oscillator. These circuits have been replicated for the following MOSFET device sizes- 350nm, 180nm, 130nm, 90nm, and 65nm; all fabricated using the TSMC MOSIS process.

Fig. 2 shows the experimental setup, which comprises the use of a semiconductor analyzer and a probing station for

capturing the voltage and current transfer characteristics of the elemental device under study in the presence of large signal RF stimulus applied using an external amplifier-based microwave source.
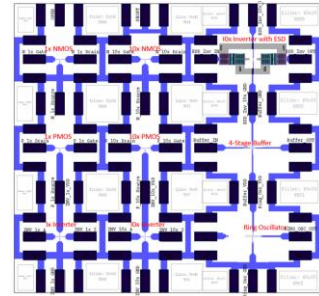

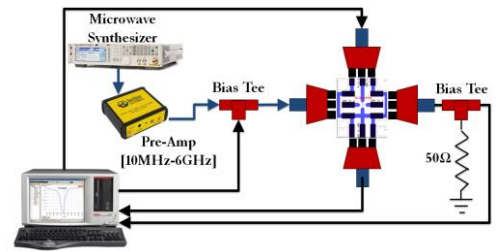Figure 1. Schematic of elemental devices under study.

Figure 2. Schematic of experimental set-up.

III. RESULTS

Fig. 3 shows the perturbed voltage transfer function (VTF) characteristics of a 1X Inverter device (350 nm) due to injected RF stimulus. The reduction in the gain and static noise margins are evident.
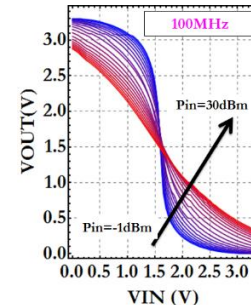

Figure 3. Change in 1X Inverter VTF due to injected l

Details on the development of the predictive models to describe such observed behavior will be presented as part of the oral presentation.

REFERENCES
[1] A. I. Kingon et al., Nature 406, 1032 (2000).

Developing Predictive Models for Erroneous Software Behavior due to Electromagnetic Interference

Sameer Hemmady[1] and Thomas M. Antonsen[2]

[1]Dept. of Electrical and Computer Engineering, University of New Mexico, Albuquerque, NM 87131
[2]Dept. of Electrical and Computer Engineering, University of Maryland, College Park, MD 20742
shemmady@unm.edu, antonsen@umd.edu

Abstract— Predicting the behavior of digital electronic and embedded systems subjected to extreme electromagnetic interference is a growing concern for military and civilian systems operating in ever denser ambient electromagnetic environments. While the interaction of the electromagnetic stimulus with the system circuitry occurs at the physical level, the manifestation of this effect is often perceived as an erroneous behavior in the software state of the system. In this research effort, we are developing Markov state vector machine models (SVM) for describing the software state of a microcontroller-based digital electronic system when subjected to an external EMI-induced glitch. We will validate these predictive models with experimental data. Such a predictive capability will help EMI/EMC engineers develop quick assessment tools for modeling the behavior of higher complexity digital electronic and embedded systems exposed to extreme electromagnetic environments.

Keywords- electromagnetic interference and compatibility, software behavior, Markov chains, RF CMOS, RF injection, Large signal RF modeling.

I. INTRODUCTION

The insistent demand for more powerful computing resources with faster clock speeds has led to the development of smaller, nanometer-scale digital CMOS devices operating with very tightening timing and voltage margins. As the CMOS device scale and operating voltages reduces, even moderate levels of injected or ambient RF interference can violate these timing and voltage margins leading to impaired system-level functional behavior, often perceived as the erroneous behavior of its operating software. In this research effort, we are developing mathematical framework to describe the probability of program flow or data flow errors within a sequence of software instructions, when a specific instruction is subjected to an external EMI-induced software glitch.

II. MATHEMATICAL FOUNDATIONS

Software execution on a microprocessor, microcontroller or embedded system can be modeled as a state machine where the individual instructions can be considered as "states" of the system (Fig.1). For an unperturbed system, the state transition probabilities from one state to the next state is unity. However, in the presence of an external EMI-induced glitch, the state transition probabilities change depending on whether the glitch causes the system to transition to the next state, skip a sequence of steps, or transition into an erroneous lock-up state (absorbing state). Here, we are developing a time-dependent Markov SVM model to describe the software behavior of the digital system subjected to external glitches.
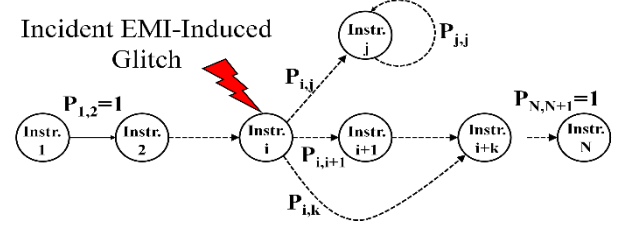

Figure 1. Schematic showing the use of Markov SVMs to model software glitches

III. EXPERIMENTAL SETUP

To validate this predictive model, we are utilizing a Field Programmable Gate Array (FPGA) to generate timed glitches into the clock stream and power supply of a microcontroller executing a sequence of instructions (Fig.2).
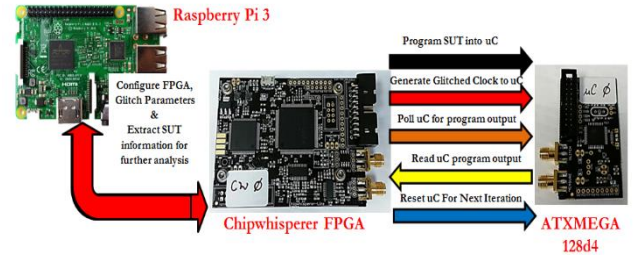

Figure 2. Schematic of experimental setup for modeling software glitches

We are generating the transition probability matrices for individual classes of instructions (Arithmetic, Logic, Branching and Machine Control) (Fig.3). These transition probability matrices will then be utilized for formulating Markov SVM models which will then be validated against experimental data for larger sequences of cascaded instructions and elementary software programs.
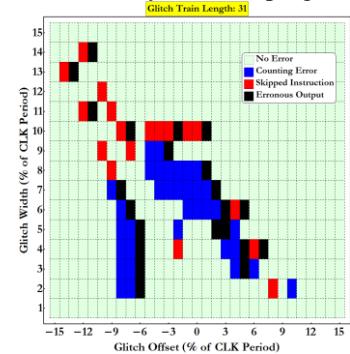

Figure 3. Glitch map generated showing erroneous software behavior

Developing a Statistical Topological Approach using Wave-chaos for Electromagnetic Effects (STUWEE)

Ghadeh Hadi, Sameer Hemmady, and Edl Schamiloglu
Department of Electrical and Computer Engineering
University of New Mexico
Albuquerque, NM 87131-0001
ghadi@unm.edu, shemmady@unm.edu, edls@unm.edu

Abstract— Predicting the statistical nature of short wavelength reverberation within random interconnections of large complicated cavities finds applications in several fields of physics and engineering. To aid in developing this predictive capability, this paper describes progress in the development of a mathematical framework that fuses the random coupling model (RCM) with the electromagnetic topology model of Baum-Liu-Tesche (BLT). We label this framework as the statistical topological approach using wave-chaos for electromagnetic effects (STUWEE). We present recent experimental results validating the predictive capability of our STUWEE framework. STUWEE is being incorporated into a computer code which will enable the user with a quick tool to assess the statistical description of the induced electromagnetic fields within user-specified, interconnected networks of large complicated cavities.

Keywords- statistical electromagnetics, wave chaos, random coupling model, multiconductor transmission lines, BLT equation.

I. INTRODUCTION

Predicting the nature of the scattering of short-wavelength waves in random interconnected networks of large complicated enclosures is routinely encountered in diverse fields such as acoustics, wireless communications, and electromagnetic compatibility engineering. The Random Coupling Model (RCM) [1], based on wave-chaos, is a statistical model describing the scattering of short wavelength electromagnetic waves in large complicated (chaotic) enclosures. The Baum-Liu-Tesche (BLT) electromagnetic topology formulation [2] is a hierarchical framework based on the multiconductor transmission line (MTL) model for describing the flow of energy between different nodes on a network of MTL segments. In this research, we fuse the RCM with the BLT electromagnetic topology to create the "Statistical Topological approach Using Wave-chaos for Electromagnetic Effects" (STUWEE) tool for predicting the statistics of the scattering of short-wavelength electromagnetic waves in random interconnected networks of chaotic enclosures.

II. EXPERIMENTAL SETUP

To validate the STUWEE framework, we have developed an experimental setup comprising a sequence of quasi-2D wave chaotic cavities (shown in Fig. 1).

Figure 1. Photographs showing our experimental setup of multiple quais-2D wave chaotic cavities that can be interconnected in random configurations to study scattering statistics.

The cross-sectional shape of these cavities can be reconfigured using metal inserts and computer-controlled, mode-stirrers to yield complicated, wave-chaotic, internal scattering environment exhibiting wave-chaotic scattering statistics.

III. RESULTS

Fig. 2 inset shows an example of one rendition of a complex interconnected network of quasi-2D wave chaotic cavities assembled at UNM. Fig. 2 shows a comparison between experimentally derived statistics of internal scattering fluctuations and predictions from our STUWEE framework.
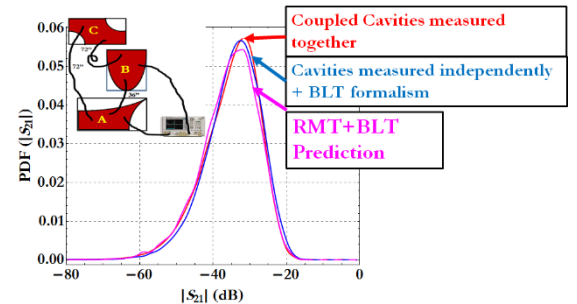

Figure 2. Inset: schematic showing network of interconnected cavities. Main: Comparison of experimentally measured internal scattering fluctuations (red), wave-chaotic cavities+BLT (blue), STUWEE (magenta).

Good agreement is observed thereby validating our STUWEE framework which involves fusing the RCM with the BLT topology.

REFERENCES
[1] S. Hemmady et.al., Phys. Rev. Lett., vol. 94, 014102 (2005)
[2] C.E. Baum, Interaction Notes 400

EMI/EMC & ESD Control Techniques in 'NAVIC' Spacecraft (IRNSS) Series

Aras Kumar R, Pal RK, Rajnish Yadav, Pallavi Y, Amit K
Systems Integration Group
ISRO Satellite Centre
Bangalore, Karnataka, India

Pramod V.Belgaonkar, Dr. V.K.Hariharan, Dr.M.Nageshwar Rao
Systems Integration Group
ISRO Satellite Centre
Bangalore, Karnataka, India

Abstract— This paper describes the methodology applied to the control of EMI and ESD and thereby achieving EMC in GEO orbit based NAVIC spacecraft series. Indian Regional Navigation Satellite System (IRNSS) series of spacecraft are configured around I-1K bus, the least dimension bus in GEO class. Seven spacecraft form the constellation in Geostationary and Geosynchronous orbit. Achieving EMC in IRNSS series of spacecraft has been quite challenging due to accommodation of systems operating at high power output & proximity of these systems with space electronics. The payload system comprises of high power navigation electronics and downlink in S-band (250W) and in L-5 band (150W). A single antenna with dual helix array (DHAA) for these bands is configured for transmission of navigation signal to the users. Further, CDMA (Code Division Multiple Access) ranging in C-band, CCRR (Corner Cube Retro reflector) laser ranging, along with conventional tone ranging supplement the navigational payload system. Atomic clocks - RAFS (Rubidium Atomic Frequency standard), the heart of navigation spacecraft, have stringent requirements on EM fields environment and are prone to plasma charging and subsequent ESD events. By analysis of potential sources of EMI and ESD in spacecraft, EMC has been accomplished by implementing concerned EMI & ESD control techniques and their verification during ground testing. This paper details, among others, the EMI/ESD Control Techniques followed in IRNSS Series of spacecraft, in order to achieve EMC.

Keywords: EMI, EMC, ESD Control measures, IRNSS, Rubidium Atomic Frequency Standard, Atomic Clocks, Grounding

I. INTRODUCTION

IRNSS satellite system named as NAVIC (Navigation using Indian Satellite Constellation) envisages establishment of Regional Navigation Satellite System using combination of GEO and GSO spacecrafts over India and region extending 1500km surrounding India. IRNSS constellation consists of seven satellites, out of them three are in GEO stationary orbit at 34degE, 83degE and 131.5degE and remaining four are in GSO (with a inclination of 29deg) crossing equatorial plane at longitude as 55degE and 111.5degE two satellite in each plane. IRNSS satellites consists of navigation payload, at L5 & S-band, it is supplemented CDMA-Ranging Payload in C-Band and laser ranging payload CCRR to accurately determine spacecraft position in its orbit. The Navigation payload broadcast precise timing Navigation service signals using Onboard Atomic Clock to the users. Satellite position data determined by ranging payloads are uploaded to satellite using TTC link.

The heart of Navigation payload is the Atomic clock units, i.e Atomic Frequency Standard (AFS). The accuracy of satellite navigation is critically dependent on the synchronization and timing accuracy of its navigation signals. Three types of Atomic Frequency Standard i.e. Hydrogen Measure, Cesium AFS and Rubidium AFS are available; RAFS and CAFS are suitable for spacecraft platforms due to weight and power requirements. The IRNSS satellites use high stability Rubidium Atomic frequency standard (RAFS) for on board clock and timing generation. The RAFS provides a 10 MHz output with frequency drift $<5 \times 10^{-13}$ Sec/day. RAFS output reference is further synthesized using Atomic Clock Monitoring Unit (ACMU). The precise timing message signals generated by Navigations Signal Generation Unit (NSGU) are synced using the RAFS Atomic clock. Navigation signals generated by NSGU are modulated in S-band and L5- band carriers in respective modulators. These modulated carriers are amplified using TWTA based amplifiers. S-band (2492.028MHz) navigation signals are amplified to 250W RF power, L5-band (1176.45MHz) navigation signals are amplified to 150W. These both navigation signals are transmitted using DHAA; one antenna array is used for L5 band signal and other array for S- band signal. The Effective Isotropic Radiate Power (EIRP) of 36dBW over 24MHz bandwidth for L-band and 39dBW over 16.5MHz for S-band. The coverage area for these signals beam is Indian main land and 1500km surrounding Indian boundaries. In future it is planned to increase coverage area by adding four more satellites in constellation.

EMC of IRNSS series of satellites is achieved by analysis of potential sources of EMI and ESD in spacecraft, and implementation of EMI/EMC & ESD Control techniques. EMC has been accomplished by analysis of potential sources of EMI and ESD in spacecraft, and by implementing concerned EMI & ESD control techniques and their verification during ground testing.
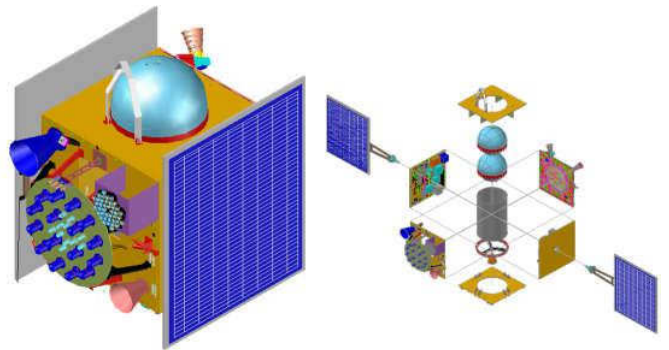

Figure 1: Stowed & exploded view of a typical IRNSS satellite

Configuration of all the seven satellites of the series is more or less identical. Satellite is realized on I-1K Bus with suitable modifications which are specific to navigation payload mission. IRNSS I-1K bus is typically a cuboidal structure with Top & Bottom panels being called as East & West decks. The main two equipment panels are North & South panels; North panel accommodates Telemetry/telecommand, AOCE, WDE, North SADA and TTC transmitters Main frame subsystem. Payload subsystems on North panel are NSGU, Navigation signal modulators and L5- band TWTAs. South panel accommodates Power subsystem, Battery, Telemetry/telecommand, IRU and South SADA of Main frame subsystems along with S-band TWTAs for Payload subsystem. Earth Viewing (EV) panel houses mainly CDMA payload with its receive and transmit horn antennas and TTC receivers. EV panel outside, DHAA antenna is mounted along with TTC antenna and CCRR payload. Anti-Earth Viewing (AEV) panel mainly contains AOCE, Star sensors and Reaction Wheels. West panel contains reaction Control System (RCS) and Liquid Apogee Motor (LAM). East panel is isolated with other panels and houses very important and critical subsystem i.e. three numbers of Atomic clocks (RAFS) and ACMU. Atomic clocks are sensitive to temperature variations and its temperature is maintained within $\pm 1^o$C using heaters in close loop. To protect thermal loads of other HK and payload subsystems on other panels of the spacecraft, EV panel is thermally isolated. To protect sun load on EV panel, spacecraft is flipped on YAW axis daily, so EV panel never faces sun and atomic clock temperature is maintained to desire value $+15\pm 1^o$C with the help of heaters. By yaw flipping North panel and South panel also changes position with respect earth north.

EMC of IRNSS series of satellites is achieved by analysis of potential sources of EMI and ESD in spacecraft, and implementation of EMI/EMC & ESD Control techniques. EMC has been accomplished by analysis of potential sources of EMI and ESD in spacecraft, and by implementing concerned EMI & ESD control techniques and their verification during ground testing.

The paper is organized as follows. Section II describes the EMI/ESD environment in IRNSS spacecraft. Section III details EMC measures undertaken in IRNSS spacecraft. Test results of EMC measures are discussed in Section IV. Finally, conclusion is presented in Section V.

II. EMI/ESD ENVIRONMENT IN IRNSS SPACECRAFT

There are many noise sources on spacecraft platform and many sensitive and critical subsystems. As IRNSS series of spacecraft are configured around I-1K bus, the least dimension bus in GEO class with approximately 1500 kg. HK and payload unit are very densely packed, gives rise to complex Electromagnetic environment. South panel contains sequential Switching Shunt Regulators (S^3R), Boost regulators (BDR) in excess to 500W DC power and 250W RF power TWTA for S-band along with other mainframe subsystems. North panel contains TTC transmitters and 150W L-5 band TWTAs and other mainframe subsystems. EV panel has TTC antenna, payload navigation signal transmitting antenna DHAA and CDMA payload and its antennas. Magnetic torquers (MTC) are placed on AEV and West panel. Sensitive subsystems i.e. TTC receivers and CDMA payload receivers are on housed in EV panel.

IRNSS spacecrafts are GEO orbit spacecraft and are prone to plasma charging and subsequent ESD events. There is possibility of differential charging of satellite external surfaces to breakdown levels and subsequently ESD events. There are three types of possible ESD events i.e. 1.) Radiated field generated due to ESD at some nearby location. 2.) ESD at a location and 3.) Structural current flow through satellite structure due to blow-off discharge to plasma. These ESD events generate EMI.

RAFS are very critical and most important subsystems of navigation satellites. RAFS are sensitive to power supply noise, therefore, Electromagnetic compatibility of RAFS is ensured with other subsystems. EMC is achieved with the use of Filter boxes, EMI gaskets, feed through filter capacitors and semi-rigid shielded coaxial cables to reduce the EMI effects. RAFS output frequency is also sensitive to temperature and magnetic fields. Considering these stringent requirements, RAFS location on the satellite was carefully chosen, RAFS are mounted on EV panel inside and thermally, magnetically isolated.

Another requirement is the radiation hardening. Radiation is a major factor in the design of space AFSs. In outer space the AFSs will continuously be exposed to energetic particles and secondary radiation. The electronics in the AFS is subject to upset, latching, and DC offset effects due to radiation. Some key components in the RAFSs are radiation hardened to significantly reduce the impact. Considerable radiation shielding is also added to further minimize the impact of the space radiation

Figure 2: Rubidium Atomic Frequency Standard (RAFS) clock used in IRNSS Spacecraft

III. EMC MEASURES IN IRNSS SPACECRAFT

To achieve the EMC of spacecraft, it is must to adopt EMI control measures from initial phase as well as various stages of spacecraft development to ensure reliable functioning of spacecraft.

Spacecraft subsystems undergo EMI/EMC testing to validate the design and find out the margins available. These tests are conducted as per MIL-STD-462 C methods. The levels are compared with MIL-STD-461 C, which are applicable to aerospace systems. The four types of tests carried out are Conducted Emission (CE), Conducted Susceptibility (CS), Radiated Emission (RE) and Radiated Susceptibility (RS).

A. Measures in Layout Design and Finalization

Subsystems placement on a layout is constrained by factors like interface and functional requirement, in addition to EMI/EMC considerations. Interface and functional requirements crop up in the form of signal flow paths. Subsystem having signal flow among them are kept close to each other.

Layout management is planned in IRNSS spacecraft is such that maximum possible isolation between receptors and emitters is provided. Power, sequential switching shunt regulator, switching subsystem BDR, high power amplifier and transmitter are co-located and isolated from sensitive and receivers.

RAFS output frequency is sensitive to temperature, magnetic field and power supply variation. To ensure high level frequency stability throughout the mission duration RAFS are thermally and magnetically isolated. Electromagnetic compatibility is ensured with other subsystems. Spacecraft structural elements and sheer webs are used to provide shielding between various section of spacecraft subsystems. Separate harness corridors for power and signal cables are provided.

B. Grounding and Bonding

To ensure EMC of spacecraft, impedance controlled reference ground plane is provided. Grounding scheme adopted in IRNSS spacecraft is Distributed Single Point Grounding (DSPG) scheme, each subsystem is grounded to reference plane close to subsystem, it ensures that ground loops are not formed. For each subsystems power returns lines are referred to power subsystem, Relay returns are referred to Bus return within the subsystem and secondary returns are referred to panel close to subsystem. The returns are connected to respective panels at one place only to avoid formation of ground loops. RF subsystems are provided with multi-point grounding. Spacecraft subsystems and units are bonded to the spacecraft structure. Panel to panel and panel to structure grounding is provided with 12 AWG wire links to form a continuous ground plane. Here it is worth to mention that EV panel where Atomic clocks are housed and this panel is isolated from other panels and structure for thermal and micro vibration reasons, it is must to provide continuous grounding plane by the use of grounding wire links. Bonding impedance measured is measured and ensured it is less than 10 mΩ.

C. Filtering

DC/DC converters used are with input EMI filters. Critical command lines are with input filters and telemetry input lines are with input filter lines. Appropriate filters are used to reduce noise within acceptable margin.

BDR System is having non-isolated architecture between input Raw Bus and output regulated 70V bus (i.e. common return, no galvanic isolation). Due to which there was some conducted emission noise on the secondary line caused by the switching
circuitry operating at 25 KHz of up to 9Vpp noise on tele-command ON/OFF lines (refer fig). After introducing appropriate filter using capacitors across Raw Bus line and Rtn (8.2kpF/200V), noise was reduced to less than 1.5Vp-p. The same is depicted in Fig. 3.
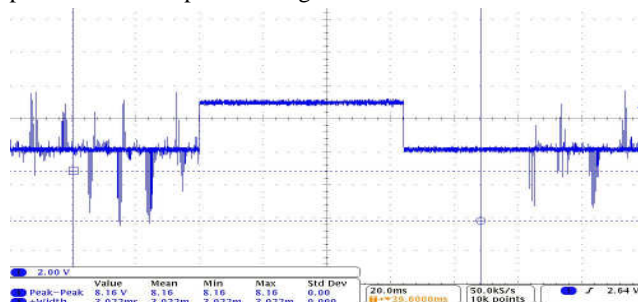

Fig. 3 Noise reduction by introduction of filter using capacitors

Radiated Emission test was conducted successfully and in the entire frequency range emissions including all the three notches were found to be well within the MIL-STD-461C limit line.

D. Electrical Distribution System Design

The electrical distribution system (spacecraft harness) forms the interface between different subsystems of the spacecraft. The design of EDS needs very much care in view of the wide variety of the signals types and their amplitude levels, the environment in which it is going to work, the IR drop for DC lines, the propagation delays of the signal lines, EMI coupling etc.. IRNSS spacecraft harness is designed in five assemblies, to provide optimum power transfer from the source or power supply bus to the receiver load, ease of integration , panel assembly and panel dis-assembly if need arises. It is be designed to meet total functional requirements and to achieve EMC of spacecraft. The other requirements of harness design are minimum weight which is achieved by reduction in harness length. Harness length is optimized with placement of subsystems as per signal flow, it also helps in minimized voltage drop and dissipation, minimized interference and coupling through harness. IRNSS series satellite harness optimized using 3D modeling of harness routing, it helped in optimization of length, harness bend radius, bundle diameter for finalization of harness corridors, clearance with all other spacecraft units. We have a plan to use 3D harness model for estimation of cable to cable coupling for EMC of harness, in future missions.

Following design guidelines are implemented in harness design of IRNSS to achieve EMC.

- Use of most appropriate wire type for the type of signal it carries.
- Sensitive signal lines are shielded, and shield is continuous and with minimum pigtail length.
- Various signal types are grouped together and isolated with other signal type.
- Payload output data to modulator interface is designed with LVDS differential signals;
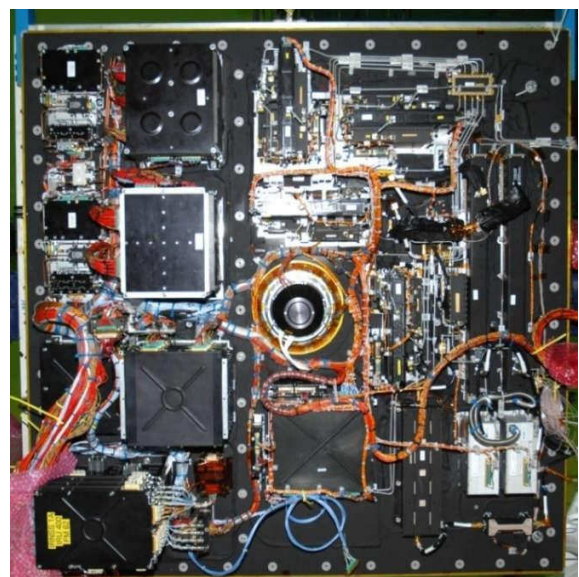

Fig. 4 EDS on flight Panels

MIL-STD 1553B bus uses special 1553 cables for balancing and impedance matching. This ensures high immunity of signals against common mode noise. Two separate MIL-STD 1553B bus one for HK and one for payload used.

RAFS output cables are flexible co-axial/ semi-rigid and are integral part of RAFS.

The harness routes for different types of signals are segregated in different groups.

E. ESD Control Measures

The IRNSS series of spacecraft are in Geo-stationary orbit and geo-synchronous orbit. These all spacecrafts of the IRNSS constellation are likely to be charged by the plasma environment to high potentials. The process of buildup of charge on external surfaces of a spacecraft with respect to plasma environment and as well differential potential build up between different parts of spacecraft. Spacecraft charging due to plasma environment is classified into two types. The first, called the absolute charging, occurs when the entire
spacecraft is charged negatively w.r.t. ambient plasma environment. The second type called the differential charging, occurs when parts of the spacecraft are charged to different negative potentials relative to each other. Absolute charging occurs very rapidly during magnetic sub-storms and in a fraction of second during eclipse. Differential charging usually occurs slowly and results in one part of surface being charged to a potential different from other parts of the spacecraft. ESD events gives rise to radiated electromagnetic fields. These radiated fields are coupled to cables and conducted to various subsystems. Blow-off discharge gives rise to structural currents which may get coupled magnetically to atomic clocks and other subsystems.

While handling of IRNSS subsystems, units and during Integration activities precautions are taken for control of ground ESD i.e. human, machine, tools and facilities.

For the proper functioning of IRNSS spacecraft, following ESD control measures are adopted:

All the structural elements of spacecraft are tied to a common electrical ground directly except solar panel substrate which is connected through an 11 kΩ charge bleed-off resistor for safety.

Structural elements which are isolated with structure are connected to structure/ ground by use of conductive copper foil tape or wire links. SADA cone which is made of GFRP is grounded to panel by the use of conductive aluminum foil tape. Continuity of these above mentioned elements is ensured by measurement.

CFRP substrate of DHAA antenna is grounded.

The spacecraft subsystem housings and other elements are bonded to spacecraft structure with approved torque value.

The exterior surfaces of the spacecraft which is mainly MLI is ITO coated to make partially conductive and grounded, all aluminized layers of MLI are interconnected with copper foil tape and grounded. Solar cells on solar panels are also ITO coated.

Cable shields are physically and electrically continuous and grounded. Harness outside the spacecraft cuboid is shielded by wrapping with copper foil tape and grounded. Flexible harness from solar

panel to SADA is wrapped with aluminized kapton and grounded.

Telemetry input lines i.e. thermistor, PRT status lines from outside spacecraft cuboid protected with transient suppressors (Transzorb) prior to input to Telemetry subsystem.

All unused input lines, spare SADA slip rings etc. Are grounded to structure through 11Kohms resistor.

IV. TEST RESULTS

A. Magnetic Field Measurements near RAFS in IRNSS Spacecraft

RAFS units are very sensitive to DC Magnetic field. Performance of the RAFS in terms of frequency stability gets affected if DC Magnetic field exceeds 5 Gauss in any direction around the package (<100mm volumetric region). Although during layout design enough care was taken to isolate all magnetic field generating elements from RAFS, actual measurements were carried out to confirm the magnetic field levels are not exceeding operational limits. There are two Magnetic torquers perpendicular to each other in IRNSS spacecraft, one on AEV Panel (Roll) and other on West Panel (Pitch). These torquers were turned ON, so that measurements can be made when maximum possible or worst case intentional magnetic field is there around the RAFS. Measured maximum magnetic field near RAFS was 0.4 Gauss (Refer Table I)

By measurements it was confirmed that maximum gauss measured, +0.4Gauss is very less when compared to maximum magnetic field under which systems function normally, 5 Gauss.

TABLE I
MAGNETIC FIELD MEASUREMENTS NEAR RAFS IN IRNSS SPACECRAFT

Criteria		Magnetic Field (Gauss)
DC Magnetic Field Generated near Magnetic Torquer		160
Ambient Magnetic field around Satellite		-0.4
DC Magnetic Field near RAFS (No current in Torquer)	X-axis	-0.29
	Y-axis	-0.02
	Z-axis	-0.3
	Vector Ampl.	+0.4
DC Magnetic Field near the RAFS (Full current in both torquer)	X-axis	-0.2
	Y-axis	0.09
	Z-axis	0.29
	Vector Ampl.	+0.34
With L band TWTA ON, magnetic field not more than 0.4 Gauss was observed near RAFS		
With S band TWTA ON, magnetic field not more than 0.4 Gauss was observed near RAFS		

B. System-level EMC Measures

The Electromagnetic compatibility of IRNSS spacecraft with launcher Polar Satellite Launch Vehicle (PSLV) is also ensured by analysis of launcher and spacecraft transmitter and receiver frequencies. The performance verification is verified in RF shielded anechoic chamber

System level EMC test was conducted to verify the Radiated EMI compatibility of IRNSS Spacecraft with the applicable PSLV launcher (PSLV).
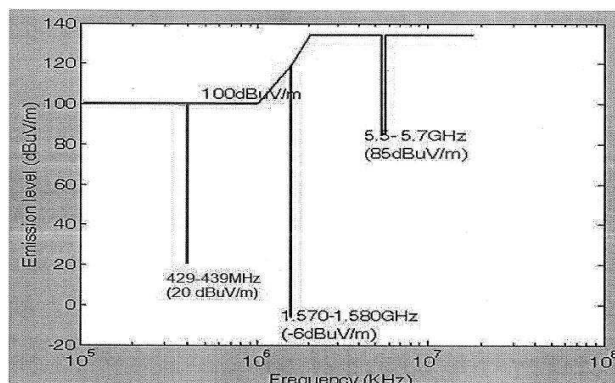

Fig. 5 Radiated Emission test in the entire frequency range

The Electromagnetic compatibility of IRNSS spacecraft with launcher Polar Satellite Launch Vehicle (PSLV) is also ensured by analysis of launcher and spacecraft transmitter and receiver frequencies. The performance verification is verified in RF shielded anechoic chamber.

TABLE III
LAUNCHER COMPATIBILITY TEST SPECIFICATIONS

Frequency, MHz	Worst Case Envelope of Launch Vehicle RS levels, dBuV/m	Notches by Applicable Launchers
0.01-1000	100	0.01 to 18GHz Range
	100 to 134	
2000-18000	134	
1570-1580	-6	PSLV GPS Rxr
5500-5700	85	PSLV GPS Rxr
429-439	20	PSLV GPS Rxr

CATF (Compact Antenna Test Facility) test was conducted at System level to validate Payload operation in radiated mode through the payload Antenna, during which overall system health in terms of interference free spacecraft operation was confirmed.
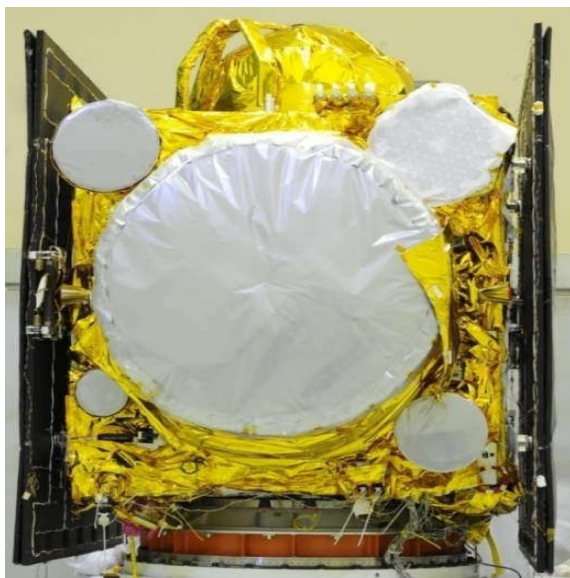
Fig. 6: IRNSS Spacecraft for system level checks

V. CONCLUSION

EMC of IRNSS series of satellites is achieved by analysis of potential sources of EMI and ESD in spacecraft, and implementation of EMI/EMC & ESD Control techniques. EMC has been accomplished by analysis of potential sources of EMI and ESD in spacecraft, and by implementing concerned EMI & ESD control techniques and their verification during ground testing. Design approach for compatibility of satellite subsystems; Atomic clocks along with high power Payload transmitters, high power switching regulators. The major design approach for the EMC includes finalization of equipment panel layout, use of structure elements for shielding, providing spatial isolation between various subsystems, grounding scheme, bonding techniques, EDS (Electrical Distribution System) design, apart from employing standard design techniques, focused on optimizing the interface cable lengths, grouping of signals and harness routing plan to achieve EMC of spacecraft.

EMC performance of IRNSS spacecraft was ensured by verification with auto-compatibility test where spacecraft performance verified in spacecraft in in-orbit mode, transmitters transmitting full power.

REFERENCES

[1] NASA-HDBK-4001, 17-02-1998: Electrical Grounding Architecture for Unmanned Spacecraft.
[2] MIL-HDBK-1857, 27-03-1998: Grounding, Bonding and Shielding Design Practices.
[3] MIL-STD 1541A (Dec. 1987): Electromagnetic Compatibility Requirements for Space Systems.
[4] Comprehensive Design Review of Electrical Integration IRNSS Document.

AUTHORS

Aras Kumar R completed BE in Electronics & Communication Engineering in 2004 from Vivekananda Institute of Technology, VTU, Karnataka. Worked as research assistant in Radio Astronomy Lab, Raman research Institue for 2 years. Later, joined ISRO Satellite Centre, ISRO, Bangalore, System Integration Group. He is involved in Technology Development projects related to automation of Harness 3D modeling and EGSE systems used for Spacecraft Testing. He has worked in the field of EMI/EMC/ESD related to spacecraft and Assembly , Integration and Testing (AIT) of Remote Sensing Satellites, Communication satellites and series of Navigation satellites. He was responsible as Project Manager for Electrical Integration Activities of GSAT-7 and IRNSS 1A to 1G satellites. Presently involved in GSAT-7A and IRNSS-H spacecraft Electrical Integration activities. **E-mail:** aras@isac.gov.in

R.K.Pal completed Diploma in Electronics Engineering from UP Technical Education Board, joined Spacecraft Integration Division at ISRO Satellite Centre during the year 1987. He has completed MCA degree from IGNOU. He has worked in field of EMI/EMC/ESD related to spacecraft and Assembly , Integration and Testing (AIT) of Remote Sensing Satellites, Communication satellites, Meteorological satellites and series of Navigation satellites i.e. IRS-1D, INSAT-3C, METSAT, Resourcesat2, CARTOSAT-2A, GSAT-3, INSAT-4CR, GSAT-5P, INSAT-3D and IRNSS series. Presently working on INSAT-3DS project. **E-mail:** palrk@isac.gov.in

Rajnish Kumar Yadav received B.Tech.in Avionics engineering from Indian Institute of Space Science and Technology IIST, Thiruvananthapuram in 2012 .Since September 2012 he has been with the Geosat Integration Division of ISRO Satellite Centre, Bangalore in the area of assembly, integration and testing of communication and navigation satellites. He has been instrumental in integration, testing and realization of all 7 satellites of the IRNSS constellation. Presently he is contributing to integration and testing of GSAT-7 and GSAT-7A satellites.
E-mail: rajnish@isac.gov.in

Amit Kumar received his B.Tech. (Avionics) from Indian Institute of Space Science and Technology, Trivandrum in 2011. He joined ISRO satellite Centre in 2011, he has been associated with the Electrical Integration Division, working in the areas relating to Integration and Testing of INSAT class of satellites. Presently, he is working for IRNSS series of spacecrafts. **Email:** amitk@isac.gov.in

Pallavi Yarlagadda has done B.Tech(Electronics & Communication) in 2006 from Jawaharlal Nehru Technological University, Hyderabad and M.E(Digital Systems) in 2009 from College of Engineering, Osmania University, Hyderabad. She joined ISRO/ISAC in 2010, since then as project engineer she contributed to integration activities of GSAT-7, IRNSS series and GSAT-7A Spacecrafts.
Email: pallaviy@isac.gov.in

Pramod.V.B received B.E. (Electronics Engineering) from Nagpur University in 1990. Joined Electrical Integration Division, ISRO Satellite Centre, Bangalore and contributed in the areas relating to Test systems & related software development, EMI/EMC/ESD aspects of spacecraft systems, Assembly, Integration and Testing (AIT) of IRS and INSAT class of satellites. As Project Manager, INSAT-4C, 4CR and RISAT (Radar Imaging Satellite), he was responsible for Integration, Testing, and evolving Grounding scheme. He was the Focal Point for Electrical Integration activities of HYLAS. Presently, he is working as Head, GEOSAT Integration Section-4, Deputy Project Director – Systems Integration for GSAT-7, GSAT-7A and IRNSS series satellites.
E-mail: pramod@isac.gov.in

Dr. V.K.Hariharan received B.Tech., (Electronics Engineering) from Madras Institute of Technology in 1984 and M.Tech., (Communication Systems) from Indian Institute of Technology (IIT), Madras in 1986. He received his Ph.D. Degree from E&ECE Department of IIT, Kharagpur in 2003. Since January 1986, he has been with the Electrical Integration Division of ISRO Satellite Centre, Bangalore. After working as EMI/EMC Test Engineer and as Project Engineer for IRS-1E, P2, P3, P4 satellites, he worked as Project Manager, Electrical Integration for : Technology Experimental Satellite(TES), CARTOSAT-1 and INSAT-3E; Subsequently as DPD-(AIT), OCEANSAT-2 and GSAT-8 and as Associate Project Director, RESOURCESAT-2 spacecraft. Concurrently, from 2005 to 2010, he was heading EMI/EMC Section, responsible for EMI/EMC/ESD testing at subsystem and system level for all the spacecraft; Refurbishment of RF shielded chamber, EMI/EMC Lab, ISAC and Establishment of RF Shielded Anechoic Chamber at ISITE for carrying out S/C Level EMI/EMC Testing, S/C-Launcher-Co-passenger Compatibility Measurements. From April 2010 to Sept. 2015, he worked as Head, GEOSAT Integration Division (GID) and as DPD-AIT for GSAT-11 and GSAT-19 spacecraft. During this period, as Head GID, he was responsible for the delivery of 13 flight worthy GEOSATs and successful launch of the same. From October 2015 to August 2016, he worked as Group Director, Systems Integration Group. Presently, he is working as Deputy Director, Integration and Checkout Area, ISAC and responsible for AIT of all satellites towards delivery of flight worthy spacecraft. He has been the author/ co-author of over 70 technical papers published in national and international Journals / Conference proceedings. His fields of interest include numerical techniques in Electromagnetics, Electrostatics, EMI/EMC/ESD studies and Systems Engineering. **E-mail:** vkh2243@isac.gov.in

Dr. M. Nageswara Rao joined ISRO in September 1982 after completing Masters in Physics with specialization in Electronics from Andhra University, Visakhapatnam. He has completed Ph.D. in Physics from Sri Krishnadevaraya University, Anantapur in July 2012. He started his career at ISRO Satellite Centre, Bengaluru. His first assignment was with Electrical Integration Division till 2006. From 1988 onwards, he was involved in the communication spacecraft assembly, integration, testing and launchactivities. He played a major role in the realization of INSAT-2 ETM, INSAT-2A, 2B, 2C, 2D, 2E, 3B, 3E and the GSAT-1 Spacecraft in various capacities. He played a major role in the realization, launch and recovery of the India's first Space Capsule Recovery Experiment (SRE) as a key project executive. During his stint with Assembly, Integration & Testing Group, he headed the Special Test & InstrumentationSection, Geo-Sat Integration & Testing and Compact Antenna Test Facility (CATF). He was Project Director of GSAT-4 and Indian Regional Navigational Satellite System (IRNSS) Space Segment and responsible for realization of a constellation of satellites. From October 2015 to August 2016, he worked as Deputy Director for Integration & Checkout Area and also held the position of Deputy Director, Communication & Power Area as additional responsibility. Presently, he is designated as Associate Director, ISAC. He has published more than 30 technical papers in various international and national journals.
E-mail: mnrao@isac.gov.in

Aircraft EM Testing in the 21ˢᵗ Century

-- What we have now that we didn't have then --

William D. Prather
Air Force Research Laboratory
Albuquerque, NM, USA,
william.d.prather@ieee.org

Abstract—There have been significant changes in the electromagnetic (EM) protection requirements for both commercial and military aircraft in the last 40 years. Modern aircraft have to meet strict EM protection standards that include electromagnetic interference (EMI), high intensity radio frequency (HIRF), electrostatic discharge (ESD), lightning, and electromagnetic pulse (EMP), as illustrated in Fig. 1. As a result, measurement methods have been developed that can be used to measure the EM shielding and protection for all these phenomena. This paper discusses the standards we have today and how they can be verified using the tools that have been developed.

Keywords: aircraft, EMP, testing, pulse, continuous wave

I. INTRODUCTION

The external electromagnetic requirements levied on new commercial as well as military aircraft, including EMI, HIRF, ESD, and EMP, have significantly increased over the past 40 years [1-3]. New aircraft address all these requirements as an integrated requirement, and the testing methods we have can be used for more than just EMP. Also, older aircraft are often upgraded to meet modern requirements, and the same tools can be used to measure the coupling to internal cables before upgrade decisions are made [4-5].

II. MEASUREMENT TECHNOLOGY

Tools are now available to measure the EM protection features on any aircraft, something we did not have many years ago. These include continuous wave (CW) illuminators, cable shield and aperture testers, CW fuselage drive techniques, as well as full threat EMP simulators and high-power pulse current injection. The time and cost required for EMP hardness verification tests today are considerably less than what they was decades ago, and having the new Military Standards make the process of verifying the hardness of an aircraft a lot more straightforward than ever before. With modern instrumentation, fiber-optics, and fast

computers, the required test time is shorter, and the recorded data is more accurate.

III. UPGRADING EXISTING AIRCRAFT

In addition to the development of new aircraft, existing fleet aircraft are often redesigned or upgraded to bring their performance up to modern standards. In such cases, it is important for the Program Office to have accurate information about the coupling of various EM environments to aid them in making engineering and
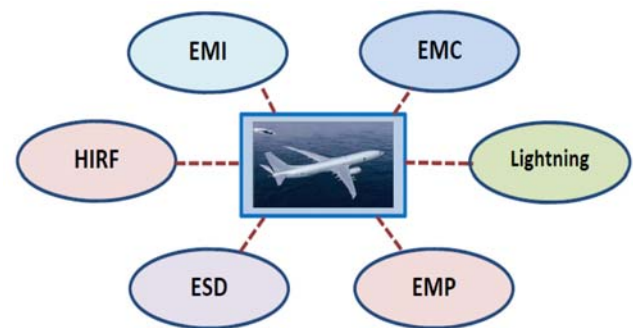

Figure 1. Integrated E3 design.

budgetary decisions. Swept CW illumination can provide such information without any danger of harming the aircraft. A system-level CW scan at the beginning of the program can greatly increase the accuracy and adequacy of the upgrade decisions and the final outcome.

REFERENCES

[1] RTCA/DO-160G, "Environmental Conditions and Test Procedures for Airborne Equipment," December 2010.
[2] MIL-STD-461G, "Requirements for the Control of EMI Characteristics of Subsystems and Equipment," December 2015.
[3] MIL-STD-464C, "Electromagnetic Environmental Effects Requirements for Systems," December 2010.
[4] W.D. Prather, "Shielding Specification Techniques & Measurement Methods for Aircraft," *Proc IEEE Symposium on EMC*, Detroit, August 2008.
[5] W.D. Prather, "Aircraft EMP Hardening in the 21ˢᵗ Century – EMP Hardening as a part of an Integrated E3 Design," *Proc. EUROEM 2016*, London, July 2016.

Malfunction of Electronic Equipment by Repetitive Ultra-Wideband Pulse

Jongwon Lee and Jin Soo Choi

The 4th R&D Institute
Agency for Defense Development
Daejeon, Republic of Korea
jwlee@add.re.kr

Abstract- This paper introduces the analysis of high-power electromagnetic (HPEM) effects on electronic equipment. We locate nine electric devices in a small building, and install D-dot sensors to measure the electromagnetic fields radiated from the signal source. Experimental result shows a low transfer rate at the frequency of 650 and 1300 MHz. It also shows a higher probability of malfunctions as the field strength and the repetition rate are increased.

Keywords- Electromagnetic Pulse (EMP), Electromagnetic Effect, Ultra Wideband (UWB)

I. INTRODUCTION

As the design technology of HPEM source has been developed, the interest in HPEM effects also rapidly rises. Therefore, it is important to experimentally measure the effects on the electronic equipment as the pulse parameters such as field strength and repetition rate are changed.

II. EXPERIMENTAL CONFIGURATION
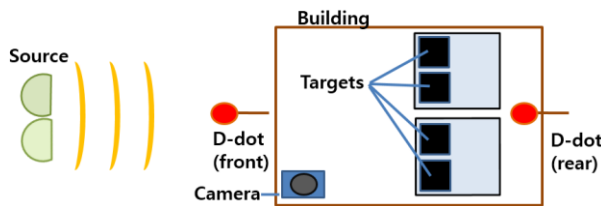
Figure 1. Setup for the measurement of HPEM effects

Figure 2. Configuration of targets

The parabolic integrated antenna source system in [1, 2] is used as the HPEM signal source. As illustrated in Figure 1 and 2, nine electric devices are located inside the small building. To measure the radiated electric fields, two D-dot sensors are installed in front of, and behind the building, respectively. We also set up the shielded camera to monitor the electric devices inside the building. The electric field strength measured at the rear sensor is in the range of 10~25 kV/m. The repetition rate of the pulse radiation is set to 1 and 100 Hz. The duration time of radiation is 1 second.
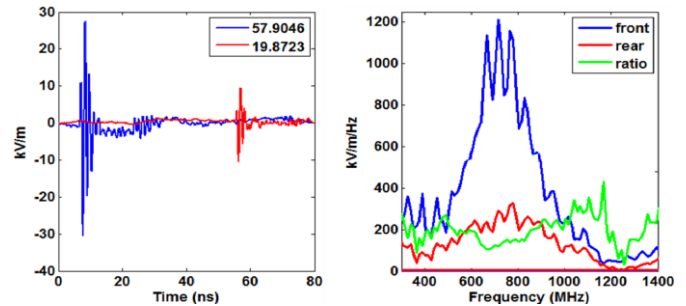
III. RESULTS

Figure 3. Measured waveforms

A. Resonance Frequency

Figures 3 shows the measured waveforms in front of and behind the structure. The signal at 650 and 1300 MHz are greatly reduced after the wave passes targets. Therefore, those frequencies would be multiple of the resonant frequency of targets.
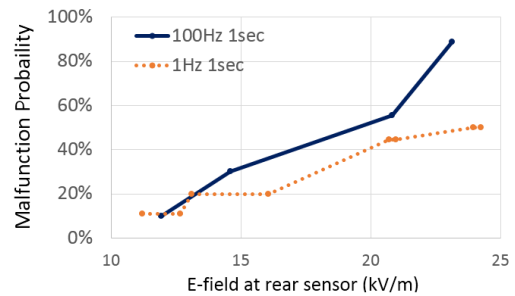

Figure 4. Malfunction Probability

B. Malfunction of Device

We define the malfunction as the state when a target cannot be returned to normal without manual operations. The malfunction probability is the ratio of the number of malfunctioned devices to the total number of devices. As shown in Figure 4, the malfunction probability increases as the strength of field rises. In addition, at the same strength of electric field, the pulse of 100Hz shows a higher malfunction probability rather than the pulse of 1Hz.

IV. CONCLUSION

HPEM effects on the electric devices inside the building are experimentally tested by using repetitive ultra-wideband signals. Measured data shows that the HPEM effect becomes more serious as the field strength or the repetition rate increase.

REFERENCES
[1] J. Ryu, and J. Lee, "An Integrated Antenna-Source System of Very High Ultra Wide-Band Gain for Radiating High-Power Wide-Band Pulses," *IEEE Trans. on Plasma Science,* vol.40, no.4, pp. 1019-1027, Apr. 2012.
[2] J. Ryu, J. Lee, H. Chin, J. Yeom, H. Kim, H. Kwon, S. Han, and J. Choi, "A High Directive Paraboloidal Reflector Antenna for High Far Voltage in an Ultra Wideband Source System," *IEEE Trans. on Plasma Science,* vol.41, no.8, pp. 2283-2290, Aug. 2013.

A Parametric Analysis A CPW Fed Novel Shaped Microstrip Patch Antenna

Paresh Jain[1]
Research Scholar
Electronics and Communication Engineering
Department,
Suresh Gyan Vihar University, Jaipur, Rajasthan
E-mail- paresh.jain@mygyanvihar.com[1]

Dr. O.S Lamba[2]
Electronics and Communication Engineering
Department,
Suresh Gyan Vihar University, Jaipur, Rajasthan,
India
E-mail- onkar.lamba@mygyanvihar.com

Abstract –A CPW fed novel shaped compact antenna is proposed in this abstract. The size of the Antenna is 50mm x 48mm x 1.6mm and it is prototyped on FR-4 substrate material which has a dielectric constant of 4.4.First, CPW-fed conventional slot antenna is designed and then the rectangular shape patch is modified to achieve higher bandwidth. The resonance frequencies are 2.4 GHz for Wi-Fi and 5.8 GHz for WiMAX applications. The proposed antenna provides bandwidth 58.42% for 2.4 GHz frequency and 17.37% for 5.8 GHz frequency which can be used for wireless applications. A parametric analysis is carried out by varying the two gaps:

1. Horizontal gap 'g_1' between the feed line and ground,
2. Vertical gaps 'g_2' between the conducting patch and ground.

The dimensional variation effects on the proposed antenna will be studied in this paper. The Return loss, VSWR, Smith Chart, Far-field radiation pattern will be studied in this paper. Simulations are carried out using Finite Element method based Ansoft High Frequency Structure Simulator.

Keywords- CPW Fed, Smith Chart, Finite Element method, Ansoft High Frequency Structure Simulator.

A Triple Band Pass Frequency Selective Surface For Augmentation In The Performance Of Wimax And Wlan

Darakshanda Noor
Electronics & Communication
Government Women Engineering College
Ajmer, Rajasthan, India
noorncet@gmail.com

Abstract— WiMax and WLAN have used at different range of bands. However, these bands suffer large attenuations, so a band pass frequency selective surface has proposed in the paper that led to the intensification in the transmission of WiMax and WLAN signal to reduce the effect of path loss. A single sided FR-4 substrate has integrated with the square and three decagon elements which results in triple band (2.5GHz, 3.5GHz and 5.5GHz) characteristics. The single sided substrate dielectric constant is 4.4 with loss tangent 0.025 and thickness 1.6mm. With respect to different incident angles, offered structure had excellent band pass response. For evaluating the performance, the CST Microwave computer simulation is used.

Keywords- Triple Pass Band Frequency Selective Surface (FSS), WiMax and WLAN 2.5, 3.5 and 5.5 GHz band.

I. INTRODUCTION

WiMax and WLAN are the most powerful as they provide high data rates with much higher speed and coverage area. In Earlier days antennas had used as reflectors but they do not show good results as current flows out of phase from antenna and cancel out. Afterwards Ben a. Munk theory of Frequency Selective Surface (FSS) came into nimble. In this current flows in-phase led to improved impedance bandwidth, angular stability and gain. Frequency Selective Surface acts as a filter at any angle of incidence for a plane wave and has band stop/ band pass frequency dependent characteristics. The most imperative factor in designing is the spacing between inter elements, patch and slot types and geometry. FSS scatters electromagnetic fields that are numerically calculated by different methods as discussed earlier as these methods differed from each other in the way of calculating different FSS configurations [7].The bandwidth are more often defined in -10dB for reflection and -.5dB for transmission. The structure has realized in CST Microwave Studio software in frequency domain solver, based on FDTD method.

II DESIGNING OF SUPERSTRATE

A. Unit Cell

A FR-4 superstrate with thickness 1.6mm and dielectric constant of 4.4 has used with dimensions W (mm) × W (mm) that is square shaped. On its one side, a patch has fixed included of two square and octagon . Due to the arrangement of square , a 2.5 GHz band has obtained. Two bands: 3.5 GHz and 5.5GHz have obtained due to second square and octagon respectively. The dimensions have illustrated in Fig. 1 and Table 1.
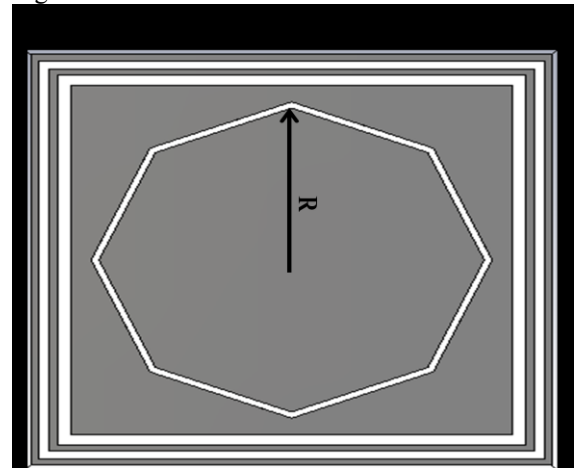

Fig1: Unit Cell

Table.1. Dimensions of proposed unit cell.

Name of Dimensions	Symbol	Value in (mm)
Width of Substrate	W	20
Radius of Outer Decagon	R	7.7
Thickness of substrate	H	1.6
Spacing between the elements	S	0.3

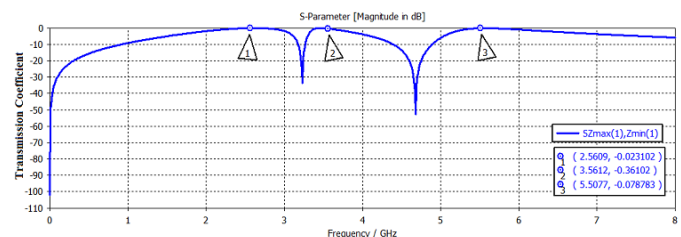## RESULTS AND DISCUSSION

Transmission Coefficient:

Fig 2: Insertion Loss Of Unit Cell

Hetero Structured 2D-Photonic Crystal Ring Resonator based Optical Wavelength Division De-multiplexer

Anila Dhingra
Research Scholar, ECE Department
Suresh Gyan Vihar University
Jaipur, India
anila_26@rediffmail.com

Dr. O. S. Lamba
Professor, ECE Department
Suresh Gyan Vihar University
Jaipur, India
lamba.ceeri@gmail.com

Abstract— In this paper, heterostructure based Wavelength Division De-multiplexer (WDDM) is designed Wavelength Division Multiplexing systems using Two Dimensional (2D) Photonic Crystal Ring Resonator (PCRR) which is essential for Photonic Integrated Circuits (PICs) and future optical networks. The structure is devised in 2D square lattice which contains circular and elliptical Si rods in air host. The designed de-multiplexer comprises three regions of ring resonator, in which region1 (having refractive index 3.255) and region2 (having refractive index 3.47) are made of circular Si rods, region 3 (having refractive index 3.255) is made of elliptical Si rods that can be used to drop three channels centered at 1471nm, 1491nm and 1530nm. Using 2D Finite Difference Time Domain (2D FDTD) method, the properties of the filter such as coupling, resonant wavelength are theoretically investigated. The Photonic Band Gap (PBG) of the designed structure is calculated by Plane Wave Expansion (PWE) method.

Keywords- Ring resonator; Photonic band gap; WDDM; FDTD; PWE; Heterostructure; Metamaterial; Photonic crystal.

I. INTRODUCTION

Photonic crystals (PhCs) are periodic dielectric structures. They are called crystals because of their periodicity and photonic because they act on light. They occur when the period is less than the wavelength of the light. PhCs may inhibit the propagation of certain range of wavelengths in either one direction or in all directions, providing the possibility to confine and trap the light in a cage. Their effect to the propagation of electromagnetic waves is similar to the periodic potential in a semiconductor crystal. The periodic potential affects the electron motion by defining allowed and forbidden electronic energy bands. Necessarily, photonic crystals contain internal regions of high and low dielectric constant that are repeated regularly as shown in Figure1.

In fiber-optic communications, wavelength-division multiplexing (WDM) is a technology which multiplexes multiple optical carrier signals on a single optical fiber by using different wavelengths (colors) of laser light to carry different signals. This allows a multiplication in capacity, in addition to enabling bidirectional communications over one strand of fiber.

With the advancement in the WDM techniques it has been a great challenge for the researchers to develop the de-multiplexers which at the receiving end can separate out these multiplexed signals effectively with highest possible efficiency. Traditionally, de-multiplexing components are realized using thin-film filters, fiber Bragg gratings (FBG), or arrayed waveguide gratings. However, such devices are not convenient for ultra-dense integration. Various concepts for realizing a de-multiplexing component utilizing the extraordinary properties of PhCs have recently been proposed. These ideas include optical micro-cavities, directional couplers, multimode self-imaging waveguides, and super-prisms.
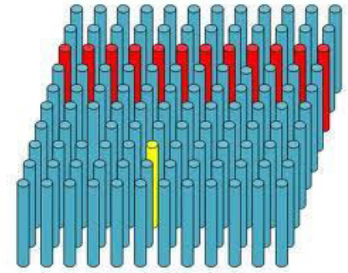

Figure1: 2D-Photonic crystal structure with Si rods in the air background

II. PROPOSED STRUCTURE

The schematic structure of heterostructure based WDDM using circular PCRR is designed using 2D-square lattice PCs. The distance between the two adjacent rods is 540 nm, which is termed as lattice constant, '*a*' and the radius of the Si rod is 0.1µm. The structure contains two regions with different refractive index of the rods in air host that is 3.255 for first & third region and 3.47 for second region, respectively. The optimized values used in the heterostructre based WDDM are obtained through gap map. The gap map gives the variation in TF/TM PBG with respect to lattice constant, radius of the rod and refractive index. The 2D Finite Difference Time Domain (FDTD) method is used to obtain the normalized transmission spectra of the structure and Perfect Matched Layer (PML) is placed as absorbing boundary condition to avoid the re flections in the computational domain.

The Metamaterial Revolution

Innovations and Challenges

Jayanti Venkataraman[1] and Jun H. Choi[2]

[1]Electrical & Microelectronic Engineering, Rochester Institute of Technology, Rochester, NY14623,USAjnveee@rit.edu

[2]Electrical and Computer Engineering, Syracuse University, Syracuse, NY13244, USA jhcho100@syr.edu

Abstract— The creation of metamaterials and artificial dielectrics have enabled a wide range of applications using low microwave power that have helped to overcome limitations of frequency dependent antenna sizes, lowering mutual coupling effects, overcoming bandwidth limitations, enhancing antenna gain, beam shaping through image formation etc. This paper presents applications of metamaterials at low power with few examples based on the research at RIT and Syracuse University. In contrast, metamaterials exposed to high power experience difficulties due to dielectric breakdown and conductor heating. At present, there is interesting research underway that is finding creative solutions for optimizing the effective material parameters to reduce the maximum field enhancement factor.

Keywords- Composite right/left hand, Double negative, epsilon near zero, dielectric breakdown, anisotropy.

I. INTRODUCTION

The metamaterial revolution that began two decades ago has opened exciting avenues of research where limitations with positive dielectric permittivity and permeability could be overcome and improvements on antenna performance could be achieved for size reduction, increased bandwidth, enhanced gain, reducing mutual coupling etc. While most of these successes are for low power applications, there are challenges yet to be overcome for high power applications.

II. INNOVATIONS WITH LOW POWER

Composite right/left-handed (CRLH) structures have been implemented in transmission lines and applied to a wide range of

Figure 1 CRLH Feed network

antenna feed networks by Itoh et.al. As an example, figure 1 [1] illustrates an all-passive CRLH phased-array feed network that allows easy controllability of radiated parameters including: polarization type, polarization orientation, cross-polarization level, directivity, and SLL. It can direct the main beam toward the desired elevation angles while allowing bidirectional operation.
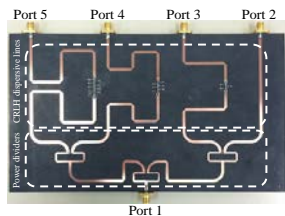
Materials exhibiting simultaneous negative permittivity and permeability materials (DNG) act as a lens creating an image of a point source. Metamaterials with permittivity ε near zero (ENZ) may be used in a similar manner to reshape the wave fronts emitted from any kind of source. As examples, are two types of novel metamaterials created at RIT. One is a DNG material that has a refractive index, n =-1 at 30.7GHz (figure 1), constructed by drilling holes in a high dielectric material [2]. The other is a thin wire grid structure acting as an ENZ material with ε=0 at 17.8GHz [3]. Experimental validation has been done to demonstrate image formation and phase reversal in the transmission plane (Figure2 for DNG lens). Gain enhancement has been achieved with the DNG lens as a superstrate and phase plane shaping has been demonstrated with the ENZ lens.

Figure 2 DNG Lens for gain enhancement
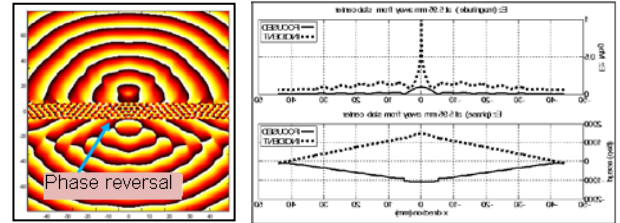
Electric field Magnitude and phase (transmission plane)

Figure 3. Image formation for DNG lens

An interesting metamaterial non-crosstalk structure with anisotropic properties, developed at RIT, is a cubical structure with multilayer metal-insulator stack-up, in the center of which are two groves cut orthogonal to each other [3]. With a dipole antenna as source, it is shown that propagation occurs along one direction and not in the orthogonal direction, Figure 3. Several unique applications using metamaterials, developed by various researchers, are available in the literature.
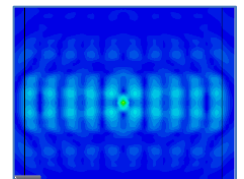
Figure 3 Anisotropic metamaterial, propagation in just one direction

III. CHALLENGES WITH HIGH POWER

Metamaterials have severe problems at high power because of dielectric breakdown and conductor heating Successful structures such as the split ring resonator (SRR) have been shown to fail with high power [4]. Research is underway for creating smart materials for high power applications. One of the techniques involves methods to reduce the maximum field enhancement factor, which is the ratio of the peak field in the structure to the incident field. Notable ones are the Sievenpiper high impedance metasurface [4] which does not allow ac currents within a forbidden frequency band. Researchers have determined that zero index and low index metamaterials are best suited for high power applications and can be designed to operate away from the magnetic resonance of the structure [5].

REFERENCES

[1] Choi J.H., Sun J.S. and Itoh T., "Frequency-Scanning phased array Feed Network based on composite right/left-handed transmission lines", IEEE Trans Microwave Theory & Tech, vol. 61, no. 8, August 2013

[2] Ali A. , Venkataraman J and Z. Lu, "Gain Enhancement of Patch Antenna Using Double Negative Superstrate Realized by a High Dielectric with Triangular Lattice of Holes," 2009 IEEE Antenna and Propagation Society International Symposium, p 934

[2] A. Khan, J. Venkataraman and Z. Lu, ""Non-crosstalk light propagation in anisotropic materials composed of multilayer metal-insulator stack" 2016 IEEE International Symposium, Antennas and Propagation (APSURSI), p983

[4] Sievenpiper et al, "High-impedance electromagnetic surfaces with a forbidden frequency band", IEEE Trans. Microw. Theory Techn., vol. 47, no. 11, pp. 2059–2074, Nov. 1999.

[5] Bossard et. al. "Mitigating Field Enhancement in metasurfaces and metamaterials for high-power microwave applications", IEEE Trans on Ant and Prop, Vol 64, Dec 2016.

Variation of E1 HEMP and IEMI Coupling to Cables

James Gilbert
Metatech Corporation
Goleta, CA, USA
James.Gilbert@metatechcorp.com

William Radasky
Metatech Corporation
Goleta, CA, USA
wradasky@aol.com

Abstract— The coupling of E1 HEMP incident electric fields to horizontal and vertical cables is dependent on the polarization and angle of incidence relative to the cable as well as the cable and ground parameters. Some of these factors are independent, but others are correlated due to the nature of the EMP generation mechanism. This presentation will show the statistical distributions that result when the variations in the coupling parameters are made in a physical manner.

Keywords-E1 HEMP, IEMI, cable coupling.

I.   INTRODUCTION

While it is straightforward to calculate the response of horizontal and vertical lines to E1 HEMP for a specific burst-line geometry, the calculation of peak current levels for varying burst locations is more difficult since the E1 EMP peak field, angle of incidence and polarization vary as a function of burst location. Fig. 1 shows the variation of peak magnitude for a burst in the middle of the continental US. The polarization also varied, with the field being nearly E-W horizontal in the high field intensity region to the south of the burst. This lowers the effect of buildup due to phasing along the line, and leads us to consider how the magnitude and polarization vary.
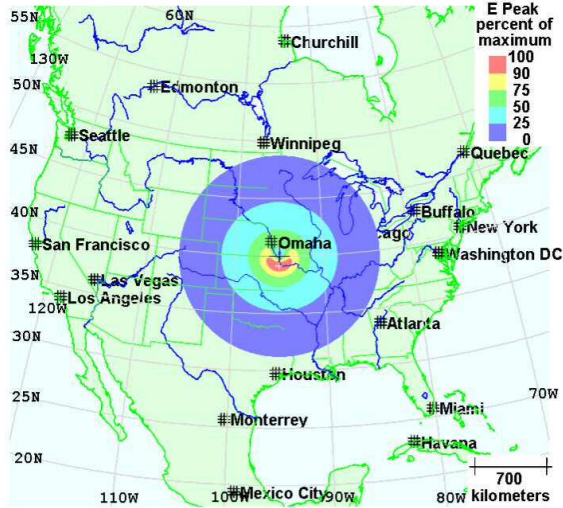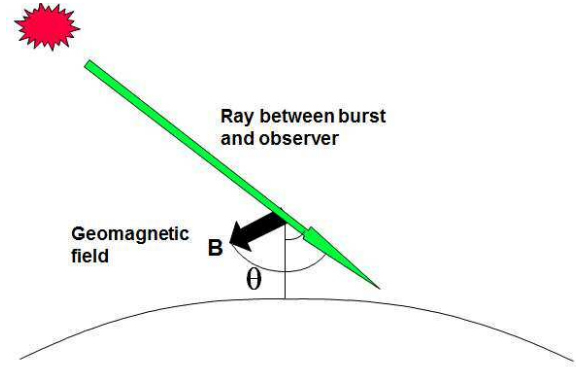

Figure 1.   Variation of E1 peak field amplitude from HEMP burst at 75 km altitude.

$$\vec{E} = \hat{\phi}\,\sin\theta\,f_1(r_g, t) + \hat{\theta}\,\sin\theta\,\cos\theta\,f_2(r_g, t)$$

Figure 2.   Symmetry of E1 HEMP electric field in ground range and geomagnetic field coordinates.

II.   SYMMETRY OF E1 HEMP FIELDS

Fig.2 shows the symmetry of E1 HEMP fields, the "smile" in Fig. 1 is produced by the interaction of terms dependent on the geomagnetic field direction (θ,φ) and terms depending on the ground range r_g. Both the E1 and the IEMI time histories are parameterized in the form

$$E = E_0 K \frac{e^{\alpha t}}{1+e^{(\alpha+\beta)t}} \qquad (1)$$

Where E_0 is the peak field, K is a normalizing constant and α and β are the rise rate and fall rate respectively. The IEC HEMP pulse has rise and pulse width times of 2.5 and 23 ns respectively, and the IEMI pulse has rise and fall times of 0.1 and 1 ns. For short cables, only the effect of f_1 needs to be taken into account.

III.   PARAMETER VARIATIONS

In this presentation we will show the probabilities of coupling from E1 HEMP and IEMI fields to short cables inside poorly shielded buildings, showing the variation for coupling to 1, 3, and 10 meter length horizontal cables at varying heights and vertical cables of the same length. The effects of varying the cable termination will also be shown.

Further Analysis of Shoreline Edge Effects for Stratified Grounds

James Gilbert
Metatech Corporation
Goleta, CA, USA
James.Gilbert@metatechcorp.com

Abstract— In this presentation we continue the development of the analysis of the ocean edge effect for geoelectric field enhancement in multilayer ground conductivities. In the ocean edge effect, the geoelectric fields resulting from a geomagnetic storm or MHD EMP are enhanced from those that would be present without the ocean. The layered geometries are computed numerically

Keywords-Geomagnetically induced current, GIC magnetic storms, Geomagnetic induction, MHD EMP

I. INTRODUCTION

The ocean edge effect occurs whenever a horizontal magnetic field resulting from a current source is applied near the edge of an ocean where the conductivity of the seawater is much higher than the conductivity of the underlying soil. This applied magnetic field results from ionospheric currents arising from geomagnetic storms or the magnetohydrodynamic (MHD) EMP from a high altitude nuclear explosion (also known as E3 HEMP). The presence of the ocean results in the reduction of the electric field in the ground beneath the ocean, but can either enhance or reduce the electric field in ground outside the ocean. Which of these two occurs depends on the orientation of the magnetic field relative to the shoreline. When the magnetic field is parallel to the shoreline, the inland geoelectric field near the edge is increased compared its magnitude if the ocean were not present, but when the magnetic field is perpendicular to the shoreline, the inland electric field near the edge is reduced compared to the it magnitude if the ocean were not present. For other orientations, the field must be resolved into the parallel and perpendicular components for analysis.

II. PREVIOUS ANALYSIS

We analyze the condition where the land has a constant slope entering the ocean, as shown in Fig.1. For a uniform ground conductivity, the behavior of the electric field near the edge was analyzed for a seawater conductivity of 4 S/m and a ground conductivity of 0.001 S/m numerically for realistic ground slopes ranging between 1/15 and 1/120. It was found for the parallel magnetic field case that the integral of the inland electric field in a scaled set of units ranged between 0.4724 and 0.4991 leading to a suspicion that the integral for the limiting case where the slope was
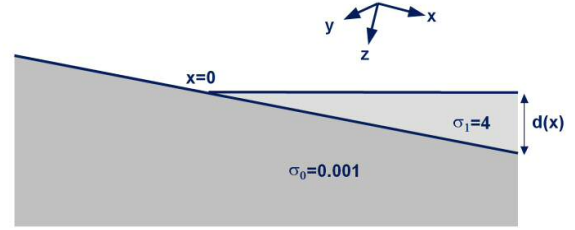
Figure 1. Geometry considered for magnetic field parallel to shoreline.

very small and the ocean conductivity was taken to be infinite that the integral would be exactly ½. An analytic analysis in [1] showed this to be true and gave a simple result for the spatial integral of the enhancement

$$\Delta V = \int_{-\infty}^{0} dx \left(E_i - Z_0 H_0 \right) = \frac{H_0}{2\sigma_0} \qquad (1)$$

where H_0 is the applied magnetic field and σ_0 is the ground conductivity.

III. CURRENT RESEARCH

Unfortunately, after extensive attempts to find an analytic solution for the layered geometry, we were forced to turn to numerical solutions. A preliminary analysis presented at EUROEM 2016 showed the enhancement effect could be calculated for stratified ground and parameterized in two parameters when the time behavior is expressed in terms of the Laplace variable s. The first is the ratio of the conductivity in the lower layer to that of the upper layer. The second is the depth of the boundary between the two conductive layers. In the presentation we will show more detailed results for the enhancement effects for the magnetic field parallel to the shoreline and show results for the reduction case with the magnetic field perpendicular to the shoreline. We will also show the fitting for the two effects and discuss the transformation back into the time domain.

REFERENCES
[1] J. L. Gilbert, "Modeling the effect of the ocean-land interface on induced electric fields during geomagnetic storms" in Space Weather, vol. 3, no 4. S04A03, doi: 10.1029/2004SW000120, 2005.

Insertion Loss Free Measuring Antenna

L. Duvillaret[1] et al.

[1]Kapteos,
Ste-Hélène du Lac, France
contact@kapteos.com

G. Gaborit[1,2]
[2]IMEP-LAHC
Université Savoie Mont-Blanc
Le Bourget-du-Lac, France
gwenael.gaborit@univ-savoie.fr

Abstract— Measuring High Power ElectroMagnetics requires ultra wide band measuring antennas but also long distance remote data acquisition system in order to put the digitizer in a safe location where the electromagnetic field strength is low enough. When dealing with frequencies ranging up to tens of GHz, the problem becomes tricky with classical electric antennas as the price and the losses of long RF cables becomes huge. Moreover, one must deal with cable insertion loss which is subject to change when installing the cable in outdoor conditions. We present here a solution that permits to get rid of insertion loss variations, that requires no time consuming with repetitive calibrations and that brings also a measurement stability of 0.01 dB during a temperature drop of several tens of Celsius degrees.

Electromagnetic Field; Optical Sensor; Metrology; Harsh Environment; Antenna Factor

I. INTRODUCTION

When dealing with metrological measurement of electromagnetic (EM) waves, the key feature is the antenna factor AF_{ant} that links (see Eq. (1)) the absolute value of the electric field E measured at the antenna location with the voltage V_{out} delivered by the antenna.

$$E = AF_{ant}(f) \cdot V_{out} \qquad (1)$$

Depending on the bandwidth covered by the antenna, the antenna factor is more or less dependent on frequency f but is also strongly linked to the RF cable or waveguide used to connect the antenna to the data acquisition system. The higher the frequency and the longer the cable, the higher will be the insertion loss (IL) and also its frequency dependence. Obviously, the cable IL can be calibrated. However, when dealing with outdoor conditions or more generally in harsh environment, such a calibration is not straightforward and at least two calibrations have to be carried out to check if the cable integrity has not been compromised during use. If these two calibrations performed prior and after the cable use do not give the same results, a new measurement is usually required with two new calibrations using either the same cable or of a new cable. Such a procedure is time consuming and if not followed, serious doubts on the validity of the measurement results will remain.

II. A MEASURING ANTENNA WITH INSERTION LOSS REAL-TIME CORRECTION

A. Principle

In order to get a real-time and automatic correction of the cable IL between the measuring antenna and the data acquisition system, two conditions are required:

(1) having a signal proportional to the IL,
(2) having IL independent of the frequency.

Indeed, if such two conditions are fulfilled, then the antenna factor $AF_{set}(f)$ of the set "antenna + cable" is simply given by:

$$AF_{set}(f) = AF_{ant}(f) + IL_{cable} \qquad (2)$$

where antenna factors are expressed in dB/m and IL in dB.

B. Proposed Solution

An optical fiber with a laser carrier modulated at the RF signal fulfills condition 2: typical IL is of the order of 1 dB/km at the frequency of 100 MHz as at the frequency of 40 GHz. An optical sensor based on the polarization state modulation [1] of a laser beam crossing an electro-optic crystal fulfills condition 1 as the average optical power is directly linked to the IL. During the conference, we will present results carried out at frequencies up to 10 GHz with a 100-m optical fiber link that requires no prior calibration nor post calibration and real-time correction of any IL variation. With a shorter 15-m optical fiber link at 4 GHz, we will present measurements showing a 0.01 dB signal stability during temperature drop of several tens of Celsius degrees applied to a few meters of the optical fiber link through the use of a freeze spray.

REFERENCES

[1] L. Duvillaret, S. Rialland, and J.-L. Coutaz, "Electro-optic sensors for electric field measurements. I. Theoretical comparison among different modulation techniques," J. Opt. Soc. Am. B, vol. 19, pp. 2692–2703, November 2002.

Issues Related with use of FDTD in Return-stroke Modeling

Rupam Pal
Department of Electrical Engineering
Indian Institute of Science
Email: palrupam@ee.iisc.ernet.in

Udaya Kumar
Department of Electrical Engineering
Indian Institute of Science
Email: uday@hve.iisc.ernet.in

Abstract— **In the recent past, a self-consistent return stroke model was proposed which could provide a deeper insight into some of the salient aspects of the phenomenon. The use of thin-wire formulation for the required computation of the dynamic field has limited its application and as a result, dispersive and non-linear media like soil could not be handled. The FDTD for field computation can overcome the problem, however large aspect-ratio and other salient features needs to be suitably handled. The thin core of the channel is handled with sub-cell approach with suitable modification for the finite conductivity. The non-conforming corona-sheath also requires special attention. Further, the field produced by the charge deposited in the corona sheath needs to be suitably incorporated in the FDTD formulation. The present work basically deals with the above listed problems. Suitable validation is provided with time-domain thin wire formulation.**

Index Terms—**Lightning , FDTD , Sub-cell modeling, Return Stroke**

I. Introduction

Modeling of the return stroke current evolution not only can aid in a better understanding of the phenomena but also finds relevance in lightning protection engineering. In the recent past, a self-consistent model for the return stroke current evolution has been presented[1] and it has been successfully applied to a few problems of practical relevance. Accordingly, one of the important aspect in modeling is an accurate evolution of the associated dynamic electromagnetic field.

Considering the large aspect ratio of the problem and a requirement on fine spatial resolution, a time-domain thin-wire formulation for the electric field integral equation was adopted in the earlier work [1]. As the required discretization is limited to the channel, it was much simpler to formulate. However, it was limited to perfectly conducting ground and hence realistic soil and buried conductors and cables could not be represented.

On the other hand, the domain based method like the Finite-Difference Time-Domain (FDTD) can, in principle, overcome the problem of modelling realistic ground and buried objects. In fact, it has been already employed to evaluate the current induced in buried cable during a strike to nearby tower. However, there are many difficulties that needs to be overcome in employing FDTD for the desired field computation in the modelling. This work basically aims to address most of them, perhaps by employing the techniques whenever they are available.

II. Formulation

Certain level of simplification would be necessary, which would be in line with that is being presently employed [1]. The channel is considered to be vertically straight and cloud-end dynamics are neglected.

A. Sub-cell approach

In order to model the channel core, whose radii is less than $1-2cm$, a sub cell based approach is essential. Otherwise, the discretization required would be unmanageable. Noting that the core has a non-linear conductance, suitable modification is employed to represent the same.

B. Modeling of the corona sheath

The channel core is always surrounded by a corona sheath, which holds almost all the charge of the leader. Its radius can span up to several meters to tens of meters. The model for the charge neutralization in corona sheath employed are, a dissipative media [1] and charge neutralizing wave . In any case, its boundary does not conform to any FDTD grid and hence special approach is required, which has to integrate with the sub-cell approach. To start with , it is represented as a lossy media.

C. Initial charge on the corona sheath

The quasi-static electric field produced by the charge lowered during the downward leader phase is the main source for the return stroke evolution. However, FDTD algorithm is not well suited for representing the static field. In fact, the spatial discretisation employed by FDTD can lead to spurious currents. A special technique has been attempted to overcome this issue.

III. Results and Discussions

After adopting/developing suitable approaches, validation is carried out with the MoM based thin-wire code. Long term stability is also verified.

References

[1] Rosy Balaram Raysaha and Udaya Kumar. "A Macroscopic Model for First Return Stroke of Lightning". In: *IEEE Trans. on Electromagnetic Compatibility* 53.3 (August,2011).

Switches for High Power Electromagnetics:
A Survey

Jane Lehr
University of New Mexico
Albuquerque, NM 87131-0001
jmlehr@unm.edu

Abstract— High performance, triggered switches are a key enabling technology for many high power electromagnetic applications such as steerable, powerful and compact antenna arrays as well as emerging technologies such as high power arbitrary waveform generators.   Moreover, there is a widespread trend toward utilizing highly modular units synchronized in time to replace the conventional single, very high peak power devices. This in turn, shifts the performance requirement to the switching elements. Here we survey the state of the art in switches appropriate for high power electromagnetics applications. Both spark gaps as well as emerging devices using wide bandgap semiconductors will be addressed.

Keywords- spark gaps, laser triggered spark gaps, photoconductive solid state switches (PCSS).

I.   INTRODUCTION

The control of transient pulses is vital to many applications of high power electromagnetics. Traditionally, the primary interest has been in arrays for peak power multiplication but now also include advanced pulse shaping for applications as diverse as materials studies and beam steering. This follows a trend away from single large peak power sources to highly modular device configurations. This paradigm shift, while seemingly straightforward, imposes new constraints on the system.

II. TRIGGERED SPARK GAPS

Spark gaps remain the switch of choice for very high power applications. Yet despite their long history, their performance in the triggered state continues to yield surprises. In their triggered state, important new insights have been gained regarding their performance.[1] In aggregate systems, proximity effects of individually triggered modules results in a wider voltage operating range requirement for the spark gap switch. [2] This will be explored in detail. The consequence of this added complexity is a severe increase in the system cost.

Recent advances in spark gap technology include performance enhancements which can be achieved by sectioning, such as in cascading [1] or by the introduction of a corona discharge [3] prior to switching and the emergence of very compact or sealed switch designs. New switching gases with low Global Warming Potential will be discussed.

III. HIGH POWER SEMICONDUCTOR SWITCHES

Tremendous changes have occurred in the semiconductor switch regime. In particular, switches made of semiconductors with very wide bandgaps, fueled by the rapid growth of wireless communications, has resulted in low loss, high-power RF switches for multifunction antenna systems. Commercial power electronics relies on silicon-based thyristors or IGBTs for power conversion.[4] Recently available Silicon Light-triggered thyristors (LTTs) have been developed [5] but suffer from slow switching speeds (hundreds of µs) and limit systems to very low switching frequencies. Wide-bandgap (WBG) semiconductor materials such as Gallium Nitride (GaN) and Silicon Carbide (SiC) [6] are being developed and have demonstrated significant performance improvements beyond what silicon can deliver. A survey of the relative merits of the key semiconductor technologies – Si, GaAs, SiC, and GaN –is presented along with a synopsis and applicability of commercial switches.

A review of photoconductive solid state switches (PCSS) and their modes of operation will be presented. Although present research in wide-bandgap photoswitches is concentrated predominantly in continuous wave applications, their applicability for pulsed applications is recognized. The emerging area of reconfigurable antennas has introduced a new way of thinking regarding switches as well as other auxiliary elements such as MEMS.

In this survey, the basic operation, performance parameters and limitations of various high power switches – both spark gaps, widebandgap photoswitches and hybrid designs –with potential for high pulse repetition rate operation are compared and contrasted.

REFERENCES

[1] J.M. Lehr, et.al., "Evaluation of spark gaps switches operated at low percents of self break voltage, presented at the Int. Pulsed Power Conf., 2009.

[2] S.F. Glover, et. al, "Genesis: A 5-MA Programmable Pulsed-Power Driver for Isentropic Compression Experiments," IEEE Trans. Plas. Sci., Vol. 38, Iss. 10, pp. 2620 – 2626, October, 2010.

 [3] J.R. Beveridege, S.J. MacGregor, M.J. Given, I.V. Timoshkin and J.M. Lehr, "A Corona-Stabilised Plasma Closing Switch," IEEE Trans. Diel. Elect. Insul, Vol. 16, Issue No. 4, pp 948-955, August 2009.

[4] Schenk, "State of the Art Bipolar Semiconductors for Very High Power Applications," in PCIM Europe, Nuremberg, Germany, 2015.

[5] Infineon, "540A/8kV Light-Triggered thyristor: For static var compensation and medium-voltage drives".

[5] Millan, "A survey of Wide Bandgap Power Semiconductor Devices," IEEE Trans.Power Elect., 2014.

[6] Hubbard, "High-resistivity GaN buffer templates and their optimization for GaN-based HFETs," *Journal of Crystal Growth,* vol. 284, no. 3-4, 2005.

Modelling EM-coupling on a Massively Composite Aircraft

J-P. Parmantier*[1], I Junqua[1], S. Bertuol[1], T. Volpert[1], Walid Dyab[2], Ahmed Sakr[2], Ke Wu[2], C. Girard[3], G. Prin[3], A. Guidoni[4], G. Samarone[4], F. Moupfouma[5], W. Tse[5], K. Nuyten[6] and A. Blommers[6]

(1) ONERA – The French Aerospace Lab, F-31055, Toulouse, France, http://www.onera.fr/en,
*jean-philippe.parmantier@onera.fr

(2) Ecole Polytechnique de Montreal, PO Box 6079 Station "Downtown", Montréal H3C 3A7, Canada

(3) AXESSIM, Parc d'innovation, Rue Jean Sapidus, Bâtiment le Pythagore, 67400 Illkirch-Graffenstaden, France

(4) IDS, Via Enrica Calabresi, 24, PISA 56121, Italy

(5) Bombardier Aerospace, 2351 Boulevard Alfred Nobel, H4S 2A9 St Laurent Que/ Canada

(6) Fokker Elmo B.V., P.O. Box 75, 4630 AB Hoogerheide, the Netherlands

Abstract— Analysis of EM coupling on massively composite aircraft requires specific modelling techniques with respect to the frequency range under study. In particular, usual scalable modeling techniques used for metallic structures have to be adapted and sometimes revised. In this paper, we present the challenges of such modelling strategies as they are addressed in an EU-Canada cooperative project called "EPICEA".

Keywords- EM-coupling, full composite aircraft, bonding, grounding, common-mode impedance

I.   INTRODUCTION

Composite lightweight materials, electrification of functions onboard aircraft and operations at higher altitude/latitude are parts of the fundamental levers for optimizing the performance of existing and future generations of commercial aircraft. However, this results in the exacerbation of Electromagnetic (EM) hazards. Specific protection measures are therefore required to guarantee safe electrical systems but they generally lead to weight penalty and refrain the emergence of new-concepts of energy-efficient Composite Electric Aircraft (CEA). Hence, the development and optimization of electrical systems integration is crucial for CEA.

EPICEA (Electromagnetic Platform for lightweight Integration/Installation of electrical systems in Composite Electrical Aircraft) is a H2020 project co-funded by Europe and Canada which started in February 2016 and will run for 36 months [1]. It has a consortium of 9 partners led by ONERA for Europe and "Polytechnique de Montreal" for Canada. The project intends to release, validate and verify a single computer environment (i.e. the EPICEA platform) helping to understand Electromagnetic issues on Composite Electric Aircraft (CEA). The EPICEA project compiles a complete set of EM issues on CEA, including EM coupling on Interconnected Systems (IS) and Cosmic Radiations on electrical systems together with new concepts of low-profile antennas designed to maintain drag performance in composite environment. In this paper, we focus on the activity dedicated to EM coupling on IS and give an overview of challenges with respect to this topic.

II.   IS EM-COUPLING MODELS AND VALIDATIONS

EM coupling models on IS must cover a wide frequency range extending from DC up to 18 GHz as recommended for Lightning Indirect effects (LIE) and High Intensity Radiated Fields (HIRF) aeronautical standards. Very different EM coupling problems on cable interconnects have therefore to be addressed together with this full composite aircraft issue: the common mode impedance and the design of current return networks both for signals and lightning at low frequency, the propagation on IS in presence of a composite reference ground at medium frequency, the absorption of energy by the lossy walls in cavities at very high frequency,

On the one hand, EPICEA numerical simulation results are compared against full wave simulations applied on Numerical Test Cases (NTCs) of increasing complexity. On the other hand, and more ambitiously, they are compared against measurements. For this purpose, the EPICEA barrel, consisting of a scale one full-composite business fuselage aircraft is provided by Bombardier Aerospace (Figure 1). It is equipped with a prototype IS provided by Fokker Elmo and dummy equipment boxes provided by ONERA. The simulations are done with commercial EM software packages as well as homemade computer codes, some of them especially plugged into the EPICEA computer platform.

The final presentation will update the content of this paper with currently available results of the project at the time of the presentation.

Figure 1. The EPICEA composite barrel (courtesy Bombardier Aerospace)

REFERENCES
[1] Electromagnetic Platform for Lightweight Integration/ Installation of Electrical Systems in Composite Electric Aircrafts, EPICEA, http://epicea-env714.eu/ .

A Study of Upward Flashes Initiated at the Säntis Tower

R. Daher [1], M. Azadifar[1], A. Smorgonskiy [2], Jacques Zuber[2], M. Rubinstein[2], G. Diendorfer[3], F. Rachidi[1]

[1] Swiss Federal Institute of Technology (EPFL), Lausanne, Switzerland

[2] University of Applied Sciences of Western Switzerland, Yverdon-les-Bains, Switzerland

[3] OVE Service GmbH, ALDIS, Vienna, Austria

roy.daher@epfl.ch, mohammad.azadifar@epfl.ch, alexander.smorgonskiy@epfl.ch,
jacques.zuber@heig-vd.ch, marcos.rubinstein@heig-vd.ch, g.diendorfer@ove.at, farhad.rachidi@epfl.ch

Abstract— In this paper, we present an analysis on upward negative flashes recorded at the Säntis Tower. The effect of time and distance constrains on the percentage of other-triggered versus self-triggered events is discussed. The results show that the majority of the upward flashes are self-triggered which is in agreement with previous studies conducted for towers located in the Alps region. The study features in addition a test of the causality relation between upward flashes and preceding nearby lightning activity. Investigation on correlated meteorological measurements reveals on average higher temperature values for flashes preceded by prior activity (other-triggered events) compared to self-triggered flashes.

Keywords- Upward lightning, self-triggered flashes, other-triggered flashes, Säntis Tower, lightning current measurement

I. DATA

Upward lightning flashes originated from tall elevated objects are classified into the so-called self-triggered and other-triggered events (e.g., [1][2]). A 'self-triggered' flash is a tower flash that is not preceded by lightning within a predefined area around the tower and within a given time interval prior to the tower flash. An 'other-triggered' flash is a tower flash preceded by cloud-to-ground or cloud flash activity within a predefined distance to the tower and within a prior time interval. The causality relation between other-triggered flashes and the preceding activity has not been established [3]. The recorded upward negative flashes recorded at the Säntis Tower [4] in the time period from 2010 to 2013 were analyzed in this study. The preceding events are determined using the provided data by European Lightning Location Network (EUCLID) [5].

II. RESULTS

Using a time interval of 5 s and a circular area of 30 km around the Säntis Tower, 92 out of the 118 (78%) analyzed upward flashes were found to be self-triggered while 26 (22%) were classified as other-triggered.

Concerning the polarity of the flashes, 24 out of the 26 other-triggered flashes were initiated by discharges of the opposite polarity (positive), which is consistent with the observations at the Gaisberg Tower [1].

In addition, the causality relation between preceding nearby flashes and upward flashes from the tower was tested by examining the events that occurred after the tower flash as proposed in [3]. Using the same time and space constraints chosen for the preceding flashes, 12 out of the 118 (10%) upward events exhibited post-tower-flash lightning activity.

Interestingly, only 4 out of the 92 (5%) self-triggered flashes were followed by lightning discharges. This leads to the conclusion that it is less likely for post-tower-flash lightning activity to occur if the tower flash was self-triggered. However, due to insufficient number of other-triggered events with post-flashes (flashes occurring after an upward tower discharge) in the period of analysis, no definitive conclusion can be made concerning any causality relation between upward flashes and nearby lightning activities.

The meteorological conditions at the time of the tower strikes were also investigated, with a focus on temperature variation, precipitation and wind speed. It was found that most of the other-triggered flashes occurred during warmer weather than self-initiated ones (mean temperature of $+8.7^{\circ}C$ and $+2.1^{\circ}C$, respectively), which is similar to the analysis performed on the Gaisberg Tower in Austria [1].

REFERENCES

[1] A. Smorgonskiy, A. Tajalli, F. Rachidi, M. Rubinstien, G. Diendorfenbr and H. Pichler. An analysis of the initiation of upward flashes from tall towers with particular reference to Gaisberg and Säntis towers. *Journal of Atmospheric and Solar-Terrestrial Physics*, 2015.

[2] D. Wang and N. Takagi, Characteristics of winter lightning that occurred on a windmill and its lightning protection tower in Japan, *IEEJ Trans. Power Energy*, **132**(6), 568–572, 2012.

[3] M. Rubinstein, J. Zuber, A. Smorgonskiy, F. Rachidi and G. Diendorfer. Correlation vs. causality in other-triggered upward lightning in tower flashes. 2016.

[4] C. Romero, M. Paolone, M. Rubinstein, F. Rachidi, A. Rubinstein, G. Diendorfer, W. Schulz, B. Daout, A. Kälin, P. Zweiacker, "A system for the measurements of lightning currents at the Säntis Tower", *Electric Power Systems Research*, vol. 82, num. 1, p. 34-43, 2012.

[5] W. Schulz, G. Diendorfer, S. Pedeboy, and D. R. Poelman, "The European lightning location system EUCLID - Part 1: Performance analysis and validation," Nat. Hazards Earth Syst. Sci., 16, 595-605, doi:10.5194/nhess-16-595-2016, 2016.

Enforcing Delayed Causality Through Spectrum Extrapolation

J. Becerra, F. Vega
Dept. of electric and electronic engineering
Universidad nacional de Colombia
Bogotá, Colombia
jmbecerrat@unal.edu.co, jfvegas@unal.edu.co

F. Rachidi
EMC laboratory
Swiss Federal Institute of Technology (EPFL)
Lausanne, Switzerland
farhad.rachidi@epfl.ch

Abstract— Delayed causality is a crucial property of real systems that must be accounted for in transient simulations. This paper presents a method for enforcing delayed causality that mitigates the phase distortion created by common enforcing methods.

Keywords; Causality enforcement; transient simulation

I. INTRODUCTION

Passive structures, such as transmission lines, produce delays on any signal that propagates through them. In the time domain, this means that the impulse response is different from zero after a positive delay   . This characteristic is known as delayed causality and is especially important when representing distributed systems in transient simulations, since ignoring it causes significant errors [1].

The common process for representing delayed causality in time domain through the impulse response involves the following steps [1]: (i) Decomposing the transfer function (TF) into minimum phase (MP) and all-pass (AP) components, (ii) extracting the delay   from the AP component, (iii) obtaining the MP impulse response by applying the Inverse Discrete Fourier transform (IDFT), and (iv) enforcing the delay over the MP impulse response.

Note that only integer multiples of the sampling time can be used to represent the delay in time domain. This causes differences between the original TF and the TF of the delayed MP impulse response, which are seen as phase distortion. Thus, large phase distortion means that that the delayed impulse response does not represent accurately the original TF, leading to erroneous transient simulations.

A method for obtaining causal impulse responses through spectrum extrapolation was presented in [2]. However, the impulse responses obtained by this method do not account for delayed causality.

In this paper, we extend the method proposed in [2] to include delayed causality and mitigate the phase distortion in the frequency domain.

II. PROPOSED METHOD

The proposed method is composed of the following steps: (i) Performing MP/AP decomposition, (ii) extracting the delay   from the AP phase, (iii) selecting the new Nyquist frequency of the extrapolated spectrum, which must be a multiple of the original frequency resolution, (iv) computing the extrapolated sampling time   as the nearest multiple of   , (v) removing the time delay due to   from the original transfer function; (vi) extrapolating the resultant transfer function, and (vii) applying the IDFT and the delay   to obtain the impulse response.

III. EXAMPLE

Consider the S_{21} parameter of a transmission line composed of two parallel coated wires. The line length is 10 m, the inner conductor radius is 0.91 mm, the wire coating thickness is 0.61 mm, and the distance between the two wires is 10 mm. The conductivity of the wires is 5.8×10^7 S/m, whereas the conductivity and relative permittivity of the coating are 1.85×10^{-12} S/m and 2.3, respectively.

The S_{21} parameter was discretized up to 50 MHz with 4097 points. On the other hand, the proposed method was applied with an extrapolation up to 70 MHz. The differences among the approaches in the frequency domain are shown in Fig. 1. The phase distortion resulting from commonly-used enforcement method can be clearly seen. On the other hand, the phase obtained using our method shows excellent agreement with the original phase.
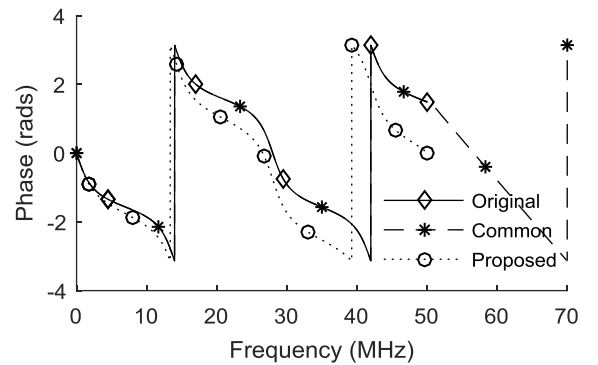

Figure 1. Phase of the original and resulting S_{21} after applying the commonly-used enforcement method and the method proposed in this work.

REFERENCES

[1] R. Mandrekar, K. Srinivasan, E. Engin, and M. Swminathan, "Causality Enforcement in Transient Co-Simulation of Signal and Power Delivery Networks," , vol. 30, no. 2, pp. 270–278, May 2007.

[2] J. Becerra, F. Vega, and F. Rachidi, "Extrapolation of a Truncated Spectrum With Hilbert Transform for Obtaining Causal Impulse Responses," , vol. PP, no. 99, pp. 1–7, 2016.

Electromagnetic Simulation of an Integrated Antenna-Source with Directional Antenna Beam Patterns

Kiho Kim*, Jiheon Ryu*, Jeonghyeon Kuk*, Jin Soo Choi*

* Agency for Defense Development, Daejeon, Republic of Korea

Abstract

In this paper, an integrated antenna-source (IAS) with directional antenna beam patterns is designed to reduce the intensity of the electromagnetic pulses radiated to the opposite site of the reflector. We simulated the electric field waveforms from the angle of 0˚ to 350˚ for the directional IAS by using CST MWS. The results show the peak electric field strength of 0.062V/m at a distance of 100m where the excited pulse has an amplitude of 1V.

Keywords: Integrated Antenna-Source (IAS), high power radiation, high-power electromagnetics (HPEM), ultra-wideband (UWB).

1 Introduction

High Power Wideband Radiators have been studied for a number of applications such as high-power electromagnetic (HPEM) effect testing [1]. We presented a high directional paraboloidal reflector antenna illuminated by an integrated antenna-source (IAS) with high ultra-wideband (UWB) gain [2]. In this paper, we propose a directional IAS to reduce the beam spill-over. In the following, electromagnetic simulation results of the directional IAS are presented.

2 Electromagnetic Simulation Results
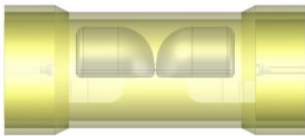
Figure 1. Simulation model of the directional IAS.

As shown in Fig. 1, we propose a modified IAS. The two electrodes are truncated. Two dielectric posts are employed to install the electrodes in the high-pressure gas case. We simulated the proposed IAS by using CST MWS [3]. Fig. 2 shows the simulated electric field waveforms and beam patterns of the directional IAS. The peak electric field is maximum at 0˚. The peak electric field decreases with the angle. Fig. 3 shows the simulation result of the directional IAS with a paraboloidal reflector. The peak electric field strength at 100m is 0.062V/m where the excited pulse has an amplitude of 1V. The UWB gain is 6.2. This value is approximately same as the UWB gain, i.e., 6.6 of omni-directional IAS with the reflector.
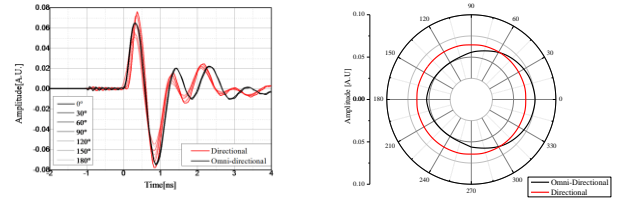
Figure 2. Simulated electric field waveforms and beam patterns of the directional IAS for the different angles.
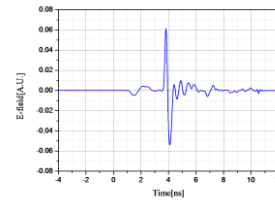

Figure 3. Simulated E-field waveform of the IAS with the paraboloidal reflector.

3 Conclusion

In this paper, a directional IAS is designed to reduce the intensity of the electromagnetic pulses radiated to the opposite site of the reflector. The simulation results show that the directional IAS with a paraboloidal reflector has the peak electric field strength of 0.062V/m at a distance of 100m where the excited pulse has an amplitude of 1V.

References

[1] Jiheon Ryu, Jongwon Lee, "An Integrated Antenna-Source System of Very High Ultra Wide-Band Gain for Radiating High-Power Wide-Band Pulses", IEEE Transactions on Plasma Science, Vol. 40, No. 4, pp 1019-1026.

[2] Jiheon Ryu et al., "A High Directive Paraboloidal Reflector Antenna for High Far Voltage in an Ultra Wideband Source System", IEEE Transactions on Plasma Science, Vol. 41, No. 8, pp 2283-2290.

[3] Jiheon Ryu, "Electromagnetic Transient Simulation of Spark-Gap Switched Pulse Generators for Predicting Pulse Waveforms", IEEE Transactions on Plasma Science, Vol. 42, No. 9, pp 2193-2197.

Study of the Active Energy Coupling Circuit of Gas Discharge Tube

Sun Wei, Han Pei
School of Mechanical and Electrical Engineering
Xi'an University of Architecture and Technology
Xi'an, Shaanxi, China
sunwei65@126.com

Sun Jinru, Chen Jingliang
State Key Laboratory of Electrical Insulation and Power Equipment
Xi'an Jiaotong University
Xi'an, Shaanxi, China
jinru2014sun@163.com

Abstract

A micro active gas surge protective gap and energy coupling circuit was investigated. The experimental results show that the voltage ratio K of MAGSPG decreased to sixty percent of that of SPG (Surge Protective Gap) with no active coupling circuit.

Keywords: trigger; active gas surge protection gap (AGSPG); voltage ratio; protection level; energy cooperation

I. THR STRUCTURE OF MAGSPG

The structure of MAGSPG is showed in Fig.1.
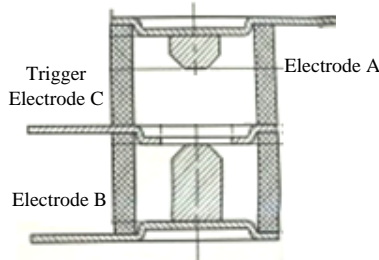
Figure 1. Structure of the MAGSPG

MAGSPG mainly consists of an anode A, cathode B and a coupling trigger electrode C. Electrodes A and B are made of brass with diameter of 5mm and surface curved 45 degree. The lengths of electrode A and B are 2.3mm and 5.4mm respectively. The trigger electrode, which is circular electrode with a 7mm hole and 1mm thickness, is installed in the middle of the MAGSPG. The all electrodes are enclosed into a ceramic insulation shell which inner diameter is 9mm and outer diameter is 12mm. the working environment is argon and the pressure is degree of 10^4Pa.

II. THE PROTECTION CHARACTERISTICS OF MAGSPG

Fig. 2 is the test circuit for measuring the impulse breakdown voltage.
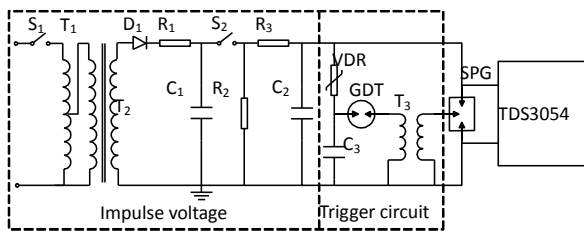
Figure 2. Test circuit of protection characteristics of MAGSPG

Active coupling trigger circuits are designed, and the circuit parameters are showed in Table I.

Table I. Parameters of trigger circuit

Parameter / Coupling No.	U_{1mA}/kV	U_{BDC}/kV	C/pF
1	2	1	200
2	2	2.8	200
3	2	3.4	200

The protection characteristics of MAGSPG Fig.3 shown in describe the relations between the impulse voltage, voltage ratio and discharging voltage of 1.2/50 impulse voltage.
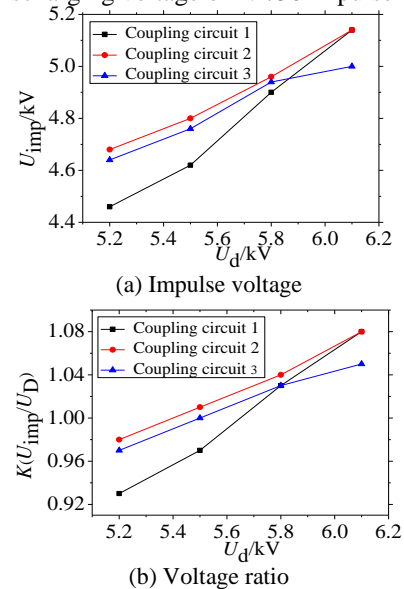

(a) Impulse voltage

(b) Voltage ratio

Figure 3. Protection characteristics of MAGSPG

III. CONCLUSION

This paper describes the design of MAGSPG, the voltage ratio of MAGSPG changes between 0.92-1.1. Comparing to SPG without active coupling trigger circuit, the voltage ratio decreases from 1.7 to about 1, the voltage protection level is improved greatly.

REFERENCES

[1] Lai J, Martzloff F D. Coordinating Cascaded Surge Protection Devices: High-Low versus Low-High[J]. IEEE TRANSACTIONS ON INDUSTRY APPLICATIONS, 1993, 29(4):680-687.

[2] Chrysanthos C, Boksiner J. Analysis of Coordination Between Primary and Secondary Protectors[J]. IEEE Transactions on Power Delivery, 1997, 12(4):1501-1507.

[3] He J, Yuan Z, Xu J, et al. Evaluation of the Effective Protection Distance of Low-Voltage SPD to Equipment[J]. IEEE Transactions on Power Delivery, 2005, 20(1):123-130.

The Performance and Test Methods for Lightning Direct Effect of Optical Ground Wires

Sun Jinru, Yao Xueling, Xu Wenjun, Chen jingliang
State Key Laboratory of Electrical Insulation and Power Equipment
Xi'an Jiaotong University
Xi'an, Shaanxi, China
jinru2014sun@163.com

Abstract
The lightning strike damage of OPGW under variable DC currents and discharge gaps are evaluated to explore the mechanism of lightning direct effect and conducting performance of OPGW. It is found that the erosion degree of aluminum-clad steel wire increases with the transfer charge of DC current increasing. With the increment in discharge gap, the temperature rise of OPGW decreases and the lightning damage degree is reduced.

Keywords: OPGW; lightning direct effect; transfer charge; discharge gap; temperature distribution

I. INTRODUCTION

The optical ground wire (OPGW) is widely used in power system as the signal transmission line and lightning protection line, which is suffered from the lightning strike occasionally [1-2]. The standard of IEC 60794 [3] stipulates the lightning test by four lightning components. But only the low-amplitude, long-duration continuous current is retained in revised standard [4]. However, the lightning strike test with current component C only cannot accurately characterize the lightning direct effect of OPGW [5-7]. In this paper, the impulse current component B (60/600μs) is used as the lead component of the DC component C. The mechanism of lightning direct effect and conducting performance of OPGW are studied with different DC current peak and discharge gaps.

II. EXPERIMENTAL PLATFORM AND METHOD

1 - Turnbuckle; 2 - Insulator; 3 - Anchoring clamps; 4 - Symmetric earthing connectors;
5 - Electrode with plane surface referring copper; 6 - Metal fuse for ignition;
7 - Tension meter; 8 - Gap between electrode and cable surface; generator;
9 - Lightning current; 10 - Rogowski coil; A - OPGW test samples
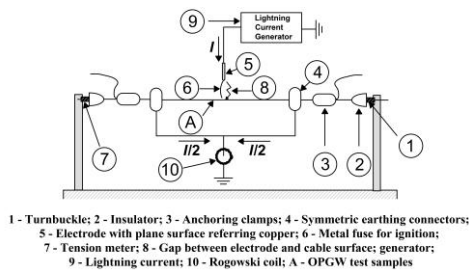
Figure 1. Lightning test device

The testing device is showed in Fig.1.

III. RESULTS AND DISCUSSION

A. Influence of charge transfer of C-component

Table I. The test waveform parameters, *d*=5cm

No.	Current B	Current C		
	I_p/kA	I_{av}/A	T_l/s	Q_C/C
A1	2.179	126.1	0.5283	66.08
A2	2.160	230.7	0.5245	120.3
A3	2.157	397.8	0.5256	206.7

Fig.2 shows the test results in the test condition in Table I.

(a) Sample A1   (b) Sample A2   (c) Sample A3
Figure.2 The damage of OPGW samples A1-A3 (*d*=5mm)

With the transfer charge and injection energy increases, the melting and ablation degree of strands is increasing. Some strands are melting to bond together or burning to break when the injection charge reaches 200C.

The temperature after lightning was measured by infrared thermometer. From relation between temperature and the charge transfer, we find the temperature increases with the increasing of charge transfer from current component C. We can estimate the instantaneous temperature of the OPGW surface after lightning strike to be 7425 °C.

B. Influence of discharge gap

The discharge gap is increased to *d*=6cm, while the conditions are unchanged. The lightning damage results of OPGW are showed in Fig.3 (*d*=6cm).

(a) Sample B1   (b) Sample B2   (c) Sample B3
Figure.3 The damage of OPGW samples B1-B3 (*d*=6mm)

It can be seen that with the increment of transfer charge, the melting and ablation degree on aluminum-clad steel wire is intensified. When the discharge gap *d* increases to 6cm, the temperature of the OPGW surface decreases and the damage degree is lightened. With the charge transfer of 200C, when *d*=5cm, serious melting and fracture occurred strands. While under the same lightning strike, the depth and degree of the melting and deformation lightning damage are relatively small with *d*=6cm. It can be explained that with the reduction of the discharge gap, the lightning energy is injected more spatially concentrated to the strands of OPGW, which will result in more serious erosion damage and higher temperature.

IV CONCLUSIONS

Based on the analysis of current standards and researches for lightning test of OPGW, the lightning component B and C are applied to the OPGW successively. It is found the ablation degree and surface temperature rise are increasing with the increment of transfer charge. The temperature of the OPGW after lightning strike reaches more than 7400 ° C with the charge transfer of 200C. With the increasing discharge gap, the temperature rise and damage degree of OPGW are both reduced, which may be related to the dispersal characteristics of the lightning current energy on the OPGW.

REFERENCES
[1] Fu Binlan．Electric Power，2005，38(10)：29-33．
[2] M. Yokoya, et al. IEEE Trans. PWRD-9 No.3, July 1994.
[3] IEC 60794-4-1-1999.
[4] IEC 60794-4-2003.
[5] Hu Yi, et al. High Voltage Engineering, 2005, 31(5): 7-9.
[6] HU Y, et al. Power System Technology, 2006, 16: 016.
[7] Goda Y, et al. IEEE transactions on power delivery, 2004, 19(4): 1734-1739

Design and Analysis of Circular Slot Microstrip Patch Antenna with FR-4 Substrate

Payal Jindal (PhD Scholar)[1]/Dr. Sudheer Sharma[2]

Dept of Electronics & Communication

Jaipur National University, Jaipur, Rajasthan

payaljindalpayal@gmail.com

sudhir.732000@gmail.com

Dr. Onkar Lamba[3]

Dept of Electronics & Communication

Gyan Vihar University Jaipur, Rajasthan

onkar.lamba@mygyanvihar.com

Abstract - Wireless communication is continuing the witness of tremendous growth and implementation of wide variety of applications. Microstrip patch antenna is widely considered to be a suitable for many wireless applications. The paper presents a new method to increase the bandwidth of microstrip antennas. This design consists of a circular patch along with the capability of covering multiple bands 1 to 15 GHz range. The simulation results of circular patch with microstrip feed arrangement with different cavity size and with the modification in cavity of these different arrangements are presented in this paper. The circular patch antenna designed with FR4b substrate (ε_r=4.54, h=0.1.6mm). Simulation results of return loss and polar radiation pattern are analyzed in this paper.

Keywords: Microstrip antenna, Return loss, Bandwidth, VSWR, Reflection Coefficient.

I. INTRODUCTION

As the increasing demand of improvement and more and more development of mobile communication and the emergence of numerous systems, it is imperative to design multiband antennas to consider various applications simultaneously. Microstrip patch antennas have found extensive application in wireless communication system owing to their advantages such as low-profile, conformability, low-cost fabrication and ease of integration with feed networks. However, conventional microstrip patch antenna suffers from very narrow bandwidth, typically about 5% bandwidth with respect to the centre frequency. This poses a design challenge for the microstrip antenna designer to meet the multiband antenna techniques.

The proposed antenna has a simple circular patch using a microstrip line feed; the patch antenna is designed using the basic concepts of the microstrip technology.

Proposed Design of circular patch

The proposed antenna is composed of a PEC (Perfect Electric Conductor) ground plane, substrate which is FR-4 (ε_r = 4.54, h = 1.6 mm) above which a circular patch is printed with inset feed line.
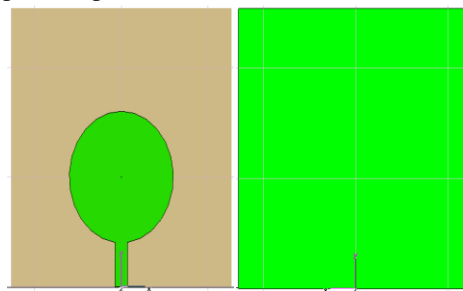

Fig. 1 Top (a) and bottom (b) view of circulator patch antenna

The dimensions of the patch are calculated using the standard design and optimized to a value of radius of the patch 15 mm , the substrates have dimension 50.8 x 50.8 mm^2, length of the microstrip feed line is optimized to 20 mm with a calculated width of 3 mm.

In this research we are using CST Microwave studio as sofware for simulation purpose. In this dissertation design and simulation of Multi band micro strip circular patch antenna which is printed on FR4 (ε_r=4.54, h= 1.6 mm) substrate in X-band is presented..At first the wavelength 'λ' was calculated for the required frequency using the height and dielectric constant.

The dimensions of the patch are calculated using the standard design equations [14] and optimized to a value of radius of the patch 15 mm , the substrates have dimension 50.8 x 50.8 mm^2, length of the microstrip feed line is optimized to 20 mm with a calculated width of 3 mm.

Simulation result of S_{11} and vswr of the circular patch antenna

S-Parameter Magnitude in dB

S1,1
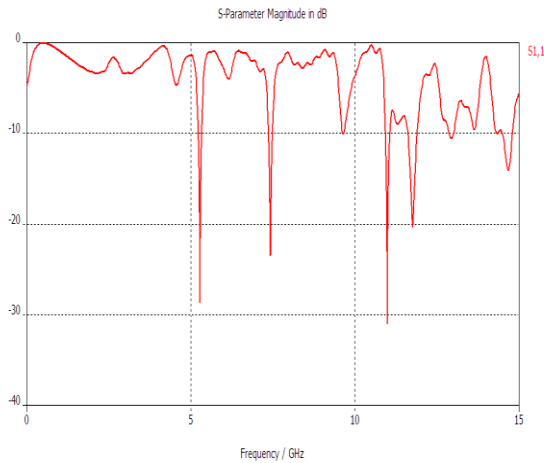
Frequency / GHz

With the given design and dimensions of the circular microstrip patch antenna obtained results of the S_{11} are summarized in the table below:

no. of bands	Central Frequency (GHz)	Return loss at central freq	frequency range(GHz)	fractional bandwidth%
5	5.28	-29	5.23-5.33	1.8939394
	7.42	-24	7.37-7.49	1.6172507
	11	-31	10.93-11.06	1.1828935
	11.8	-20	11.62-11.90	2.3829787
	14.7	-14	14.5-14.8	2.0435967

Votage Standing Wave Ratio (VSWR)

VSW

Frequency / GHz
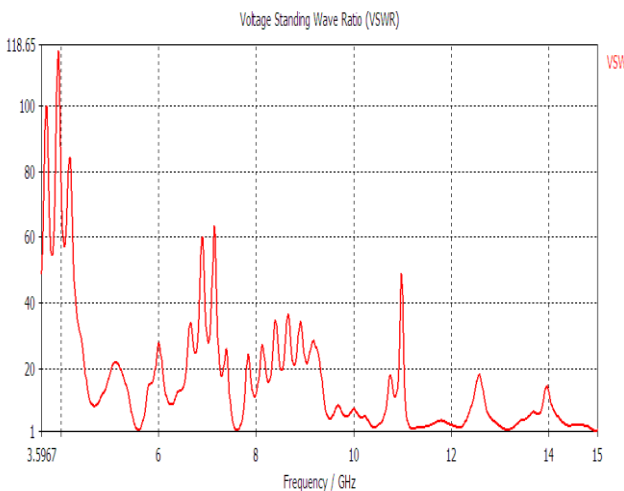
I.

II. CIRCULAR PATCH ANTENNA WITH CAVITY

With the motivation of the study of the behavior of the circular patch antenna, the design is simulated with inserting a cavity in the substrate. The patch used to make the above structure of multi band antenna is observed with circular cavity in the substrate at the center of the patch. A high permittivity substrate will make the metal patch look electrically larger by changing the wave propagation speed; another method used in tuning a microstrip antenna is loading the patch with slots. There are two helpful models that can be used to explain change in resonant frequency.
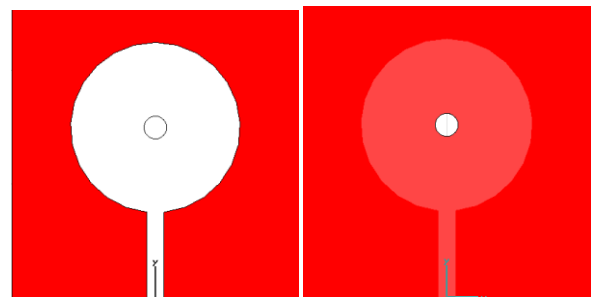
Fig . Structure with cavity

References:-

1)L. H. Weng, Y. C. Guo, X. W. Shi, and X. Q. Chen, "An overview on defected ground structure" *Progress In Electromagnetics Research B*,vol. 7, pp. 173-189.

2) P. Geng, J. J. Li, R. H. Jin, S. Ye, X. L. Liang and M. Z. Li, "The development of curved micro strip antenna with defected ground structure" *Progress In Electromagnetics Research, PIER* 98, pp. 53-73.

3)J. Malik and M. V. Kartikeyan "A stacked equilateral triangular patch antenna with sierpinski gasket fractal for WLAN applications," *Progress In Electromagnetics Research Letters,* vol. 22, pp.-71-81, 2011.

4)A. Azari and J. Rowhani, "Ultra wideband fractal microstrip antenna design", *Progr. Electromag. Res. C*, vol. 2, pp.7–12, 2008.

5) M. Bai, J. Xing, Z. Wang, and B. Yan. "Design of an H-shape cross slotted aperture-coupled microstrip patch antenna", in *Proc. IEEE Int. Worksh. Electromagnetics; Applications and Student Innovation IWEM 2012*, Sichuan, China, 2012.

Lightning strike to tower side of Tokyo Skytree

Toru Miki, Mikihisa Saito, Takatoshi Shindo, and
Hideki Motoyama
Electric Power Engineering Research Laboratory
Central Research Institute of Electric Power Industry
Kanagawa, Japan
torumiki@criepi.denken.or.jp

Masaru Ishii
APET (Center for Advanced Power & Environmental
Technology), School of Engineering
The University of Tokyo
Tokyo, Japan

Abstract— Lightning observations have been carried out at Tokyo Skytree, which is a 634-m high freestanding broadcasting tower located in a flat terrain at 1 m ASL. 25 downward and 37 upward lightning have been observed at the tower during 2012 to 2016. This paper describes observed lightning strikes to tower side. Among 25 downward flashes since 2012, tower-side strikes occurred 3 times. Its ratio is 12% in all of the downward flashes.

Keywords-downward flash; lightning current; tall structure; lightning shielding; lightning observation

I. INTRODUCTION

Direct observation of lightning current at Tokyo Skytree by using a pair of Rogowski coils started in the end of February 2012 [1]. 25 downward and 37 upward lightning have been observed at the tower as shown in Table I. It is well known that upward lightning initiated by an upward leader usually propagates from the top of the tower. The authors expected that downward lightning also would mostly strike the top of the tower. However, among the 25 downward flashes, 3 flashes to lower and middle levels of tower side were confirmed, which are detailed in Table II.

II. LIGHTNING STRIKE TO TOWER SIDE

Lightning strikes to tower side occurred at 2012/05/10 14:09, 2014/05/09 15:17 and 2016/08/02 11:19,

TABLE I. Confirmed lightning flashes at Tokyo Skytree during 2012−2016

Year	Downward /Upward		Positive /Negative /Bipolar			Return Stroke [times]
2012	D:2*	U:8**	P:0	N:6	B:1	14
2013	D:12***	U:5	P:0	N:15	B:2	57
2014	D:6*	U:10	P:0	N:14	B:1	13
2015	D:0	U:13	P:1	N:9	B:3	20
2016	D:5*,****	U:1	P:0	N:6	B:0	12
Total	D:25	U:37	P:1	N:50	B:7****	116

* The authors confirmed 3 downward flashes to lower and middle levels of tower side detailed in Table II.
** 2 upward flashes were confirmed by optical and EM observations in April and May 2012 (no recorded current).
*** includes a subsequent return stroke branched from a downward flash which struck elsewhere.
**** All the bipolar flashes started with positive upward leaders.

___

TABLE II. Downward flashes to lower and middle levels of tower side occurred at Tokyo Skytree during 2012-2016

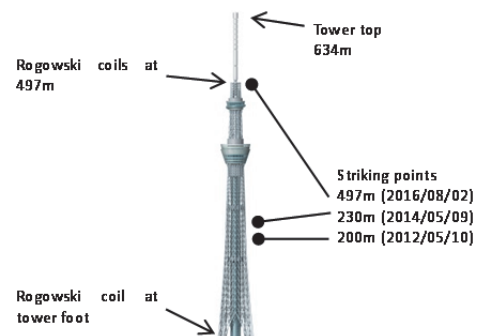| Date	Triggered time	Polarity	Altitude of Striking Point	Altitude of −10 degree Celsius
2012/05/10	14:09:26	Negative	200m	3900m
2014/05/09	15:17:25	Negative	230m	4000m
2016/08/02	11:19:03	Negative	497m	6800m

Figure 1. Striking points of lower and middle levels of tower side.

respectively. The first two flashes are considered downward first return strokes. The third flash is inferred a subsequent return stroke branched from a downward flash which struck elsewhere. Figure 1 shows the striking points of tower side. Every striking point was confirmed by optical images. All the three lightning channels came down from the north direction of the tower, where there were no tall buildings. The altitudes of −10 degree Celsius isotherm when these flashes occurred were 3900m, 4000m, and 6800m, respectively, as shown in Table II. According to the calculated results obtained by a digital model of atmosphere NuWFAS [2], the altitudes of −10 degree Celsius isotherm when downward flashes to the tower occurred in 2012 to 2014 were almost higher than 5500m. The authors continue the lightning observation, and are trying to evaluate these phenomena from the viewpoint of shielding.

REFERENCES
[1] T. Miki, T. Shindo, A. Asakawa, H. Motoyama, M. Ishii, Y. Suzuhigashi, K. Fukuda, "Measurement of Lightning Currents at TOKYO SKYTREE and Observation of Electromagnetic Radiation Caused by Strikes to the Tower", Proc. 31th Int. Conf. on Lighting Protection (ICLP) 152, Vienna, Austria (Sep. 2012).
[2] T. Miki, M. Saito, S. Sugimoto, T. Shindo, H. Motoyama, M. Ishii, H. Taguchi, A. Tajima, and A. Fujisawa: "Meteorological Condition Influencing Lightning Characteristics Hitting Tokyo Skytree," ICOLSE2015, TOU-59, Toulouse, France (Sep. 2015)

Improvements Needed for MIL-STD-188-125-1

William A. Radasky* and Sergio N. Longoria[†]

*Metatech Corporation, Goleta, CA 93117 US, wradasky@aol.com
[†]ETS-Lindgren Inc., Austin, Texas, US, Sergio.longoria@ets-lindgren.com

Abstract – MIL-STD-188-125-1 provides protection and test requirements to build a shielded building against the threat of High-altitude Electromagnetic Pulse (HEMP) produced by a nuclear detonation in the upper atmosphere. Over the years it has become apparent that improvements are needed in the standard.

Keywords – HEMP; protection; testing

I. INTRODUCTION

The military standard, "High-Altitude Electromagnetic Pulse (HEMP) Protection For Ground-Based C4I Facilities Performing Critical, Time-Urgent Missions, Part 1: Fixed Facilities, MIL-STD-188-125-1 [1], updated in 1998, was originally written in 1990 and has had some modifications over the years. While intended for military applications (and in particular for only a particular class of military systems), it is being used today in some commercial applications. Unfortunately the standard does not use normal commercial test procedures to allow the standard to be applied uniformly. In addition, there are questions concerning some of the levels required for testing that are not practical and may not be necessary. This paper will point out some of the flaws in the current standard with the hope that the military will consider improvements in the future.

II. DISCUSSION

The potential improvements to be considered include:

- To provide alternative power entry geometries to reduce the conducted environment [2], [3]

- To provide alternatives to the surface power conduit requirement to include highly shielded cables

- To replace the E3 HEMP "DC" injection test at the building with a harmonic test [4]

- Correct the pulse width of the E1 HEMP injection test to align with published data [2], [3]

- Identify the tolerances for all tests defined in the standard, including E1 HEMP injection parameters [5]

- Identify how to process time domain injection data considering frequency domain sensor sensitivity data

- Reevaluate the residual requirement for power line injection testing to consider the normal current and voltage operational levels

This paper will discuss each of these recommendations in some detail.

III. CONCLUSIONS

MIL-STD-188-125-1 has been a very good standard for many years, but since the latest version has not been updated in 12 years, an effort should be made to improve its usage. In addition, even for military applications there are too many ambiguities in the standard to allow different test teams to acquire the same results when testing the same facilities. It is hoped that the individuals in charge of this standard will make an effort to improve its usability in the future.

REFERENCES

1. MIL-STD-188-125-1, "High-Altitude Electromagnetic Pulse (HEMP) Protection For Ground-Based C4I Facilities Performing Critical, Time-Urgent Missions, Part 1: Fixed Facilities, 7 April 2005.

2. IEC 61000-2-10 Ed. 1.0 (1998-11): Electromagnetic compatibility (EMC) – Part 2-10: Environment – Description of HEMP environment – Conducted disturbance. Basic EMC publication

3. IEC 61000-2-9 Ed. 1.0 (1996-02): Electromagnetic compatibility (EMC) – Part 2: Environment – Section 9: Description of HEMP environment – Radiated disturbance. Basic EMC publication

4. W. A. Radasky, "Impacts of Geomagnetic Storms on High Voltage Power Systems," CIGRE SC C4 2012 Hakodate Colloquium, Hakodate, Japan, September 2012, pp. 229-232.

5. IEC 61000-4-25 Ed. 1.1 (2012-05): Electromagnetic compatibility (EMC) – Part 4-25: Testing and measurement techniques – HEMP immunity test methods for equipment and systems. Basic EMC publication

Review of Geomagnetic Storm Environments – 2017

W. A. Radasky

Metatech Corporation, Goleta, California, US, wradasky@aol.com

Abstract – Over the past four years, Cigré Study Committee C4 has investigated measurements of geomagnetic disturbances at the Earth's surface in order to understand the variations of geomagnetic storms over the past 30 years. The variations of interest include the time-dependence of the measurements, the variations of the signals with latitude and longitude, and also the variations that are apparent due to the nature of the emission of charged particles from the Sun. The focus on the work is to develop and understanding of the potential impact of geomagnetic storms on the operation of the high voltage power grids throughout the world.

Keywords – geomagnetic storms, geomagnetic disturbance (GMD), sudden impulse (SI), coronal hole high speed stream (CHHSS), electrojet storms

I. INTRODUCTION

Geomagnetic disturbances (GMDs) on Earth, originating from the Sun, cause slowly varying currents to flow in the Earth and in electrical power systems, metallic communication lines, railways and pipelines. Under some conditions, these currents can disrupt the proper functioning of those infrastructure systems, with the potential to affect societies dependent on reliable electricity supplies. Therefore it is clear that the exposure to GMDs and the responses of power systems require the attention of electricity utilities, manufacturers and regulators.

II. WHAT IS CIGRÉ?

For these reasons, Cigré (Conseil International des Grands Réseaux Électriques, known in English as the International Council on Large Electric Systems) Study Committee C4 (System Technical Performance) initiated a research study to examine the measured data from different types of geomagnetic storms with emphasis on the data acquired and saved in electronic form. This means that while some very large storms have occurred in the past and are important, it was felt that we should concentrate on storms that have occurred in the modern era. In some cases we have been able to correlate measured ground magnetometer data with satellite solar wind measurements. This paper summarizes the accomplishments of the C4.32 working group, as we are nearing the completion of a technical brochure to be published when the work is completed.

III. LARGE STORMS OF THE PAST

In recent years several important geomagnetic storms created problems for the operation of power networks in different parts of the world. For example a severe geomagnetic storm occurred in March 1989, and it initiated the collapse of the Hydro-Quebec power system, giving the storm its name: "The Quebec storm". In addition to the blackout, several high voltage transformers were damaged, both by the storm itself and also by the collapse of the Quebec network. In October 2003 the "Halloween storm" disrupted power supplies in Sweden and damaged transformers in South Africa. In July 2012 an event thought to be comparable to the Carrington storm in 1859 was measured by a satellite in the same orbit as the Earth around the Sun, but the ejected plasma did not intercept the Earth, so the effects were not observed on the Earth.

IV. DIFFERENT TYPES OF GMDS

There is more than one type of GMD, and each has different characteristics and different parameters that make them important to power grids. The Cigré work characterizes the parameters of GMDs as a basis for examining the consequences for power systems and supports the preparation of appropriate approaches for prevention, mitigation and response to reduce the risks to power utilities and society. The three classes of GMDs considered in the Cigré work include the sudden impulse storms, the electrojet storms, and the coronal hole high speed stream storms. Each of these will be described in the presentation, and the data acquired and analyzed will be summarized. In addition the relative importance to electric power grids for each type of storm will be discussed.

V. CONCLUSION

This abstract summarizes the detailed paper to be presented at the URSI General Assembly in August 2017, and those interested should consult that paper for more information [1].

REFERENCES

[1] W. A. Radasky, "Summary of the Cigré Study Committee C4 Project on Geomagnetic Storm Environments," URSI General Assembly, Montreal, August 2017.

A Key Aspect in Estimating the Effects of Ultrashort EMP on Electronic Devices

Yury V. Parfenov[1], Leonid N. Zdoukhov[1], Vladimir M. Chepelev[1], Boris A. Titov[1], William A. Radasky[2]

[1]Russian Academy of Sciences, Joint Institute for High Temperatures, 125412 Moscow, Izhorskaya 13, bld.2, Russia,
e-mail: parfenov@ihed.ras.ru
[2]Metatech, Corp, 358 S. Fairview Ave, Suite E, Goleta, CA, USA, 93117, e-mail: wradasky@aol.com

Abstract–The method of estimating the effects of ultrashort EMP on electronic devices is offered. This method is based on the use of key parameters of the pulse electric disturbances induced in critical circuits of equipment and allows choosing the most effective simulator for tests.

Keywords–ultrashort electromagnetic pulse; pulse electric disturbance; key parameters.

I. INTRODUCTION

For estimating the effects of ultrashort EM pulses on electronic devices, C. Baum suggested the use of scalar parameters (norms) [1]. We propose a similar method, which is based on the use of so-called "key parameters" determining the possibility of various failures of electronic devices as a result of the influence of high power EM pulses. Such failures can be described as follows: irreversible (permanent) failure of some elements; transition of active elements to the saturation mode; and incorrect transfer of data between digital devices [2]. The possibility of failure occurrence depends on the disturbance key parameters.

The condition of electronic device element irreversible failure is the simultaneous performing of the following inequalities (criteria): $U_{in}>U_{el.br}$; $J_{in}>J_{therm.br}$. Here U_{in} the amplitude of pulse voltage induced at the input of the given element; $U_{el.br}$ is the voltage value of electric breakdown initiation; $J_{in} = \int_0^T I_{in}^2(t)dt$ is the Joule integral; $I_{in}(t)$ is the pulse of current flowing through the element after electric breakdown occurrence; T is the duration of this pulse; and $J_{therm.br}$ is the Joule integral minimum value providing thermal breakdown.

For stable transition of active elements to saturation mode, the performing of the following conditions is necessary: $U_{in}>U_{sat}$; $J_{in}>J_{sat}$; $f > \frac{1}{\Delta T}$. Here U_{sat}, J_{sat} and ΔT are respectively: the minimum voltage value for the transition of active elements to the saturation mode; the Joule integral minimum value, providing a stable transition to this mode; and the duration of the process departing from saturation after the cutoff current flows through elements. The pulse repetition rate is f.

II. DISCUSSION

As the criteria of digital device failures caused by occurrences of errors in data packets transmission, the following inequalities can be accepted: $N_{err}>N_{err.crit}$; $R<R_{crit}$; $P_{err}>P_{err.crit}$.

Here N_{err} and R are the numbers of data packets containing errors and the data transmission rate under conditions of repeated pulse disturbance influence, P_{err} is the probability of error occurrence in data packets transmission, as a result of disturbance influence, and $N_{err.crit}$, R_{crit} and $P_{err.crit}$ are critical values of these parameters. In turn, $N_{err.crit}$, R_{crit} and $P_{err.crit}$ depend on the induced pulse disturbance parameters: pulse energy and its repetition rate. Listed above the parameters of the induced pulse disturbance are the key parameters, and their values characterize the danger of the electromagnetic influence. Below we illustrate the method.

Let us assume that we have two simulators:
- Simulator 1 forms mesoband waveforms having a central frequency of 0.8 GHz; the *pbw* parameter of 10% (here the *pbw* parameter is characterizing the relative width of the frequency band of radiated pulses) and a pulse repetition rate of 1 kHz;
- Simulator 2 forms ultrawideband waveforms having the low frequency edge of 660 MHz, and the high edge of a frequency of 2.95 GHz. The *pbw* parameter is 127% and the pulse repetition rate of 30 kHz.

We calculated the key parameters of pulse disturbance induced in a double-wire power supply line, where one of the wires is connected with the grounding metallic pellet. The calculated results for three key parameters are presented in Table 1; the validation of these calculations will be discussed in the presentation.

TABLE 1. THE VALUES OF KEY PARAMETERS

Key parameters	U_{in}, V	$J_{in} \cdot 10^{11}$, J/ohm	P_{err}
Simulator 1	49	29	$6.4 \cdot 10^{-3}$
Simulator 2	34	5.3	$1.4 \cdot 10^{-1}$

It is easy to see that the maximum values of the U_{in} and J_{in} parameters are observed using Simulator 1. At the same time the maximum value of P_{err} parameter is observed for high frequency pulses emitted by Simulator 2.

REFERENCES

[1] Baum C.E., "Comparative system response to resonant and unipolar waveforms," Intern. Symp. on EMC, Magdeburg, October 1999.
[2] Yury V. Parfenov, et al., "Physical patterns of the influence of pulse electromagnetic fields on electronic devices," IEEE Trans. on Electromagnetic Compatibility. To be published.

Channel Current Predicted by a Self Consistent Return Stroke Model for Different Leader Charge Models

Sukesh A
Research Scholar
Department of Electrical Engineering
Indian Institute of Science
Bengaluru, India - 560012
Email: sukesh.pilicode@gmail.com

Udaya Kumar
Professor
Department of Electrical Engineering
Indian Institute of Science
Bengaluru, India - 560012
Email: udaya@ee.iisc.ac.in

Abstract—It is customary in ligthning protection engineering to relate the charge on the leader channel to the peak of prospective return stroke current. The charge as such is obtained by integrating the measured current up to a specified time duration, which could further be related to the charge deposited over a given section of the leader. Recently, a self consistent return stroke model has been proposed which had a good agreement with the current understanding of the evolution of the return stroke current. Therefore, it would be interesting to obtain the charge and peak current relation from such a model. The result thus obtained would be useful in many ways and in comparison across different leader charge models. As a related exercise, the role of critical field employed to fix the radius of the leader corona sheath is also intended to be assessed.

I. INTRODUCTION

In lightning protection of ground based structure, the ambient field produced by the downward leader decides upon the inception and propagation of upward discharges and hence final strike point. The ambient field as such is related to the charge on the leader, a quantity which is not readily availbale. On the other hand, reasonbly good knowledge exists on return stroke current statistics, the peak current in particular. In order to simplify the day-to-day-usage, it has been customary to relate the strength of the charge on the leader to peak of the prospective return stroke current. With regard to the charge on the leader, it is estimated by integrating the measured return stroke current over a time duration, which is related to the return stroke transit across the channel. As such, the charge distribution on the leader is not a measured quantity and that the total charge does not provide any information on the spatial distribuion of the charge, some uncertainty can exist.

One convenient way of addressing this issue would be correlate the peak of the return stroke current and the charge on the leader through suitable theoretical models. Due to its practical utility, there are several models for the spatial charge disribution on the leader channel viz. Golde's model, Eriksson's model, model by Dellara and Garbagnati and Cooray's model.

With regard to the model for the return stroke current evolution, we need a model which consistently describes the current evolution. In other words, without assuming the current anywhere in the channel or its propagation characteristics, the model should describe the current evolution. In the recent past, such a model seems to have been proposed in [1] with certain acceptable simplification on the channel geometry. Cloud charge is modeled as an ellipsoidal structure. Streamer charge distribution and streamer segment radii are computed iteratively. Consideration of a thin wire structure for the leader channel makes it possible to use the electric field integral equation (EFIE). Point sectional collocation form of Method of Moments (MoM) was used to solve the EFIE equation as an initial value problem. Toefler's spark law was used for the streamer section and a first order arc equation was used for the leader section.
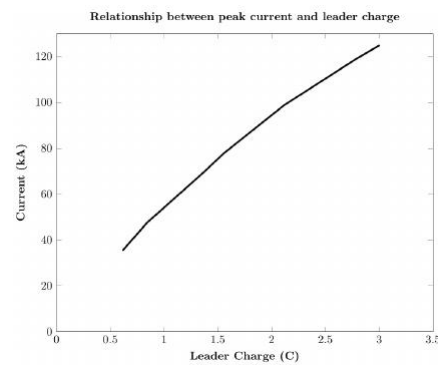
As the result obtained on the current evolution, remote electromagnetic fields and certain aspects of strike to tower was very satisfactory, the same model is intended to be used with different leader charge models to quantify the charge and peak current relations. A sample result for Cooray's model is shown in the figure.

REFERENCES

[1] Rosy B R and Udaya Kumar "A Macroscopic Model for First Return Stroke of Lightning", IEEE Trans. on EMC, Vol.53, No.3, Aug 2011

Development of a Mesoband Immunity Test Source and Method

R. Hoad, B. Petit, T. Rees and G. Eastwood
QinetiQ Ltd.,
Cody Technology Park, Farnborough, Hampshire,
GU14 0LX, UK
rhoad@qinetiq.com

Abstract— Standardized test methods are required to determine the immunity of equipment and systems to radiated Mesoband and Hyperband environments. This paper summarises a method proposed to the International Electrotechnical Commission (IEC), Sub-Committee 77C for a tractable and cost effective test methodology.

Keywords-component; *HPEM, IEMI and EMC*

I. INTRODUCTION

Several published standards [1, 2, 3] indicate that a wide variety of Intentional Electromagnetic Interference (IEMI) sources are available which produce Mesoband and Hyperband environments. These sources could be considered to pose a potential threat to equipment and systems which underpin Critical National Infrastructure (CNI), for example.

When assessing the risk from these IEMI sources to CNI [4] one must either;

a) assume an immunity level, based on EMC limits or sparse effects data, which will likely have an inherent high degree of uncertainty; or

b) conduct an immunity test on actual or representative equipment with an actual or representative simulation of threat sources.

For case b) above, whilst the environment definition exists, details concerning how to perform the test do not. A test method has therefore been developed and proposed.

II. DISCUSSION

A test method requires definition of the technical aspects listed below. Additionally it is important, for the IEC, to use as much existing EMC type approaches as possible so that the testing can be cost effective;

- Derivation and definition of test levels and other waveform parameters;
- Definition of the test environment and test set-up;
- Definition of how to calibrate the E-field in the test volume.

Full scale simulators, capable of producing very intense (10's kV/m) environments are available and have been categorized within a compendium [5]. However, often these sources cannot offer a wide variety of threat environments in one location, and they tend to have a limited parameter range (fixed frequency, pulse widths etc.)._____

Furthermore it can be shown that using the approach described in [1 and 3] that very intense levels are not needed for an immunity assessment. This is because separation distance and physical barriers between the source and the victim equipment greatly increase path loss leading to a reduction in the field intensity at the victim. This means that threat waveform simulation at lower intensity levels (less than 5 kV/m) can be acceptable.

Figure 1 shows the QinetiQ Mesoband and Hyperband immunity test source, named TRIGR within a Semi-Anechoic Chamber.
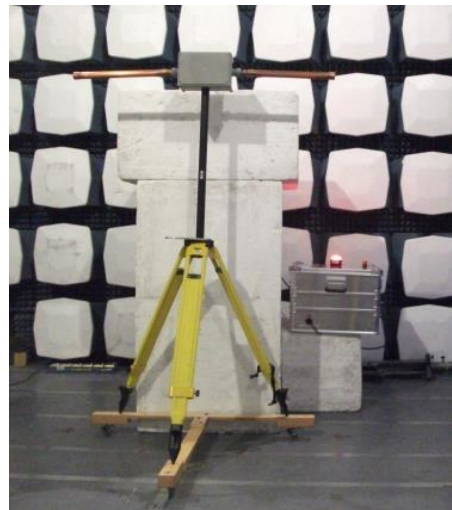
Figure 1. QinetiQ TRIGR Mesoband test source

This paper will discuss the derivation of immunity test parameters and method for Mesoband and Hyperband sources.

REFERENCES

[1] IEC 61000-4-36 Ed. 1.0:2009 'IEMI immunity test methods for equipment and systems'
[2] Mil-Std-464C, Military Standard, Electromagnetic Environmental Effects, Requirements for Systems, 1 Dec 2010
[3] ITU-T K.81, SERIES K: Protection Against Interference, 'High-power electromagnetic immunity guide for telecommunication systems', November 2009
[4] L. Chatt, B. Petit, R. Hoad, 'High Power Radio Frequency Risk/Hazard Assessment Tool', EUROEM 2016, Imperial College, London, UK, 11 to 15 July 2016
[5] IEC 61000-4-35: 2009, 'HPEM simulator compendium'

High Power Electromagnetic (HPEM) Research Activities in India

Pande DC
LRDE, DRDO, MoD, CV Raman Nagar
Bengaluru 560093 (India)
pande.dc@gmail.com

Abstract

The HPEM research activities in India are being carried out in various Government Research Organisations and also in Academic Institutes. Initially research and development work started in the Research Establishments as per their charter of duties and specific applications. The research and development work in the field of lightning have been carried out extensively in the industry and academic institutes. At present the indigenously developed lightning test facilities are available to test power systems and also aerospace systems.

Defence R&D Organisation (DRDO) and Department of Atomic Energy (DAE) is actively involved in the research and development of Nuclear and Non–nuclear Electromagnetic Pulse (EMP). The activities are focused towards the interaction and coupling analysis of EMP coupling to the complex structures, development of mitigation techniques and simulators development for hardness verification testing of the critical infrastructures. The EMP test facilities for radiated transient fields and conducted transients testing are available with Public Sector Undertakings and also with Private Sectors as per the applicable Military & IEC Standards. Indian Industries have also developed the EMP protection components and devices to meet the country's need.

The number of research projects and technology development projects are going on both at DRDO Labs and DAE Labs in High Power Microwave (HPM) and Ultrawide Systems. The Narrow Band and Hyper Band systems are based on both Marx Based and Explosive pulse power systems.

DAE is one of the prime research establishments in the country where the pulse power systems are being developed in the country from late seventies till date towards specific applications in flesh X-rays, LASER, Intense Relativistic Electron Beam (IREB), Magnetic Forming etc. These pulse power systems are known as Kilo Ampere Linear Injector (KALI). These KALI systems are available upto 5000 J energy. DRDO & DAE worked in these systems for the generation of High Power Microwave using VIRCATOR, Relative Klystron and BWO configurations in L, S and X Bands of frequencies. AT the same time these two organisations have developed the number of Sub Hyper and Hyper band systems for the susceptibility and vulnerability studies of the electrical and electronic circuits and systems. Their applications in GPR, TWIR and neutralising IEDs are being investigated.

In this plenary talk the HPEM activities being carried out at various research establishments and future scope of work in the country is being highlighted.

UWB HPEM Simulator
in accordance with IEC 61000-4-36

Jin-Ho Shin
Replex Co., Ltd.
Seoul, Republic of Korea
hpett@replex.co.kr

Young-Kyung Jeong
Replex Co., Ltd.
Seoul, Republic of Korea
ykj@replex.co.kr

Dong-Gi Youn
Replex Co., Ltd.
Seoul, Republic of Korea
admin@replex.co.kr

Tae-Heon Jang
Korea Testing Laboratory(KTL)
Ansan-si, Republic of Korea
thjang@ktl.re.kr

Abstract— In this paper, we present a UWB HPEM simulator to be capable of generating hyperband HPEM signal corresponding to IEC 61000-4-36. The simulator has energy band from 50MHz to 2100MHz as hyperband. It can be operated stand-alone with charging battery and has compact size of 1450mm × 400mm × 400mm in length, width and height, respectively. The simulator can produce 217kV(far-voltage) and 100Hz pulse repetition rate.

Keywords-component; high power electromagnetics; HPEM standard; UWB HPEM simulator

I. INTRODUCTION

Modern civil systems are based on electronic components and subsystems composed of electronic parts. Therefore, the vulnerability of electronic devices to High Power Electro-Magnetic(HPEM) threats has been increased widely [1]. In this paper, we present a UWB HPEM simulator in accordance with IEC 61000-4-36. This simulator satisfies the standard and light-weight/compact size to operate.

II. Development of UWB HPEM simulator

A. Design and Construction of UWB HPEM simulator

The UWB HPEM simulator consists of 4 modules, which Power Supply(PS) with battery, High Voltage Generator(HVG), Pulse Forming Line(PFL) and UWB Antenna are shown in the Figure 1.
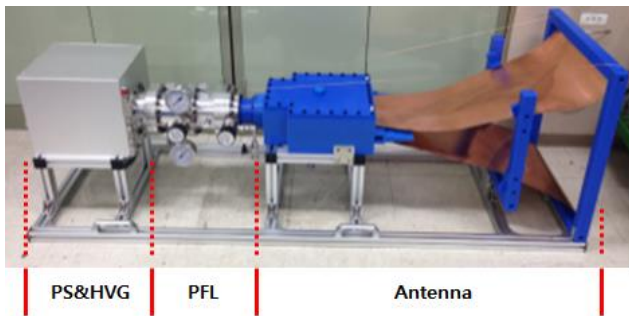
Figure 1. UWB HPEM simulator

B. Results

The electric field of UWB HPEM simulator was measured by TEM sensor at anechoic chamber. The measured far-voltage was 217kV as shown Figure 2.
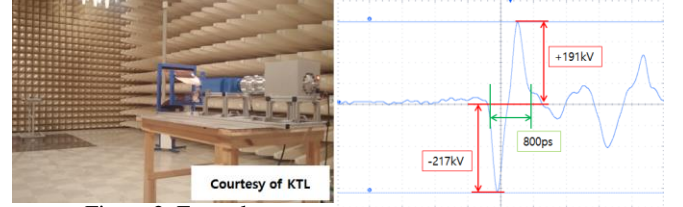
Figure 2. Far-voltage measurement set up and waveform

The spectral magnitude calculated by far-voltage was shown in the Figure 3. The 90% energy band was from 50MHz to 2.1GHz and percent bandwidth corresponds with hyperband simulator standard. Table I represents comparison between the UWB HPEM simulator and "Generic Hyperband Test Parameters" of IEC 61000-4-36 standard.
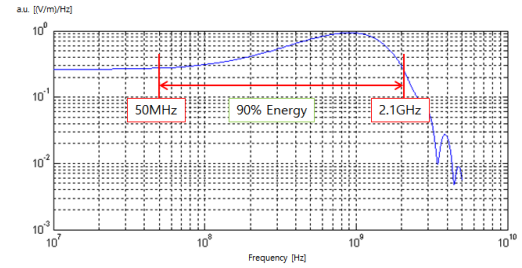
Figure 3. Spectral magnitude of far-voltage waveform

TABLE I. Comparison of parameters

Section	Rise time [ps]	Pulse width [ns]	Pulse repletion rate [Hz]	Burst duration [s]
Standard test parameters[2]	100~500	0.2~5	1~1000	1~10
UWB HPEM simulator	150~200	0.7~0.8	1~100	1~10

As shown in the TABLE I, the UWB HPEM simulator satisfies with all the parameters and RMS deviations of far-voltage, rise time and pulse width are under 10%. Also these parameters can be adjusted as test demands or user requests.

REFERENCE

[1] Sabath, Frank. "System oriented view on high-power electromagnetic (HPEM) effects and intentional electromagnetic interference (IEMI)." Proceedings of the XXIX URSI General Assembly (2008).

[2] IEC 61000-4-36 Ed 1.0, p.21.

Challenges in Designing and Testing of EMP Ethernet (RJ45) Filter

Aswin R
Research and Development Department
EMI Solutions PVT LTD
Bangalore, Karnataka, India
development@emisindia.com

Abstract— Electro Magnetic Pulse: EMP has always been a matter of concern for Engineers. An electromagnetic pulse (EMP) is a high energy radio wave that can destroy, damage, or cause the malfunction of electronic systems by overloading the circuits. Electronic systems will suffer from an EMP largely depending on its magnitude and location of strike. Some systems are inherently protected against EMP whereas other sensitive Electronic devices must be protected against EMP so that these devices are not harmed. MIL STD-188-125-1/2 and IEC 61000-4-24 are the specifications for defining the requirements for HEMP protection.

Keywords- Pulse Current Injection (PCI), HEMP, Residual Current

I. INTRODUCTION

MIL STD-188-125-1/2 and IEC 61000-4-24 specifies the standards for PCI (pulse current injection) testing. PCI testing is a measure of integrity of the protection system. They require specialized test equipments which inject high voltage/high current pulses (Double Exponential Pulse) into the HEMP Protection System. The residual current through the protection system plus other parameters like Root Action, Peak Rate of Rise are monitored as per the standards. It is a measure of the efficacy and compliance of the protection system. MIL STD-188-125-1/2 defines three PCI pulse for testing the HEMP protection system, E1 (short pulse), E2 (intermediate pulse) and E3 (long pulse). Short Pulse E1 is a 5 kA peak 20/550ns pulse for common mode and 5kA/$\sqrt{n}$ 20/550ns pulse for differential mode (where n is the number of lines) and has an electric field pulse amplitude of the order of tens of kV/m. Intermediate pulse E2 is a 250A peak 1.5/4000μs pulse and has a electric field pulse amplitude of several hundred V/m. Long pulse E3 is a 1000A peak 0.2/20s pulse and has a very low amplitude pulse on the order of tens of V/km or mV/m.

II. TESTING PROCEDURE

For checking the compliance of a HEMP filter with MIL STD 188-125-1/2, a short pulse E1 pulse is injected into the input side of the HEMP filter and the residual current flowing through a 50 ohm resistive load is measured(For differential mode).The maximum acceptable limit of residual current through the 50 ohm load is 100 mA as per MIL STD 188-125-1/2. For the Intermediate pulse E2, pulses are injected into EMP Filter but there is no requirement to measure the residual current pulse. The filter must withstand the pulse without damage to the EMP Filter.
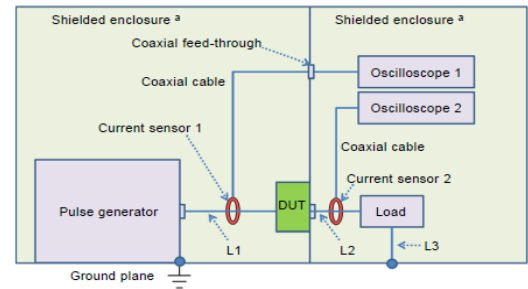
Fig.1. PCI Test Setup

III. CHALLENGES IN THE DESIGN

The main challenge in design of High speed Data line filter with EMP protection is that the total Shunt Capacitance and Series Inductance of the components must be very less in order to achieve the high data speed. So the commonly used Surge Protection Devices like MOV, TVS etc cannot be used in the design. These over voltage/current protection devices have high inherent capacitance which increases the insertion loss in the Pass Band.

Second Challenge is to meet the permitted residual current of 100 mA on a 50 Ohms load as per the MIL STD 188-125-1/2. The normal operating voltage of the Data Line Filter is ± 3V and the maximum operating voltage is ± 55 V. According to MIL STD 188-125-1/2 the permitted residual current is 100 mA which corresponds to 5V peak on a 50 Ohms Load. So a compromise on either MIL STD 188-125-1/2 or on the maximum operating Voltage has to be done.

The simulations were carried out in EMCoS PCB VLab Software and it was found that   total shunt capacitance and series inductance was in the order of pF and nH respectively. A multi stage low pass filter was designed giving the cut off frequency corresponding to 1000Mbps data rate. The over voltage protection devices was selected based on the designed shunt capacitance and series over current protection devices was selected based on the designed series inductance. Over Current Protection along with Over Voltage protection is mandatory for achieving the residual current as per MIL STD 188-125-1/2 and IEC 61000-4-24.

REFERENCES

 [1] International Standard IEC 61000-4-24 Electro Magnetic Compatibility.

[2] High-Altitude Electromagnetic Pulse (Hemp) Protection For Ground-Based C I Facilities Performing Critical, 4 Time-Urgent Missions – MIL STD 188-125

Research on Lightning Electromagnetic Environment of Electric Multiple Unit

Li Mingxiao
School of Electrical Engineering
Xi'an Jiaotong University
Xi'an, Shanxi, China
eucalypi@126.com

Zhang Hongye
School of Electrical Engineering
Xi'an Jiaotong University
Xi'an, Shanxi, China
zhanghongye@stu.xjtu.edu.cn

Abstract—Accidents caused by lightning stroke on the electric multiple units (EMU) are attracting widespread social concerns. In this paper, a field-circuit combined model is established in CST to simulate the lightning stroke on EMU. This paper simulated the current path after a lightning stroke on catenary and calculated the transient electromagnetic field generated by lightning impulse based on transmission line matrix methods (TLM). The result shows that electromagnetic field is strongest right below the pantograph while electric and magnetic field strength could respectively reach to 161.8kV/cm and 5.98×10^3A/m. It should be avoided to place electronic devices and seats below the pantograph.

Keywords-EMU; lightning stroke;TLM; electromagnetic field(key words)

I. INTRODUCTION

Rail transport especially the passenger transport has come into a high-speed period in China marked by the widespread use of bullet trains like electric multiple units (EMU). However, accident caused by lightning occurs occasionally. In 2011, a great crash accident happened in Wenzhou due to the communication equipment fault which caused by lightning stroke. Existing research on lightning electromagnetic environment mostly focus on the influence of bow net arc or the shielding effect of metal train body shell[1]. In fact, some electronic devices like controller of high voltage isolating switch is placed on the roof of train. And for the requirement of integration, more equipment will be integrated in high voltage box which is placed on the top of the train. Therefore it is of great importance to analysis the electromagnetic field generated by transient lightning impulse outside the train.

II. SIMULATION MODEL OF LIGHTNING STROKE ON EMU

A. Analysis of Lightning Stroke Progress

Generally, lightning strikes the catenary. Lightning current flows in both directions along the line. Also, it will flow through the pantograph to the high voltage equipment atop the train. In this case, arrester will work and leads the large lightning current to flow through the train body shell and earthing system to the ground.

B. Simulation Model of Lightning Stroke on EMU

The TLM model includes pantograph bracket, deflector, high voltage isolating switch and its supporting insulators. Waveform of lightning current is double exponential function with the maximum of 200kA, rise time of 1.2μs and fall time of 50μs[2]. The lumped circuit part includes the wave impedance of catenary and earthing system which can be obtained by measurement.

III. SIMULATION RESULT

Four locations are selected as viewpoints to observe the electromagnetic calculation result. The four viewpoints are: right below the pantograph bracket (point 1), 0.2m (point 2) and 1m away from deflector (point 3) and nearby the switch controller (point 4). The maximum electric and magnetic field strength is as shown in Table I. Fig.1 and Fig.2 show respectively electric field and magnetic field distribution at 0.5μs.

TABLE I   MAXIMUM OF ELECTRIC AND MAGNETIC FIELD STRENGTH

	Point 1	Point 2	Point 3	Point 4
E(kV/cm)	161.8	84.9	47.5	22.8
H(A/m)	5980.8	5212.8	2718.1	1665.2
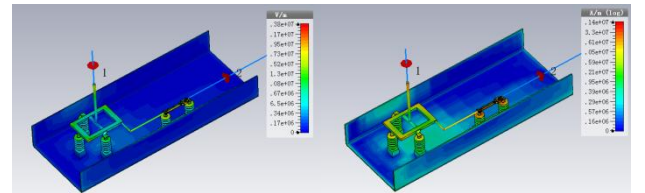
Figure 1.Electric field distribution   Figure2. Magnetic field distribution

IV. CONCLUSION

Electromagnetic field is strongest right below the pantograph. With the lightning current peak of 200kA, the maximum of transient electric and magnetic field strength can respectively reach to 161.8 kV/cm and 5.98×10^3 A/m. Electric field decreases by 52% in 1m after crossing the deflector. Metal body shell of EMU has certain effects of electric field shielding, but it is not recommended to place electronic devices and seat right below the pantograph.

REFERENCES

[1] Qin Binquan, Xiang Mi, and Ren Yan, "Analysis of person safety and lightning protection in straddle-type monorail transportation," Asia-Pacific international conference on lightning. 2011: 40–43.

[2] Youpeng Huangfu, Shuhong Wang, "Transient Lightning Impulse Performance Analysisfor Composite Transmission Line Tower," IEEE transactions on electromagnetic compatibility [J].57:378-381,2015.

ASIAEM 2017- Limit for the circuit model for Rogowski Coil

Santosh Janaki Raman and Udaya Kumar,
Department of Electrical Engineering,
Indian Institute of Science, Bangalore, India
Email id – santoshj@ee.iisc.ernet.in

Sridhara B,
SIT College, Tumkur

Abstract - Rogowski coils have been used to measure lightning currents in tall towers and in high voltage circuits. Many a times, the frequency content in the measured currents are beyond the upper frequency limit of the Rogowski coils. In such a scenario, the response of the coil obtained by circuit based models tends to be inaccurate since it fails to capture the high frequency effects. To address this issue, the response of the coil is obtained by the full wave electromagnetic solution. The currents obtained by the full wave solution is compared with the circuit based solution and an upper frequency limit on the applicability of the distributed circuit model is proposed

Keywords – Full wave solution; interpolation function; time- domain electric field integral equation (TD-EFIE)

I.   INTRODUCTION

The Rogowski coil current transducer has been extensively employed for measurement of currents ranging from the power frequency to fast rising impulses. Among the two modes of operation of the coil, the Self-Integrating Rogowski(SIR) coil is preferred for fast rising impulse currents and its performance under controlled conditions are shown to be quite satisfactory.

However, there are several practical scenarios in which the measurement is affected by the high frequency response of the coil. In [1], a detailed analysis for the coil's response is made. After deriving a novel governing equation for the Coil's high frequency response, solution for canonical case was deduced. It is then shown that the asymmetry in the excitation can seriously limit the measurement made through SIR coils.

 Further the wire length and the wavelength of the highest frequency to be resolved tend to become comparable. Therefore, question arises on the range of validity of the distributed circuit model which is generally employed for the requisite analysis. In order to address this issue, a full-wave solution is sought along with its low frequency counterpart.

II.   METHODOLOGY

Considering the geometry of the coil, a thin-wire approximation is employed and the role of former is neglected. A numerical solution using the method of moments in time-domain is applied on the electric field integral equation [2]. The low frequency solution is also obtained from the same code with appropriate changes made to the velocity of propagation. This ensures that the spatial resolution employed for the low frequency or the quasi-static solution (for which the circuit based approach is valid) remains the same.

III.   PRELIMINARY RESULTS

The geometry considered for the numerical simulation has been shown in Fig. 1 and the current distribution obtained from full-wave electromagnetic solution has been shown in Fig. 2.
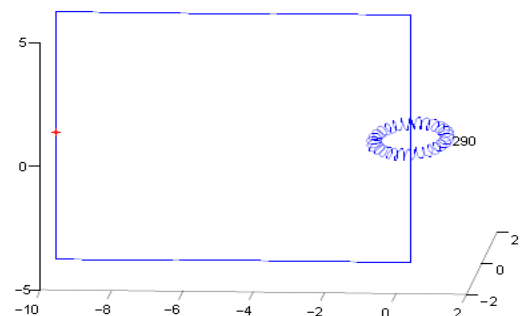
Fig. 1 Geometry of the Rogowski coil under consideration
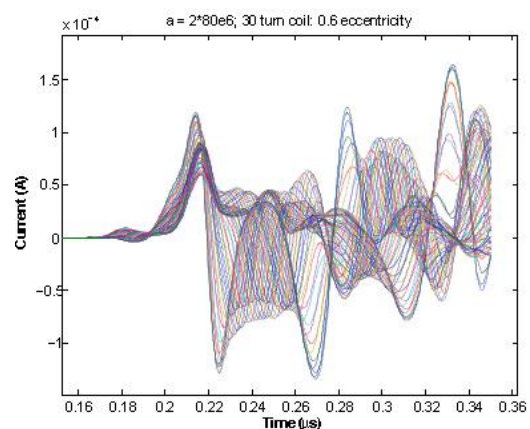
Fig. 2 Currents obtained using full wave solution

References:
1.   Udaya Kumar, "Performance of Rogowski Coils at Higher Frequencies", International Conference on Lightning Protection (ICLP2010), Cagliari, Italy.
2.   Miller E.K., Poggio A.J. and Burke G.J., "An integro-differential equation technique for the time-domain analysis of thin wire structures: I. Numerical method", Journal of Computational Physics, vol. 12, pp. 24 - 48, 1973.

Far Field Boundary Characterization of Half Impulse Radiating Antenna (HIRA)

Rakesh Kichouliya and Sandeep M Satav
Research Centre Imarat
P.O. Vigyanakancha, Hyderabad

D. Rama Krishna and Divya Divi
Department of Electronics Engineering
Osmania University, Hyderabad

Abstract—This paper presents the experimental characterization of the far field boundary for the time domain half impulse radiating antenna (HIRA) by experimentally characterizing the E_ϕ and E_r components with respect to E_Θ in the respective far field region in the frequency range of 200 MHz to 1.5 GHz. The distance, at which the frequency domain fields of HIRA follows the same variation as experimentally characterized, becomes the far field boundary of the HIRA.

Keywords-Far field; HIRA; UWB;

I.   INTRODUCTION

The HIRA is a UWB source whose far field boundary can be empirically computed based on the rise time and reflector diameter [1].The experimental results show that the computed far field boundary is overestimated [2]. In classical theory of far field [3] boundary the E_Θ will be dominating component as compared to other two E_ϕ and E_r components of the field. We have first experimentally characterized the E_ϕ and E_r components with respect to E_Θ from 200 MHz to 1.5 GHz in the far field region. The Simulation of the HIRA carried out using CST Microwave studio software and validated experimentally. After validation of the HIRA model the three components of the field computed at various distances in bore sight in frequency domain from 200 MHz to 1.5 GHz. The distance at which the E_ϕ and E_r component of HIRA follows the same variation as experimentally characterized in frequency domain from 200 MHz to 1.5 GHz that distance becomes the far field boundary of the HIRA.

II. HIRA MODEL VALIDATION

The HIRA system model simulated in CST software and the E_θ field is compared with the measured field with D dot sensor and it is shown in figure 1 and 2.
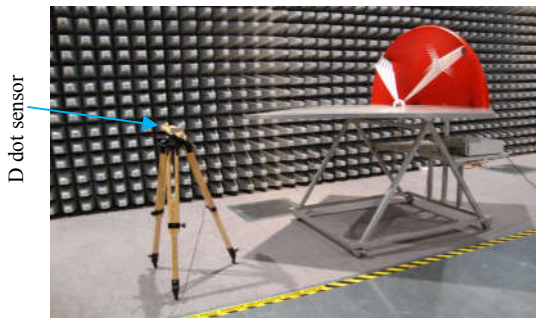
Figure 1. HIRA field measurement set up
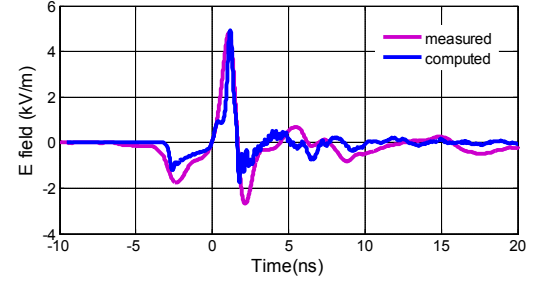
Figure 2.HIRA time domain field at 2m

III. MEASUREMENT OF FIELD IN FREQUENCY DOMAIN

The frequency domain far field measurement carried out using 3-axis field probe, from 200 MHz to 1.5 GHz for all three field components. The measurement set up is shown in figure 3.
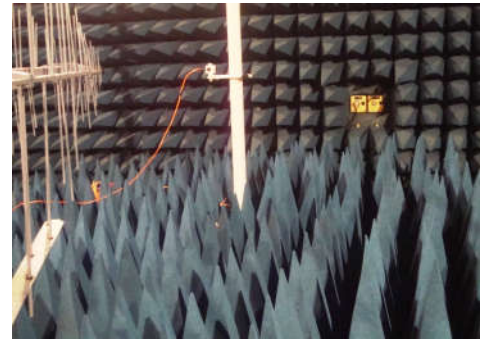
Figure 3. Field measurement set up in frequency domain
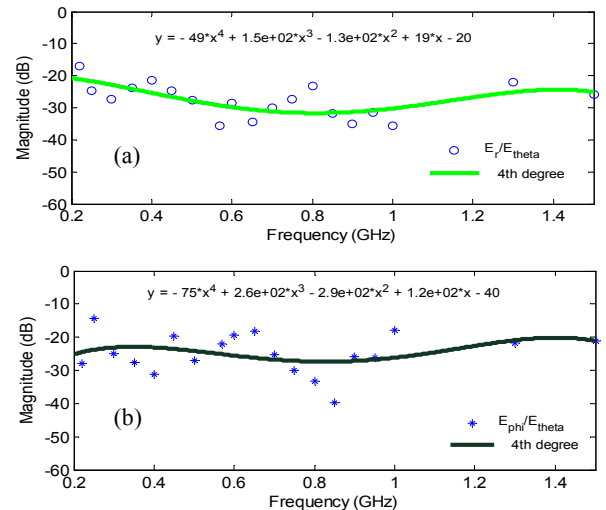
Figure 4. E_r and E_ϕ normalized to E_θ forming Limit lines (a) E_ϕ (b) E_r

The measured E_r and E_Φ field components are normalized to E_θ and they are plotted in figure 4. The 4th degree polynomial fit applied to the measured field data to form the limit lines for the E_r and E_Φ field components in the far field region.

IV. DTERMINATION OF FAR FIELD DISTANCE

The normalized frequency domain field data of the HIRA is computed in bore sight at various distances from 3m to 22 m, and they are plotted against the measured far field limit line in section III. The distance at which the frequency domain fields of HIRA are lesser than or equal to the limit line will be far field distance of HIRA. The HIRA fields are plotted at 5 m to 11 m distance from the HIRA in figures 5 to 11.
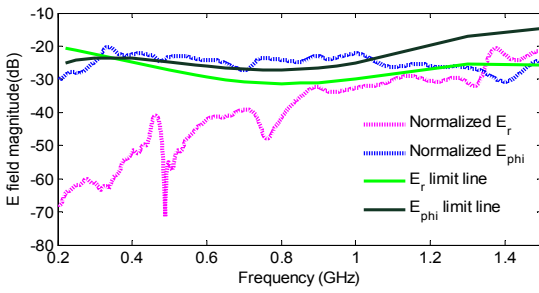
Figure 5. Field variation at 5 m from HIRA
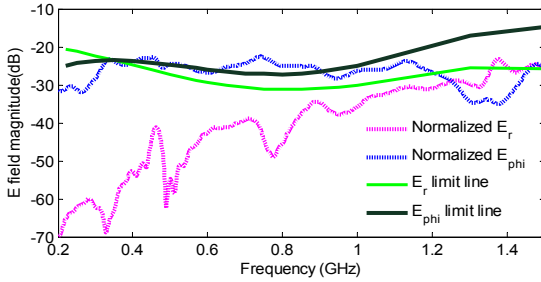
Figure 6. Field variation at 6 m from HIRA
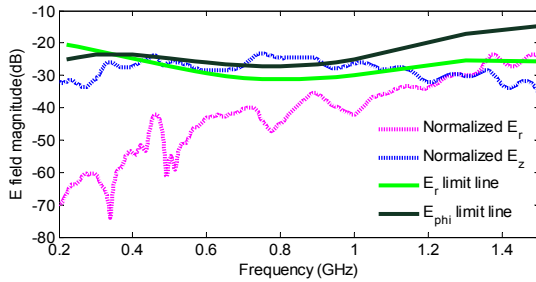
Figure 7. Field variation at 7 m from HIRA
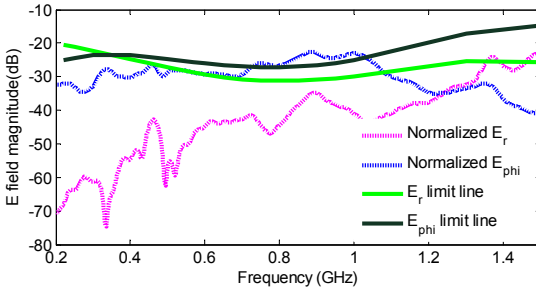
Figure 8. Field variation at 8 m from HIRA
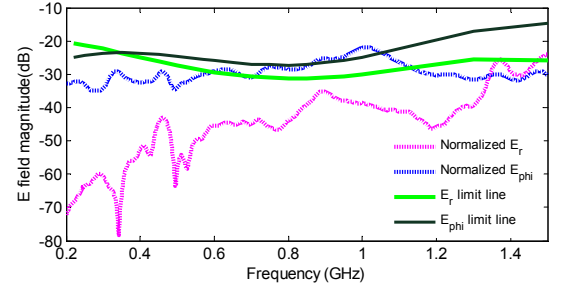
Figure 9. Field variation at 9 m from HIRA
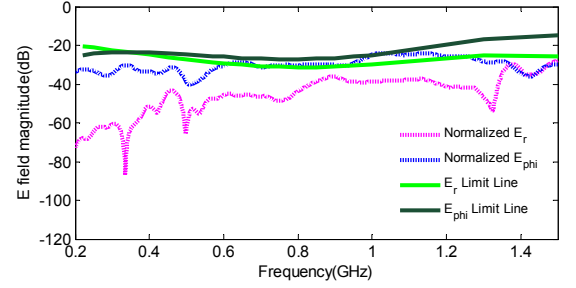
Figure 10. Field variation at 10 m from HIRA
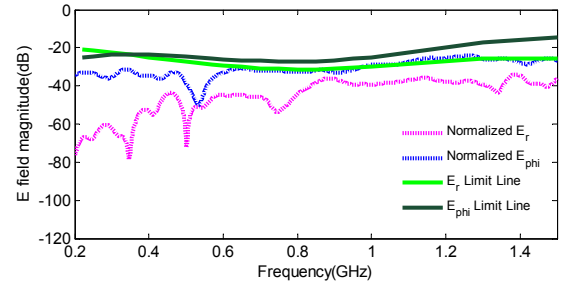
Figure 11. Field variation at 11 m from HIRA

V. CONCLUSION

The normalized field E_r and E_φ are plotted against their respective limit lines from figure 5 to 11. It can be seen from the figures that the E_r component (pink dotted) of the field is exceeding its limit line (parrot green) above 1.35 GHz, while below 1.35 GHz it is well below the limit line. Similarly the E_φ component (blue dotted) of the field is exceeding its limit line (green) up to 9 meters. At a distance of 10 m and above (figure 10 and 11) , both the electric field components are equal to or below their respective limit line.

Therefore, from this experimental and computational study , 10 m is found to be the far field boundary of HIRA UWB system considered in this work.

REFERENCES

[1] James Benford John A Swegle, B and Edl Schamiloglu, "High Power Microwaves," Third Edition, CRC press, New York, pp. 210–214, 2016.
[2] Technical Note, "Impulse Radiating Antenna, HIRA-180" on www.montenaemc.com
[3] Balanis C. A, "Antenna Theory and Design,", Wiley India, p. 210–214, 2016.

Numerical Evaluation of an Analytical GPR Model

Indulata Sahu, Sonu Dasi and Subrata Maiti
Department of ECE, NIT Rourkela
Email:1indulata@gmail.com, dasisonu@gmail.com

Abstract—**In this work we have evaluated a time efficient analytical ground penetrating radar model by comparing its accuracy with an well known FDTD based model. The results show that analytical model's performance is promising in terms of accuracy for describing the response due to layered media.**

Index Terms—**GPR, Green's function, layered media**

I. INTRODUCTION

Numerical models are very accurate to simulate ground penetrating radar (GPR) with complex scenarios. However, they are inefficient for real-time GPR detection. An FDTD based popular model is gprMax [1], which is suitable to simulate various types of GPR environments. Analytical models are generally time efficient and application specific. MPWM-2 proposed by Maiti et. al. [2] is based on analytical solution of a full wave model (FWM). This model [2] is found to be time efficient to represent layered media. In this work, MPWM-2's accuracy is compared with gprMax by synthetic experiments.

II. PROPOSED METHOD

The derivation of MPWM-2 is elaborately discussed by Maiti et. al. [2]. Here the spatial domain Green's function $G_{xx}^{\uparrow}(\omega)$ at the source point $((x, y, z) = 0)$ is defined as the ratio between x - directed received electric field (E_{r_x}) and transmit electric field (E_{t_x}) as follows:

$$G_{xx}^{\uparrow}(\omega) = E_{r_x}/E_{t_x}. \quad (1)$$

Applying Huygen's principle, the equivalent magnetic current density is related to electric field density as $M^s = -2\hat{n} \times \hat{x}E_x^t = -2E_x^t\hat{y}$. Therefore, (1) can be modified as

$$G_{xx}^{\uparrow}(\omega) = -2E_{r_x}/M_y. \quad (2)$$

The M_y is magnetic current density acting in y - direction at source. (2) is useful to find Green's function by gprMax simulation. MPWM-2 is based on monostatic GPR system.
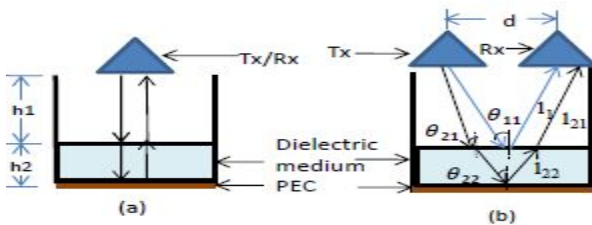
Fig. 1. Reflections in case of a) monostatic antenna, (b) bistatic antenna

On the other hand, gprMax simulates a bistatic model. To compare these two, there is a requirement to modify MPWM-2 to account for extra travel path and angle of incidence deviating

from 90° as shown in Fig. 1 (a) and (b). Therefore, for single layer media as target, MPWM-2 [2] is modified as

$$G_{xx}^{\uparrow}(\omega) = \frac{r_{12}cos\theta_{11}}{2\pi}\left\{\frac{e^{-2\gamma_1 l_1}}{\frac{2l_1}{\gamma_1}} + \frac{e^{-2\gamma_1 l_1}}{4l_1^2}\right\}$$

$$+ \frac{\hat{r}_{23}}{2\pi}\left\{\frac{1}{2\left(\frac{l_1}{\gamma_1} + \frac{l_{22}}{\gamma_2}\right)} + \frac{\left(\frac{l_1}{\gamma_1^3} + \frac{l_{22}}{\gamma_2^3}\right)}{4\left(\frac{l_1}{\gamma_1} + \frac{l_{22}}{\gamma_2}\right)^3}\right\}cos\theta_{22} \quad (3)$$

where $\hat{r}_{23} = e^{-2(\gamma_1 l_1 + \gamma_2 l_{22})}r_{23}\left(1 - (r_{12}cos\theta_{21})^2\right)$. Here $cos\theta_{11} = h_1/l_1$, $l_1 = \left(h_1^2 + (d/2)^2\right)^{1/2}$, $\cos\theta_{21} = h_1/l_{21}$ and $\cos\theta_{22} = h_2/l_{22}$. θ_{21} and θ_{22} can be calculated by applying suitable geometry. MPWM-2 assumes that the planar media is infinite in cross section. However, gprMax can simulate a finite domain based on available computational resources.

III. RESULTS AND CONCLUSION

To compare MPWM-2 and gprMax, we consider two cases: 1) a PEC placed at 35 cm from the antenna and 2) a sand layer of thickness 10 cm located at 35 cm from the antenna. Simulation in gprMax is carried out for a domain size of $100 \times 80 \times 50$ cm^3 with a spatial step of 4 mm in all directions. Therefore, the cross-section of medium is limited to 100×80 cm^2. Antenna spacing is taken as 14 cm. A gaussian monopulse centered at 2 GHz is generated. The simulation outcomes are presented in Fig. 2. There is a significant matching between the Greens's function obtained for both the targets. The cross-correlation coefficients are found to be 0.9998782 and 0.9997241, respectively, for PEC and sand. Hence, this analysis demonstrates that MPWM-2 is significantly accurate to represent layered medium.
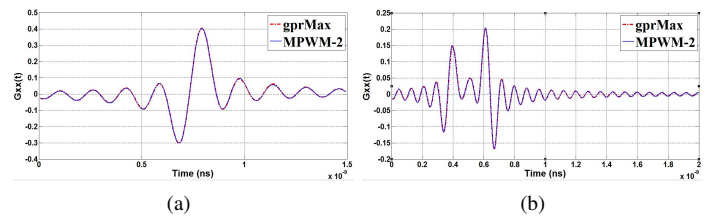

Fig. 2. Simulated Green's function for (a) PEC, (b) Sand layer

REFERENCES

[1] C. Warren and A. Giannopoulos, "Creating finite-difference time-domain models of commercial ground-penetrating radar antennas using taguchis optimization method," *Geophysics*, vol. 76, no. 2, pp. G37–G47, 2011.

[2] S. Maiti, S. K. Patra, and A. Bhattacharya, "A modified plane wave model for fast and accurate characterization of layered media," *IEEE Transactions on Microwave Theory and Techniques*, (under press).

Characteristic Analysis of Conducted and Radiated Switching Transients of GIS

ZHANG Hong-ye, XIE Yan-zhao
State Key Laboratory of Power Equipment and Electric Insulation
National Center for International Research on Transient Electromagnetic Environments and Applications
School of Electrical Engineering, Xi'an Jiaotong University
Xi'an, Shaanxi, China
zhanghongye@stu.xjtu.edu.cn; yzxie@mail.xjtu.edu.cn

Abstract—This paper presents analysis of characteristics of measured switching transients including conducted VFTO inside the gas insulated substation (GIS) and radiated electromagnetic fields outside the GIS. In order to figure out the regularities of these switching transients, both some main parameters and their influential factors are studied. This work provides some basic data for better grasping the properties of switching transients of GIS.

Keywords- gas insulated substation; switching transients; typical characteristics; VFTO; radiated electric field

I. INTRODUCTION

Switching operations could generate inside GIS VFTO, which threatens the safety of GIS equipment. What's more, during the propagating process of VFTO, when it encounters points of discontinuous impedance, strong transient electromagnetic fields could be stimulated outside the GIS, which can cause to the secondary electronic device electromagnetic interferences or even damages. Therefore, it is necessary to study the characteristics of switching transients. In this paper, based on a large number of experimental data, the main properties consisted of the amplitude, the front time, the dominant frequency and the damping factor of switching transients are summarized in detail, and their influential elements are also analyzed. Based on the actual characteristics of switching transients, this paper aims to clarify the present research situation in this domain and provide a data base for more future work.

II. SWITCHING VFTO

In general, the characteristics of switching VFTO in GIS are concluded as follows: 1) The amplitude is generally around 2p.u., but may exceed 3p.u., which scale with the voltage level of GIS. 2) The front time is around 3~20ns. 3) The frequency spectrum includes basic oscillation frequency (several tens to hundreds of kHz), high-frequency oscillation of tens of MHz, and UHF oscillation of hundreds of MHz.

III. SWITCHING TRANSIENT E-FIELD

Measured switching transient electric fields (E-fields) are in form of a series of pulses, of which every individual pulse is in damping sinusoidal waveform as shown in Figure 1, measured in a 220kV GIS [1]. Based on many measurements [2], some parameters of switching E-field pulses due to closing operations of disconnecting switches (DS) are shown in table I.

The characteristics of switching E-field pluses are summarized below: 1) The highest amplitude is of several to several tens of kV/m, which scales with GIS voltage level. 2) For individual pulses due to DS closing operations, their front time is around 2~25ns. 3) The dominant frequencies are between 0.5MHz and 120MHz which vary inversely with GIS voltage level. 4) The damping factor of a switching E-field pulse is around several million, which vary inversely with GIS voltage level. The characteristics of measured switching transient E-fields depend on the switch type, the GIS voltage level, and the measurement location, etc. Peak field component amplitudes scale approximately as 1/r with distance from the bus. For the same switch, closing operations produce much higher transients than opening operations. DS operations produce transients of larger amplitude and greater number than circuit breakers, and the dominant frequency of the former is higher than that of the latter, for the same voltage level.
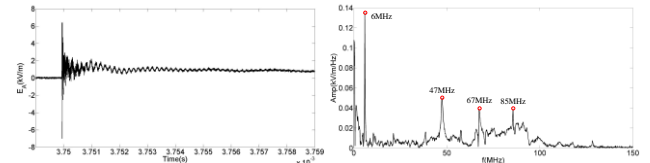

Figure 1. Typical waveform and frequency spectrum of an individual pulse measured in a 220kV GIS

TABLE I.   E-FIELD DUE TO DS CLOSING OPERATIONS

Voltage Level (kV)	Maximum Amplitude (kV/m) / Distance from the Bus (m)	Front (ns)	Dominant Oscillation Frequency (MHz)	Damping Factor
230	5/<1	2	115	9.0e6
330	1.3/3	13	17	5.1e6
420	20/0.09	9	10~40	—
500	19/2	11	20	—
800	57 /0.09	23	10	1.3e6

IV. CONCLUSIONS

This paper has summarized the main characteristics of switching transients of GIS, including conducted VFTO and radiated E-fields, and analyzed their influential factors. This work should help many researchers to better realize the regularities of switching transients, but much work is still needed to verify and improve these conclusions.

REFERENCES

[1] KONG Xu, GUO Fei, LIANG Tao, et al. Measurement and Analysis of the Transient Radiation Electric Field Excited by the Switching Operation of the Breaker in GIS[J]. Proceedings of the CSEE, 2016, 36(18):5087-5093.

[2] C. M. Wiggins, S. E. Wright, Switching transient fields in substation, IEEE Trans. on PD, vol. 6, no. 2, pp. 591-600, 1991.

Characterization of Attenuation of various Civil Structures for High Intensity Transient EM Field

Asian Electromagnetic Symposium (ASIAEM-2017)

M. Ratna Raju, Scientist - D
EMI-EMC Tech Centre
Research Centre Imarat (RCI), DRDO
Hyderabad, Telangana, India
ratnam.raju@rcilab.in

D. Ratan Sanjay, Scientist ó E
Compact Antenna Range facility
Research Centre Imarat (RCI), DRDO
Hyderabad, Telangana, India
d.ratnasanjay@rcilab.in

Sandeep M. Satav, Scientist - F
EMI-EMC Tech Centre
Research Centre Imarat (RCI), DRDO
Hyderabad, Telangana, India
sandeepm.satav@rcilab.in

*Abstract*ô This paper, presents the practical test results of attenuation characterization of various civil structures for high intensity transient electromagnetic filed generated by particular class of High Power Electromagnetic (HPEM) system. In this paper a standard measurement procedure for measurementof EM filed of HPEM systemhas been explained as part of calibration of the system for characterization of attenuation. By using calibratedsystem, variousstructures of building such as concrete roof, brick wall, grilled windows, metal doors, air conditioning ducts of building have been characterized for their shielding effectiveness to transient EM field.Consolidated test results of attenuation of structures are tabulated and various inferences have been drawn.

Keywords-Attenuation, Shielding effectiveness, High Power Electromagnetic (HPEM),

I. INTRODUCTION

It is essential to evaluate the attenuation of various structures of building for particular class of HPEM field; so that it will be very useful for evaluating the breakdown/upset levels of equipment installed in a building for HPEM threats. For attenuation measurement of different structures of building, an indigenously & in-house developed compact HPEMsystem has been used. The system has E*r product of 240 kV.

II. HPEM SYSTEM CALIBRATION

The measurement process which have been adopted for HPEM system characterization has been shown in figure 1
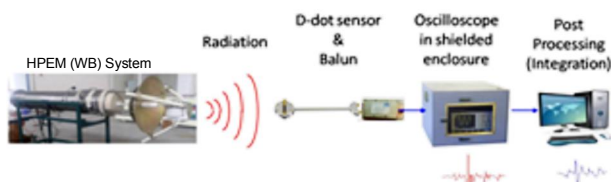
Figure 1 HPEM system calibration setup

The peak values varied between 240kV/m to 300kV/m at 1m as shown in Figure 2; plotted sensor output in MATLAB for successively measured 100 pulses on the same graph to ensure repetitiveness of the system.

III. ATTENUATION MEASUREMENT

The HPEM system which has been calibrated for E-field in the above paragraph is used for attenuation measurement for various obstacles. Consider the concrete roof of building; photograph of attenuation measurement setup and corresponding test results are given in figure 3 and 4
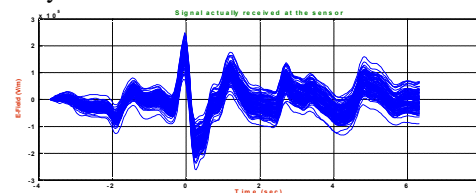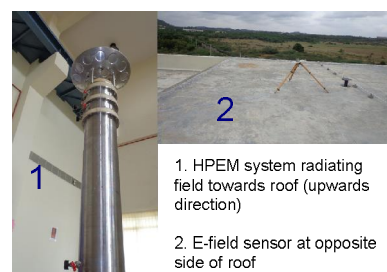
respectively.

Figure 2 E-field value at 1m distance from HPEM System

1. HPEM system radiating field towards roof (upwards direction)

2. E-field sensor at opposite side of roof
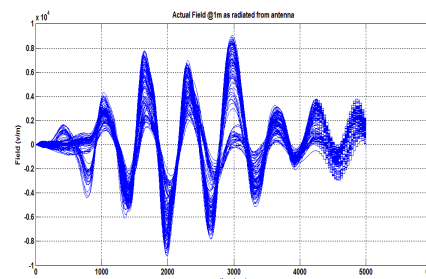
Figure 3 Setup for attenuation measurement of roof

Figure 4 E-field measured in opposite side (for system)of roof

Detailed explanation for system calibration and attenuation measurement of remaining obstacles will be discussed in main paper. Consolidated test results are given in table 1

TAMBLE 1 ATTENUATION MEASUREMENT

.	stacle	Reference E Field	
		r c *t r* *bstac*	*Att* *at* *r*
1	Brick wall	90 kV	8.52
2	Grilled window	50 kV	13.62
3	Metal door	2.6 kV	39.30
4	Concrete roof	7.0 kV	30.70
5	AC honeycomb ducts	80 kV	90.5

REFERENCES
[1] Simple sub 50ps rise time high voltage generator by MM Kekez, institute of information technology, Ottawa, Canada
[2] D V Giri, Radiated spectra of impulse radiating antennas, sensor and simulation notes 386, 1995

Development of Compact,Wide Band (WB), High Power Electromagnetic (HPEM) System Electronic Vulnerability Study (EVS)

Asian Electromagnetic Symposium (ASIAEM-2017)

M. Ratna Raju, Scientist - D
EMI-EMC Tech Centre
Research Centre Imarat (RCI), DRDO
Hyderabad, Telangana, India
ratnam.raju@rcilab.in

Sandeep M. Satav, Scientist - F
EMI-EMC Tech Centre
Research Centre Imarat (RCI), DRDO
Hyderabad, Telangana, India
Sandeepm.satav@rcilab.in

D. Ratan Sanjay, Scientist ó E
Compact Antenna Range Facility
Research Centre Imarat (RCI), DRDO
Hyderabad, Telangana, India
D. Ratnasanjay@rcilab.in

Abstract— This paper presents the design and development of a compact, Wide Band (WB), High Power Electromagnetic (HPEM) system, indigenously& in-house developed by the EMI-EMC Tech Centre, RCI for performing vulnerability studies on various types of electronic systems. The HPEM system consists of a HV power supply, a HV pulse generator, a discone antenna with a spark gap at the feed in compact size and a 1.8m parabolic reflector to direct the field. This system has E*r value of 720 kV. It is 24 V DC operated System. A 14-stage Marx generator scheme with a high pressure spark gap at peaking gap is used for pulse generation. The radiating system consists of a Discone antenna with a spark gap at its feed immersed in oil and placed at the focus of the reflector. A 3.5 GHz free field sensor (D-dot) and 2.5 GHz bandwidth digital storage oscilloscope is for characterization of the systems. Vulnerability studies are conducted on various types of electronic like personal computer (PC), Industrial PC, communication equipment, test & measuring instruments etc. Details of the system & characterization results of the system are presented. Data of electronic vulnerability studies are also presented.

KEYWORDS- HPEM, Marx Generator, Discone Antenna, Reflector, EM Field

I.   INTRODUCTION

A HPEM environment can be a single pulse with many cycles of a single frequency, an ultra-wideband transient pulse.The last two decades have witnessed increased interest in HPEM, particularly generation of high-power electromagnetic fields and their effects on electronics.In this paper we present the design and development of a HPEM (WB) system to conduct vulnerability studies on different electronics. It delivers a WB signal, directed by a parabolic reflector of diameter 1.8m.
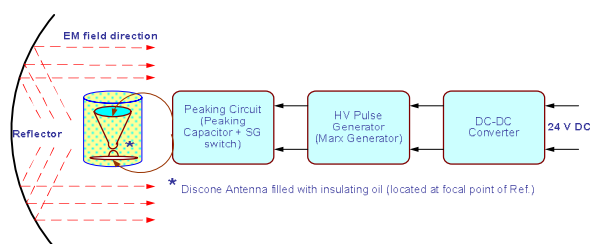

Figure 1 Block diagram of compact HPEM (WB) system

II.   SYSTEM DESIGN & DEVELOPMENT

The Block diagram of compact HPEM (WB) system as shown in figure.1 consists of a compact HV fast rise time impulse generator including battery fed DC-DC Convertor, a peaking circuit and an oil filled conical antenna. Detailed system design and development will present in main paper and experimental setup is given figure 2.

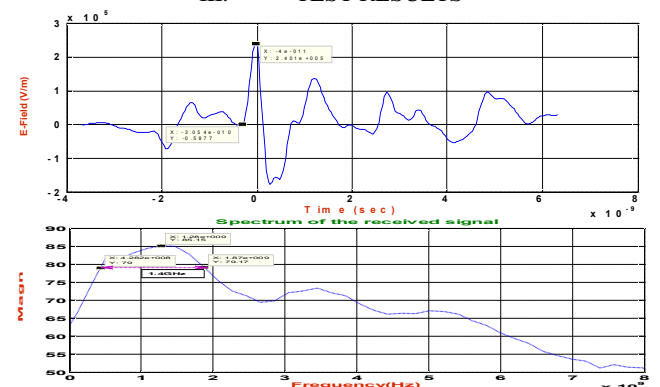Figure 2Experimental setup of compact HPEM (WB) system

III.   TEST RESULTS

Figure 3Test results (mag. & spectrum) of HPEM (WB) system

We achieved field strength 250-300 kV/m at 1 m distance and magnitude spectrum has peak amplitude at 1.4 GHz with band width 400 MHz. Details of test results will present in main paper.

III.   VULNERABILITY STUDIES

TABLE I.   VULNERABILTY STUDIES CONCLUSION

s	Target	Effect	Field strength	Dist.	PRF
1.	Function gen.	4 kV/m	Operational upset	50 m	22
2.	Oscilloscope	4 kV/m	Operational upset	50 m	22
3.	Radio set	3.5 kV/m	Funct. damage	60 m	22
4.	PC (HP)	6 .5 kV/m	Operational upset	40 m	22
5.	Ind. Computer	7.5 kV/m	Operational upset	26 m	22
6.	Missile OBC	8.6 kV/m	Operational upset	20 m	22
7.	Mobile Phone	10 kV/m	Funct. damage	18 m	22

REFERENCES
[1] Marx Gen. design & performance; by WJ Carey &JR Mayes
[2] Electrode design by N.Giao Trinh, Senior IEEE member

Fast Rise-time, Transient High Voltage Divider

Sandeep Satav
Scientist-F, EMI-EMC Tech Centre
Research Centre Imarat
PO Vignyanakancha, Hyderabad, TS, India
sandeepm.satav@rcilab.in

Dr. V. M. Pandharipande
Professor (Emeritus)
ECE Dept. CoE, Osmania University
Hyderabad, TS, India
vijaympande@yahoo.com

Abstract — Measurement of High Voltage (HV) impulse, transient signal waveform is required in several applications like operation and maintenance of Electromagnetic Pulse (EMP) simulator, Marx generator and in EMI testing like CS115, CS116, ESD & lightening tests of MIL-STD-461G. Other methods of measurement like resistive and capacitive divider have limited band width and have other limitations for measuring HV signals in the sub-nanosecond rise time range. In the proposed method no lumped element is used, electromagnetic field generated due to flow of signal is detected and measured. It is an invasive device. In this paper measurement principle is explained and construction details of a high voltage prototype are presented. Calibration of the device is presented along with the final measurement results.

Keywords- High voltage, fast transient, derivative sensors

I. INTRODUCTION

Characterization and measurement of HV fast rise time transient signal is essentially required in the design, development, operation and maintenance of several systems like EMP simulator, IEMI, ESD or transient generator used in EMI-EMC testing. These voltages can be in the range of 600 kV with rise time as fast as 1 ns to 400 ps. All step / pulse / impulse generator define their waveform into specific broadband resistive impedance mostly 50 Ω. Waveform characteristics of generator changes when connected to an antenna which is having a dynamic impedance beyond its operative frequencies. It is important to know the exact incident waveform into the antenna input connector. Also for transient signal, radiated response of different antennas is different. For an example, a step function given to an Impulse Radiating Antenna (IRA) will be differentiated by the antenna and radiated field will be of an impulse, which is first derivative of the step signal.
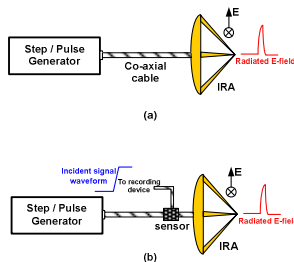
Fig. 1 Measurement requirement

In such cases, there is a definite need of measuring the voltage signal flowing through the coaxial cable to the antenna input connector or output of any impulse generator. As shown in figure 1 (a) in absence of a suitable sensor, no information about the incident waveform is available, while in figure 1 (b), a measurement device gives information about the incident waveform. Hence, a relationship between incident waveform and radiated waveform from an antenna can easily be established. Similar measurement can also be done with the help of Resistive or Capacitive Divider. However due to parasitic capacitance and wire/cable inductance rise time of such divider has restriction. For example, fastest rise time Resistive divider of 200 kV has rise time of only 20 ns, whereas requirement is for 400 kV, 400 ps – 1 ns range.

II. WORKING PRINCIPLE

The working principle of the sensor is a miniature ground plane d-dot sensor installed within a coaxial structure. It picks the derivative (time rate of change) of electric flux density (D). The output voltage of sensor is proportional to the derivative of the D;
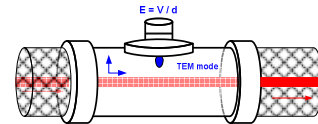

Fig. 2 Schematic of a V-dot sensor

$$V_{sensor} \; \alpha \; \frac{dD}{dt} \tag{1}$$

$$V_{sensor} = R \; A_{eq} \; \dot{D} \tag{2}$$

where, R is load impedance (Ω) and A_{eq} is equivalent area of the sensor (m^2) depending upon its geometrical shape and capacitance.

$$V_{(on\,centre\,cunductor)} \; \alpha \; E\text{-field}\,_{(inside\,coaxial\,geometry)} \tag{3}$$

REFERENCES

[1] Everett G. Farr *et. al.*, "A Comparison of Two Sensors Used to Measure High-Voltage, Fast-Risetime Signals in Coaxial Cable," Measurement Note 58, March 2004.

Effects of millisecond pulsed electromagnetic field on C6 cell's viability and apoptosis

Yao Xueling, Xu Wenjun, Sun Jinru, Le Yangjing, Chen jingliang, Lu Xiaoyun
State Key Laboratory of Electrical Insulation and Power Equipment
Xi'an Jiaotong University
Xi'an, Shaanxi, China
xlyao@mail.xjtu.edu.cn

Abstract
This paper established the electromagnetic environment with rise time 0.18ms, the duration time 1.396ms. The magnetic intensity is 6mT. The cell viability the apoptosis is observed. The results showed that in the fourth day showed significant inhibition by 14.16%($P<0.001$). There was no obvious apoptosis in apoptotic observation.
Keywords: Pulsed electromagnetic field, Mice glioma cells(C6), cell viability, Apoptosis

I EXPERIMENTAL METHODS

The 96-well plate was cut into 4x4 units and used after 24 hours of sterilization under ultraviolet light. The digested mouse glioma C6 cell line (supplied by the Department of Biology, Xi'an Jiaotong University School of Biomedical Engineering) was added to 96-well plates (4x4) and cultured at 3000/100 μL per well. The medium was a high glucose medium containing 10% FBS and incubated in a 5% CO_2 cell incubator at 37 °C. Adhere to 12 hours after the experiment. The Exposure magnetic intensity is 6mT, frequency is 30s per time, last 4 hours per day, continuous for 4 days.
The MTT method was used for cell viability test, and Hochest method was used for apoptosis test.

II EXPERIMENTAL RESULTS

2.1 Cell Viability Result

The MTT results for cell viability is shown in Figure 1. It's the result for 4 days for both control group and exposure group. There was no significant difference in cell viability between the irradiation group and the control group. The cell viability was significantly inhibited on the fourth day (P <0.001), and the inhibition rate was 14.16%.
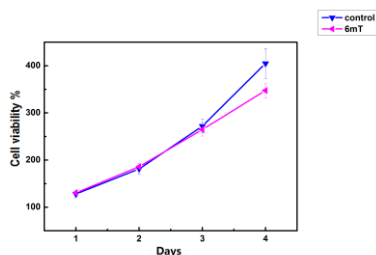
Figure1 Cell viability test result for 4 days

2.2 Apotosis Result

The Hoechst apoptosis results are shown in Figure 2. Compared with the control group and exposure group, there was no obvious apoptosis or micronucleus.
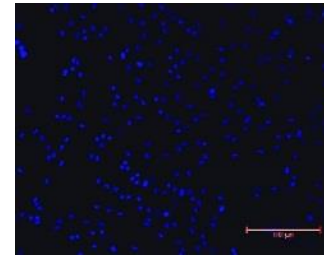
(a)Control group
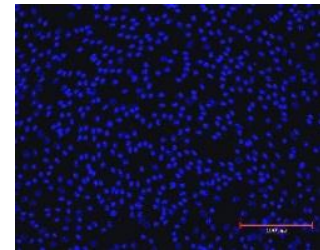
(b)Exposure group
Figure2 Cell apoptosis test result

III CONCLUSION

This paper established a millisecond exponential wave electromagnetic field. The rise time is 0.16ms, the duration time is 1.396ms, and the exposure is 30s per time, 4 hours a day for 4 days. The intensity of the magnetic field is 6 mT. MTT method is performed for testing cell viability each day and Hoechst method is used to observe the apoptosis in the 4th day. The following conclusions are obtained: the cell viability response after electromagnetic field exposure is nonlinear and had a significant cumulative effect. There was no significant difference between the exposure group and the control group in the first three days. In the 4th day, the experimental results showed that the cell viability is significantly inhibited by 14.16%. Apoptotic observation showed no obvious apoptosis between these two groups.

REFERENCES

[1].Verginadis, I., et al., Beneficial Effects of Electromagnetic Radiation in Cancer. 2012. 249-268.
[2].Sun Yueming et al.The research progress of human golima cell line U251,SHG-44,U87. Practical Journal of Cardiac Cerebral Pneumal and Vascular Disease, 2015(2):p.7-9

The Simulation and Experiment Research for Lightning Direct Effect of CFRP Subjected to Current Component A

Yao Xueling, Guo Canyang, Sun Jinru, Xu Wenjun, Chen jingliang
State Key Laboratory of Electrical Insulation and Power Equipment
Xi'an Jiaotong University
Xi'an, Shaanxi, China
xlyao@mail.xjtu.edu.cn

Abstract

The mechanism of the damage in carbon fiber reinforced polymer (CFRP) with lightning current component A strike was explored in this paper. The experimental results show that the damage modes are comprised of the decomposition of epoxy, carbon fibre breakage and sublimation.
Keywords: CFRP; coupled electrical-thermal analysis; direct effect of lightning current; Finite element model.

I EXPERIMENTAL METHODS

In order to simulate lightning strike, this paper establish a lightning current component A generator as shown in Fig.1.
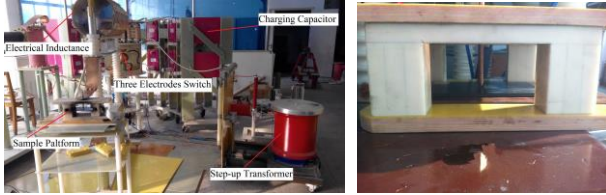
Figure 1. Lightning current component A generator

The lightning current component A is designed according to the standard SAE ARP5412. The experimental current waveform which is applied on CFRP is showed in Fig.2
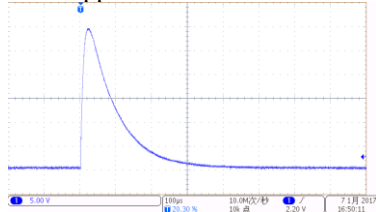
Figure 2. the lightning current waveform of 30kA

II EXPERIMENTAL RESULTS

The lightning damage and scanning results on the upper surfaces of CFRP specimens under the impulse current $(20/85\mu s)$ with peak current of 20kA and 35kA respectively are showed in Fig.3.
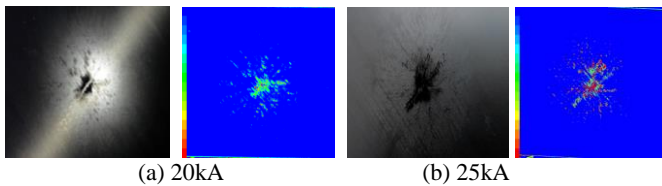
(a) 20kA   (b) 25kA
Figure.3 Photograph of the specimen after lightning strike

From Figure 3, It can be found that the main damage zones distribute vertically. The deep colour region like red represents much more serious damage than the light colour like green.

III. NUMERICAL SIMULATION

Coupled thermal-electrical analysis is conducted using multi-physics. The three-dimensional finite element model is constructed, as shown in Fig.4. The model is 8-ply quasi-isotropic $([45/0/-45/90]_{4s})$ type. The specimen is 150 mm length and the 100mm width and 1mm thickness.
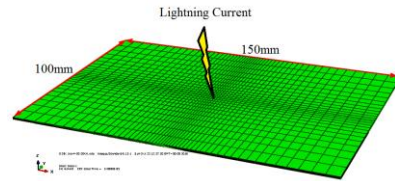

Figure 4. The finite element model

The surface damage is shown in Fig.5 and the temperature distribution is showed in Fig.6.
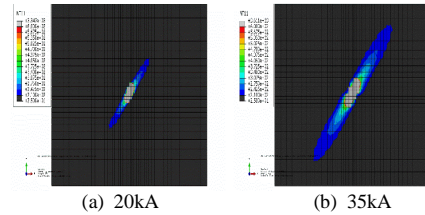

(a) 20kA   (b) 35kA
Figure 5. The surface damage of CFRP
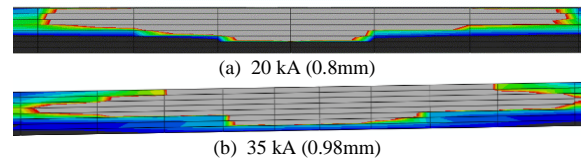

(a) 20 kA (0.8mm)

(b) 35 kA (0.98mm)
Fig.6 The damage depth of CFRP

IV CONCLUSION

Lightning tests and numerical simulation were performed to explore the mechanism of the damage behaviour of CFRP. The lightning current component A causes visible damage to the carbon/epoxy laminate and the damage mainly includes the decomposition of epoxy, fibre breakage and carbon fibre sublimation. The propagation of the fibre breakage is vertical. With the increase of the lightning current I_{peak}, the damage depth of CFRP increases obviously.

REFERENCES

[1] Chemartin L, Lalande P, Peyrou B, et al. Direct effects of lightning on aircraft structure: analysis of the thermal, electrical and mechanical constrsins. J Aerospace Lab 212,5(AL05-09):1-15.
[2] Ogasawara T, Hirano Y, Yoshimura A. Coupled thermal-electrical analysis for carbon fibre/epoxy composites exposed to simulated lightning current. Composites: Part A 2010,41(8):973-81.

HEMP radiated environment distribution simulated by Monte Carlo method

Ning Dong, Yan-zhao Xie
State Key Laboratory of Power Equipment and Electric Insulation
National Center for Reasearch on Transient Electromagnetic Enviroments and Applications
School of Electrical Engineering, Xi'an Jiaotong University
Xi'an, Shaanxi, China
dongning96@163.com; yzxie@mail.xjtu.edu.cn

stract—The HEMP radiated environment at one certain position with fixed latitude and longitude is a consequence of nuclear bursts around the observation point. In this paper, aiming for better clarifying HEMP radiated distribution environment, it is determined as functions of the latitude, longitude and height of the burst and is simulated by Monte Carlo method. The result of this paper can be referential to more future research in this domain.
Keywords: HEMP; radiated environment; Monte Carlo method

I. INTRODUCTION

The radiated environment due to a high altitude nuclear burst is related to the altitude and the local geomagnetic inclination which is determined by the latitude and longitude of the burst [1]. Thus the waveform characteristics of the early-time HEMP surround the burst are function of the burst's latitude, longitude and height.

The radiated environment at certain position is consequence of the bursts happened around the observation point; the bursts are regarded as uncertain events with uncertain parameters. The radiated environment distribution can be simulated by Monte Carlo method and described using a probabilistic method, which shows more realistic situation than considering the radiation as 50kV/m standard waveform all around.

II. PHYSICAL MODEL OF CALCULATION

When λ radiated released by high-altitude nuclear explosion interacts with air molecule, they produce Compton current and secondary current, which interact with the geomagnetic filed and result in HEMP.
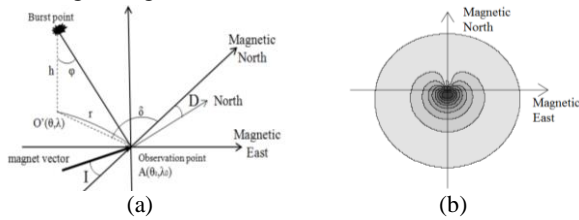

(a)   (b)

Figure 1(a) Burst, observation point and the definition of varieties
(b) Peak electric field intensity on the earth's surface of HEMP

Based on the physical process, the peak electric field intensity, polarizing angle and elevation angle ($,\alpha,\psi$) of the HEMP wave at O could be deduced as the function only with respect to the latitude, longitude and height ($\theta,\lambda,$) of the burst：

$$(\theta,\lambda,) = {}_0\sqrt{\begin{array}{l}\sin^2\varphi\sin^2\delta\sin^2 I + \sin^2\varphi\sin^2\delta\cos^2 I \\ +(\sin\varphi\cos\delta\sin I - \cos\varphi\sin I)^2\end{array}} \quad (1)$$

$$\alpha(\theta,\lambda,) = \tan^{-1}\left[\frac{\sin\varphi\sin I + \cos\varphi\cos\delta\cos I}{\sin\delta\cos I}\right] \quad (2)$$

$$\psi(\theta,\lambda,) = \cos^{-1}((+) / *\sin\varphi) \quad (3)$$

Due to function(1) , the Peak electric field intensity on the earth's surface surrounding the burst is calculated as shown in Fig.1(a), for a magnetic dip equals 45°.

The geomagnetic inclination I(θ,λ) is the angle between magnetic north and the earth's magnetic field vector. The angle will change with the variation of latitude and longitude. It could be calculated based on the No.11 International Geomagnetic Reference Field model by Schmidt semi-normalized associated Legendre functions [2].

TABLE I Relation of geomagnetic inclination to the change of latitude and longitude (unit: °)

Latitude/°N	longitude/°E			
	40	80	120	160
40	57.04	56.44	55.46	54.57
60	73.57	73.46	73.14	73.11
80	85.03	85.05	85.02	84.78

III. RESULT OF CALCULATION

Assume the high-altitude nuclear explosion surrounding one certain observation point is uncertain. The height，longitude and latitude of the burst are arbitrary parameters and considered as uniformly distributed. Utilize Monte-Carlo simulation to calculate the peak electric field intensity.
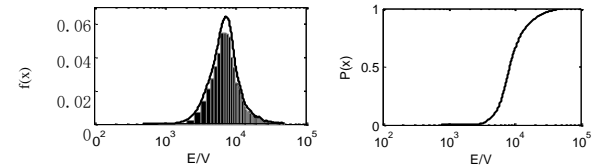

Figure 2 Histogram and PDF, CDF of peak electric field intensity

By combining 10000 calculation results for the Peak electric field intensity, the probabilistic method provides the probability function, probability distribution function and confidence level of the radiated environment.

TABLE II Probability to exceed different value of peak electric field intensity of HEMP

Prob(E>x)	0.9	0.5	0.1
Peak electric field intensity/V	19030	8421	4995

REFERENCES
[1] Ianoz M, Nicoara B I C, Radasky W A. Modeling of an EMP conducted environment[J]. IEEE Transactions on Electromagnetic Compatibility, 1996, 38(3):400-413.
[2] International Association of Geomagnetism and Aeronomy Working Group V-MOD. Participating members, Finlay C C, Maus S, et al. International Geomagnetic Reference Field: the eleventh generation[J]. Recent Developments in World Seismology, 2012, 183(3):1216–1230.

Half Impulse Radiating Antenna for High Voltage UWB System

S. K. Singh, S. Mitra, K. Senthil, R. Chaurasia, Archana Sharma

Accelerator and Pulse Power Divison
Bhabha Atomic Research Centre
Mumbai Maharashtra, India
sandeeps@barc.gov.in[1],sabyam@barc.gov.in[2]

Abstract—This paper discusses the design and analysis of a Half Impulse Radiating Antenna ('HIRA') for a high voltage 'UWB' (Ultra Wide Band) system developed at APPD, BARC Mumbai. High voltage pulser in this system consists of a Marx generator and a solid dielectric pulse forming line with an embedded peaking switch. A 100 Ω HIRA antenna has been designed to match with the pulse forming line impedance. Simulated results of reflections coefficient, VSWR and gain in frequency domain are presented in this paper. Time domain response of the antenna is also discussed. Designed antenna shows good performance over entire frequency range of 250 MHz – 1.25 GHz, which is determined according to pulse parameters.

Keywords-UWB; HIRA; far field; rise time.

I. INTRODUCTION

Antennas capable of radiating and receiving fast pulses are required in high power UWB applications. High gain, low dispersion and low return loss over a wide frequency range are the requirements for UWB antennas used in these systems [1, 2]. Designed antenna was intended to work in 250 MHz-1.25 GHz frequency range according to the pulse parameters of the system (3.5 ns FWHM,300 ps rise time). A Half Impulse Radiating Antenna is designed for these pulse parameters, this antenna can be directly fed using an unbalanced source. Practical and simulated time response of complete antenna structure is presented in this paper. Peak power pattern of antenna is also measured practically in horizontal plane.

II. DESIGN

Based on the pulse parameters, design frequencies were calculated. Half Impulse radiating antenna is used for radiation of UWB pulses in this system. This antenna is a paraboloidal reflector antenna with a TEM feed. Antenna diameter was chosen to be 2 m for appropriate electromagnetic field radiation. Antenna design was carried out using analytical formulas [3, 4]. Same structure was modelled and simulated in CST microwave studio. Two constant impedance coplanar TEM feed lines are used for feeding the reflector antenna. Some new type of feed structures have also been suggested recently [5]. Impedance of each feed line was 200Ω. Each feed arm is terminated with a 200 Ω copper sulphate aqueous resistor to provide low frequency impedance matching.

III. RESULTS

Based on above considerations an antenna was designed as shown in figure 1. Waveform of radiated electric field is shown in figure 3. A figure of merit of ~200 kV has been achieved using this UWB system. Peak power pattern of antenna was measured in horizontal plane; half power beam width of antenna was 5 degrees as shown in figure 2.Simulated gain of antenna at 1 GHz frequency was 17dB. Power measurement for peak power pattern was performed at low power.
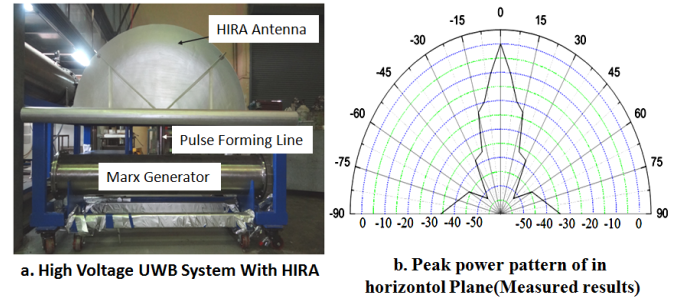

a. High Voltage UWB System With HIRA
b. Peak power pattern of in horizontol Plane(Measured results)

Fig.1 High UWB System and its peak power pattern

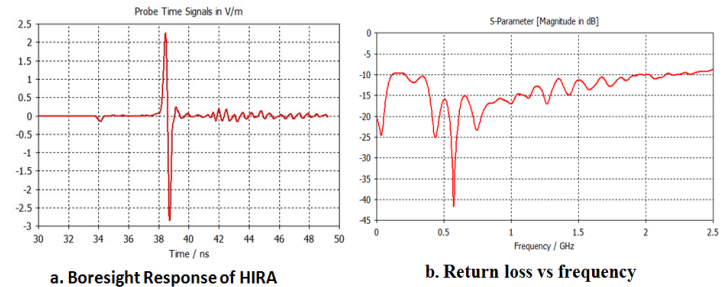a. Boresight Response of HIRA
b. Return loss vs frequency

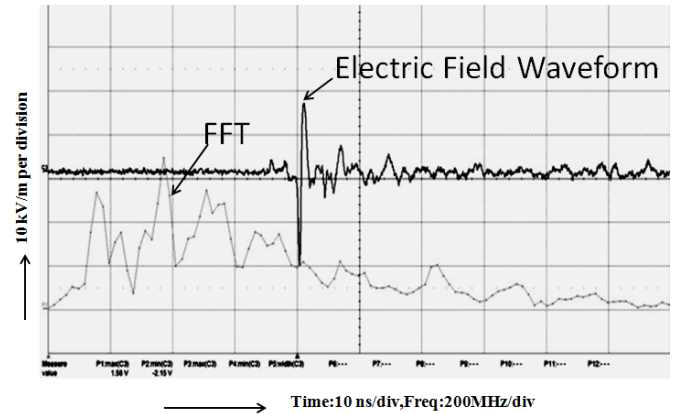Fig.2 Boresight response and return loss for HIRA

Fig.3 Radiated Electric Field Waveform (Measured) along with FFT

REFERENCES

[1] D. V. Giri, F.M. Tesche and C.E. Baum "An Overview of High-Power Electromagnetic (HPEM) Radiating and Conducting Systems" Circuit and Electromagnetic System Design Notes, Note 50 (Feb 2006).

[2] D.V. Giri, "High Power Electromagnetic Radiators Nonlethal Weapons and Other Applications", Harvard University Press, 2004.

[3] E. G. Farr and G. D. Sower, "Design Principles of Half Impulse Radiating Antennas," Sensor and Simulation note 390, 1995.

[4] C. E. Baum et. al., "JOLT: a highly directive, very intensive, impulse-like radiator", Proceedings of the IEEE Volume: 92, Issue: 7, July 2004.

[5] Dhiraj K. Singh et. al., "Gain enhancement of reflector based impulse radiating antennas: An innovative approach", Progress in Electromagnetic Research C, Vol. 38, pp153-164, 2013.

ASIAEM 2017- Design of antenna systems with Tx/Rx Isolation for Handheld GPR

Preeti Dongaonkar
Electronics & Radar Development Establishment
DRDO
Bangalore,Karnataka,India
preeti.dongaonkar@lrde.drdo.in

Abstract—This paper describes the design of two types of antenna systems which can be used in a handheld GPR. These antenna systems are particularly suitable for GPR which transmit Stepped Frequency Continuous Waveform (SFCW).The antenna system for Handheld GPR typically consist of a single radiating element for transmit and a radiating element for signal reception.Since in SFCW GPR transmit antenna (Tx antenna) is continuously transmitting and receiver antenna(Rx antenna) is receiving there should be high isolation between Tx and Rx antenna so that receiver does not get saturated.This paper brings out design and performance comparison of a monopole based as well as a frequency independent element based antenna system for SFCW GPR.These antenna systems have been designed with Tx/Rx isolation of <-30 over 150% bandwidth.

Keywords-UWB antenna;SFCW based GPR;monopole antenna,log-periodic antenna;handheld GPR

I. INTRODUCTION

Handheld GPR is a useful technique for detection of Anti-personnel mines(APM),Anti Tank Mines (ATM) and Improvised Explosive Devices (IED's).GPR systems are required to operate over an Ultra Wideband (UWB) to achieve target resolution of the order of few cms. Also as the depth of penetration into the soil is inversely proportional to frequency,the operating frequency starts from few 100 MHz. Thus the antenna has to be UWB and at the same time it should be compact for a handheld GPR. In addition to this for SFCW based GPR there should be sufficient Isolation between Tx and Rx antenna over UWB. These requirements present very big challenge for antenna design.

II. DESIGN OF UWB ANTENNA SYSTEMS

In the first design a monopole antenna has been designed to operate over an UWB and the isolation between Tx and Rx antenna has been reduced by use of a Flat absorber and an aluminium plate. Fig 1 shows the photograph of the antenna which consists of a Tx and a Rx monopole element separated by absorber and an isolation plate.By using these,isolation was improved to -30 dB over the band from initial value of -14 dB. Fig 2 shows measured Return

loss and Isolation of this antenna system.

In the second design an antenna system based on frequency independent element has been designed.The results of this design will be presented.
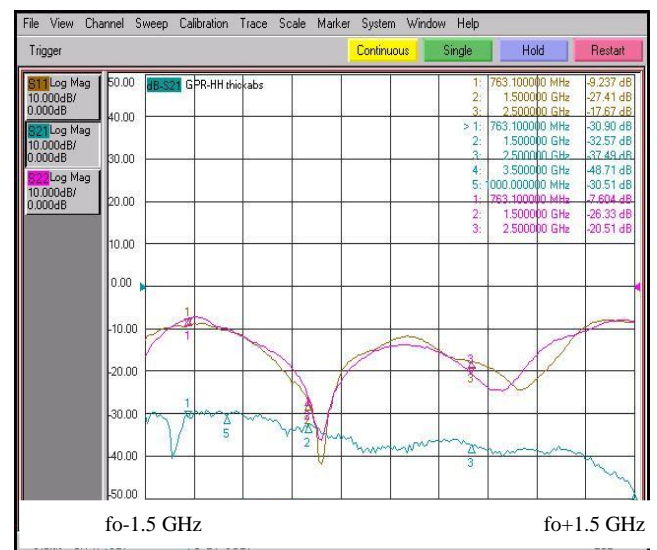

Figure 1.Monopole based HH GPR Antenna.

Figure 2.Measured Return loss and Isolation of Tx/Rx antenna

REFERENCES
[1] D.J.Daniels, "Ground Penetrating Radar", Encyclopedia of RF and Microwave Engineering,Vol.2, Jhon Wiley and Sons, Ins., Hoboken, New Jersey, United States,2005
[2] Dhiraj K Singh,D. C. Pande,A Bhattacharya "Development of Low Profile Hybrid Printed UWB Monopole Antenna for Handheld GPR Applications",9th International Radar Symposium India-2013 (IRS-13).
[3] R Bawer & J.J Wolfe "The Spiral Antenna",1958 IRE International Convention Record (Vol 8).
[4] G. Dyson, j., "The Equiangular Spiral Antenna" Antenna and Propagation , IRE Transactions on, Vol 57, no.2,pp.181-187,April 1959

A Full-Scale Experimental Test of Electromagnetic Time Reversal Applied to Locate Faults in Power Lines

Zhaoyang Wang[1,*], Shaoyin He[2], Qi Li[2], Buying Liu[2], Reza Razzaghi[1], Mario Paolone[1], Yanzhao Xie[2,*] and Farhad Rachidi[1,*]

[1] Swiss Federal Institute of Technology (EPFL), Lausanne, Switzerland

[2] State Key Laboratory of Electrical Insulation and Power Equipment,
Electrical Engineering College, Xi'an Jiaotong University, Xi'an, Shaanxi, China

zhaoyang.wang@epfl.ch, yzxie@xjtu.edu.cn, farhad.rachidi@epfl.ch

Abstract—We present a full-scale experimental test of the electromagnetic time reversal applied to locate faults in power network.

Keywords—Fault location; electromagnetic time reversal; distribution networks.

I. INTRODUCTION

The functionality of fault detection with higher performances in terms of location time and accuracy is of paramount importance in today's and future transmission and distribution power networks [1].

Motivated by improving the applicability and efficiency of the currently developed fault location methods in power system, a promising technique based on the theory of electromagnetic time reversal (EMTR) [2] has been recently applied to locate faults in power networks [3]. The proposed method is applicable to topologically complex and inhomogeneous networks and active distribution networks. Furthermore, it shows superior performance in terms of accuracy and robustness against uncertainties with respect to the existing methods.

In this paper, we present the results of a field experiment illustrating the ability of EMTR-based method to locate faults along a 10-kV overhead line. In particular, the paper shows, for the first time, the experimental validation of the EMTR-based fault location method in a field environment of power system. The experiments were performed on a 677-m long 10-kV distribution line in Yuncheng city, Shanxi Province, China.

II. ELECTROMAGNETIC TIME REVERSAL APPLIED TO FAULT LOCATION

Based on the reversibility in time of the wave equations [2], an EMTR-based fault location method was proposed in [3]. The method is implemented in three steps, namely: *i)* measurement of the fault-generated electromagnetic transients at observation point(s), *ii)* simulation of the back-injected time-reversed measured fault signals for different guessed fault locations (GFLs), and *iii)* assessment of the fault location by analyzing the energy of current flowing through each GFL [3]. The real fault location is characterized by the highest energy concentration.

III. EXPERIMENT

In November 2016, an experiment aiming at validating the EMTR-based technique to locate faults in a real distribution line was conducted. The tested line is a 677-m long 10-kV distribution line located in Shanxi Province, China. The line includes 11 overhead-line towers. To emulate a phase-to-ground fault occurrence, a pulse generator was connected between a phase conductor and the ground, injecting a pulse with rise time around 3 ns. The full width at half maximum (FWHM) of the pulse is approximately 1.15 µs. The faulty phase of the line was grounded at both ends through a 1500 pF thin-film capacitor, representing the high-frequency input impedance of the power. The induced transient current signal was measured at one end of the line. According to the EMTR technique [3], the measured current signal was time-reversed and back-injected into the model of the line simulated in EMTP-RV [4] and the fault location (pulse injection point) was accurately identified.

REFERENCES

[1] "*IEEE guide for determining fault location on ac transmission and distribution lines – redline,*" IEEE Std C37. 114-2014 (Revision of IEEE C37. 114-2004) – Redline, pp. 1 – 128, Jan. 2015.

[2] M. Rubinstein, F. Rachidi and M. Paolone, "Time reversal: a different perspective," in *Electromagnetic Time Reversal: Application to Electromagnetic Compatibility and Power Systems*, ch. 1, Wiley, 2017.

[3] R. Razzaghi, G. Lugrin, H. M. Manesh, C. Romero, M. Paolone, and F. Rachidi, "An efficient method based on the electromagnetic time reversal to locate faults in power networks," *IEEE Transactions on Power Delivery*, vol. 28, no. 3, pp. 1663 – 1773, Jul. 2013.

[4] J. Mahseredjian, S. Dennetière, L. Dubé, B. Khodabakhchian and L. Gérin-Lajoie: "On a new approach for the simulation of transients in power systems," *Electric Power Systems Research*, vol. 77, issue 11, pp. 1514-1520, Sept. 2007.

Research on High-Voltage GTEM cell for E1 pulse

Jeong-Ju Bang
Aerospace EM Technology Center
Korea Testing Laboratory(KTL)
Jinju, Republic of Korea
jjbang@ktl.re.kr

Tae-Heon Jang
Aerospace EM Technology Center
Korea Testing Laboratory(KTL)
Jinju, Republic of Korea
thjang@ktl.re.kr

D.V. Giri
University of New Mexico
PRO-TECH
11-C Orchard Ct, Alamo, CA 94507 USA
giri@DV.com

Abstract— In this paper, high-voltage Gigahertz Transverse Electromagnetic (GTEM) cell for E1 pulse is investigated. The GTEM cell which consists of a tapered rectangular waveguide loaded with septum is discussed. The TDR and S parameter of GTEM-cell was measured with the oscilloscope. The measured results were compared with the simulation results performed with CST.

 Keywords- GTEM cell; E1 pulse; Gigahertz Transverse Electromagnetic;

I. INTRODUCTION

In the modern society, Information systems and electronic systems are composed of semiconductor elements. However, in such information equipment and electronic systems, serious failures and breakdowns can occur due to high-power electromagnetic waves. Interest in high-power electromagnetic waves is increasing.
In this paper, we describe a high-voltage GTEM cell for high-power electromagnetic immunity test.

II. Development of high-voltage GTEM cell

Design of GTEM cell
 The schematic of GTEM cell is shown in Figure 1. GTEM cell interior is divided into barriers. The input side volume is filled with gas for insulation. The end of the septum is terminated by distributed resistors.
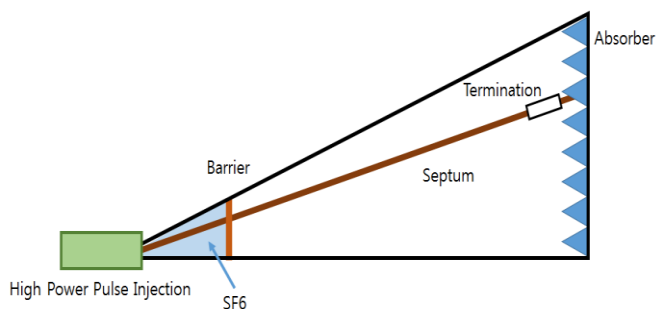

Figure 1.   Schematic of GTEM cell

Simulations were performed to characterize the GTEM cell. The TDR and S parameter were simulated by CST. Figure 2 shows GTEM cell modeling for simulation.
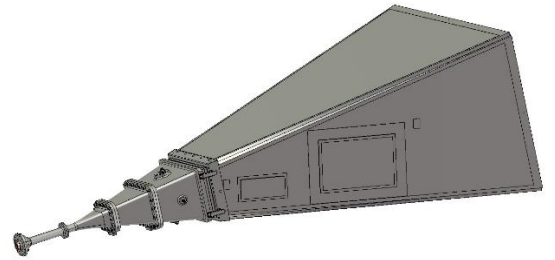

Figure 2.   GTEM cell modeling for simulation

The S parameter is shown Figure 3. The S11 of this commercial GTEM cell is below -5dB in the frequency range up to 2GHz. Figure 4 shows Electric field of GTEM cell.
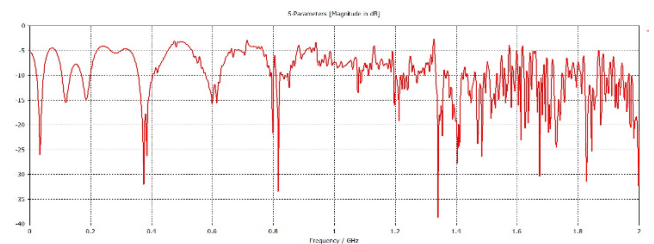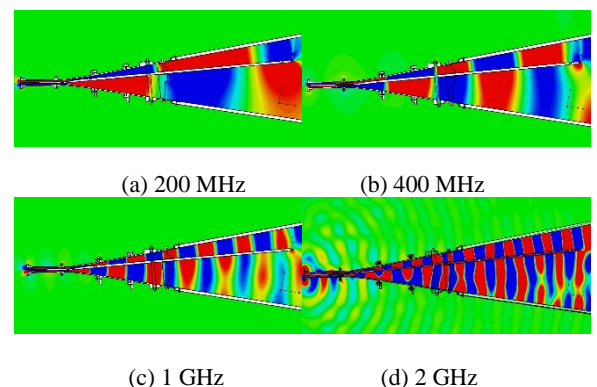

Figure 3. S parameter of GTEM cell (S11)

(a) 200 MHz   (b) 400 MHz

(c) 1 GHz   (d) 2 GHz

Figure 4. Electric field of GTEM cell

REFERENCES
[1]F. Sabath, "Classification of Electromagnetic Effects at System Level", 2008 International Symposium on Electromagnetic Compatibility, pp. 1-5, 2008.
[2] R. Hoad, A. Lambourne, and A. Wraight, "HPEM and HEMP Susceptibility Assessments of Computer Equipment", 2006 17th International Zurich Symposium on Electromagnetic Compatibility, pp. 168-171, 2006.

Circuit Approximation of the Reflection Coefficients for the Asymptotic Approach and the SEM Method

S. Tkachenko, F. Middelstaedt, J. Nitsch, R. Vick
Otto-von-Guericke University, Magdeburg, Germany
e-mail: sergey.tkachenko@ovgu.de

F. Rachidi
Swiss Federal Institute of Technology, Lausanne, Switzerland

Abstract— The SEM method allows to describe the high - frequency electromagnetic response of different scattering objects both in frequency and time domain. The case of a long transmission line can be treated by the so named asymptotic approach, which yields parameters for the SEM expansion. The key role in the application of the asymptotic approach for the SEM play the reflection coefficients for TEM waves. In earlier work they were obtained using an iteration method. In this paper we have shown that these reflection coefficients can be obtained using a concept of the additional terminal impedance (terminal reactance plus terminal radiation resistance) and usual equations of TL theory, and apply then these knowledge for the SEM.

Keywords-SEM; reflection coefficients; transmission lines

I. INTRODUCTION

Different kinds of transmission lines can serve for the transmission of energy and useful signal, but also works as receiver of natural and intentional disturbances, both in frequency and time domain. Numerical methods (MoM, FDTD, etc.) allow to obtain a response of such objects for specific cases, but do not give the general picture of interaction. The classical transmission line (TL) approximation yields the results in general analytical form, but it does not work for high frequencies, when the transversal dimension of the line is large or comparable to the characteristic wavelength and radiation is important.

However, analytical results for the high frequency case can be obtained by the Singularity Expansion Method (SEM). This method was developed by C.E. Baum, F.M.Tesche, D.Giri and other researchers in the earlier 70th (see review in [1]). In the SEM the scattering object is represented as a set of oscillators, which complex frequencies are poles of the response function (defined by one way or another), and don't depend on the kind of excitation of the system. This set of oscillators yields the main contribution to the coupling response of the object both in frequency and time domain. They also define the radiation of the system, the scattering amplitude, etc. Moreover, the SEM poles can be used for identification of systems. However, the main method of obtaining of the SEM expansion for the system of general view is the processing of numerical (e.g., Method of Moments) data.

On the other hand, the application of the SEM to the thin-wire systems (antennas and transmission lines) has several specific features, which make obtaining and the investigation of the SEM expansion essentially easier, especially when the response function is known in analytic form. For the long line (L>>h) such response function can be obtained by using the so-called asymptotic approach, when the current in the central, asymptotic region of the line can be represented in a three - term form, including the forced wave in the infinite line and two forward and backward running TEM waves, caused by the reflection processes at the terminals [2]. The amplitudes of these waves are defined by the so-named reflection and scattering coefficients for current waves. Formally the solution in the asymptotic region looks like a classical TL solution, but the reflection and scattering coefficients have to be calculated for the high- frequency case, when the wavelength can be about the height of the wire above ground. These coefficients can be calculated using perturbation theory for thin wires [2,3,4], or by an analysis of numerical results. The solution for the current includes the resonance denominator, which contains only the reflection coefficients. The zeros of the denominator yield the SEM poles of the first layer (see examples for the open and short circuited horizontal wire in [3,4]). Thereby, the reflection coefficients for the current waves play a key role in the application of the asymptotic approach for the SEM.

II. RESULTS

In this paper we develop another method to define the high frequency reflection coefficients for open and short-circuited lines with an arbitrary geometry of terminals. To do that we introduce additional terminal impedance of the line. On the first step, by using the method of induced EMF [6], we calculate the additional complex power on the terminal by integrating a product of complex conjugate current and scattered field with negative sign (with subtracted TL contribution) along the wire. The scattered field can be found as an integral of the current with the corresponding scalar Green's function kernel using the Mixed Potential Integral Equations (MPIE). In this way the additional complex power is given by the double integral of the product of the current and the complex conjugate current with different argument and their derivatives and some kernels constructed from the scalar Green's function. Then we define the terminal impedance using the usual electrical engineering relations between power, terminal current and lumped impedance for the short circuit line and power, terminal voltage and lumped impedance for the open-circuit wire. The terminal impedance can be represented as terminal reactance (inductive for the short circuit line and capacitive for the open-circuit line) plus terminal radiation resistance. Then the reflection coefficient is defined by the usual equation from the classical transmission line approximation. By direct analytical calculations it was shown that, at least in the first approximation of the small TL parameters ($1/2\ln(2h/r_0)$, where h is a height of the line, r_0 is a radius of the wire), reflection coefficients obtained by the circuit approximation and perturbation theory coincide both for the open circuit and short circuit wire.

Some numerical examples for the calculation of the SEM poles calculated by different methods are presented.

REFERENCES

[1] C.E. Baum, "The Singularity Expansion Method in Electro-magnetics",D.V.Giri and F.M.Tesche(ed.),Lulu Enterprises 2012.
[2] S.Tkachenko, F.Middelstaedt, J.Nitsch, R.Vick,G.Lugrin, F.Rachidi, "High–Frequency Electromagnetic Field Coupling to a Long Finite Line with Vertical Risers", *GA URSI 2014* Beijing.
[3] S.Tkachenko,J.Nitsch,R.Vick,F.Rachidi,D.Poljak,"Singularity expansion method (SEM) for long terminated transmission lines", 2013 Int. Conf. on EM in Adv. Appl. (ICEAA), Torino, 2013.
[4] F.Middelstaedt, S.V. Tkachenko, R.Rambousky, and R. Vick, " High-Frequency Electromagnetic Field Coupling to a Long, Finite Wire with Vertical Risers Above Ground", IEEE Trans. on Electromagn. Comp., Vol. 58 , No. 4 , pp.1169 - 1175, 2016 .
[5] E. K. Miller, "PC's for AP and other EM reflections," IEEE Antennas Propagat. Mag., vol. 41, pp. 82–86, Apr. 1999.

Research on calibration accuracy of D-Dot sensor

Jiang Yunsheng, Meng Cui*
Department of Engineering Physics, Tsinghua University
Key Laboratory of Particle & Radiation Imaging, Ministry of Education
Beijing, China, 100084
jys16@mails.tsinghua.edu.cn

Abstract— The calibration method of D-Dot sensor is needed when measure the EMP environment, but the calibration coefficients' difference obtained in different equipment is always ignored. By means of the comparison of numerical simulation, theoretical calculation and experimental calibration, this paper analyzes the calibration difference of D-Dot sensor in two practical TEM cells, and the consistency is verified.

Keywords- D-Dot sensor; calibration; accuracy; theoretical calculation; simulation; experimental calibration

I. INTRODUCTION

The calibration method of D-Dot sensor is described detailed in IEEE Std 1309-2013, which presents calibration B that uses TEM cell to produce standard EM field, to obtain the response of the sensor. However, it is observed that the calibration coefficients in different TEM cells are different. This paper analyzes the difference through theoretical calculation, numeral simulation and experimental calibration.

II. THEORETICAL CALCULATION

D-Dot turns the differential electric field strength to voltage output. According to the theoretical analysis of D-Dot, the relationship between the incident electric field strength E and the integration of output voltage Y can be written as follows[1]:

$$E(t) = K \cdot \int V(t)dt = K \cdot Y(t) = \frac{1}{R \cdot A_{eq} \cdot \varepsilon_0} Y(t) \quad (1)$$

Where R is the matching impedance, which is 50 Ω in circuit, A_{eq} is the equivalent area [2], and ε_0 is vacuum dielectric constant.

For the D-Dot sensor used and simulated in this paper, the probe height is 15mm, the radius of the plane is 2.5cm, and the half angle of the probe is $\theta = 46.96°$. The

Fig. 1. D-Dot sensor stereogram

sensor is shown as Fig 1. Due to the parameters above, the equivalent area can be calculated as $A_{eq} = 6.8779 \times 10^{-4}m^3$. And thus, the theoretical calibration coefficient is $K_{the} = 3.286 \times 10^{12}m^{-1}s^{-1}$.

III. NUMERICAL SIMULATION

The following simulation aims at the calibration of the specific D-Dot sensor described before in 300MHz-TEM cell and 400MHz-TEM cell in CST MWS.

The TEM cells are modelled in real size. The 300MHz-TEM cell is 0.5 m height, whereas the 400MHz-TEM cell is 0.3 m height.

The D-Dot sensor is placed on the exact point in the calibration space. The output voltage signal detected through a 50 Ω resistance is integrated and the integrated signal is processed linear fitting with the calculated electric field strength. So the calibration coefficient K can be read out easily.

The simulated coefficients are listed in Table I. The two fitting correlation coefficients are greater than 99.99%.

IV. EXPERIMENTAL VERIFICATION

Corresponding to the simulation, experiments are performed to get the calibration coefficients to verify the simulation and the theoretical calculation.

Double exponential pulse source is used to excite the electromagnetic field in the TEM cells. And the sensor is placed on the middle point of the calibration space as accurate as possible. An oscilloscope is used to detect the output voltage signal.

The experimental calibration coefficients are listed in Table I. And the correlation coefficients are 99.49% in 300MHz-TEM experiment and 99.99% in 400MHz-TEM experiment, separately.

TABLE I. CALIBRATION COEFFICIENTS AND RELATIVE ERRORS IN THREE WAYS

Calibration Equipment	Calibration coefficient ($\times 10^{12} m^{-1} s^{-1}$)			Relative error to theoretical value	
	Theoretical calculation	*Numerical simulation*	*Experimental*	*Numerical simulation*	*Experimental*
300MHz-TEM	3.286	3.7875	3.757	15.3%	14.3%
400MHz-TEM		4.2516	4.789	29.5%	31.4%

V. CONCLUSION

Due to the above analysis, it can be concluded that:

- The theoretical calculation, numeral simulation and experimental calibration shows good consistency;
- The relative error to the theoretical value can approach 32%. This value is larger than the uncertainty referred in IEEE Std 1309-2013[3].
- From Table I, it is obvious that the relative error in 400MHz-TEM cell is about twice larger than it in 300MHz-TEM cell, which represents that the field perturbation increases when the cell size decreases.

REFERENCES
[1] IEC 61000-4-33-2005, B.8, pp. 47
[2] Yang C, Test Technology and Application of High power Electromagnetic Field [D].Beijing: Tsinghua University,2016:42
[3] IEEE Std 1309-2013, pp. 36

F r ea F lded a eg ide l   a e tr ct re f r illi eter a e T Ts

Swagata Ray
University of Burdwan, Physics Department
West Bengal, India713104
swagata25ray@gmail.com

Latha Christie
Microwave Tube Research and Development Centre
Bangalore, India 560013
christie@mtrdc.drdo.in

Abstract A 94 GHz four beam folded waveguide SWS (FW SWS) for a millimetre wave TWT is designed and simulated. As the number of beams increase, interaction impedance and hence power level of the TWT increases. The design is carried out such that the four linear beams pass through small holes in the broad wall of the folded waveguide. The design for the four beam FW SWS with longitudinal orientation of the beam holes has also been compared with that of a conventional one beam FW SWS. The Simulation has been carried out using 3D CST Studio. It has been found that the bandwidth of both the structures is around 18%, while the four beam FW SWS gives more interaction impedance as compared to the conventional one beam FW SWS.

Keywords- Folded Waveguide TWT, Ultra Wideband, millimetre wave, interaction impedance, multi-beam, power

I. INTRODUCTION

Travelling wave tubes (TWTs) are normally used for high power, ultra wideband radar applications that require high resolution at mm wave frequencies. Folded waveguide SWS (FW SWS) is the preferred slow wave structure in millimetre wave frequencies due to its robust construction. The power level of the conventional FW SWS can be increased by improving the interaction between RF wave and electron beam that can be done by increasing the number of beams. In this paper, a four beam FW SWS has been designed and simulated using 3D CST Studio and compared with that of a one beam FW SWS.

II. DESIGN OF FOUR BEAM FW SWS

Initial design of the FW SWS is carried out using parametric analysis. Then the design is modified to accommodate multi beams using the simulations carried out in CST Microwave Studio. The operating frequency is chosen as 94 GHz and the beam voltage as 19 kV. Fig.1 (a) and (b) gives 3D view of one beam and four beam FW SWS. Fig. 2 gives the comparison of the dispersion and interaction impedance characteristics of the two different FW SWSs.

First a conventional FW SWS is designed for a center frequency of 94 GHz and then four beam-holes are inserted. The radius of beam hole for the one beam FW SWS is 0.0532λ and the radius of the beam hole for four beam FW SWS is .0250λ. Fig. 1 gives the 3D view of the one beam and the four beam the FW SWS.
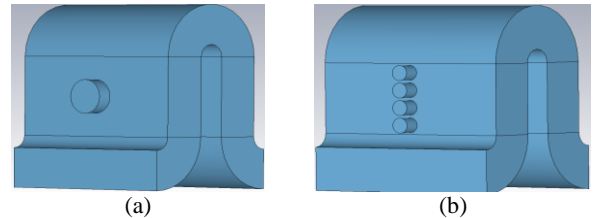

Figure 1. 3D view of (a) one beam FW SWS (b) four beam FW SWS

The dispersion and interaction impedance characteristics are derived from CST STUDIO and is given in Fig. 2.
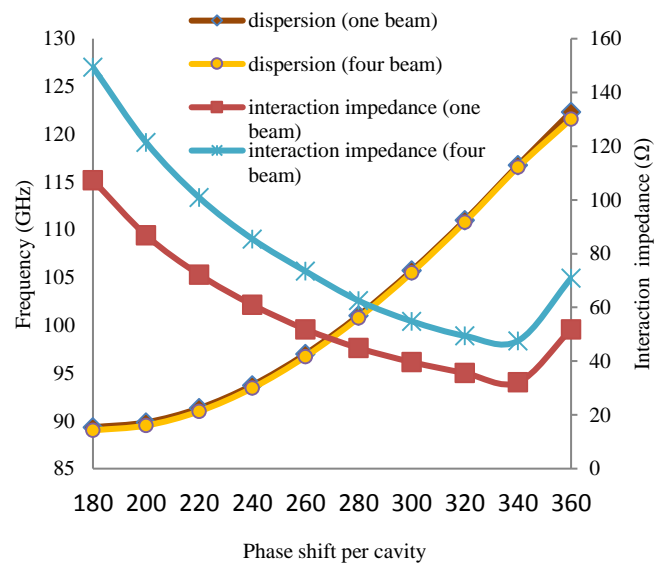

Figure 2. Dispersion and interaction impedance characteristics of one beam and four beam FW SWS

III. Conclusion

The design and simulation has been carried out for one beam and four beam FW SWSs. The interaction impedance of four beam hole FW SWS is higher compared to that of conventional FW SWS and hence more power can be achieved with a four beam structure.

REFERENCES
[1] Shengmei Yan, Wei Su, Yajun Wang, Ao Yu, "Design and theoretical analysis of multibeam folded waveguide travelling-wave tube for subterahetz radiation". IEEE Trans. On Plasma Science, vol. 43, no. 1, January 2015
[2] Wenxion Liu, Ke Li, Yong Wang, Miaomiao Cao, "Investigation of high-frequency characteristics of beam-wave interaction system of terahertz two-beam folded waveguide".

Design and i lati n f an ltra ide and l a e tr ct re f r a illi etre a e T T

SanjuktaNej
Department of physics, University of Burdwan,
West Bengal 713104, India
sanjuktanej@gmail.com

Latha Christie
Microwave Tube Research & Development Centre
Bangalore 560013, India
christie@mtrdc.drdo.in

Abstract A W-band coalesced mode Inductively Loaded Inter Digital SWS has been designed using equivalent circuit approach and simulated using CST Studio. The coalesced mode approach gives an ultra-wide band and also it gives an increase in both the transverse and longitudinal dimensions which is much useful at millimetre wave frequencies as it reduces fabrication difficulties. The structure gives a bandwidth of around 20 to 25% at W band.

Keywords- Inter digital TWT, coalescent mode, millimetre wave, dispersion, impedance, ultra wideband

I. INTRODUCTION

Conventional TWTs fall short of power and gain requirements at the band edges mostly at the lowest frequencies when extrapolated to operate for wide band range. By operating in the coalesced mode region, an Inductively Loaded Inter Digital SWS (ILID-SWS) is able to give an ultra-wide band operation. Such ultra-wideband amplifiers at mm wave frequencies will be of great use in radars used for imaging and also for jamming purposes. For an ultra-wideband amplifier, the beam velocity should be in synchronism with the RF wave velocity over a very wide frequency range. In coalescent mode operation, the upper cut-off frequency of the lower pass band or cavity band and the lower cut-off of the upper pass band or slot bandis coalesced or merged and hence there is no dispersion for a very wide range of frequencies. In this paper, the design and simulation of an ILID SWS with an operating frequency of 94 GHz, and a beam voltage of 17.5 kV has been carried out. It is found that almost 20 to 25% of bandwidth has been achieved by this structure.

II. DESIGN AND SIMULATION OF ILID SWS

The design of the ILID SWS has been carried out at W-band using an equivalent circuit approach, which gives the initial dimensions of the structure. Later the structure is modelled using 3D software package CST Studio and the dispersion and interaction impedance characteristics computed. Fig 1 gives the schematic of ILID SWS and fig. 2 and 3 gives the dispersion and interaction impedance characteristics of ILID SWS respectively.
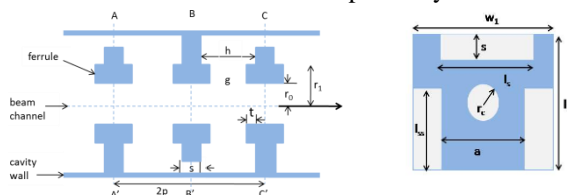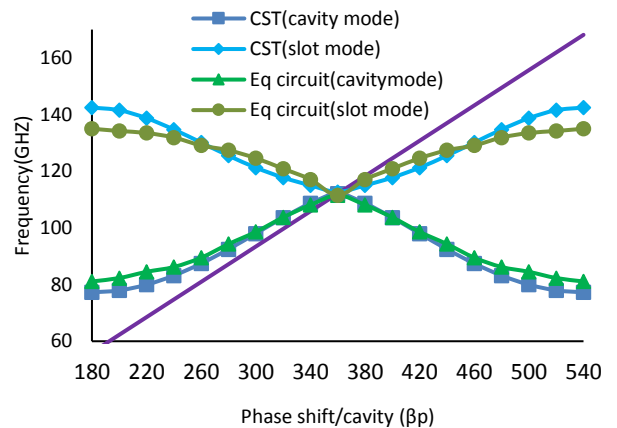

Fig.1. Schematic of ILID-SWS
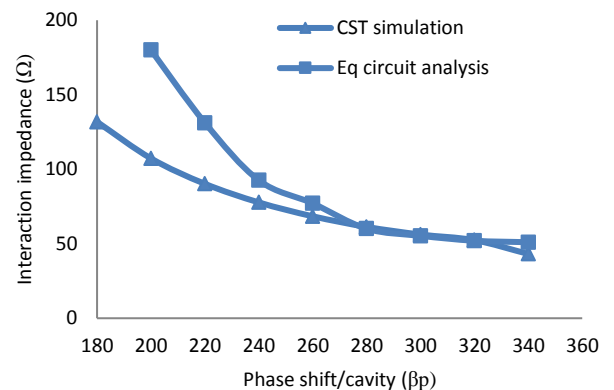

Fig.2.Dispersion characteristics of ILID SWS

Fig.3.Interaction Impedance characteristics of ILID SWS

III. CONCLUSION

The ILID SWS is ideally suited for an ultra-wide band TWT used in imaging radars. The design shows that the pitch is increased and the bandwidth around 20 to 25%.

REFERENCES

[1] Latha Christie and Lalit Kumar and N. Balakrishnan, "Design simulation of inductive loaded inter-digital SWS" in proc. IEEE International Vacuum Electronics Conference, Monterey, USA, April 2006

[2] Shunkang Liu, "Expanding to the bandwidth of the coupled cavity TWTs in MMW" International journal of infrared and millimetre waves, Vol. 22, No. 2, 2001

Development of Multi-channel Waveform Recorder

Kong Xu, Xie Yan-Zhao

State Key Laboratory of Power Equipment and Electric Insulation

National Center for Research on Transient Electromagnetic Environments and Applications

School of Electrical Engineering, Xi'an Jiaotong University

Xi'an, Shaanxi, China

Kongxu.nachuan@foxmail.com, Yzxie@mail.xjtu.edu.cn

Abstract—This paper develops a multi-channel waveform recorder for nanosecond level electrical signal measurement. First, it can detect the coupled signal in hermetically sealed cavities as it does not need fiber or coaxial-cable. Second, commonly used norms or super-norms of the measured waveform can be acquired by the signal processing software. The maximum sampling rate of the multi-channel norms detector is 2 GSPS and the memory depth can be 32 kB. The estimated operation bandwidth is 1 kHz - 460 MHz.

Keywords - digital measurement, electrical signal, FPGA, High-speed ADC, norm, signal integrity.

I. INTRODUCTION

One often has to measure the coupled electrical signals in various cavities, such as the cockpit of aircraft or vehicle under electromagnetic compatibility test [1]. Hence, a kind of measuring device without an external communication or power line is needed [2]. On the other hand, norm has been widely accepted by electromagnetic pulse researchers and has been included in several international standards [3]. So, this paper presents a multi-channel waveform recorder without external connecting line. It can measure the coupled electrical signals in hermetically sealed cavities and calculate the commonly used norms of the measured signal via specially designed signal processing software.

II. SYSTEM DESIGN OF THE MULTI-CHANNEL WAVEFORM RECORDER

The schematic of the multi-channel waveform recorder is shown in fig.1. The waveform recorder can digitize and store the measured signals based on high-speed ADC and FPGA.
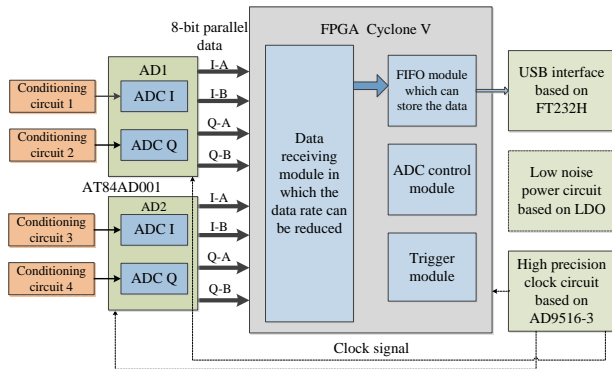

Figure 1. Schematic drawing of the waveform recorder

The working process of the multi-channel waveform recorder is shown in fig.2. It can realize single pulse acquisition and pre-trigger function guarantee that the whole pulse, including the waveform before trigger signal, can be recorded.
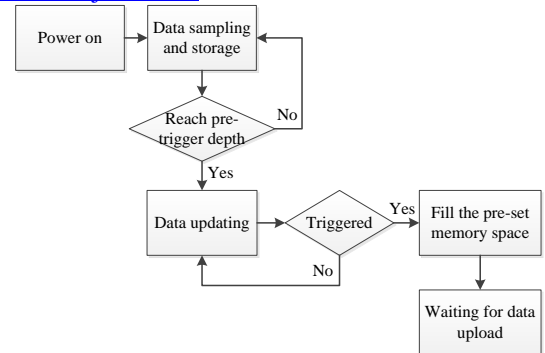

Figure 2. Working progress of the multi-channel waveform recorder

III. PERFORMANCE OF THE MULTI-CHANNEL WAVEFORM RECORDER

The calibration result of square pulse is shown in fig.3. The 10%-90% rise times of the two waveforms are both about 1 ns. The frequency response curve of the multi-channel waveform recorder is shown in fig.4. According to calibration results, the operation bandwidth is 1 kHz-460 MHz.
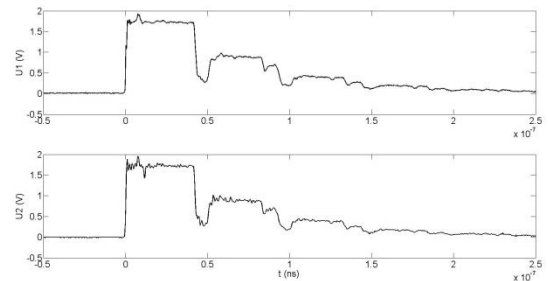

Figure 3. Waveform comparison between the 50 ns square pulse measured by the oscilloscope (upper graph) and the four-channel waveform recorder (lower graph)

REFERENCES

[1] D. V. Giri and Carl E. Baum, Design guidelines for flat-plate conical guided-wave EMP simulator with distributed terminators, Sensor and Simulation Note 402, Oct. 1996.

[2] Carl E. Baum, Norm detectors for multiple signals, Measurement Notes, Note 40, Oct. 1991.

[3] William A. Radasky, et al. Introduction to the Special Issue on High-Power Electromagnetics (HPEM) and Intentional Electromagnetic Interference (IEMI) [J]. IEEE Trans. on EMC, vol. 46, no. 3, pp. 314-321, Aug. 2004.

The Criteria to Evaluate the Performance of High-Power UWB Antennas

Shaofei Wang, Yanzhao Xie
State Key Laboratory of Power Equipment and Electric Insulation
National Center for International Research on Transient Electromagnetic Environments and Applications
School of Electrical Engineering, Xi'an Jiaotong University
Xi'an, Shaanxi, China
wsf2013@stu.xjtu.edu.cn; yzxie@mail.xjtu.edu.cn

Abstract— In this paper, a set of criteria to evaluate the performance of the high-power (HP) UWB antennas are proposed based on electromagnetic norms and mechanism for effect of electromagnetic pulse. Conventional antenna characterizations such as efficiency, gain, etc. are redefined for the UWB antennas and method to calculate these proposed criteria is presented.

Keywords: high-power; UWB antenna; performance

I. INTRODUCTION

For the antennas which transmit short pulse with wideband spectrum, conventional antenna characterizations [1] are usually function of frequency. That makes the assessment of the performance of UWB antenna more difficult [2]. In this paper, we try to propose a set of criteria to evaluate the performance of UWB antennas based on their properties in the time and frequency domain, so that the performance of different UWB systems can be quantitatively evaluated and compared.

II. ANTENNA CHARACTERIZATIONS

In this section, the radiation efficiency and antenna gains are defined for the UWB antennas, based on the relationship of electromagnetic norms and EMP effect.

TABLE I.   RELATIONSHIP BETWEEN NORMS, EFFECT AND ANTENNA CHARACTERIZATION [3]

p-Norm	Norm Quantity	Example of use	Antenna Characterizations
$\lVert E \rVert_\infty$	$_1 = \lvert\ (\ )\rvert$	Circuit upset	Effective Potential Gain
n/a	$_2 = \lvert \partial\ (\ )/\partial\ \rvert$	Component arcing; circuit upset	Transfer Function and Convolution $(\ ) = \dfrac{(\ )}{(\ )}$ $(\ ) = {}^{-1}\big[\ (\ )\ (\ )\big]$
n/a	$_3 = \left\lvert\displaystyle\int_0\ (\ )\right\rvert_{\max}$	Dielectric puncture	
$\lvert E\rvert_1$	$_4 = \displaystyle\int_0^\infty \lvert\ (\ )\rvert$	Equipment damage	
$\lvert E\rvert_2$	$_5 = \left\{\displaystyle\int_0\ \lvert\ (\ )\rvert^2\right\}^{1/2}$	Component burnout	Energy Gain

Energy reflected back to the feeder and consumed by the matching load (if any) should be considered for the definition of efficiency of the UWB antenna,

$$\eta = \eta\,\eta\ . \tag{1}$$

where η and η are the reflection efficiency and load-loss efficiency respectively.

In the frequency domain,

$$\eta(\ ) = \eta\ (\ )\eta\ (\ ). \tag{2}$$

For the input voltage with spectrum of $(\ )$, the efficiency of the UWB antenna can be calculated as,

$$\eta_0 = \frac{\int \eta(\ )^{\ 2}(\ )}{\int\ ^2(\ )} \tag{3}$$

The energy gain can be calculated in the time domain as,

$$_0 = \frac{2\pi\ ^2 \int\ ^2(\ )}{\int\ ^2(\ )} \tag{4}$$

And in the frequency domain,

$$(\ ) = \frac{2\pi\ ^2\ ^2(\ )}{^2(\ )}$$

$$_0 = \frac{2\pi\ ^2 \int\ ^2(\ )}{\int\ ^2(\ )} = \frac{\int\ (\ )\ ^2(\ )}{\int\ ^2(\ )} \tag{5}$$

The effective potential gain can calculated as,

$$= \frac{\ }{\ } \tag{6}$$

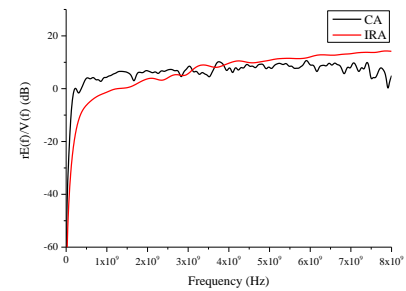$$(\ ) = \frac{(\ )}{(\ )} \qquad (\ ) = \int_{-\infty}^{\infty}\ (\ )\ (\ )\ ^{2\pi} \tag{7}$$

Figure 1. Transform functions of Combined Antenna (CA) and Impulse Radiating Antenna (IRA) with the same maximum dimension of 0.4 m

REFERENCES

[1] Balanis C A. Antenna Theory Analysis and Design [M]. 3rd. Hoboken, New Jersey: John Wiley & Sons, Inc., 2005.
[2] O. E. Allen, D. A. Hill and A. R. Ondrejka. Electromagnetic Compatibility, IEEE Transactions on, 1993, 35(3): 339-346.
[3] Electromagnetic compatibility (EMC) –Part 4-33: Testing and measurement techniques –Measurement methods for high-power transient parameters, IEC Standard 61000-4-33, 2005.

Cone Antenna Design for D-dot Sensor Calibration

Tae Heon Jang
Aerospace EM Technology Center,
Korea Testing Laboratory,
Jinju-si, Gyeongsangnam-do, Korea
thjang@ktl.re.kr

Je Hun Lee
Aerospace EM Technology Center,
Korea Testing Laboratory,
Jinju-si, Gyeongsangnam-do, Korea

Abstract— For the radiated immunity test against mesoband and hyperband transient E-field, it is important to evaluate field uniformity in test area and to verify the test parameters in time domain using a derivative sensor, such as a d-dot sensor. The calibration result of the derivative sensor will affect the measurement result of the field uniformity and test parameters. This paper is for the design of a cone antenna to be used for calibration of d-dot sensors.

Keywords- calibration method, d-dot sensor, mesoband and hyper-band, cone antenna

I. INTRODUCTION

IEC TC 77 SC C is recently working to develop the immunity test method of equipment and system against mesoband and hyperband transient E-field, as well as the calibration method of derivative sensors in the IEC 61000-4-36. For the radiated immunity test, it is important to evaluate field uniformity in test area and to verify the test parameters in time domain using a derivative sensor, such as a d-dot sensor. And hence the calibration result of the derivative sensor will affect the measurement result of the field uniformity and test parameters such like peak of E-field, rise time of the pulse, maximum rate of rise, pulse width or action integral. As for calibration methods, three kinds of methods are considering, which are a method using a cone antenna over the ground plane, a substitution method in GTEM waveguide and three antenna method in free space. This paper is for the design of a cone antenna to be used for calibration of d-dot sensors.

II. DESIGN OF A CONE ANTENNA

A cone antenna over ground plane is as shown in Fig. 1. The impedance of the cone over ground plane is a function of the cone half angle (θ) as in (1) [1]. With $\theta = 4°$, the impedance becomes approximately 200 Ω.
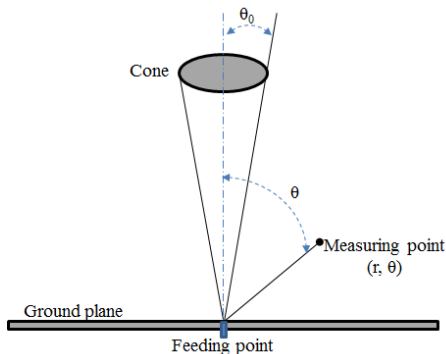

Figure 1. Configuration of a cone antenna to be designed

$$Z_C(t) = 60 \ln[\cot(\theta_0 / 2)] \tag{1}$$

The electric field generated by this antenna has the simple time domain analytic form as in (2) [2].

$$E_\theta(t) = \frac{V_{GEN}(1+\Gamma)}{r \sin\theta \ln[\cot(\theta_0 / 2)]} \tag{2}$$

Where   and θ denote the location of the sensor under test, θ is the solid angle of the cone, and   is the output of a pulse generator to be fed at the base of the cone.

Fig. 2 shows the results of TDR and E-field simulation for the cone in CST MW studio for several different shapes.
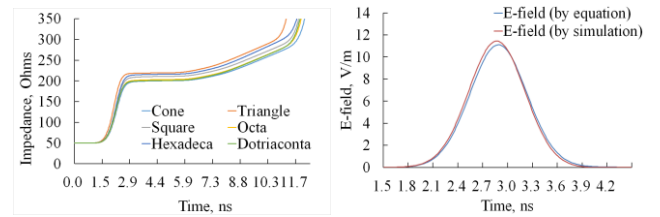

Figure 2. TDR and E-field simulation

Fig. 3 shows the TDR measurement of the fabricated cone antenna and E-field measurement of a d-dot sensor in it.

Figure 3. TDR and E-field measurement

III. CONCLUSION

This paper is that a cone antenna over ground has been designed, fabricated and measured its performance for calibration of derivative sensors to be used in the mesoband and hyperband transient radiated immunity tests. The E-field measurement from a d-dot sensor in cone antenna will be compared with the theoretical [3].

REFERENCES
[1] NBS technical note 1008, Antenna and the associated time domain range for the measurement of impulsive fields, 1978
[2] NIST technical note 1392, Time-domain calibrations of D dot sensors, 1998
[3] IEC 61000-4-33, Testing and measurement techniques - Measurement methods for high-power transient parameters

Particle-in-Cell Simulation of S-Band 500 MW Relativistic Backward Wave Oscillator

Sanjay Kumar Gupta, Dr. S.Umamaheswara Reddy

Microwave Tube Research & Development Centre,
Bangalore 560013, India
Tel: +91-080-28388325, Fax: +91-080-28381750, E-mail:
sanjay@mtrdc.drdo.in

Abstract: S-band relativistic backward-wave oscillator with a resonance reflector is designed using the "CST 3D Software [2]". Backward-wave oscillators (BWO) is high power Microwave sources [1] based on relativistic electron beams it is capable to producing high-power coherent radiation in the centimeter and millimeter wavelength regimes. In this paper we present the design and PIC Simulation of S band 500MW conceptual large diameter coaxial relativistic BWO in which a coaxial corrugated waveguide is used. It's having advantage of wide frequency tuning ability by varying the energy of the beam.

Keywords: High Power Microwaves, BWO, Corrugated structure, Beam Instability, Magnetic field confinement

I   EIGEN MODE & PIC SIMULATION

SWSs are used in BWOs in order to slow down the phase velocity of the electromagnetic wave so that the electron beam can resonantly interact with the wave which is the prerequisite of microwave generations. Coaxial corrugated cylindrical waveguide has been designed and used as Slow Wave structure for high power coaxial relativistic backward wave oscillator. The coaxial corrugated cylindered waveguide are described by

$$R=R0*(1+ l0*sin\ ((2*\pi*L)/d))$$

Eigen mode analysis carried out by CST Eigen mode solver [2] to evaluate dispersion plot & beam line is drown to estimate the synchronous operating voltage as shown in fig 1.
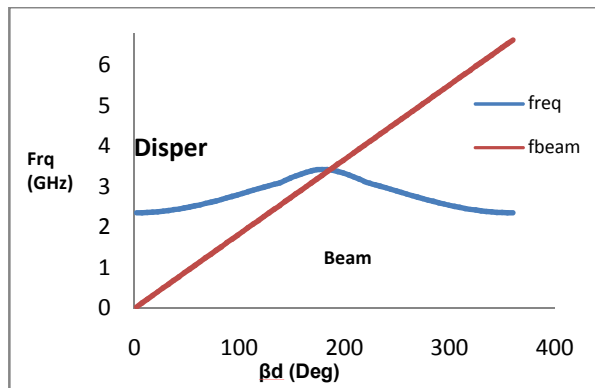

Fig 1: Dispersion characteristics of the BWO

CST is a 3-dimensional, relativistic and fully electromagnetic particle-in-cell code which automatically accounts for beam space charge and nonlinear effect in the

Beam wave interaction. It can stimulate the interaction and Electromagnetic fields as they evolve in time and space from some defined initial conditions. Wideband lumped reflector placed nearby the input edge of the SWS. Adopting the SWS configuration of fig.3, a coaxial RBWO is simulated with a beam under a voltage of 450 kV and current of 7.6 kA applied external magnetic field used 1.2 T to guide the electron beam.
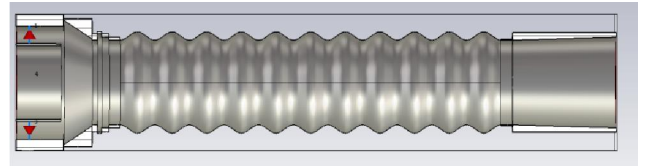

Fig 2: BWO Simulation Model

Table 1

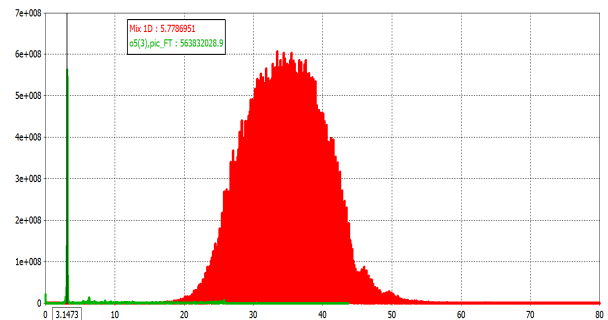| Parameter	Value
Beam Voltage (kV)	450
Beam Current (kA)	7.6
Frequency (GHz)	3.14
Power(MW)	>500
Magnetic Field (T)	1.2
Operating Mode	TM01

Fig 3; Power Plot at outport port

CONCLUSION

PIC simulations provided insight into the beam-wave interaction in the coaxial relativistic BWO. Simulation results are good agreement with the expected performances of the device. An outline of design & PIC Simulation for compact and efficient backward wave oscillator which can work in the frequency range of S band and power more than 500 Mega watts this frequency range and power will be useful [1] for advanced radars, HPM Application etc.

REFERENCES

[1] J. Benford , J. Swegle and Edl Schamiloglu High-Power Microwaves second edition Taylor & Francis Group
[2] CST MWS Tutorials, available at: http://www.cstchina

Estimating time-dependent radiation impedance of software instructions with applications to the Random Coupling Model

Joe M. Chen, Ghadeh Hadi, Rusmir Bilalic, David Dietz, Sameer Hemmady, Salvador Portillo, Manel Martinez-Ramon, Edl Schamiloglu

Department of Electrical and Computer Engineering, University of New Mexico

Albuquerque, NM 87131-0001

sportil@unm.edu, shemmady@unm.edu, edls@unm.edu

Abstract— As part of ongoing effort to develop a black box model of microelectronic susceptibility to electromagnetic interference the University of New Mexico is currently researching the use of the Random Coupling Model to develop predictive models for the coupling of extreme EM fields to electronic systems contained within complicated enclosures. In this model the coupling efficiency of a sensitive port is quantified by the radiation impedance. This radiation impedance is dependent on the software instruction that is being executed at time of interrogation. We propose to use a time-domain technique where the phase measurements of a single tone input and the reflected signal are used to calculate the port impedance of these microcircuits. This paper presents the measurement technique, a numerical model utilizing the transfer function of the system, characterization results of the technique, and initial instruction-dependent impedance measurements of a DUT.

Keywords- Time-domain measurements; instruction-dependent impedance; electromagnetic susceptibility.

I. INTRODUCTION

Understanding the time-dependent impedance behavior of advanced microelectronics with respect to instruction set is critical to the development of a black box model of electromagnetic susceptibility. Our group at the University of New Mexico is actively researching the use of the Random Coupling Model (RCM) to develop such a predictive model. For active digital electronic systems, the input port radiation impedance can change based on the software instruction being executed by the system. In this body of research, we are experimentally studying the nature and variation in the radiation impedance of a microcontroller pin as a function of its software execution, from which we will develop predictive models. The predictive models developed will help EMI/EMC designers better characterize the susceptibility of their electronic systems in extreme EM environments.

II. TIME-DOMAIN S-PARAMETER APPROACH

The time-domain approach to measuring S-parameters and ultimately the impedance of an integrated circuit pin is based on measuring phase differences between the incident and reflected signals. A single tone sinusoidal signal is sent into individual input and output pins of the microcontroller via a well characterized 4-port bidirectional coupler. The microcontroller is running a simple counting program of known execution length. An oscilloscope captures the

amplitude of the input and the phase measurement is given by the S34 output of the coupler reflected signals. The data from the reflected port is then put through a bandpass filter centered at the monochromatic frequency of the input signal. The test circuit is an 8 bit Atmel microcontroller operating at 1 MHz and the bespoke circuit board for the microcontroller has been characterized to operate up to 100 MHz. The input signal comprises a large number of equally-spaced discrete frequencies spanning the range from 100 kHz to 100 MHz. The automated system captures 2000 signals at each discrete frequency to produce an average value and, thus, reduce the random noise. The difference in phase between the two digitized signals yields the S-parameters and ultimately the port impedances.
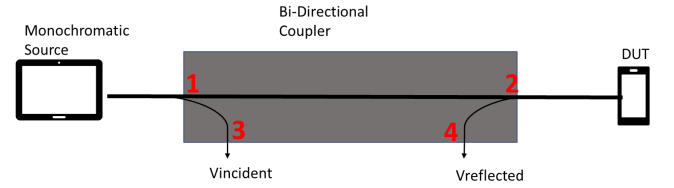

Figure 1. Diagram of the time-domain port impedance measurement. Ports are denoted by the red numbers.

V_{incident} and $V_{\text{reflected}}$ can be calculated from (1) and (2)

$$V_{\text{incident}} = \frac{1}{|S_{31}|} * e^{jS_{31}} \tag{1}$$

$$V_{\text{reflected}} = \frac{1}{|S_{42}|} * e^{jS_{42}}. \tag{2}$$

Using the canonical relationship for $S_{11}=V_{\text{reflected}}/V_{\text{incident}}$ yields the port impedance (3)

$$Z = 50\frac{(1+S_{11})}{(1-S_{11})} \tag{3}$$

III. RESULTS

The time-domain approach for measuring S-parameters and port impedances was tested using a 50 Ω load, and open and short circuit calibration loads. Results of these experiments as well as initial results from pin impedance measurements of a microcontroller will be presented.

REFERENCES

[1] S. Hemmady, X. Zheng, E. Ott, T.M. Antonsen, and S.M. Anlage, "Universal Impedance Fluctuations in Wave Chaotic Systems," Phys. Rev. Lett., vol. 94, 014102 (2005).

Review on Test Parameters and Tolerances of E1 HEMP Simulator

Tae Heon Jang
Aerospace EM Technology Center,
Korea Testing Laboratory,
Jinju-si, Gyeongsangnam-do, Korea
thjang@ktl.re.kr

Je Hun Lee
Aerospace EM Technology Center,
Korea Testing Laboratory,
Jinju-si, Gyeongsangnam-do, Korea
light@ktl.re.kr

Abstract—The radiated HEMP environment and immunity test are specified in IEC publications for civil application and Mil-Std-461F RS105 and VG 96903–50 for military systems. They have test parameters: peak amplitude of electric field, rise time, pulse width and the ratio of E and H. However, their tolerances are different, so that some HEMP simulators could not satisfy with the both tolerances in civil application and in military application simultaneously. This paper reviews the tolerances for test parameters of HEMP simulators by measurement to reflect into IEC standards.

e   rds- radiated HEMP, simulator, test parameters, tolerances, RS-105

I.   INTRODUCTION

IEC TC77 SC C has published several standards for radiated HEMP phenomena: definition of environment, test level and test method – IEC 61000-2-9, IEC 61000-4-25 and IEC 61000-6-6. IEC 61000-4-20 published by TC77 SC B has HEMP transient testing requirements in Annex C.

In military side, Mil-std-461F RS105 specifies test level and test method for radiated susceptibility, transient electromagnetic Field. Germany has military standard, VG 96903–50 - Test methods, test equipment and limiting values: Field test with NEMP simulators.

These publications have almost same test parameters: peak amplitude of electric field, rise time, pulse width (FWHM) and the ratio of E and H (wave impedance). However, their tolerances are different, so that some HEMP simulators could not satisfy with the both tolerances in civil application and in military application simultaneously.

II.   REVIEW OF THE TOLERANCES

The parameters of the standards are summarized in Table I.

TABLE I.   Comparison of test parameter of radiated HEMP Test

P licati ns	E field	rise ti e	F	E
IEC 61000-2-9 (Radiated HEMP Environment)	50 kV/m	2,5ns	23ns	377Ω
IEC 61000-4-25 Small radiated test facilities	50 kV/m 0 to 6 dB	2ns to 2,5ns	25ns to 30ns	377Ω ±50Ω
IEC 61000-4-25 Large simulators type I	50 kV/m 0 to 6 dB	2,5ns ±0,5ns	25ns to 75ns	377Ω ±50Ω
IEC 61000-4-25 Large simulators type II	50 kV/m ± 10 dB	2ns to 10ns	25ns to 500ns	377Ω ±50Ω
IEC 61000-6-6	50 kV/m	2,5ns	25ns	
IEC 61000-4-20 Annex C	50 kV/m 0 to 6 dB	2,25ns ±0,25ns	27,5ns ±2,5ns	377Ω ±50Ω
Mil-Std-461F, RS105	50 kV/m 0 to 6 dB	1,8ns to 2,8ns	23ns ±5ns	-
VG 95371-50, (Germany)	50 kV/m ±10 %	2,5ns ±10 %	23ns ±20 %	377Ω ±20%

Fig. 1 shows the measurement setup for reviewing test parameters and the tolerances in HEMP simulator.

Fig. 2 describes the measuring points in HEMP simulator and shows the measured waveform of E1 HEMP with peak E-field, rise time and pulse width. Table II is the proposed tolerances for amendment of IEC standards.

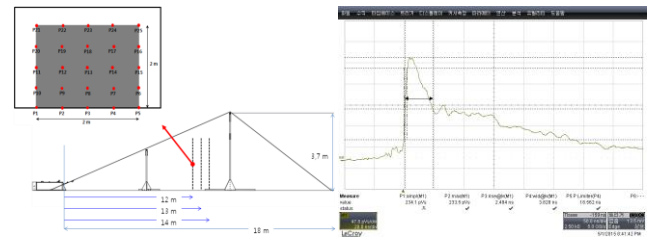
Figure 1. Measurement setup in HEMP simulator

Figure 2. Measuring points in HEMP Simulator

TABLE II. Proposed tolerances for IEC Standards

P licati ns	E field	rise ti e	F	E
IEC 61000-2-9 (Radiated HEMP Environment)	50 kV/m	2,5 ns	23 ns	377Ω
IEC 61000-4-25 Small radiated test facilities	50 kV/m 0 to 3 dB	2,5 ns ±10 %	23 ns ±20 %	377Ω ±20%
IEC 61000-4-25 Large HEMP simulators type I	50 kV/m 0 to 6 dB	2,5 ns ±20 %	23 ns -20%, +30%	377Ω ±20%
IEC 61000-4-25 Large HEMP simulators type II	50 kV/m ± 10 dB	2 ns to 10 ns	25ns – 500ns	377Ω ±50Ω
IEC 61000-6-6 (in Table 1)	50 kV/m	2,5 ns	23 ns	
IEC 61000-4-20 Annex C	50 kV/m 0 to 3 dB	2,5 ns ±10 %	23 ns ±20 %	377Ω ±20%

This paper reviewed the parameters and tolerances of the radiated HEMP requirements in the publications with a HEMP simulator.

REFERENCES

[1] IEC 61000–4-25:2012, HEMP immunity test methods for equipment and systems.
[2] IEC 61000-4-20:2010, Emission and Immunity testing in transverse electromagnetic (TEM) waveguides
[3] Frank Sabath and Stefan Portthast, "Tolerance values and the confidence level for High-Altitude Electromagnetic Pulse (HEMP) Field Tests", IEEE EMC Transactions, 2013

Study of an Helical Flux Compression Generator Used for Driving a High Power Microwave Source

Ashish Sharma
Pulsed Power and EMC Lab
Department of Electrical Engineering
Indian Institute of Science, Bangalore
ashsharma032@gmail.com

M. Joy Thomas
Pulsed Power and EMC Lab
Department of Electrical Engineering
Indian Institute of Science, Bangalore
jtm@ee.iisc.ernet.in

Figure 2. Electrical equivalent circuit of the system before opening the opening switch.

Abstract— A 2D numerical model for predicting the performance of an explosively driven helical flux compression generator (HFCG) which feeds a High Power Microwave (HPM) source is presented in this paper. Using the 2D filamentary approach along with the dynamic matrix concept, a numerical code is developed and the computed results are presented in this paper.

I. INTRODUCTION

There has been considerable interest in developing High Power Microwave (HPM) sources for nonlethal directed energy weapon applications. The technology that is used to develop such sources has its roots in pulsed power. HPM system comprises of four main components which include primary or seed energy source, pulsed power system for generating high magnitude voltage/current pulse from the seed energy source, power conditioning circuit and the microwave device. Field-deployed devices require the system to be stand-alone which could be transported easily. HPM with conventional pulsed power sources are bulky and fails to meet such design constraint. Explosively-driven HPM source that uses a flux compression generator (FCG) (see fig.1) as the pulsed power source can serve as a viable replacement for conventional pulsed sources. An explosively-driven HFCG consists of a hollow cylindrical metal tube called the armature filled with high-energy explosives, placed within a helical coil called the stator. The explosives when detonated cause the armature to expand leading to the compression of the magnetic flux present within the annular space between the stator and armature. This flux is initially set up by the seed current flowing in the circuit using a seed current source. This compression of magnetic flux results in the generation of a high magnitude current pulse. The current pulse from HFCG is converted into a fast-rising voltage pulse using a power conditioning circuit comprising of an energy storage inductor and an opening switch which drives the HPM source.

In order to achieve high energy gain, inductance of the energy storage inductor L_{ES} (see fig.2) is required to be small as compared to the initial HFCG inductance as the gain at the end of operation is proportional to the ratio of initial HFCG inductance to the inductance of the energy storage inductor.
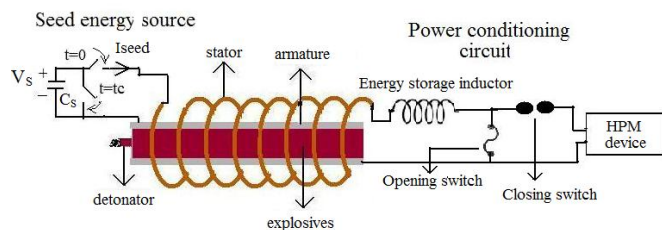
II. PROBLEM DEFINITION

The electrical equivalent circuit of HFCG can be represented by a first-order series R-L circuit with time-varying elements once seed energy source is disconnected. Then, the governing equation for the time-variant system is given as-

$$\frac{d}{dt}[(L(t) + L_{ES}) \times I(t)] + I(t) \times (R(t) + R_{ES}) = 0 \quad (1)$$

To solve for the generator current I(t) of equation (1), time-varying inductance L(t) and resistance R(t) of the HFCG generator are required which are obtained through a 2D numerical code developed for modeling the generator.

III. RESULTS

Time-varying inductance and resistance are evaluated and equation (1) is solved for the generator output current. A 20 Ω resistor is connected to the system as dummy load to represent HPM device. A current gain of 12 is achieved for the generator parameters mentioned in table 1.

Figure 3. Equivalent inductance

TABLE I. HFCG PARAMETERS

Stator coil diameter	60 mm
Stator coil length	500 mm
Stator coil turns	70
Armature diameter	30 mm
L_{ES}	1 uH
R_{ES}	10 mΩ
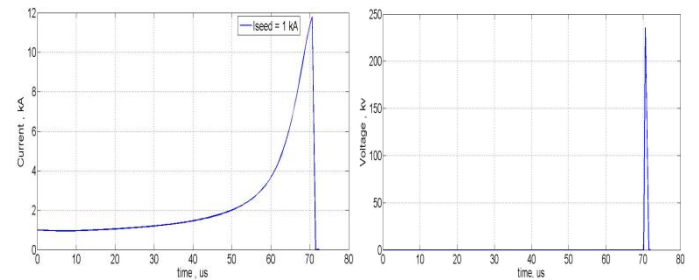
Figure 4. Generator output current for seed current of 1 kA.

Figure 5. Voltage across the HPM device.

Figure 1. HPM generator with HFCG connected to seed source.

REFERENCES

[1] B.M Novac, I.R Smith, M.C Enache, "Simple 2D Model for Helical Flux- Compression Generators," Laser and Particle Beams, Vol. 15, No.3, pp. 379-395.

Modified Ground Plane for High-gain UWB Wearable Antennas

Shilpi Ruchi Kerketta, Debalina Ghosh, P. K. Sahu

School of Electrical Science
Indian Institute of Technology Bhubaneswar
Bhubaneshwar, Odisha, India
srk10@iitbbs.ac.in, deghosh@iitbbs.ac.in*, pks@iitbbs.ac.in

Abstract—An UWB wearable antenna suitable for medical applications is presented in this paper. The narrowband monopole antenna is mounted on a modified ground plane thus extending its bandwidth and enhancing the gain. The ground plane is modified by using an inverted semicircular plate for achieving a bandwidth of 1:10 from 3.1 GHz to 31 GHz. In the process, the form factor of the antenna is kept within limits for integration with wearable devices. The method of enhancing the bandwidth with minor modifications of the ground plane is shown to be applicable for a wide range of planar antenna designs as demonstrated through this paper.

Keywords-Ground Plane, Monopole antenna, Planarized antenna, Wearable antenna, UWB.

I. INTRODUCTION

Thus there is a growing demand for wearable antennas in healthcare applications. Ultra-wideband (UWB) based techniques offer several advantages over other narrowband microwave or optical techniques .Various compact printed microstrip slots and monopole antenna have been designed to increase impedance bandwidth. Other techniques are by using simple bevel, with round smooth element, using shorting pins, with fractal design, wide open slots, adding parasitic elements, various substrate thicknesses and various patches [1-3].

II. DESIGN OF ANTENNA

The radiating element is circular with radius

$$r = \frac{87.94}{f_r \sqrt{\varepsilon_r}} \qquad (1)$$

where f_r is the resonant frequency and ε_r is the relative permittivity of the substrate[4]. The antenna is fabricated on 1.016mm thick Rogers 5880LZ ($\varepsilon_r = 1.98$) substrate and has surface area of 30mm x 40mm. It is fed by 50Ω microstrip feedline. In order to improve the impedance matching, an inverted semicircle is merged with the ground plane as shown in the Fig.1.

III. RESULTS AND DISCUSSION

A. For monopole Antenna

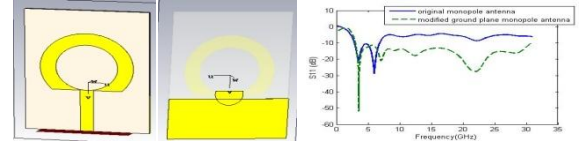The antenna performance was evaluated using CST.

Fig. 1. Monopole Antenna Design with Semi-Circular Extension with simulated and measured return loss

TABLE 1. COMPARISON OF GAIN OF ANTENNA

	Original Antenna		Modified Antenna	
	Freq (GHz)	*Gain (dB)*	*Freq (GHz)*	*Gain (dB)*
Start of Operation Band	2.85	2.39	3	2.96
End of Operation Band	6.86	5.6	30.84	5.23
Max gain in the Operation Band	6.86	5.6	21.457	6.4737

The original structure with a partial ground gives an impedance bandwidth from 2.8 GHz to 6.8 GHz and with the modified ground plane the bandwidth 3 GHz to 31 GHz measured with the help of R&S ZVA 24 analyzer. A study of the effect of the modified ground plane has been done for various other shaped monopole and textile antennas and it is observed that the bandwidth of all the antennas are enhanced in Fig.2.
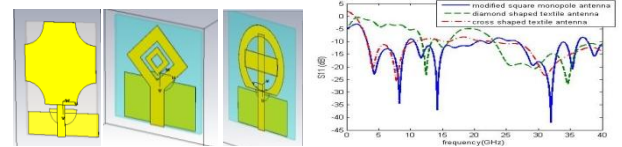

Fig. 2. Return Loss for Various Monopole Antennas with Modified Ground Plane

REFERENCES

[1] Mamdouh Gouda, Mohammed Y. M. Yousef, "Bandwidth Enhancement Techniques Comparision", Journal of Theoretical and Applied Information Technology 31st January 2012. Vol. 35 No.2

[2] Hossein Malekpoor, Shahrokh Jam, "Analysis on bandwidth enhancement of compact probe-fed patch antenna with equivalent transmission line model", IET Microw. Antennas Propag., 2015, Vol. 9, Iss. 11, pp. 1136–1143

[3] Kung Bo Ng, ChiHouChan, Haiyin Zhang, and Guoxun Zeng, "Bandwidth Enhancement of Planar Slot Antenna Using Complementary Source Technique for Millimeter-Wave Applications", *IEEE Trans. Antenna Propag.*, vol. 62,no. 9, Sept. 2014.

[4] N. Singh, A. K. Singh, V. K. Singh. "Design & Performance of Wearable Ultra Wide Band Textile Antenna for Medical Applications" , Open Eng.Vol 5,pp.117–123 ,2015.

Simulation Analysis of Circular Polarization using Single Microstrip Patch Antenna

Swapnil Narke[1], C Bhattacharya[2]

[1] Savitribai Phule Pune University, Pune 411007, India

[2] Armament Research and Development Establishment, Pune 411021, India

Abstract - The microstrip patch antenna are common in usage because of their small size, light weight, low profile and low manufacturing cost. Linearly polarized transmission is the prevalent mode for microstrip patch arrays. However, in cases of using two-antenna assembly, circular polarization is beneficial to provide the required electrical isolation between the two antennas. Circular polarization can be achieved using some perturbation in aperture of an antenna such as nearly square diagonal-fed antenna as shown in below Fig. 1(a), truncated corners square patch antenna as shown in below Fig. 2(a), etc. Here, we are presenting simulation of circular polarization using two different techniques in which first is truncated corner as shown in Fig. 1(a). Because of different dimensions of diagonals, resonant frequency along the chopped diagonal is higher than unchopped diagonal. The frequency of operation and the feed points are chosen in such a way that two modes are excited in phase quadrature. In Fig 2(a), the circular polarization is obtained because the two modes of resonance are spatially orthogonal. The antenna is excited at a frequency in between the resonant frequencies of these two modes in order to obtain the phase quadrature between the two modes. Circular polarization is defined with axial ratio. Axial ratio is the ratio between minor axis and major axis of an ellipse containing rotating electric field vectors on the polarization ellipse. In case of circular polarization, major axis and minor axis should be equal so that axial ratio becomes zero in the dB scale. The simulation analysis is carried out in HFSS.
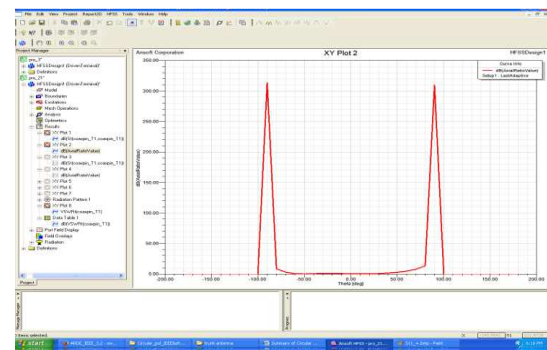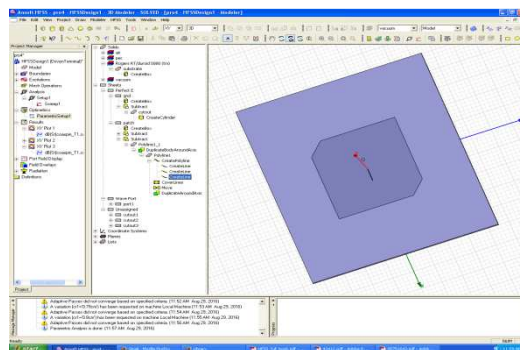
(a)   Geometry of truncated corner patch antenna,   (b)   Axial Ratio w.r.t. theta (in the elevation plane).

Figure 1. Circular polarization with resonant frequency at 3.16 GHz.
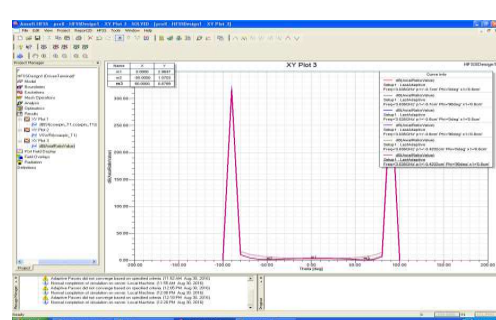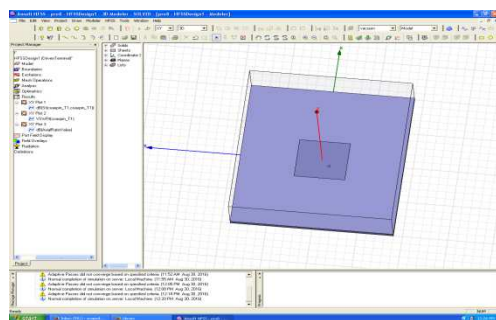
(a)   Geometry of diagonal fed rectangular patch antenna, (b) Axial ratio w.r.t. theta (in the elevation plane)

Figure2. Circular polarization with resonant frequency at 3.16 GHz.

REFERENCE

[1] C. Sharma and Kuldip C. Gupta, "Analysis and optimized design of single feed circularly polarized microstrip antennas", *IEEE Trans. Antennas and Propagation*, vol. AP- 31, no.6, November 1983.

Studies of Vulnerabilities on Electronics Gadgets against HPM

Senthil Kumar D[@], Shanmuganathan, Saket Khandekar, Srinivas Nekkenti, Manik Das, Laloo Alex, and SUM Reddy

[@] senthil@mtrdc.drdo.in

Microwave Tube Research & Development Centre, DRDO, Bangalore

Abstract - This paper describes the various experimental studies carried out on commercial electronics gadgets against High Power Microwaves (HPM) radiation. Toy electronics such as Remote Controlled (RC) car, robot, helicopter and mobile phones are the commercial electronic gadgets used for studies. Effects of narrow band repetitive RF radiation by magnetron based source and single pulse shot duration radiation from advanced vircator a narrow band HPM (NBHPM) source are investigated. Electronic Power Conditioner (EPC) unit of Microwave Power Module (MPM) is also subjected to the single shot NBHPM and the results are discussed in this paper.

Key words - HPM vulnerability, effects of high power RF radiation.

I.   Introduction

In recent years HPM have found variety of applications in defence and industrial systems. Directed Energy Weapons (DEW) and enhanced / new radar systems are some of the inspiring applications of HPM in defence. Microwaves on the order of 100's of MW peak power and frequency in the range of 1-300 GHz are characterized as HPM. Varieties of systems demands microwave sources of high peak power capabilities and simple in construction. In most of the devices HPM are generated by the interaction of an intense relativistic electron beam with a microwave interaction circuit. HPM radiation can inflict hard kill, where the electrical components are physically damaged, or a soft kill, where the components are temporarily disabled. In a hard kill the HPM pulse induces currents high enough to melt the metal on a circuit board, or a voltage that will result in a flashover in sensitive electrical components. A soft kill upsets a digital circuit or disturbs communication between various modules, when the induced voltage by the HPM pulse is of the order much higher than the operating voltage of the component being used in those circuits.

II.   Experiments

In this paper we present the functional disturbance observed during repetitive and single pulse/shot HPM radiation. The Magnetron craved out from the commercial microwave oven generating 900W peak power having ~0.750µs pulse width and ~13µs pulse repetition time is used as repetitive RF radiation source. The schematic of the repetitive experimental set

up is shown in figure 1. A reflex triode based advanced vircator generating ~80MW peak RF power ~80ns pulse width operating at single shot mode is used as NBHPM source. The photograph of the gadgets under test during NBHPM radiation is shown in figure 2. The electric field was measures at various distances from the repetitive source as well as single shot NBHPM sources.
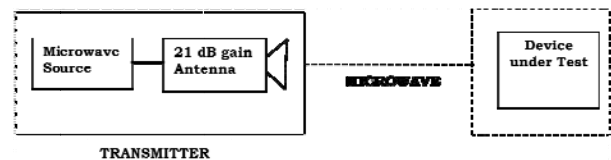

Figure 1. Schematic of low power NBHPM

Figure 2. Experimental setup of high power NBHPM

III.   Results and discussions

During all the experiments it was observed that the commercial mobile phones and toy electronics gadgets are temporarily stops functioning during the exposure. However in many occasion it resumes its function after radiation ceases. Of the order of 600v/m by the repetitive radiation could create the same effect by the single shot NBHPM where ~15kV/m was generated. EPC of MPM encountered permanent damage when it was exposed with single shot high power NBHPM. Upon further investigations some of the circuit tracks in the PCB as well as semiconductor components were damaged in the EPC unit.

REFERENCES
[1]. Robert J Barker & EDL Schamiloglu, High Power Microwave Sources & technologies, IEEE Press, 2001.
[2]. James Benford and John Swegel, High Power Microwaves, Artech House, Boston, London 1992.

Ultra-Thin Wide Band Metamaterial Absorber

Prakash Kumar Panda, Debalina Ghosh
School of Electrical Sciences
IIT Bhubaneswar
Bhubaneswar, India

R. Vasudeva Reddy
Dept. of Electronics and Telecommunication
IIIT Bhubaneswar
Bhubaneswar, India

Abstract—This paper describes the implementation and characterization of an ultra-thin wide band metamaterial absorber covering the entire X-band frequency (8-12GHz). The proposed structure consists of an inner square shaped closed ring resonator confined in another outer square shaped ring with an open slot. The proposed metamaterial absorber have good absorbance characteristics for both TE and TM modes at an angle of incidence normal to the resonator wall. The proposed metamaterial absorber find wide applications in wireless power transmission, bolometer, radar cross-section, IR camouflage, thermo photovoltaic's etc.

—Metamaterial Absorber, Wideband, Polarization angle, Full Width at Half Maximum (FWHM).

I. INTRODUCTION

The metamaterial absorber comes under resonant absorbers in electromagnetic spectrum. Due to its resonant absorptivity, it absorbs electromagnetic wave at designed frequencies. The metamaterial absorber started its journey with single band [1], dual band, triple band [2] and so on. The potential applications need broadband absorbers with compact size. Ding et.al [3] used multiple layered structure with different dimensions to obtain broadband absorption from 8.15 GHz to 14 GHz. Here the wideband absorption is obtained by adding a lumped resistor into the unit cell. It shows similar absorption characteristics for both TE and TM mode of incidence.

II. CHARACTERIZATION OF ABSORBER

The proposed unit cell consists of square shaped closed ring resonator enclosed in another square shaped open ring resonator. The outer ring is also called as the double split ring resonator with two slots C1 and C2 as shown in Fig.1. The outer double split ring resonator and the enclosed ring resonator are connected with a slit. The resonant structure is etched over an FR4 substrate having dielectric constant $\varepsilon_r = 4.4$, and loss tangent tan $(\delta) = 0.02$, of thickness t, which is backed with a complete metal plate. The relation between the absorbance A(ω), reflectance R(ω) and transmittance T(ω) is obtained as,

$$(\omega) = 1 - (\omega) - (\omega) \qquad (1)$$

Where, R(ω) = $|S_{11}|^2$ & T(ω) = $|S_{21}|^2$. As the back side of the unit cell is of metallic plate, so $|S_{21}|$ is zero. Hence equation 1 can be written as

$$(\omega) = 1 - (\omega) = 1 - |_{11}|^2 \qquad (2)$$

Initially, the dual band absorber structure is designed at 9.4 GHz and 13.4 GHz with absorptivity 99.88% and 97.26% respectively. The dual band characteristics are achieved by the capacitive and inductive coupling between the outer and inner rings. Then, to achieve the wideband absorptivity two slots in the outer ring have been created for additional capacitance. Again to achieve more wideband absorptivity, a lumped resistor R_1 (100Ω) is placed in the top slot of the outer ring. Then, the 90% absorptivity covers the band from 8.05 GHz to 14.0 GHz.The optimized design parameters for wideband absorber are listed in Table I.

Fig. 1. MA Unit Cell's Top View

TABLE I. MA PARAMETERS

s r er	Para eters in				
	P	G	G_1	W	W_1
Wide Band		0.4	0.65	0.4	0.15

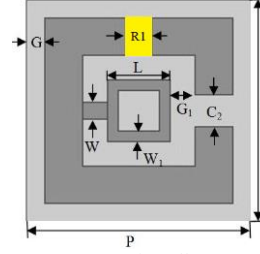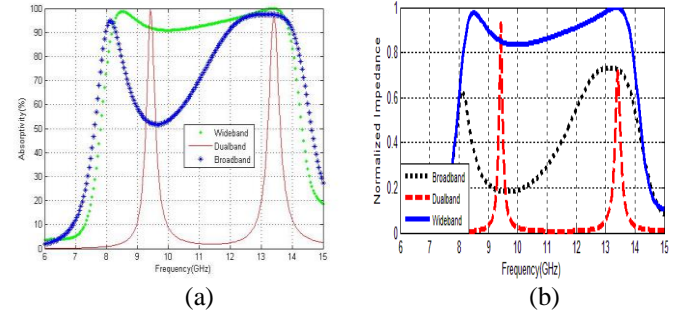| (a)	(b)

Fig. 2. (a) Absorptivity (b) Normalized impedance

III. CONCLUSION

An ultra-thin wideband metamaterial absorber is designed and simulated. The wideband absorption is achieved by adding a lumped resistor to the designed structure. The proposed absorber works well for TE and TM polarization.

REFERENCES

[1] Landy NI, et al. "Perfect Metamaterial Absorber." Phys. Rev. Lett., Vol.100, May2008.

[2] H. Zhai, C. Zhan, Z. Li, and C. Liang, "A triple-band ultrathin MA with wide-angle and polarization stability," IEEE Antennas & wireless propagation letter., vol. 14, pp. 241-244,2015.

[3] F. Ding, Y. Cui, "Ultra broadband terahertz metamaterial absorber," Apply. Phys. Lett. 100,103506-2012.

Ubiquitous nature of Asymptotic Conical Dipole Profile for Ultrawideband Antenna Design

Dhiraj K. Singh

Electronics and Radar Development Establishment(LRDE),Bangalore,India
dhirajkumarsingh@lrde.drdo.in

Abstract— **Asymptotic conical dipole(ACD) profile derived using equivalent charge method has been extensively used as ultrawide sensor for time domain electromagnetic pulse measurement.ACD has been used as feed for reflector Impulse radiating antennas and demonstrated substantial improvement in the performance compared to conventional conical feed IRAs. This paper discusses the ubiquitous nature for ACD profile derived from different combinations of charge distributions for designing different types of ultrawideband antennas for different applications.**

Index Terms— **ACD,IRA, UWB, GPR,TWIR**

I. INTRODUCTION

Ultrawideband antenna design specially towards lower center frequencies are of great importance for both civilian as well as military radar applications.The short range radars like Ground penetrating Radar(GPR) and Through wall imaging Radar(TWIR) are realized in either in time domain or in frequency domain [1].The antenna design for both these applications calls for contradictory requirement of low frequency for better penetration and ultrawide band for better range resolution. The common ultrawide band antenna element design relies on heuristic approach and numerical simulation. Equivalent charge method is used here to derive different ACD profiles using different combinations of equivalent charge distributions. The time domain full wave simulation of these profiles shows that these antenna profile possess large instantaneous bandwidth, high directionality and pulse fidelity.

The equivalent line charge $\lambda(z)$ on the *z*-axis is defined as:

$$\lambda(z) = \begin{cases} \lambda_0, & 0 < z < z_0 \\ -\lambda_0, & 0 > z > -z_0 \\ 0, & z = 0, z > z_0 \end{cases}$$

$$Q = \begin{cases} Q_0, & z = z_0 \\ -Q_0, & z = -z_0 \end{cases}$$

where mean charge separation $z_0 > 0$, charge density $\lambda_0 > 0$, and discrete charge $Q_0 > 0$.The equivalent charge distribution is shown in figure1 and few of the antenna profile derived is shown in figure2.
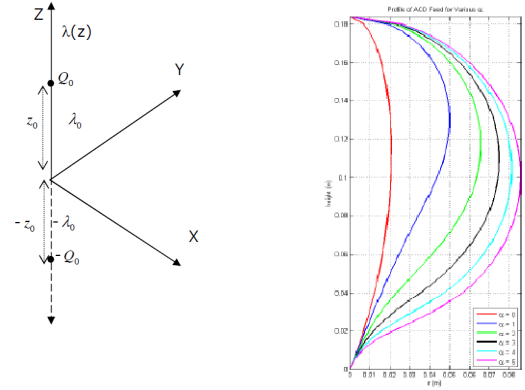
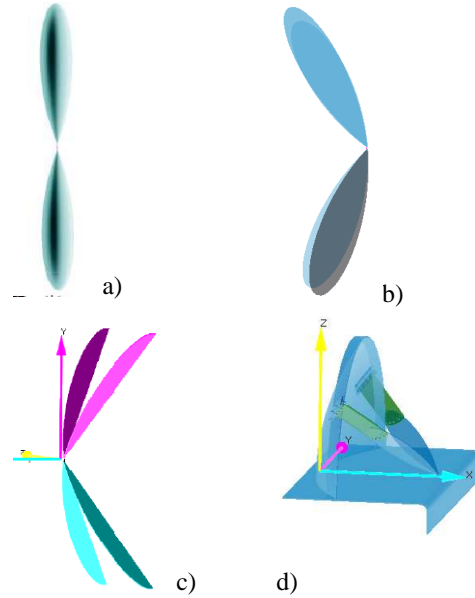

Fig. 1.Equivalent Charge Distribution

Fig. 2.Basic UWB Antenna Profiles Derived

REFERENCES

[1] D. J. Daniels, "Ground Penetrating Radar", *Encyclopedia of RF and Microwave Engineering*, vol.2, John Wiley & Sons, Inc., Hoboken, New Jersey, United States, 2005.

[2] Dhiraj K Singh et al., "Selection of Ideal feed profile for Asymptotic conical dipole fed Impulse Radiating Antenna" Progress in Electromagnetics research C,Vol.35,95-109,2013.

Study of Finite Rate of Innovation Signal for Detection of Landmines

Vijayakumar Solaiselvam
Dept. of Electrical Engineering
Indian Institute of Science, Bengaluru, India
e-mail-svijayin@gmail.com

Dr. Joy Thomas M
Dept. of Electrical Engineering
Indian Institute of Science, Bengaluru, India
e-mail-jtm@ee.iisc.ernet.in

Abstract—Sub surface detection of Landmines poses many unique challenges due to complex soil medium and influence of various environmental conditions. This paper studies the feasibility of using Finite Rate of Innovation (FRI) signal with compactly supported kernel for detection of Landmine/UXO. FRI signal based detection provides a faster detection algorithm with better resolution, but time varying nature of reflected pulse act as a dampener for utilizing the advantage of FRI techniques. This work concentrates on studying the performance of FRI sampling in landmine detection system for landmines buried at different depths in soil with varying moisture content. Though over parameterization in FRI sampling may reconstruct the original signal but at the cost of physics of the reflected signal and higher sampling rate, which nullify the advantage of FRI technique. Here we study the suitability of FRI sampling scheme for landmine detection system with normal FRI method and FRI method with an average soil model, so that, it can be explored in the sense of a failsafe algorithm in the detection system. To focus on the suitability of the method and for the sake of simplicity, this work uses one dimensional Finite Difference Time Domain (FDTD) simulation with Piecewise Linear Recursive Convolution method to implement the double Debye soil model, weighted least square (WLS) algorithm with some modification is used to fit the soil model with the available experimental data.

Keywords-Finite rate of innovation, Landmine, Soil Moisture, Double Debye Model, Dispersive Medium

I. INTRODUCTION

Detection of buried unexploded ordnance (UXO) poses one of the greatest humanitarian challenges in the 21st century. To improve the probability of detection, many researchers proposed multi sensor and algorithm based landmine detection system, in that Ultra wide band (UWB) microwave subsurface imaging is one of the technique showing promising results.

III. FRI TECHNIQUE

Good number of studies has been carried out using the finite rate of innovation based signal reconstruction for detection applications like radar, ultrasonic imaging systems..etc. Vetterli et al.[1] proposed a sampling method for the general class of FRI signals. Tur et al.[2] proposed compactly supported sum of sinusoid (SoS) as kernel for FRI signal sampling. Bhandari et al proposed method of FRI sampling for time varying pulses. Though dispersive nature of the soil medium is a dampener for considering FRI signal technique but its advantage over other methods like, its ability to use lower sampling rate, directly calculating the delay time of the reflected pulses from

the target and its resolving ability/resolution in the relatively lower bandwidth frequency spectrum motivates us to use the FRI sampling and explore the methods to overcome the current problems. This paper uses Gaussian signal as incident excitation source with standard deviation of $\sigma_\omega = 62.8, 31.41, 18.8$ and $6.28 \times 10^9 \, rad/s$.

IV. RESULT

Performance of FRI sampling for UXO detection has been studied by numerous simulations for different buried depth and soil moisture conditions. Here Soil-1 is a clay soil with the volumetric moisture content of $m_v = 13.5\%$ and, conductivity $\sigma = 5mS/m$, Soil-2 is a clay soil with $m_v = 7.5\%$, $\sigma = 5mS/m$ and Soil-3 is a dry loam soil with $m_v = 2.3\%$, $\sigma = 1mS/m$.

(a) Reflected E-field for a mine buried at depth 5cm, Incident Gaussian wave σ_{freq}=10 GHz

(b) Reflected E-field from Soil-Mine Interface

(c) Reflected E-field from Mine-Soil Interface

(d) FRI Reconstruction in Soil-3 for L=8

(e) FRI Reconstruction in Soil-2 for L=10

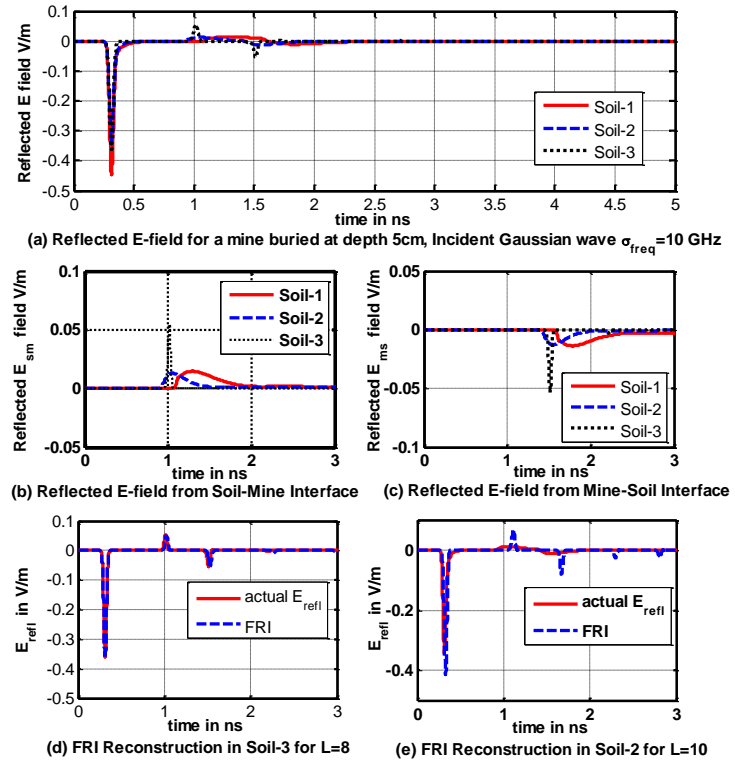Fig.1. Reflected EM wave with $\sigma_{freq} = 10GHz$ from landmine buried at a depth of 5cm and its conventional FRI reconstruction

Figure.1 shows that for 7.5% moisture soil, FRI is able to find pulses time, improvements can be made to achieve the correct magnitudes, so it can be used as fail safe algorithm.

REFERENCES

[1] M. Vetterli et al, "Sampling signals with finite rate of innovation," IEEE Trans. on Signal Process., vol.50, no. 6, pp. 1417–1428, June 2002

[2] R. Tur et al, "Innovation rate sampling of pulse streams with application to ultrasound imaging," IEEE Trans. on Signal Process.., vol. 59, no. 4, pp. 1827–1842, April 2011.

Improved Large Mode Area Low Confinement Loss Photonic Crystal Fiber With Flattened Dispersion

Mrs.Sandhya Sharma
(PhD Scholar)
Dept of Electronics & Communication
Suresh Gyan Vihar University Jaipur, Rajasthan
himanshu.makkar@mygyanvihar.com

Dr. O.S. Lamba
(Professor)
Dept of Electronics & Communication
Suresh Gyan Vihar University Jaipur, Rajasthan
onkar.lamba@mygyanvihar.com

Abstract: In this paper improved large mode area high birefringence photonic crystal fiber with single mode is proposed.The conventional single mode fiber suffer from limited output power due to small core diameter about 8 µm to 10 µm.This short coming can be overcome by using currently photonic crystal fiber of large mode area low confinement loss with single mode. [2]These properties provide scaling potential for fiber laser and amplifier systems.This type of fiber gives higher output power. The LMA 7-rod core fibers are obtained by removing the air-holes belonging to the first ring and the central one in the fiber cross-section. The 7-rod core photonic crystal fibers can provide high effective area values and single mode operation by properly choosing low air filling fraction and relatively small hole to hole distance. In this paper we compare the dispersion and confinement loss of 7-rod core photonic crystal fibers with 1-rod core.

Index terms: *Photonic Crystal Fiber (PCF), Finite difference time domain (FDTD),Large mode area(LMA),confinement loss, Birefringence.*

Introduction*:* The photonic crystal fiber has many unique properties, such as low non linearity,endlessly single mode operation, Large Mode Area (LMA),and high birefringence.These properties provide scaling potential for fiber laser and amplifier systems.This type of fiber gives higher output power. For high power optical beam, effective area of optical fiber is limited by increasing core size. An all silica PCF with different ratio of hole diameter to pitch d/Λ was studied in this paper.It is shown from numerical results that we can design low loss LMA in single mode. One rod core triangular PCFs have shown that their ESM region is defined by $d/\Lambda < 0.406$.

By narrowing the air-holes for a fixed pitch or by enlarging the pitch for a fixed d/pitch value, it is possible to increase the PCF effective area. But because of the losses, an upper limit on the guided mode area exists. That is because the decrease in the air-filling fraction causes an increase of the leakage losses.

To overcome all these problems, recent works are being done on another LMA with 7-rod core. Simulation results have shown that for a fixed d/Λ value the single mode region for 7-rod core PCFs is smaller than that of the traditional triangular fibers. The endlessly single mode regime for the 1-rod core PFC is defined by $d/\Lambda < 0.406$.while for large core triangular PCFs d/Λ is < 0.035.

Analysis*:* All the analyses of PCF properties have been done by using OPTI FDTD8.0.This method gives sufficient accuracy, efficiency and reliability. The triangular lattice PCFs present wider effective area for large pitch Λ so that they can be applied practically for high power delivery. For this it is necessary to work in single mode operation.

Design model: The proposed PCF is made of pure silica and has a circular array of air holes running along its length.This is index guiding PCF. For designing large area 7 rod PCF, first ring of air holes is removed.The total no. of air holes rings are nine.

In layout of 1-rod core with 9 rings $\Lambda = 1.55$ µm , d=1.0µm, $\Lambda = 2.5$µm. Similar layouts have been made for 7-rod core with 9 rings.
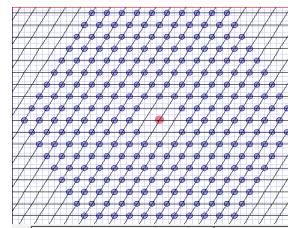

Figure 1: Layout of of seven rod PCF

Simulation results: In this paper, we have compared the dispersion & confinement loss obtained for 1-rod core fibers and 7 rod core fibers. As the number of air-hole rings is increased in the fiber, dispersion reduces. Furthermore, when the dimensions of the core are increased almost flat graphs for dispersion are obtained. The dispersion decreases with increase in the air-hole rings. As the air filling fraction increases, the dispersion also increase.

The increase of air hole rings leads confinement of light in core region, due to this, there is smaller losses than those with less air hole rings. By increasing the air holes diameter, we can increase air filling fraction and losses can be decreased.

Four designs with $d/\Lambda=0.27$ & 0.25 for one rod core and seven rod cor**e.** Here we take $\Lambda = 2.3$ and d= 0.60 and 0.65.

Conclusion:It has been found that when the dimensions of the core are increased almost flat graphs for dispersion are obtained. Thus 7-rod core fibers act as a better dispersion compensation fibers.We also see that in seven rod core confinement loss is low and birefringence is very high with respect to single rod fiber. It is shown from our numerical results that it is possible to design a low loss & high birefringence PCF with LMA at 1.55µm. We believe that our proposed design is useful for laser application.

Establishment of India's Largest Outdoor RS105 Test Facility as per MILSTD 461F/G

B. Venkata Ramana
Scientist-C
SAMEER-E3,
Visakhapatnam, A.P, India
bvramana.sameer@nic.in

P. Siva Kumar
Scientist-C
SAMEER-E3,
Visakhapatnam, A.P, India
skp.sameer@nic.in

Dr. B Subbarao
Scientist-F
SAMEER-E3,
Visakhapatnam, A.P, India
bsubbarao@ieee.org

Abstract – Electromagnetic Pulse (EMP) is a short burst of electromagnetic energy which can disrupt the electrical & electronic systems. There is a need for the electronic Systems to comply with the levels of EMP produced as per MIL STD 461 F/G. The communication, defense and now extended to civilian sectors are major victims for the electromagnetic pulse. The Ministry of Electronics & Information Technology, Government of India has funded the project for establishment of India's largest outdoor RS105 EMP test facility at SAMEER-E3 centre, Visakhapatnam, Andhrapradesh. Proposed system is establishing to meet the compliance testing for RS105 as per the MIL standards with generated test levels of upto 50 kV/m and covering the EUT test volume of 18mX13mX3m, sufficient to test the large defense and civilian systems.

Keywords - EMI/EMC, Electromagnetic Pulse, B-Dot & D-Dot sensors, transmission line, Pulse generator.

I. INTRODUCTION

An electromagnetic pulse (EMP) is defined as a high amplitude, short duration, broadband pulse of electromagnetic energy which can have devastating effects on unprotected electronic equipment and systems. Electromagnetic Pulse (EMP) origination may be a natural occurrence or man-made and can occur as a radiated, electric or magnetic field or a conducted electric current, depending on the source. The Electronics, communication and computing networks and electrical systems are vulnerable for the intense electric field level & fast rise time of such pulse(s). The test RS105 in military EMI-EMC standard at subsystem level qualification (MIL-STD-461F/G) is an important test to evaluate various electronic systems against EMP threat. The RS105 test method describes a transient electromagnetic pulse of up to 50 kV/m, double exponential wave with a rise time in the nanosecond range, which is applied to the equipment under test (EUT) at least 5 times. The EUT should not exhibit any signs of performance degradation.

To fully explain the physics behind how EMPs are created extends beyond the scope of this paper, but can be simplified to a short sequence of events -

A natural or man-made payload detonated at an altitude within or above the earth's atmosphere. During the explosion, Gamma rays (high energy photons) are rapidly released in all directions from the detonation. These gamma rays interact with air molecules in the earth's atmosphere which creates electromagnetic energy. This interaction process is called the "Compton's Effect." When a gamma ray "incident photon" collides with an atom in the atmosphere, it knocks a stationary electron free on a trajectory away from the detonation. These electrons "Compton's electrons" being smaller than their corresponding positively charged atom travel at a higher rate of speed rapidly increasing the charge separation distance between them. This separation time is expected to define the EMP rise time to peak voltage. The electrons quickly recoil back to their proton to conserve energy "Compton's recoil electrons." This recoil time is expected to determine the EMP fall time from peak voltage much like that of charging and discharging a capacitor.

II. TEST SETUP AS PER THE STANDRD

The RS105 test method specified in MIL-STD-461F addresses the risk of radiated exposure to an EMP event. RS105 testing is generally applicable for equipment installed in exposed and partially exposed environments. Defense Systems requires RS105 testing for nearly every installation platform, surface ships, submarines, and aircraft, to ground applications. Below is the typical setup as per the standard.
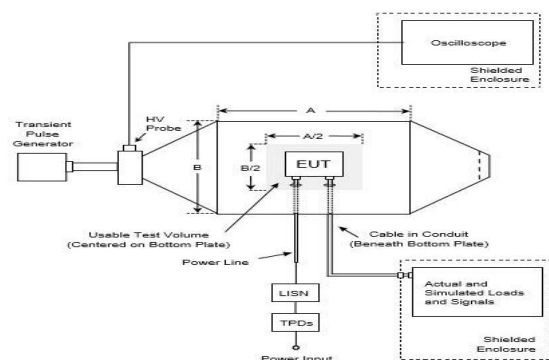

Figure 1. Typical test setup using parallel plate radiation system.

III. ABOUT THE PROPOSED TEST FACILITY

The proposed RS105 test facility at SAMEER-E3, Visakhapatnam for testing large objects as per requirements of MIL STD 461F/G has the following key features.

Tolerances and characteristics of the RS105 limit as per the MIL STD 461F/G shall be as follows:

- Rise time (between 10% and 90% points) between 1.8 ns and 2.8 ns (electric field continuously increasing).
- Full width half maximum (FWHM) pulse width equal to 23 ns ± 5 ns.
- Peak value of the electric or magnetic field for each grid position: 0 dB ≤ magnitude ≤ 6 dB above limit.

$$E_1(t) = 0 \quad \text{when } t \leq 0$$
$$= E_{01} \times K_1 \left(e^{-a_1 t} - e^{-b_1 t} \right) \quad \text{when } t > 0$$

$E_{01} = 5 \times 10^4$ V/m
$a_1 = 4 \times 10^7$ s^{-1}
$b_1 = 6 \times 10^8$ s^{-1}
$K_1 = 1.3$
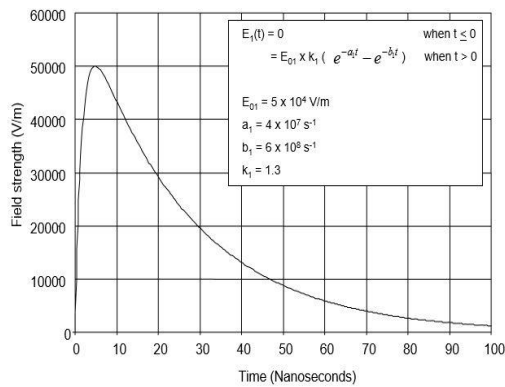
Figure 2. RS105 limit for all applications.
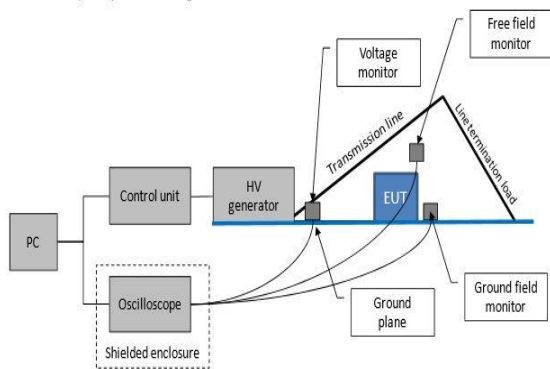
Figure 3. Block Diagram of the proposed test setup

The HV generator delivers the high voltage pulse to a transmission line mounted on a metallic ground floor. The line termination load absorbs the pulse and avoids reflections. A control unit monitors the HV generator and triggers the pulse generation. D-dot and B-dot sensors are used to monitor the generated electric & magnetic fields and V-dot sensor to monitor the generator output pulse voltage and shape.

An oscilloscope collects the measurements from the field and voltage sensors for display and eventually storage in the control PC. In order to ensure correct measurement the oscilloscope has to be placed in a shielded enclosure, protecting it from the strong E-field pulse. Other accessories as LISN or TPDs can be required but are not shown in the above drawing.

The proposed system is being executing by M/s. Montena Technology, Sa, Switzerland as turnkey project to install the system as outdoor facility within SAMEER Centre for Electromagnetic Environmental Effects (E3) at Vishakhapatnam, Andhra Pradesh.

Proposed facility is installing as outdoor facility within the SAMEER Centre for Electromagnetic Environmental Effects (E3) at Vishakhapatnam, Andhra Pradesh. Within the 13 acres of total extent, suitable location for installing the proposed facility was finalized by consulting the domain experts. Finalized location is covered by hills towards the termination end, which has the advantage of natural attenuation. Simulations are performed to study about the effect of the soil properties and presence of control building. The position of the control building was finalized based on the simulations with reference to axis of the antenna.

The electrical ground plane is made of metallic mesh installed over the soil. Metallic plates are used to cover the ground plane in the test zone, to allow the testing of heavy equipment. The soil under the RS105 test system will be made of concrete.

The equipment/sub systems of size max. 18 m x 13 m x 3 m (L x W x H) with weight of 30 tons can be tested for RS105 compliance specifically major defense systems for safety Critical equipment and subsystems located in an external installation.

The concrete pad below the Ground plane is of size: 70m x 30m (L x W) with a slope of at least 1.5% for water drainage and the slope is toward the generator shelter end from load end. The reinforced concrete pad under the test zone allows testing of EUT of a maximum weight up to 30 tons.
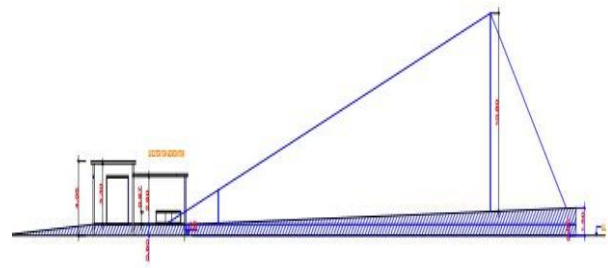

Figure 4. Side view of the Concrete Pad.

To realize the ground electrode, it is necessary to install a ground loop around the concrete pad as shown in the figure 5.
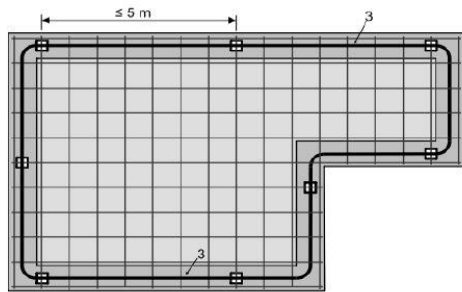
Figure 5. Sample of ground loop.

The steel tape or the steel cable for ground loop are made of galvanized steel. The loop must be entirely in the concrete and connected to the reinforcement of the concrete pad at every 5m distance. It is necessary to install seven earth terminals on the ground plane for grounding of the test system. Earth terminals are distributed as follows on ground plane- in the generator shelter, near the support of the output plate, two on each side of the first portal, two on each side of the main portal, and two on each side of the termination plate. The earth terminals are built into the concrete slab and connected to ground loop.
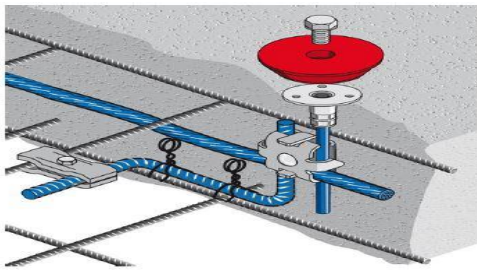
Figure 6. Sample of Earth terminal

As per standard the antenna will be of type Transverse electromagnetic (TEM) cell of transmission line with a matching termination resister bank permanently installed.

The antenna/transmission line radiates the field on the equipment under test (EUT). The line must be optimized for good waveform fidelity and therefore must have low reflection at the end of the structure formed by a resistive load adapted to the generator impedance. The radiating line is made of multiple copper wires terminated with distributed load resistors. The lines are hold and mounted on plastic poles. The radiating line is installed on the floor, on a metallic ground plane. The antenna structure is designed to withstand the winds of around 80 to 100km/h limit.

The proposed antenna is a 10.8 m high and long bounded wave line. It is made of a nonmetallic structure supporting stainless steel cables. Chains of termination resistors are connected at the far end of the antenna wires.
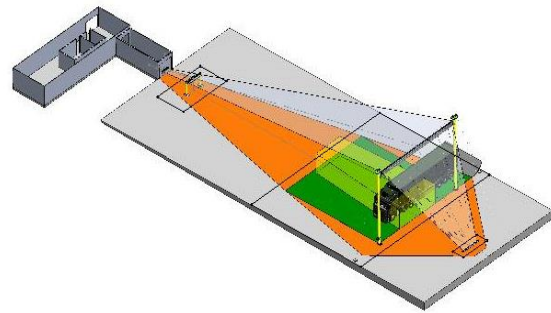

Figure 7. Schematic of Antenna Structure.

The environment to be simulated is dependent on the EUT and can be categorized in 2 types [13]: 1) aerospace systems are concerned by free field electromagnetic pulses; 2) ground or sea systems: the transient wave is more complicated due to the addition of the incident and the reflected waves.

To simulate these environments, different RS105 simulators are possible: 1) radiating simulators 2) bounded wave (or guided wave) simulators 3) hybrid simulators. Bounded wave type of simulator is chosen based on requirements in terms of the technical specifications viz. Polarization, homogeneity of the field, influence of the ground plane, wave form distortion etc.

Figure 8. Examples of three different RS105 simulators

A high voltage pulse generator of about 1 MV peak voltage delivers the desired fast electrical pulse to the antenna. The generator is installed inside a non-metallic shelter with adaptations to connect to the antenna. The ground plane inside the non-metallic shelter should be flat and horizontal. Transient pulse generator generates mono, plus, and minus polarity pulses as per standard to test for both polarities. The high voltage transient pulse generator connected permanently to the antenna and placed in a non-metallic shelter for protection from environment and other interference.

Figure 9. 1MV pulse Generator

The RS105 test system generates quite strong electromagnetic pulse which will disturb the electronic equipment in the vicinity of the test setup. It is required to install the control and measurement equipment in a shielded room. This shielded control room will be inside a small building with some additional storage room. The measurement equipment is installed in a control room building next to the pulse generator.

The external dimensions are: 4.0 x 3.0 x 2.5m.

Figure 10. Shielded Control Room

Figure 11. RS105 test facility- Construction Progress.

FAT has been carried out at M/s. Montena sa, Switzerland for verification of the Pulse generator's characteristics. The antenna radiation lines are simulated using a metallic plate and the termination is considered to be a bank of resistors, simulating the RS105 test system's termination impedance. Generator is verified for different set voltage levels to check the generated E-Field, using an E-Field sensor. The following figures show the test setup of Generator verification and position of D-dot sensor for E-field measurement.

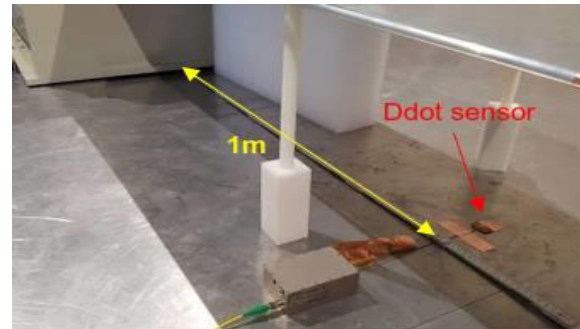Figure 12. Verification of RS105 Generator - Metal plate & bank of resistors

Figure 13. Electric Field measurement using D-dot sensor

The generated Electric Field picked up by the sensor is shown in below figure.
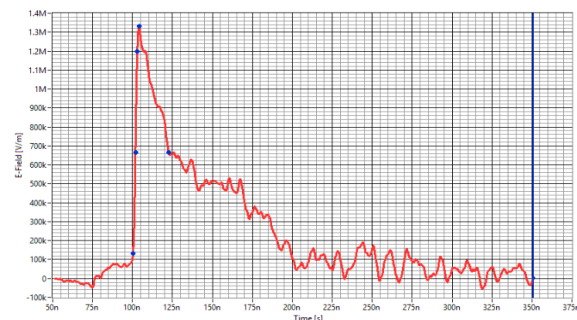

Figure 14. Electric Field level picked up by the sensor

The RS105 generator is verified for different voltage levels as listed in below Table 1:

TABLE I: The Generated Electric Field & Output Voltage Levels

.n .	Percent le el	t t ltage	E Field generated
1	40%	393 kV	674 kV/m
2	50%	493 kV	810 kV/m
3	75%	743 kV	1330 kV/m
4	90%	890 kV	1440 kV/m

The installation of RS105 test facility is planned in the month of August, 2017; the testing for defense, commercial & telecommunication equipment will begin soon after the installation.

The proposed establishment of test facilities at SAMEER-E3 shown in below figure, also includes, Shielded Semi-anechoic Chamber and EMI/ EMC test instrumentation as per MIL STD 461 F/G to serve the nation in wide range of sectors viz. commercial, telecommunications, medical, etc.

Figure 15. Proposed RS105 test facility installation at SAMEER-E3, Visakhapatnam, Andhra Pradesh, India.

IV. CONCLUSION

The Ministry of Electronics & Information Technology, Government of India has funded the project for establishment of India's largest outdoor RS105 test facility at SAMEER-E3 centre, Visakhapatnam, Andhrapradesh. Proposed system is establishing to meet the compliance testing for RS105 as per the MIL standards with generated test levels of upto 50 kV/m and covering the EUT test volume of 18mX13mX3m, sufficient to test the defense and civilian systems. This RS105 test system is presently being in realizing state, executing by M/s Montena Technology, SA, Switzerland as turnkey project to installs the system as outdoor facility within SAMEER Centre for Electromagnetic Environmental Effects (E3) at Vishakhapatnam, Andhra Pradesh. Compliance testing services as per MIL STD 461 will be offered for evaluation of electronic subsystems once the facility is operational, tentatively services will be started by mid of the year 2017.

REFERENCES

[1] RS 105 – Radiated Susceptibility – transient electromagnetic field, MIL STD 461 E/F/G

[2] MIL-STD-461 & 462 D: Requirement of the Control of Electromagnetic Interference, Emission and Susceptibility & Test Methods. US DoD MILSTD, 11 Jan 1993

[3] Technical Competence and Factors involved in realizing EMP Test Facility as per MIL-STD, K. Suryanaranayana (Retd.), V.V. Rama Sarma, Sandeep M. Satav, K. Rajeshwar Rao, M. Ratna Raju

[4] Technical articles from InCompliance & Intererence Technology magazines

[5] Technical excerpts from IEEE Electromagnetic Compliance magazine

[6] Testing for Immunity to EMP by Jeffrey Viel, National Technical Systems , IN Compliance 2010.

[7] http://www.montena.com

[8] http://ece-research.unm.edu/summa/notes/Sensor.html

[9] http://ece-research.unm.edu/summa/notes/Theoretical.html

[10] Developments in Early-Time (E1) High-Altitude Electromagnetic Pulse (HEMP) Test Methods Anthony Wraight, William D. Prather, Senior Member, IEEE, and Frank Sabath, Senior Member, IEEE

[11] Electromagnetic Compatibility (EMC): Part 4. Testing and Measurement Techniques—Section 32: HEMP Simulator Compendium, IEC 61000-432, 2002.

[12] A brief survey of available EMP simulators, D. V. Giri, 1986.

ASIAEM 2017- Size reduction of log periodic antenna using folded arm structure

NILESH KUMAR MANKER
Delhi University South Campus ,
Deparment of Electronics Science
Delhi , India
email: nmanker@gmail.com

Abstract— This paper describe the design of a printed log periodic dipole array antenna using folded arm structure. Log periodic(LP) antenna is ultra wide band antenna and the purpose of using folded arm structure in LP antenna is only to reduce size of antenna without affecting gain and bandwidth as we got in normal (oth iteration) design.With folded arm structure size of LP is reduced upto 25% this type of size reduction is possible in 2 iteration design of fractal koch geometry method but folded arm structure is simpler than fractal koch geometry.This antenna is design with <10db return loss for Ultra wide band (.5GHz to 3 GHz).

Keywords-UWB antenna , log periodic antenna ,size reduction.

I. INTRODUCTION

Log periodic antenna is a frequency independent antenna .Wide bandwidth devices play an important role and should be forefront object in wireless communication research activities. In addition to the wide bandwidth, the devices should also have a compact dimension to suppress down the cost of fabrication. Numerous method related to the size reduction; one of the popular method is fractal structure .But this paper deal with the new design folded arm structure, purpose of fractal and folded arm design is same ,size reduction without affecting gain and bandwidth as we got in 0th iteration design. Size reduction of log periodic antenna is important because LPDA is wide band antenna .

II. DESIGN OF LOG PERIODIC ANTENNA

In this paper log periodic antenna is presented with folded arm structure.For folding each dipole element we divide each element into equal parts.This method is simpler than fractal geometry method for size reduction.

Design   ecificati n

Operating Frequency	: 1.5 GHz-3 GHz
Spacing factor(σ)	: 0.098
Scaling factor(τ)	: 0.78
Dielectric used	: FR4
Thickness of dielectric	: 1.5mm

III. Design calculations;

$$\tau - \frac{l_n}{l_{n+1}} - \frac{d_n}{d_{n+1}} - \frac{s_n}{s_{n+1}} \qquad N = 1 + \frac{\ln(B_S)}{\ln\left(\frac{1}{\tau}\right)}$$

$$B_s = BB_{ar} = B[1.1 + 7.7(1 - \tau)^2 \cot \alpha$$

Table 1. Dimension of designed 0th iteration printed LPDA fractal Koch antenna

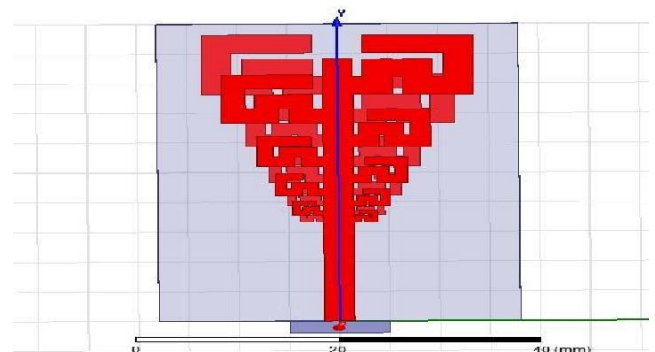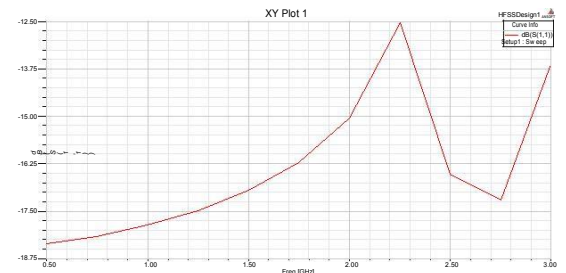| Element n^{th}	l (mm)	d (mm)	s (mm)
1	48.0	3.0	5.9
2	39.4	2.4	4.8
3	32.3	2.0	4.0
4	26.5	1.6	3.3
5	21.7	1.3	2.7
6	17.8	1.1	2.2
7	14.6	0.9	1.8
8	12.0	0.7	1.5
9	9.8	0.6	1.2

figure 1: LPDA using folded arm structure

figure 2: Return loss of antenna

REFERENCES:

[1] J. H. Reed, An Introduction to Ultra Wideband Communication Systems, New Jersey: Prentice Hall, 2005.

[2] R. Gharpurey and Peter Kinget, Ultra Wideband: Circuits, Transceivers and Systems(Integrated Circuits and Systems), New York, Springer, 2008.

[3] L. Zhu, S, Sun and R. Li, Microwave Bandpass Filters for Wideband Communications, New Jersey: John Wiley & Sons, 2012.

[4] K. Falconer, Fractal Geometry: Mathematical Foundations and Applications, 2nd Edition, New Jersey: John Wiley & Sons, 2003.

[5] J. Volakis, Antenna Engineering Handbook, 4th Edition. New York: McGraw-Hill, 2008.

[6] P. Jarry and J. Beneat, Design and Realizations of Miniaturized Fractal Microwave and RF Filters, New Jersey: John Wiley & Sons, 2009.

Electric Field Levels on Ground after High Altitude EMP

Carl Friedrich Rädel[1], Michael Hagel[1], Lars Ole Fichte[1], Sebastian Lange[2], Frank Sabath[2], Marcus Stiemer[1]
[1]Faculty of Electrical Engineering
Helmut Schmidt University, Hamburg, Germany
[2]Bundeswehr Research Institute for Protective Technology – NBC Protection, Munster, Germany

Abstract— Based on a model for the generation of high altitude nuclear electromagnetic pulses, the electric field distribution on the ground is determined by a line of sight calculation. The method is optimized by using parallel CPU processing and adaptively reducing the resolution of the diagram. To visualize the results, support by Google Maps, 2017 is added.

I. INTRODUCTION

The electromagnetic pulse (EMP) is a threat to electrical structures, such as electronic devices or power grids. A nuclear explosion in an altitude of approximately 30 km or more creates an EMP on that part of the earth's surface directly visible from the burst point. The EMP is commonly divided in three different phases: A quick early-time pulse (E1), due to gamma radiation stripping electrons from molecules and ionized atoms in the air, a secondary pulse from scattered gamma radiation and neutron interaction (E2), and finally a much slower pulse caused by deformation of the geomagnetic field (E3) [1]. The highest frequencies and maximum field strength arise in the early-time pulse (E1). To model its impact, we apply the well-known model of K. D. Leuthäuser [2]. The underlying theory describes the occurring phenomena based on electromagnetic (EM) wave and particle interaction. Using both MATLAB and the C++ programming language, the area affected by the EMP is calculated depending on its parameters such as the production rate of gamma radiation or the position of the burst point and the observer. The computing time is immensely reduced by consequent parallelization. The computed results are visualized with the help of Google Maps, 2017 [3].

II. THEORY

The gamma radiation can be considered as emitted by a point source at the burst point above the affected area. Gamma rays hit molecules and atoms, ionizing them and freeing electrons via the Compton effect. The production rate of fast Compton electrons $\dot{n}_c(r, t)$, responsible for the E1-EMP, depending on the radius vector between the burst point and the observer location r and the time t is modeled by a source function, which is the quotient of a sum of exponentials (QEXP)

$$\dot{n}_c(r,t) = \frac{\pi}{(\alpha+\beta)\sin\left(\pi\frac{\alpha}{\alpha+\beta}\right)} \frac{g(r)}{\exp(-\alpha\tau)+\exp(\beta\tau)} \qquad (1)$$

with retarded time $\tau = t - r/c$ (here, c denotes the speed of light), rise-parameters α, β > 0, and a function $g(r)$ proportional to the unscattered gamma flux [2]. Depending on the atmospheric density, secondary electrons are released due to an avalanche effect. The detached electrons are deflected by the earth's magnetic field, which is approximated as a dipole field. They follow a spiral trace around the magnetic field lines. This rapid change in direction causes an EM wave. The currents in the upper atmosphere and the resulting electromagnetic fields are computed by the presented computer code and propagated along a line of sight from the burst point to the observer location. This produces the typical smile diagram, as shown in Fig 1, see [2] for further details.

III. OPTIMIZATION

Computing the EM field strength at each point on the ground along the line of sight is time consuming. While the computation can be performed in parallel across multiple CPUs for distinct points in a canonical way, it is already demanding in terms of memory and CPU time for the numerical determination of the EM field in one single point of the affected area on the ground. Hence, we optimized the EM field computation in a single point by CPU based parallel processing, which yields a solution in a considerably reduced time. Further, to create the smile diagram, we adaptively reduced the density of points from the center outwards, thus diminishing the overall number of points needed to create the diagram. The demand for resources is thus decreased, such that the calculations of the resulting EM-field for large areas can finally be performed on a laptop computer rather than on a parallel computer cluster. The scaling factors achieved by this strategy are 1.8 for 2 threads, 2.8 for 4 threads and 4.2 for 8 threads. Particularly, if a single point of the diagram is of interest, it can quickly be evaluated.

The calculated results are visualized over a world map. In Fig. 1 the normalized electric field strength over Bangalore is presented for the instant, which the peak value is reached in. Due to the local geomagnetic field the smile diagram looks like a bow tie.
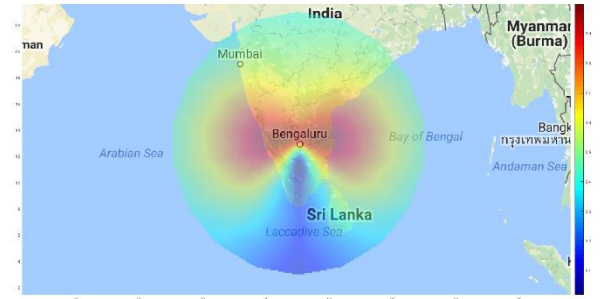

Figure 1. Smile diagram over Bangalore, normalized total electric field strength at peak value.

REFERENCES

[1] K.S.H. Lee (ed.), "EMP Interaction: Principles, Techniques and Reference Data – A Summa Book", Hemisphere Pub. Corp 1986.

[2] K.D. Leuthäuser, "A complete EMP environment generated by high altitude nuclear bursts", Theoretical Note 363, Fraunhofer-Institut, Euskirchen (Germany), Oct. 1992.

[3] Zohar Bar-Yehuda, 2015, plot_google_map, MATLAB Central File Exchange.

A Critique of the Bandwidth Definition for a Pulsed EM Based Detection System

Vijayakumar Solaiselvam
Dept. of Electrical Engineering
Indian Institute of Science, Bengaluru, India
e-mail-svijayin@gmail.com

M. Joy Thomas
Dept. of Electrical Engineering
Indian Institute of Science, Bengaluru, India
e-mail-jtm@ee.iisc.ernet.in

Abstract—Ultra wide band (UWB) electromagnetic waveforms are widely used in many applications. But there exists no clarity between different definitions for the bandwidth based on application and those suggested by regulatory agencies. The work presented in this paper aims to perform a critical analysis on the UWB system bandwidth. This paper analyses the signal bandwidth of pulsed electromagnetic system and studies the actual influence of different time parameters of the various Electromagnetic Pulse (EMP) waveforms on its bandwidth. It also studies the definition of bandwidth in the case of UWB pulsed waveform for detection applications in general and subsurface detection application in particular.

Keywords-Electromagnetic Pulse, Bandwidth, Subsurface detection, Ultra wide band

I. INTRODUCTION

The high frequency component in the receiver output of a detection system contains important details of the target. Usefulness of the high frequency also depends on many system parameters like receiver response, signal to noise ratio, input waveform correlation etc. So bandwidth of the detection waveform must include all the useful frequency components. This requirement is very important in the case of subsurface detection system. This paper gives some guidelines for arriving at the bandwidth for commonly used EMP waveforms [1] in the context of detection application. In this abstract, details of double exponential waveforms along with its derivatives are analyzed. Also importance of rise time and fall time in arriving at the frequency bandwidth is presented.

II. RESULTS AND DISCUSSIONS

As an example, bandwidth definition of double exponential waveform (DEW) is analyzed, for the sake of simplicity rise time(t_r) of the DEW signal is defined as time between zero value to signal peak, fall time(t_f)is defined as time between signal peak to its 50% magnitude. As per the Parseval's theorem, energy contained in both time and frequency domain should be same. For a DEW signal with $t_f > 10t_r$, most of the energy in the time domain signal is contained in the tail (falling edge) section of the signal. Percentage of energy contained in rise time section of the signal is very minimal. It is found that for a DEW signal with varying rise time and constant fall time, effect of rise time on frequency bandwidth is observable only after -60dB of spectral magnitude. This contradicts with the normallyused thumb rule of $0.35/t_r$, though waveform with lowest rise time has higher frequency components but their magnitude is very minimal (lower than -70dB), This will be lower than noise level in the detection application. So we may not be able to use
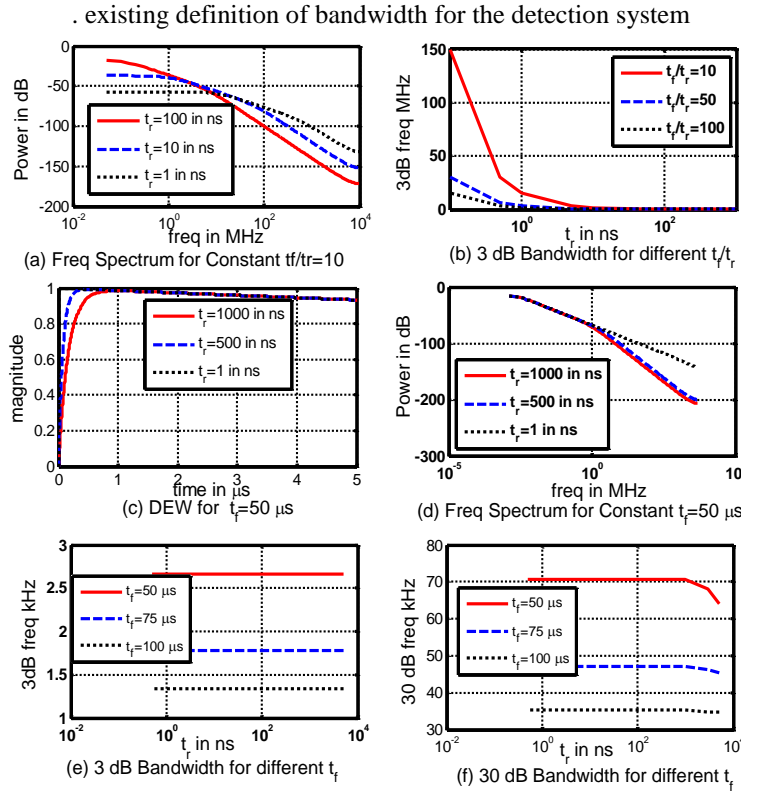
. existing definition of bandwidth for the detection system

Fig.1. FrequencySpectrum of DEW for various rise and fall time

Figure.1. shows that the bandwidth of the double exponential waveform up to 60 dB is fully depends on fall time than rise time and hence the advantage of a fast rise time pulse may not be useful for detection application, but derivative of DEW signal will have totally different frequency pattern which is influenced by the rise time, since many radiators will have field response which is derivative of the input DEW. So for those applications rise time still has a significant impact on the final detection.

III. BANDWIDTH THUMB RULE

Name		Bandwidth (approx)		% Energy in Variance
		3dB	20dB	
Gaussian		0.1349/σt	0.41994/σt	67.56
Diff. Gaussian	fmax	0.265/σt	0.43996/σt	59.6
	fmin	0.081/σt	0.01/σt	
DEW		0.133/tf	1.0856/tf	93.33 for tf=10tr

REFERENCES
[1] D.V. Giri, "High Power Electromagnetic Radiators", Harvard University Press, 2004

Image Focusing of Stepped Frequency Ultra Wideband Radar using Time Reversal Technique

Paramananda Jena
LRDE, DRDO
Bangalore, Karnataka, India
pj11@iitbbs.ac.in

Debalina Ghosh
School of Electrical Sciences
IIT, Bhubaneswar
Bhubaneswar, Odisha, India
deghosh@iitbbs.ac.in

A. Vengadarajan
DRDO
Bangalore, Karnataka, India
vengadarajan@yahoo.com

Abstract— This paper presents a Time Reversal(TR) based image focusing scheme for co-array based Stepped Frequency Continuous Wave (SFCW) UWB radar. A practical co-array based SFCW radar is considered for imaging applications. The image of a typical Through-the-Wall Imaging Radar (TWIR) target (human being) merges with multipath reflections from scatterers such as furniture like tables and chairs. Ghost targets are also generated due to large numbers of multipath, and it is difficult to discern the actual target due to poor Signal-to-Clutter-Ratio(SCR). It is found that with the application of TR technique, there is a substantial improvement in cross range resolution and SCR which will aid to better target detection and imaging.

Keywords: co-array UWB radar; Time Reversal(TR), Stepped Frequency Continuous Wave(SFCW).

I. INTRODUCTION

A Co-array MIMO(multiple Input Multiple Output) [1] UWB SFCW radar is designed to achieve required resolution. TR signal processing technique can be achieved physically or synthetically i.e. the TR retransmission is done mathematically instead of physical retransmission. In TWIR, physical TR has been used[2] which is not suitable for practical radar application. In this paper, the synthetic TR is applied with consideration of real time implementation in TWIR. In typical TWIR radar small array is practical for portability, which leads to poor cross range resolution. TR exploits the presence of large numbers of scatters present in the TWIR scenario for better cross range resolution despite having a small antenna array. Here, for the sake of simplicity, the penetration effect through wall is not considered which does not have any impact on the findings.

II. TR for Co-ARRAY SFCW UWB RADAR

The co-array based UWB radar with two transmitters, fourteen receivers, targets and multipath scatterers is shown in Fig.1. Fig.2 shows the conventional imaging-back projection - of scenario as shown in Fig. 1, wherein large number ghost have appeared. It creates large number of undesired image artifacts, which further complicates the image interpretation. The mathematical TR techniques is applied on the aforementioned scenario and there is a significant reduction in ghost targets. Further, it is found that large number of scatterers provide better focusing. The image focusing metric is captured as Signal-to-Clutter ratio(SCR) improvement as shown is Table-1. The SCR is the ratio of target power and average clutter power in the vicinity of the target. More the numbers of scatterers, the improvement is SCR is better with TR, which goes against the conventional wisdom. When there are no scatters focusing and conventional imaging gives same result.
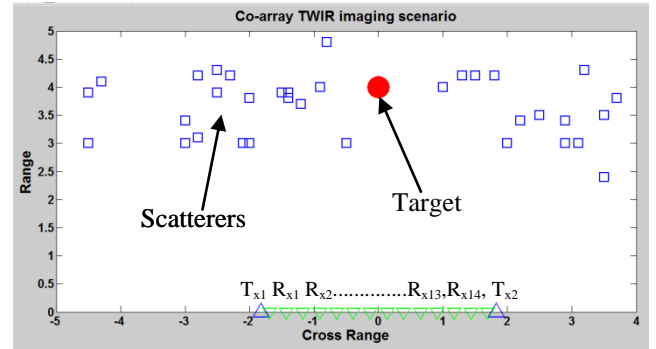

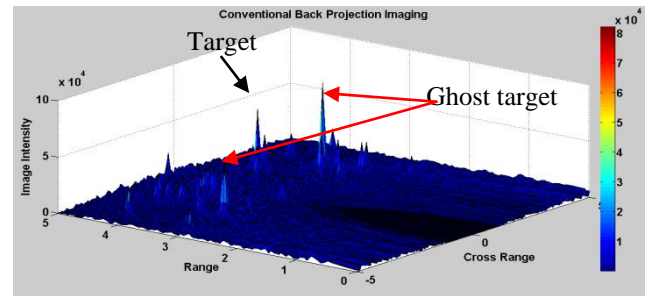Figure 1 Co-array UWB radar imaging scenario
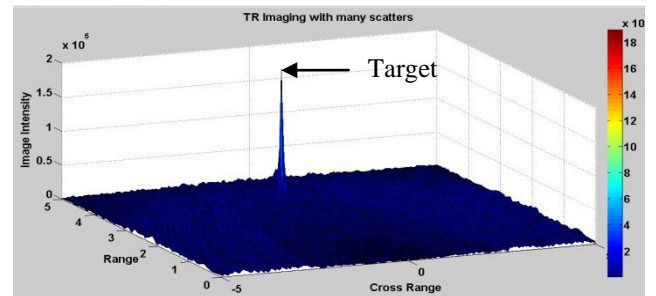

Figure 2 Conventional Imaging Back Projection

Figure 3 Image Focusing with Time Reversal

Table-1 SCR improvement with TR		
No. of Scatterers	SCR(Signal-to-Clutter-Ratio) dB	
	TR	Without TR
20	31	17
9	31	20
0	34	34

REFERENCES

[1] Z. Li, T. Jin, B. Chen, and Z. Zhou, "A coarray based MIMO array design method for UWB imaging," in Proceedings of the IET International Conference on Radar Systems, pp. 1–4, Glasgow, UK, October 2012.

[2] W. Zheng, Z. Zhao, and Z. Nie, "Time Reversal-Based Processing for Human Targets Detection in Realistic Through-The-Wall Scenarios" Progress In Electromagnetics Research, PIER 87, 279–296, 2008.

EM Modelling of Ultra Wideband Time Reversal

Paramananda Jena
LRDE, DRDO
Bangalore, Karnataka, India
pj11@iitbbs.ac.in

Debalina Ghosh
School of Electrical Sciences
IIT Bhubaneswar
Bhubaneswar, Odisha, India
deghosh@iitbbs.ac.in

A.Vengadarajan
DRDO
Bangalore, Karnataka, India
vengadarajan@yahoo.com

Abstract: **This paper attempts to verify the effectiveness of the super resolution capability of Ultra Wide Band (UWB) Time Reversal (TR) in the presence of discrete scatterers using EM solver. Conventionally, modeling of imaging scenario is done with statistical signal processing approach. In this paper physical modeling in the EM perspective is done to validate the UWB TR .**

I. INTRODUCTION

The Electromagnetic Time Reversal (TR) technique is based on the time invariance property of electromagnetic waves. For every forward electromagnetic wave, there exists a back propagating wave which follows the same path. If the medium is lossless and inhomogeneous, then TR provides better cross range resolution named as super resolution; since it is better than Rayleigh resolution limit. Super resolution property of TR can be validated in the lossless and less lossy medium. It is modeled by placing scatterers of different dielectric properties mimicking the practical scattering environment. Conventional environmental modeling with signal processing techniques are inadequate to capture all the physical phenomena such as scattering, diffraction, reflection and depolarization. However, EM solver can model the aforementioned physical phenomena. UWB TR using Gaussian impulse excitation of bandwidth 900 MHz is used to validate the concept of super resolution.

II. TIME REVERSAL SUPER RESOLUTION

The simulation set up is shown in Fig. 1. The source is a dipole antenna operating from 100 MHz to 900 MHz corresponding to a range resolution of 18 cm. There are seven antennas forming an array of transceivers. This is referred to as Time Reversal (TR) array. The elements of the TR array have a spacing of 30 cm corresponding $\lambda_c/2$, where λ_c corresponds to the center frequency of 500 MHz. Scatterers with different sizes and different dielectric constants are placed in a box of 300 cm x 350 cm x 60 cm. The signal received at the TR array is time reversed and retransmitted back through the medium. For verification of the super resolution property of TR, the same setup is analysed with and without scatterers. Fig. 2. (a) shows the electric field inside the medium without scatterers, the cross range resolution is 60 m. Fig. 2. (b) shows the electric field inside the medium with scatterers-cross range resolution of 50 m. It is seen that the electric field gets focused back at the source proving the property of TR. The simulation is extended with more numbers of scatterers and the focusing of the TR field is in the order of 45m as shown in Fig. 3.(a). Active source localisation using TR is effective for communication and radio location applications. But for the radar application, the important factor is the focusing of passive reflectors such as human being target in the Through-the-Wall Imaging Radar(TWIR) and mines in Ground Penetrating Radar(GPR). Another simulation of passive reflector focusing is aslo carried out using TR and focusing effects on passive scatterers is shown in Fig.4. In summary,TR provides better cross range resolution in

scatterer rich medium - cross range resolution : 60 m (No scatterers), 50 m (6 scatterers) , 45 m (9 scatterers).
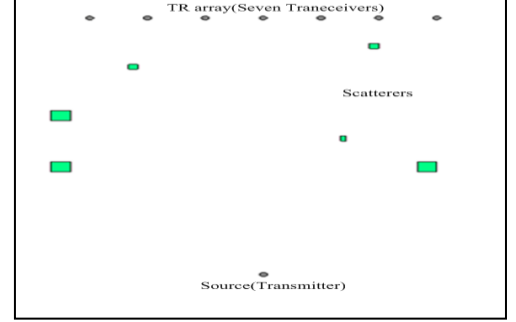

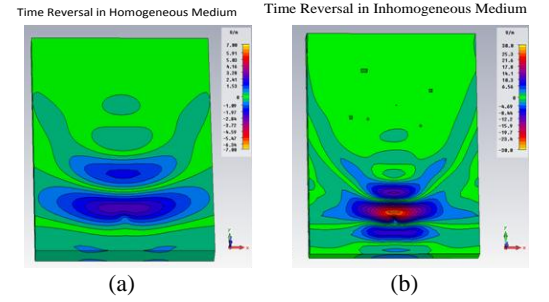Fig. 1. TR array for simulation

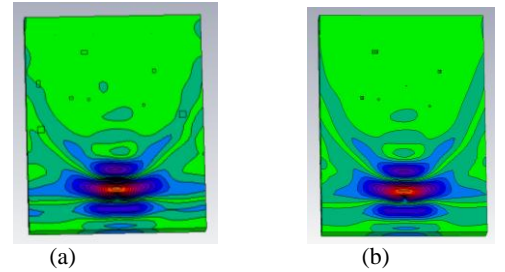Fig. 2. (a) TR in homogeneous medium (b) non-homogeneous medium

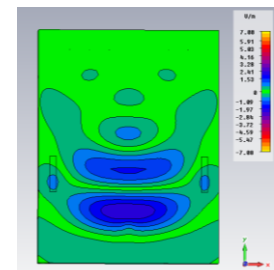Fig. 3. (a) TR with more nos. of scatterers (b) TR with less nos. of scatterers

Fig. 4. TR focusing on passive scatterers

REFERENCES

[1] Ahmet GurukanCepni, "Experimental investigation of time-reversal techniques using electromagnetic waves," PhD Thesis, year 2005, Carnegie Mellon University, Pittsburgh , Pennsylvania, USA.

[2] M. Yavuz and F. Teixeira, "Ultrawideband Microwave Sensing and Imaging Using Time-Reversal Techniques: A Review," Remote Sensing, vol. 9, pp. 466–495, 2009.

Wideband High-Power Microwave Module on the Basis of Two RF-Outputs Magnetron

G.I. Churyumov
Microwave & Optoelectronics Lab.
Kharkiv National University of Radio Electronics
Kharkiv, Ukraine
g.churyumov@ieee.org

A.I. Ekezly
Microwave & Optoelectronics Lab.
Kharkiv National University of Radio Electronics
Kharkiv, Ukraine
ekezli@gmail.com

Abstract— **This paper shows one of a possible way of obtaining the nanosecond duration high-power microwave pulses. For realization it we used the microwave module containing a non-relativistic microwave generator (magnetron with two RF outputs), a resonant microwave compressor and a matched load as an antenna for radiating electromagnetic pulses. The power, frequency and time characteristics and parameters of electromagnetic radiation at X and K_u bands are presented. Besides it, possibility of application of this approach for creating microwave module at mm range of wavelength is discussed. It is shown that the microwave module can be presented as non-lethal directed energy weaponry and to be used for electronic attacks.**

Keywords- high-power microwave, resonant microwave compressor, two RF outputs magnetron, electromagnetic weapon

I.   INTRODUCTION

The prospects for developing the high-power microwave electronics is associated with creating the high-power relativistic microwave devices which are provided generation of high-power microwave pulses (peak power is units and tens GW) [1]. However, the application of such devices is connected with considerable technical and technological difficulties, especially, when need to produce very short microwave pulses (duration less then 100 ns). In this case for forming microwave pulses there is more simple approach based on the pulse compression technology, namely, the resonant microwave compression method. A central idea of this method is slow storage of electromagnetic energy in the microwave resonator and then its removal from the high factor resonator for shorter duration to a matched load (antenna) [2]. Among advantages of this method it is necessary to note its ease of its realization, the possibility of application the industrial magnetrons as well as the standard elements of waveguide techniques.

In this paper we consider an operation of the microwave module, in which is used the magnetron having the two RF outputs of energy.

II.   STATEMENT OF THE PROBLEM

Fig. 1 shows a block diagram of the microwave module. The magnetron that is used in this experiment has the two RF outputs of energy: active and passive. For tuning and controlling by a frequency of the magnetron we used the tunable short-circuit waveguide as the reactive load of the passive RF output . The frequency-tuning curve is shown in Fig. 2.
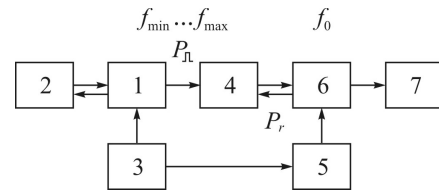
1 – a magnetron with two RF outputs; 2 – a tunable short-circuit waveguide; 3 - a power supply (modulator); 4 - ferrite isolator; 5 – a generator of controlling pulses; 6 - a microwave cavity; 7 – a matched load (antenna)

Figure 1.   Block diagram of the microwave module.

III.   ANALYSIS OF RESULTS

The analysis shows that for increasing an efficiency of compression and formation of the high-power nanosecond microwave pulses necessary to reduce a loss of power P_r. Assuming that $f_{min} < f_0 < f_{max}$ with the help of a short-circuiting piston we adjust an oscillation frequency of the magnetron to a resonant frequency of the microwave cavity and as a result the power P_r, reflected from microwave cavity is decreased.
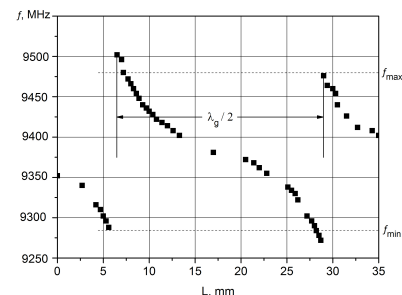

Figure 2.   Experimental curve of frequency tuning of the two RF outputs X-band magnetron.

Thus, we have tested the microwave module using the magnetron with the two RF outputs for forming high-power nanosecond microwave pulses.

REFERENCES

[1] A.S. Gilmour, Jr., *Klystrons, Traveling Wave Tubes, Magnetrons, Crossed-Field Amplifiers, and Gyrotrons.* Artech House. 2012. – 837 p.

[2] Benford J., Swegle J.A. and Schamiloglu E. *High Power Microwaves*. Second Edition. CRC Press. 2007. – 556 p.

High Power Millimeter Wave Pulse Measurement Using Cross-waveguide Resistive Sensor

Anil Allampalli[1], Amitabha Bhattacharya[2]

Dept. Electronics & Electrical Communication Engineering
Indian Institute of Technology, Kharagpur-721302, India
[1]*anilsai@iitkgp.ac.in*, [2]*amitabha@ece.iitkgp.ernet.in*

Abstract—**In this paper, a novel method that enables the determination of high power microwave pulse is discussed. A resistive sensor (RS) is basically made up of an n-type semiconductor and its performance is based on the well-known electron heating phenomenon in the semiconductor. The resistance of the semiconductor changes when electric field incident on it. By measuring the resistance change, the pulse power propagating through the waveguide can be measured. The voltage standing wave ratio (VSWR), electric field distribution and electric field dependencies on the frequency have been determined.**

Keywords: **Electromagnetic wave, mode TE$_{10}$, semiconductor obstacle, resistive sensor, X-band waveguide**

I. Introduction

High power microwave (HPM) devices are used in various application in the recent years [1]. The semiconductor diodes are being used for the measurement of HPM pulse measurement. The diodes can't handle high power level. An alternative device has been developed for the HPM pulse measurement, i.e. resistive sensor (RS). The sensing element (SE) is made up of an n-type semiconductor with ohmic contacts on both sides. The sensing element acts as a variable resistor when electric fields incident on it. The resistance change in the semiconductor is independent on the direction of applied electric field [2].

II. Fabricated Resistive sensor

The sensing element is made up of an n-type silicon wafer with an orientation $\langle 110 \rangle$. The resistivity of the silicon wafer is 5Ω-cm and thickness of 0.275 mm. A sensing element placed at the center of a waveguide with dimensions of 9 mm $\times$ 2.5 mm. The metalization area on the sensing element is 1 mm $\times$ 1.5 mm. Silver paste has been used to connect the metal wires to sensing element.

III. Results and Discussion

The sensitivity of the RS in the linear region is proportional to the pulse power P propagating through the waveguide. The sensitivity of RS in linear region is defined as follows [3].

$$\xi = \frac{4\beta\sqrt{\frac{\mu_0}{\epsilon_0}}}{ab\sqrt{1 - \left(\frac{f_c}{f}\right)^2}} \left[\frac{1}{2} + \frac{1}{1 + (2\pi f \tau_e)^2}\right] \langle \frac{E_m^2}{E_0^2} \rangle \quad (1)$$

where $\langle E_m^2 \rangle$ is an average of a square of the electric field amplitude in the sensing element and E_0 is an electric field

at the center of the waveguide. In the waveguides frequency band, ratio f_c/f changes from 0.8 to 0.5. The sensitivity of the RS decreases monotonously due to waveguide dispersion. By increasing the average electric field incidence on the semiconductor, the monotonous decrease in the sensitivity can be compensated. The reflection coefficient inside the waveguide should be as small as possible. The experimental VSWR value shows a good match with the simulated result as shown in Fig.2
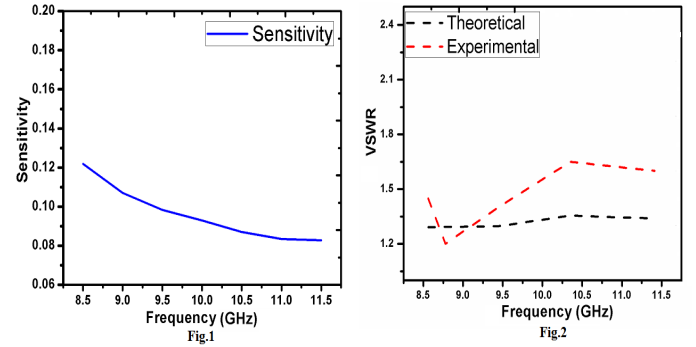

Fig. 1. Sensitivity of the sensing element (kW^{-1}) and Fig.2 Theoretical and experimental results of VSWR

IV. Conclusion

CST-simulations were performed to investigate the interaction of the n-type semiconductor sample with High Power microwave pulse. The VSWR was calculated and compared with the experimental result. The proposed sensor is able to measure the pulse powers up to 12.5 kW.

V. Acknowledgment

References

[1] J. Benford, J. A. Swegle, and E. Schamiloglu, *High power microwaves.* CRC Press, 2015.

[2] E. M. Conwell, *High field transport in semiconductors.* Academic Press, 1967, no. 9.

[3] M. Dagys, I. Kancleris, R. Simniskis, E. Schamiloglu, and F. J. Agee, "The resistive sensor: a device for high-power microwave pulsed measurements," *IEEE Antennas and Propagation magazine*, vol. 43, no. 5, pp. 64–79, 2001.

LIGHTNING. THUNDERSTORM ACTIVITY DIAGNOSTICS

A.A. Serkov, Dr. Sci.
Information Systems dept., Univ. NTU "KPI" and
"New Line Technologies",
Kharkov, Ukraine,
e-mail: saa@kpi.kharkov.ua.

S.A. Nikitin, PhD.
Information Systems dept., Univ. NTU "KPI" and
"New Line Technologies",
Kharkov, Ukraine,
e-mail: s.nikitin@newline.tech.

Abstract - Thunderstorm activity diagnostics is caused by the need to minimize the damage caused by lightning strikes. Particular attention is paid to the reliability of the forecast of thunderstorm activity and the time of its formation. Small time span between the formation of the storm hazards forecast and the onset of adverse events does not allow to take timely efforts to minimize the damage caused. Therefore, the solution of problem of thunderstorm danger diagnosis is actual.

Keywords – lightning; thunderstorm danger; intelligent data analysis; visualization.

I. INTRODUCTION

Increasing the reliability of the thunderstorm hazard diagnosis requires processing of diverse information, which differs in both form and content. Such data is provided a result of receiving of operative information about the results of the instrumental measurement with its subsequent processing in real time. At the same time, the spatial reference of obtained data is being carried out to ensure the completeness, clarity and timeliness its presentation. Conjugation of heterogeneous information from one or more sources in each point of a given region is a source data array and the initial phase of the complex information analysis in which various mathematical processing methods are applicable.

II. FORMULATION OF THE PROBLEM

With the development of convective cloud, there is a gradual increase in the density of spatial charges and increased storm activity. The duration of prestorm condition can reach 16 minutes, with an average value of 8 minutes [1]. And if for 14-16 minutes the cloud does not become stormy condition, it usually breaks. Thus, the registration and identification of the intercloud discharge allows the time interval of 15 minutes before the first dangerous discharge of "cloud-to-ground" type. Pulse electric field of intercloud discharge has horizontal polarization. This is the basis to identify them from the general mass of discharges. An additional feature is the definition of electrostatic field gradient during the prestorm activity, and the identified intercloud discharge is used as the reference point.

III. RESULTS

Designed standalone module allows to carry preprocessing and transmission of information on the collection server for data mining and storage of the results. The device contains two capacitive sensors and an electrostatic discharge sensor producing signals which are input to the ADC of the embedded MCU. The server provides the ability to represent data on the current electrostatic situation in the selected region as the overlay information on the geographical map of the area. At the same time server performs the forecast of storm front propagation direction with the definition of the place and time of probable "cloud-to-ground" lightning. Data are transmitted via the mobile DECT standard communications system. Autonomous modules coverage areas overlap and coincide with the service area of the base station (Fig.1).
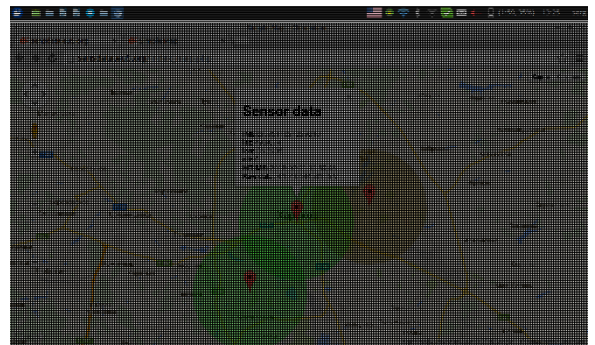

Figure 1. Visualization of thunderstorm activity

The satellite maps and map information are stored in a database. The original algorithm is used for matching map information and the corresponding area, and displaying the results of the measurement. Distributed information about lightning hazard is stored in a database and transmitted to the central computer over a mobile communication network using a method developed. The developed information retrieval system is based on queries to database allocated to the server. It can be accessed from any computer in the global network.

REFERENCES

[1] Mac Gorman, D., Apostolakopoulos, I., Nierow, A., Murphy, M., Demetriades, N., Cramer, J., Krehbiel, P.: Improved timeliness of thunderstorm detection from mapping a larger fraction of lightning flashes. Lightning Imaging Sensor Intl. Workshop, 11–14 Sept., Huntsville, Ala., Univ. of Ala. Huntsville and National Space Sci. and Tech. Center, 2006.

UWB Pulse Generator Using Step Recovery Diode

J.Prajapati[1], C. Prabhakar[1], M.S. Ansari[2], A. Chatterjee[1], R. S. Kshetrimayum[1], and R. Bhattacharjee[1]

[1]Department of Electronics and Electrical Engineering,
Indian Institute of Technology Guwahati, Guwahati, Assam-781038, India
[2]Raja Ramanna Centre for Advanced Technology,
Indore, Madhya Pradesh-452013, India

Abstract- The UWB applications require a very narrow pulse in the time domain as well as sufficient power within the limit of the FCC guidelines. In this paper we present an UWB pulse generator with the help of transmission line and Step Recovery Diode (SRD). The proposed circuit is simulated in HSPICE. The results show generation of a very sharp pulse whose bandwidth is in UWB band.

 Keywords- HSPICE; Step Recovery Diode; UWB Pulse;

I. INTRODUCTION

The UWB system has a large relative bandwidth that exceeds 20% or a large absolute bandwidth of more than 500 GHz. The frequency band for UWB ranges from 3.1-10.6 GHz [1]. The prime requirement of UWB system is a narrow pulse to support large bandwidth communication. In this communication, we present a narrow pulse generation by using the transmission lines acting as different electrical components and SRD. The SRD supports a very high repetition rate and high output voltage amplitude for UWB pulses. The circuit diagram, working principle and results of the UWB pulse generator are explained in sec. II.

II. UWB Pulse Generator

A. Circuit Diagram

 The proposed circuit diagram of UWB pulse generator is shown in Figure 1.
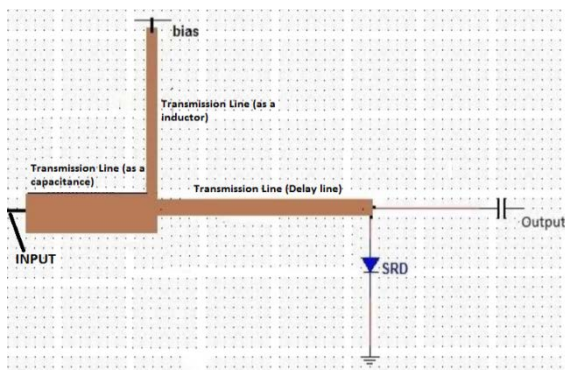

Figure 1. Circuit diagram of UWB pulse generator in HSPICE

The input voltage is applied at the one end of transmission line having dimensions as length (L) =24mm, width (w) =5mm, height (h) =1mm, and thickness (t) =0.5mm acting as a capacitance unit. A bias voltage is applied to make SRD in forward bias condition. The dimensions of the transmission line acting as an inductor unit are L=3.2mm, w=1mm, h=1mm, and t=0.5mm. The transmission line to produce the delay of 10ps to the reflected pulse, have dimensions as L=6mm, w=2mm, h=3mm and t=0.04mm.

The impedances of corresponding transmission lines are 11.76Ω, 63.17Ω and 89.32Ω.

B. Working Principle and Results

The input voltage applied is a negative voltage pulse having peak amplitude of -5V as shown in Figure 2(a). Initially the SRD is in forward bias, when the negative pulse reaches to the SRD, it quickly changes from low impedance to high impedance. This fast transition of impedance at SRD generates a sharp pulse which travels in both directions, towards output as well as towards input side of the delay line. Due to high mismatch at the interface of the transmission line (capacitance unit and delay line), the pulse gets reflected back to the output which then combined with the pulse coming from SRD and form a Gaussian pulse as shown in Figure 2(b).
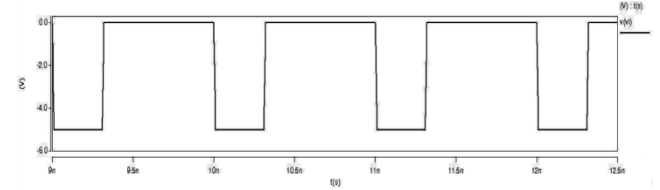
(a) Input pulse
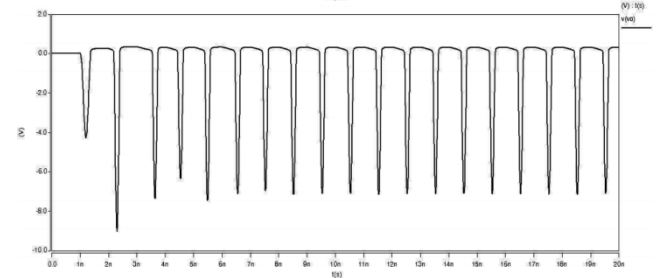
(b) Output pulse
Figure 2.

The spectral density shows that the bandwidth of the output pulse (up to first null) is within the UWB band specification as shown in Figure 3.
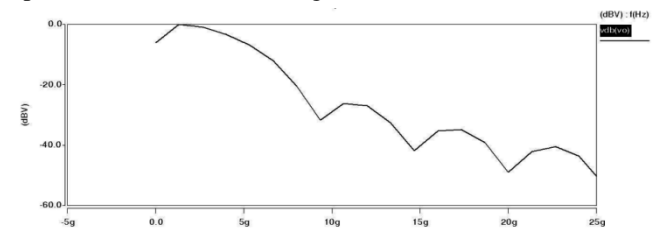

Figure 3. Output pulse in frequency domain

REFERENCES
[1] R. S. Kshetrimayum, "An Introduction to UWB communication system," IEEE *Potentials*, vol. 28, no. 2, pp. 9-13, March/April 2009.

Research on the Coupling Processes of Transmission Lines and Network with Diffused Field within Reverberation Chamber.

Qingguo Wang, Rui Jia, Zhaoming Qu, Erwei Cheng

The Research Institute of Electrostatic and electromagnetic Protection,

Mechanical Engineering College, Shijiazhuang, China

Email: Qingguowang99@aliyun.com

The electromagnetic field within a reverberation chamber is called diffused field or "in cavity field" formed by numerous reflections of electromagnetic wave and is of statistical characteristics. In a well stirred reverberation chamber, a statistically uniform, isotropy and random polarized field can be formed within it. The energy coupling process between diffused field and transmission lines is very important for the analysis of coupling mechanism and protection measures.

In this paper, four problems are discussed using theoretical and experimental methods.

1. The simulation model of diffused field based on limited number of plane waves and Mont Carlo statistics is first proposed and the loading effects on the field distribution is then analyzed.

2. Based on the above simulation models, the diffused field stimulated by electromagnetic pulse is discussed and a uniform field within a reverberation chamber can be obtained with the 3dB standard deviation which has been verified by experimental results. According to the experimental research, it is found that a pulsed electromagnetic field can stimulate a attenuated oscillation within a chamber and lasted for 3000ns in a big chamber sized. 10.4m×8m×4.3m. This will provide enough time for the electromagnetic waves to be reflected for over 100 times and so this give the possibility to form a statistical uniform diffused field within a reverberation chamber. In the uniformity calculation, the average peak values of pulsed field obtained during 12 paddle positions are applied to calculate the standard deviation. The X, Y and Z components are all meet the 3dB requirements similar to the results for continuous electromagnetic wave.

3. The coupling properties of parallel conductors, non-uniform strait conductor and typical networks with diffused field in a reverberation chamber are simulated using multi-plane wave superposition model. The dependences of induced voltage and current on the resistor loads, length of conductors or tubes in a network are calculated and compared.

4. A modeling and simulation method for the coupling calculation of transmission lines with diffused field has also been proposed using multi-planes wave for the pulse stimulate reverberation chamber by using super matrix equation and inverse-Fourier transformation. And the loading effects and dependences of length of induced voltage and current are also discussed. It is found that, attenuated oscillating of current on the load forms.

Impact Characteristics of Single Extended Grounding Electrode

Liu Xing
School of Electrical Engineering
Xi'an Jiaotong University
Xi'an Shaanxi China

Guo Jie
School of Electrical Engineering
Xi'an Jiaotong University
Xi'an Shaanxi China

Abstract—Full-scale experiment was used in this paper to research the impulse characteristics of grounding electrode. Compared with reduced-scale experiment or simulation method, full-scale experiment can obtain comprehensive impulse grounding impedance characteristics of the grounding device directly. The modified three-pole-method was used in full-scale experiment. A large number of experiments were done to research the effect of impulse current amplitude, grounding electrode size and current injection point on the impulse grounding impedance characteristics. The experiment result shows these conclusions: (1) the impulse grounding impedance decreases with the increasing amplitude of current and the soil ionisation shows saturation effect as the current increases. (2) the impedance decreases significantly with the increasing grounding size and it also shows saturation effect when grounding size is large enough. (3) the impulse grounding impedance is lower when the current injection point is the middle point of grounding electrode.

Keywords- grounding electrode; impulse characteristics; full-scale experiment; soil ionisation; inductance effect

I. INTRODUCTION

Impulse grounding impedance is a significant factor which affects the level of lightning protection and lightning trip-out rate of transmission lines [1]. While it's difficult to obtain the impulse impedance of grounding electrode accurately because of the soil ionisation under impulse current. Therefore the study of the impulse characteristics of grounding electrode is significant to lightning protection [2]. The study of the impulse characteristics of grounding electrode is mainly divided into theoretical simulation and experimental method. Theoretical simulation develops quickly in recent years, but experimental study is still the most effective method. Experimental study includes full-scale experiment and reduced-scale experiment. Compared with reduced-scale experiment or simulation method, full-scale experiment can obtain comprehensive impulse grounding impedance characteristics of the grounding device directly [3].

II. RESULTS AND DISCUSSIONS

A. Impulse Current Effect

The current waveforms of the grounding electrode under various charging voltages is shown in Fig.1. The impulse grounding gets smaller when the current amplitude increases. The reason is the soil ionisation: when the electric field strength around the grounding electrode exceeds the breakdown field strength of the soil, the soil will be partial breakdown, then the area of current flow will expand. Thus the impulse impedance decreases. And the soil ionisation become more intense as current increasing. The soil ionisation also shows saturation effect with increasing current.

B. Grounding Electrode Size

the impedance decreases significantly with the increasing grounding size, and it also shows saturation effect when grounding size is large enough The impulse grounding impedance shows not only soil ionisation but also inductance effect under the impulse current.

C. Current Injection Point Effect

Impulse grounding impedance is lower, when current applied at midpoint, compared with endpoint injection. When current applied at midpoint, the current could be diffused rapidly from the middle point to the two sides, inductive impedance and impedance are both lower.

III. CONCLUSION

It is concluded that (1) the impulse grounding impedance decreases with the increasing amplitude of current and the soil ionisation shows saturation effect as the current increases. (2) the impedance decreases significantly with the increasing grounding size and it also shows saturation effect when grounding size is large enough. (3) the impulse grounding impedance is lower when the current injection point is the middle point of grounding electrode, thus the position of the ground lead should be selected in geometric center of the grounding electrode

REFERENCES
[1] R. Kosztaluk, M.Loboda, D.Mukhedkar, "Experimental Study Of Transient Ground Impedances," IEEE Transactions on Power Apparatus and Systems, 1981, 100(11): 4653-4660.
[2] L. Grcev, F. Dawalibi, An electromagnetic model for transients in grounding systems," IEEE Trans. Power, Del., vol. 5 no. 4 pp. 1773-1781 Oct. 1990.
[3] S. Visacro, M. B. Guimarães, L. S. Araujo, "Experimental impulse response of grounding grids," Electr. Power Syst. Res., vol. 94 pp. 92-98 Jan. 2013.
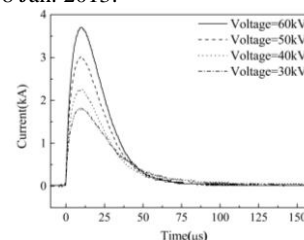
Figure 1. Current curve under different charging voltage

Evaluation of HEMP Tests by Binary Regression Models

Lars Ole Fichte, Marcus Stiemer
Helmut Schmidt University
mailto: lo.fichte@hsu-hh.de

Chaouki Kasmi
Agence nationale de la sécurité des systèmes
d'information, Paris, France

Keywords - Statistical evaluation, generalized linear model

Abstract— High Altitude Nuclear Electromagnetic Pulses (HEMP) are among most extreme external signals that can interfere with electric devices. To ensure the survival of vital components even in case of a HEMP event, several procedures have been designed to test DUTs in a lab environment. An estimation of the level which causes a failure of the DUT due to the external HEMP will allow engineers to fix better field levels for HEMP susceptibility tests and to avoid overtesting. This paper will apply standard binary regression models [2,3] such as as *logit* or *probit* on the results of HEMP tests from literature, with the aim to estimate a failure probability function, from which an appropriate test level can be derived in the future.

I. INTRODUCTION

We predict the outcome of HEMP susceptibility tests by estimating a failure probability function by the application of standard binary regression models [1,2] Since the large data sets needed for valid statistical evaluation are not available in the literature, we will focus on a German dissertation [3].

II. RESULTS

Here, we want to introduce simple statistical models to quantify the influence of the field strength x (continuous quantity) to failure Y (1 - does fail, 0 - does not fail). Contrary to the classic linear regression model we write

$\pi_i = P(Y_i=1) = h(\beta_0 + \beta_1 x_i),$

for the probability π_i that the trial i at field strength x_i results in $Y_i=1$. Thereby, h: $\mathbf{R} \to [0,1]$ denote the *response* function.

In Fig. 1 the three profiles of the binary regression models are given, i.e. the curves $h(\beta_0 + \beta_1 x)$, where $h()$ is chosen according the related model. Here, we estimate the breakdown failure probability of a computer [1], based on the measured field magnitude (• in Fig.1) and derived from the different regression models.
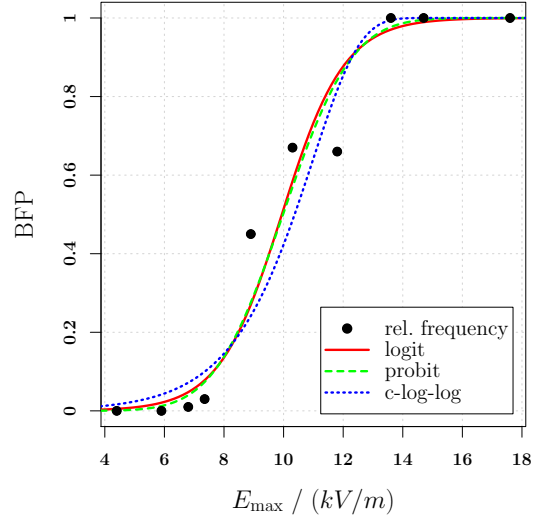

Fig.1: Response profiles of the three binary regression models for the data from Fig. 6.1 in [3].

The above example allows to conclude that binary regression models form a suitable tool for modeling the impact of the field strength to the tendency of the SUT to fail during a HEMP test.

III. CONCLUSION

If one is able to identify representative robust and vulnerable SUTs, then a binary regression model (either the popular *generalized linear model* (*glm*) variety or the slightly more exotic approaches in [1] should be fitted.
For serious treatment of the problem one should do more research to consider, for example, measurement uncertainty and optimal design for *glm* appropriately [4].

[1] Agresti, A.: Categorical Data Analysis, Wiley, Hoboken, N. J., 3rd edition, 2013.
[2] Bliss, C.I. :"The method of probits". Science, 79 (2037), pp. 38–39.
[3] Camp, M.: "Empfindlichkeit elektronischer Schaltungen gegen transiente elektromagnetische Feldimpulse", PhD thesis, University of Hannover.
[4] Nelder, J. and McCullagh, P.: "Generalized Linear Models", Chapman and Hall/CRC Press, 2. Edition, 1989

A Review of the Existing Techniques for Complex Natural Resonance Extraction

Andrés Gallego
Department of Electric and
Electronic engineering
Universidad Nacional de Colombia
Bogotá, Colombia
ajgallegog@unal.edu.co

Felix Vega
Department of Electric and
Electronic engineering
Universidad Nacional de Colombia
Bogotá, Colombia
jfvegas@unal.edu.co

Sebastian Eslava
Department of Electric and
Electronic engineering
Universidad Nacional de Colombia
Bogotá, Colombia
jseslavag@unal.edu.co

Abstract— We present in this paper a comparative review of the methods for calculating the Complex Natural Resonance extraction of backscattering signals. Existing techniques are characterized in terms of computational cost, noise sensibility and early time sensibility.

r s—Singularity Expansion Method, Cauchy's Method, complex natural resonance, matrix pencil method, Laplace transformation, radar, Half Fourier Transform.

I. INTRODUCTION

The Singularity Expansion Method (SEM), proposed by Carl Baum in 1971[1], is a technique used to characterize the response of an object to electromagnetic stimuli using its Complex Natural Resonance (CNR). This response, unique for each object is aspect independent and can be used for object identification.

This method has been applied to several domains and applications, especially Automatic Target Recognition (ATR). Several techniques are used to extract the CNR of the signal, among them we have: the Matrix Pencil Method, the TLS-Prony's Method and the Cauchy's Method.

With the aim of implementing an FPGA version of SEM, for real time application, we performed a comparative analysis of the existing techniques for CNR extraction.

II. CNR EXTRACTION METHODS COMPARISON

The results of the analysis are presented in Table 1. The analysis characterizes each method in three aspects: Early Time (ET) -Late Time (LT) incorporation, Computational cost and Noise influence. The analysis was performed from both, theoretical point of view and using simulation results of canonical geometries.

As a conclusion, the most feasible method to be implemented in a portable, real time processing unit is the method based in the Half Fourier Transform.

REFERENCES

[1] C. E. Baum, "On the singularity expansion method for the solution of electromagnetic interaction problems," 1971.

[2] W. Lee, "Identification of a target using its natural poles using both frequency and time domain response," 2013.

[3] F. Sarrazin, A. Sharaiha, P. Pouliguen, P. Potier, and J. Chauveau, "Analysis of two methods of poles extraction for antenna caracterization," IEEE Antennas Propag. Soc. AP-S Int. Symp., pp. 1–2, 2012.

[4] S. Jang, W. Choi, T. K. Sarkar, M. Salazar-Palma, K. Kim, and C. E. Baum, "Exploiting early time response using the fractional Fourier transform for analyzing transient radar returns ,"IEEE Trans. Antennas Propag., vol. 52, no. 11, pp. 3109–3121, 2004.

TABLE I. METHODS COMPARISON FOR SEM CNR EXTRACTION

eth d erf r ance	Date	R	tati nal st	D ain f erati n	Earl ti e res nse inc r rati n	erall FP i le entati n s ita ilit
atri Pencil	1990	High	Moderate	Time	Moderate	High
a ch	2007	Low	High	Frequency	Moderate	Low
T Pr n	1987	Moderate	High	Time	Low	Moderate
FT	N/A	Low	High	Frequency	Moderate	Moderate
FT	1980	N/A	Low	Frequency	High	High

High Frequency Coupling with Stochastic Transmission Line in Rectangular Resonator

S. Tkachenko, J. Nitsch, R. Vick
Otto-von-Guericke University, Magdeburg, Germany
e-mail: sergey.tkachenko@ovgu.de

R Rambousky
Bundeswehr Research Institute for Protective Technologies and NBC Protection (WIS), Munster, Germany

Abstract— In this paper, we investigate propagation of high-frequency current waves along stochastic transmission line in rectangular cavity using as a basis the model of transmission line with symmetry of resonator. The stochastisation of the line is created by the stochastically arranged chain of loads. Using this model one also can take into account stochastic geometry of the line. The research have shown a significant difference between the propagation of the current wave along the transmission line with stochastically arranged loads (TL with stochastic geometry) in free space and in the resonator. In the first case, the average square of the absolute value of the transmission coefficient exponentially tends to zero with increasing length of the line because of interference phenomena for current waves. In the second case, in the average, the current can penetrate through the stochastical chain of the loads (TL with stochastic geometry) due to the re-reflection of the signal from the walls of resonator.

Keywords- resonators; stochastic transmission lines

I. INTRODUCTION

Investigation of electromagnetic coupling to antennas and transmission lines inside resonator - like objects (shielded rooms, computer cases, aircraft fuselages, satellites, etc.) is one of the most challenging task in modern electromagnetic compatibility. The developing of corresponding calculation methods is quite advanced mathematical problem. In reality the problem is more complicated, because of the exact geometrical and electrical parameters of transmission line, which define such coupling, are unknown in practical applications. As result one can only talk about the probability of the one or the other parameters.

The numerical methods (like MoM, TLM, etc.) which are usually applied for the solution of this group of problems are applicable for specific cases only and they are computationally intensive. In contrast to that, analytical and semi-analytical methods are applicable on general cases, and allow to make a fast analysis of the problem. They are based on different approaches of mathematical physics. The method of small antennas allows to consider electrically small scatterers and radiators (dipole and monopole antennas, loop antennas, etc.) in a resonator [1]. However its application is restricted to small dimensions of the scattering objects. Another approximate method: the method of analytical regularization [1] for thin wires allows to consider thin wires line or antennas in a resonator using the resolution operator in TL approximation and taking into account several nearest resonance frequencies [1]. However, this method also has some restrictions. From another hand, as usual in theoretical physics, an exact solution for the system "transmission line in resonator" can be found for a high-symmetrical system, where wire and cavity have the same symmetry. For a rectangular resonator the wire is conducted parallely to four walls of the resonator and connects two other opposite walls. This system allows an exact analytical solution by a spatial Fourier transformation for any kind of excitation, including any finite number of lumped sources and loads, which can be considered as controlled voltage sources [2]. In the case of multiple loads the problem is reduced to the solution of linear system of Nth order (N is a total number of sources and loads) [3]. This method is computationally effective, fast (contains only double mode sums) and allows to solve stochastic problems with relative large statistical samples.

II. RESULTS

In this paper, we investigate propagation of high-frequency current waves along stochastic transmission line in rectangular cavity using as a basis the model of transmission line with symmetry of resonator. The stochastisation of the line is created by the stochastically arranged chain of lumped impedances, which can have as reactive as well losses components [4]. Using this model one also can take into account stochastic geometry of the line, by the expansion of the deviation of the vertical coordinate of the transmission line from the horizontal one into a sin - Fourier series, further definition a deviation of the inductance and capacitance per - unit length from their uniform values and quantization of these values ([5],[4]).

Calculations in the considered method are greatly facilitated by the fact that, for the each Fourier mode, an amplitude of the lumped potential and its position define only numinator of corresponding Fourier series coefficient through simple trigonometric function. The denominator, including one-dimensional summation and depending from transversal geometry of resonator, is the same for each elements. This circumstance also gives a possibility to develop analytical perturbation theory up to the second order on the value of lumped impedances. The method can be used to obtain statistical moments of current and square of its absolute value as well as the PDF of these values.

The research have shown a significant difference between the propagation of the current wave along the transmission line with stochastically arranged loads (TL with stochastic geometry) in free space and in the resonator. In the first case, the average square of the absolute value of the transmission coefficient exponentially tends to zero with increasing length of the line because of interference phenomena for current waves [4,5]. In the second case, in the average, the current can penetrate through the stochastical chain of the loads (TL with stochastic geometry) due to the re-reflection of the signal from the walls of resonator.

REFERENCES

[1]. S.Tkachenko, J.Nitsch, R.Rambousky, R.Vick, "Electromagnetic coupling to thin wire structures inside resonators", *Int. Symposium EUROEM* 2016, 11-14 July 2016, London, UK.
[2]. S.Tkachenko, R.Rambousky,J.Nitsch, "Electromagnetic Field Coupling to a Thin Wire Located Symmetrically Inside a Rectangular Enclosure", *IEEE Trans.EMC,* **55**(2), No.2, 2013.
[3]. S.Tkachenko, J.Nitsch, R.Rambousky, "Electromagnetic Coupling to Transmission Lines with Symmetric Geometry inside Rectangular Resonators", F.Sabath, E.Mokole (eds.), *Ultra-Wideband Electromagnetics* 10,Springer,NY 2014. pp. 31-48
[4]. S.Tkachenko, H.-J.Scheibe, X.Wang, R.Vick, "Propagation of Current Waves along a Transmission Line with Randomly Located Non-Uniformities", *2013 Int. Conf. ICEAA*, Torino, 9-13 Sept. 2013, pp: 1286 - 1289.
[5]. S.Tkachenko, R.Vick, "High-Frequency Stochastic Properties of Transmission Lines", Final Report of DFG Project Nr. VI 207/3-1, 2014, Magdeburg.

Noninvasive Method to Diagnose Early Insulation Fault during Circuit Breaker Test by Radiated E-Field Measurement

Kong Xu, Xie Yan-Zhao, Sun Li-qiong
State Key Laboratory of Power Equipment and Electric Insulation
National Center for International Research on Transient Electromagnetic Environments and Applications
School of Electrical Engineering, Xi'an Jiaotong University, Xi'an, Shaanxi, China
Kongxu.nachuan@foxmail.com, Yzxie@mail.xjtu.edu.cn, lqsun@mail.xjtu.edu.cn

Abstract—This paper introduces a noninvasive method to diagnosis the early insulation fault inside the circuit breaker. It is found that some early insulation fault can be diagnosed by measuring the radiated electric field (E-field) during the switching operation of the circuit breaker. Although the discharge quantity of the early insulation fault is too small to be detected by traditional voltage or current measurement, the radiated E-field can be very distinct. It can be a potential noninvasive method to diagnose the early insulation fault by the switching E-field measurement.

Keywords - circuit breaker, switching E-field pulse, measurement, insulation fault diagnosis.

I. INTRODUCTION

The on-site experiments for more than two years in Xi'an high voltage apparatus research institute (XIHARI) show that the switching operation of the circuit breaker can excite transient E-field around the breaker. It is found that the early insulation fault of the circuit breaker is very hard to be detected by the traditional current or voltage probes due to very limited quantity of charges during the partial discharge process, however this process can radiate E-field pulses which can be detected by E-field sensor with fiber-optic link [1]. This paper presents some results to show the effectiveness of this noninvasive method.

II. SWITCHING E-FIELD MEASURING RESULTS OF CIRCUIT BREAKER WITH EARLY INSULATION FAULT

A) Measuring result of 800 kV breaker made by Tan-an switcher factory in Oct. 28, 2014
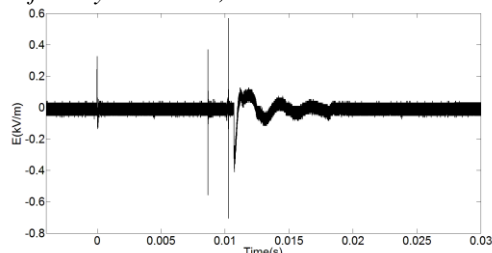

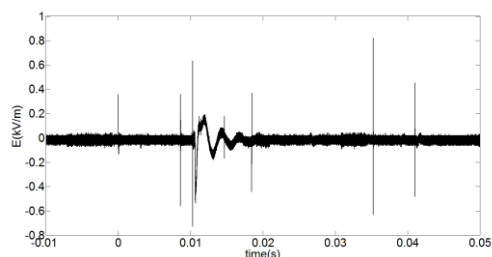Figure 1. Normal E-field waveform of the breaker during synthetic test

Figure 2. E-field waveform when the breaker has early insulation fault

B) Measuring result of 550 kV breaker made by Beijing switcher factory in Apr. 25, 2015
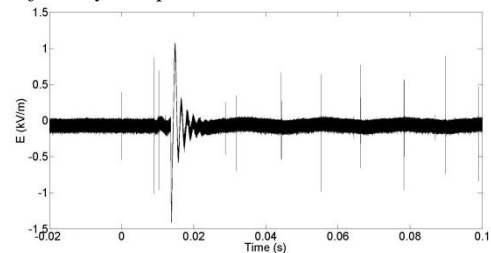

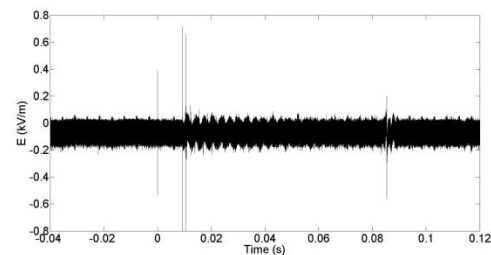Figure 3. E-field waveform when the breaker has early insulation fault

Figure 4. E-field waveform when the breaker is breakdown

C) Measuring result of 420 kV breaker made by Ping-zhi switcher factory in Dec. 28, 2015
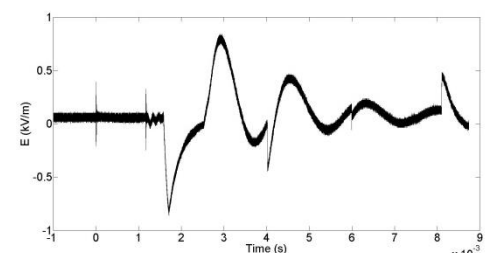

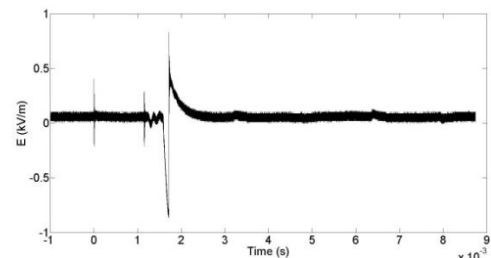Figure 5. E-field waveform when the breaker has early insulation fault

Figure 6. E-field waveform when the breaker is breakdown

REFERENCES

[1] Xu Kong, Yan-Zhao Xie, et al. High-voltage circuit-breaker insulation fault diagnosis in synthetic test based on noninvasive switching electric-field pulses measurement, IEEE transaction on power delivery, vol. 31, no. 3, pp. 1168-1175, Jun. 2016.

Simulation Analysis of Tower Grounding Impedance under Impulse Current

Wei Qi
School of Electrical Engineering
Xi'an Jiaotong University
Xi'an, Shaanxi, China

Guo Jie
School of Electrical Engineering
Xi'an Jiaotong University
Xi'an, Shaanxi, China

Abstract—With the rapid development and extension of power system, the operating experience shows that most accidents occurred on transmission lines are caused by lightning. The lightning current, which can be dozens or even hundreds thousands amps, flows through tower grounding electrode and it leads to non-linear soil ionization around the electrode. To improve the lightning prevention of transmission lines, it is necessary to take the non-linear soil ionization into consideration in the simulation of tower grounding electrode, which is essential for the design. Currently most theories and models neglect the non-linear soil ionization or use simplified models. In this article, Finite Element Method is applied to build a optimized model by comsol-multiphysics software. Besides, the non-linear soil ionization phenomenon is taken into consideration. With this model, a grounding electrode simulation with a high amplitude can be done.

Keywords-tower grounding impedance; Finite Element Method; non-linear soil ionization; lightning

I. INTRODUCTION

Most accidents occur when lightning hits transmission lines or towers. Currently, it is usually applied that power frequency grounding resistance multiply a coefficient to replace tower grounding impedance. However, soil ionization and inductive effect works when lightning current flows through the tower and grounding impedance will be non-linear. Based on electromagnetic field theory, Finite Element Method has its own superiority to analyze grounding electrode. Discretizing soil element is core of this model so that spark field and distribution along electrode can be simulated.

II. SIMULATION MODEL AND ANALYSIS

To verify the experiment results, a model is built in comsol-multiphysics software, which contains a 1m-long steel electrode and soil field. Impulse current curve is 8/20 μs. Soil resistivity is 43.5 Ω·m. Grounding impedance under different amplitude of impulse current are found.

The structure and size of electrode are changed to verify the model. It contains a 2m-long vertical electrode, a 2m-long horizontal electrode and a cross electrode, which are made by steel. In the simulation, all these model are buried in 0.8m depth and soil resistivity is 100 Ω·m(We use 43.5 Ω·m in II. to verify that the simulation model is correct because soil resistivity in the experiments is 43.5 Ω·m. 100 Ω·m is a typical soil resistivity value and is often used.).

Inductive effect cannot be neglected because of high frequency of lightning. Three type of models in are chosen and amplitude of impulse current is 10kA. The relation between grounding impedance and current frequency are found.

III. CONCLUSION

There are several conclusions after calculating: (1) this simulation model is accurate in that deviation from experiment results is 10%. (2) soil ionization works under high-amplitude impulse current and grounding impedance will be lower with increasing of current. The decline tendency has saturation effect. (3) impulse grounding impedance is greater than power frequency grounding resistance because of high frequency of impulse current. Grounding impedance will increase when frequency of current increase.

TABLE I. GROUNDING IMPEDANCE OF THREE KINDS OF ELECTRODES UNDER DIFFERENT FREQUENCY

Current frequency/kHz	Type of electrode		
	Horizontal	Vertical	Cross
0.05	19.02∠0.05	18.42∠0.05	16.34∠0.06
0.5	19.06∠0.35	18.43∠0.37	16.36∠0.41
5	19.38∠1.92	18.79∠1.96	16.72∠2.20
50	20.99∠6.52	20.35∠6.58	18.28∠7.34
500	27.35∠19.85	26.51∠19.39	24.57∠21.13

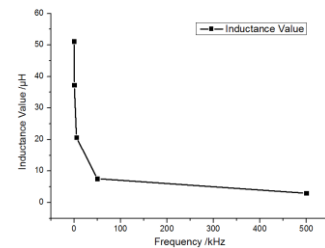Figure 1. Inductance of grounding electrode under different frequency.

REFERENCES

[1] A. Geri, G. M. Veca, E. Garbagnati, G. Sartorio, "Non-linear Behaviour of Ground Electrodes Under Lightning Surge Currents: Computer Modelling and Comparison with Experimental Results," IEEE Transactions on Magnetic, 1992, 28(2): 1442-1445.
[2] HE Jinliang, "Grounding technology of power system," Beijing, China: Science Press, 2007.

R D T R D E F R P ED RR TE
PP T

Muthukumar M, Dr.D.Ramakrishna, Dr.V.M.Pandharipande
Department of ECE, Osmania University, Hyderabad
muthukumarece@gmail.com

stract Transmit/Receive Module (TRM) is a key component in Phased Array Radar system. In this paper, construction technique of hybrid TRM PCB to reduce the size and cost has been described. The architecture has been chosen such a way that the TRM can be manufactured using available COTS components. The reliability of the TRM has been improved by proper thermal management and component design. The TRM have a bandwidth of more than 1GHz at X-band. Phase and amplitude are controlled by a 6-bit phase shifter and a 6-bit attenuator, respectively. The output power is 5W and the receiver noise figure is 3.5 dB. The entire module has been shielded for better EMI/EMC compliance. The required power supplies are derived internally. The module has special features like temperature monitoring, RF Output monitoring, Power supply health status..etc. Engineering proto-type has been fabricated and tested. The measured results are presented and shows good agreement with design predictions. The module has a footprint of 90mm (L)X 14mm (W) X 8mm (H).

Multi-Layer T/R Module has been designed and developed to address the following practical problems:

- Size – Using Hybrid Technology
- Cost – Using COTS Packaged SMT Components and Automated Assembly
- Limited Scan Angle – By reducing the TRM Size
- Thermal Issue – By using proper Thermal Via design and cooling techniques
- Integration Issue – Major components will be integrated in Single Module as a brick
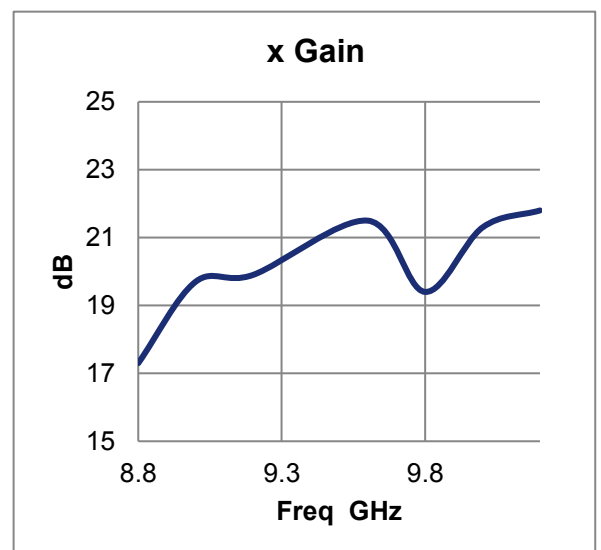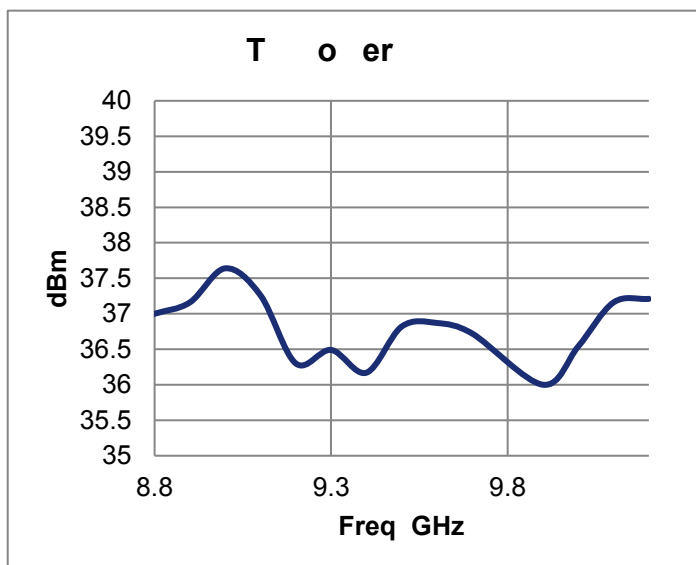
Statistical Analysis of the Radar Cross Section of Colombian Improvised Explosives Devices

art ‡ a‡ a r† ac s sta a t

‡

†

jfvegas@unal.edu.co

Abstract—This paper presents the radar cross section of several Colombian IED models. This work aims the construction of a database suitable for statistical analysis of the characteristics associated with different IED topologies.

e rds - Improvised explosives devices, Radar Cross Section, UWB Radar

I. INTRODUCTION

As its name suggests, improvised explosives devices (IEDs) are manufactured using artisanal, non-standardized methods of construction. Moreover, IEDs have low metal content and are variable in shape and size. These characteristics limit the effectiveness of using metal detectors, or other methods currently used for the detection of conventional landmines.

In [1] the backscattering of 22 IEDs was measured and characterized in frequency domain. In [2] the authors of this paper presented one method for measuring the characteristic response of IEDs in time domain.

In this paper we will analyze the same set of devices in order to get more information leading to the generation of a classification algorithm.

II. EXPERIMENTAL SETUP

The RCS was measured using a computer-controlled M-sequence, polarimetric, MiMo radar platform. Four dual-polarized Vivaldi antennas, working at lower GHz range, were mounted on tripods. One of the antennas was used as polarimetric transmitter and the remaining three were used as receivers. The IED under test were mounted on a turntable in front of the antenna array.

The calibration of the system was performed measuring the RCS of a metal corner reflector, a plate and a cylinder. These objects have a known Radar Cross Section (RCS).

20 IEDs were tested in this experiment. The devices were placed on top of a styrofoam turntable in vertical and horizontal positions. The test was performed outdoor.

Each specific model of IED was illuminated with two polarizations, at two orientations. Cross and co polarized backscattering was measured at the receiving antennas. This means that for each IED 24 datasets were measured. The RCS measurements were processed and a set of common features, leading to identification was extracted.

Fig. 1 shows the behavior of the RCS of the IED # 20, shown in Fig. 2. Now we will getting behavior for all IED used and thus we will get the typical features for these specific models of IEDs.
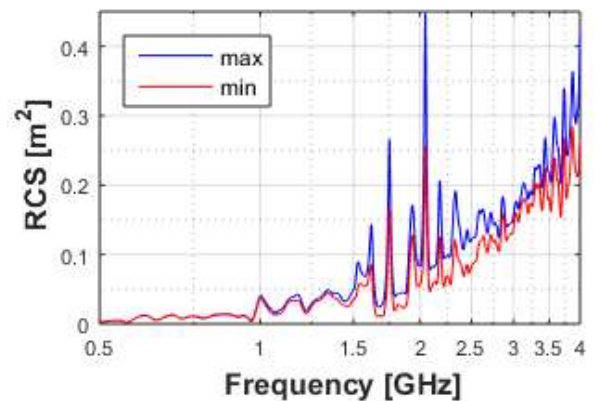

Figure 1. Behavior Co-polarized RCS for IED # 20.

Figure 2. IED 20 used for this test.

REFERENCES

[1] J.J. Pantoja, N. Peña, F. Rachidi, F. Vega, F. Roman, "Characterization, Modelling, and Statistical Analysis of the Electromagnetic Response of Inert Improvised Explosive Devices," in Electromagnetic Compatibility, IEEE Transactions on vol.56, no.2, pp.393-403, April 2014.

[2] D. Martinez, S. Gutierrez, S. Rodriguez, F. Vega, R. Bustamante, J. Sachs, C. Baer, "UWB Backscattering Characterization of Improvised Explosives Devices", European Electromagnetics International Symposium EUROEM 2016, London, UK, 2016.

Exfoliated Human Cells Response to Microwaves and Magnetic Field Exposure

Kuznetsov K.A., Shckorbatov Y.G.
Research Institute of Biology
V.N. Karazin Kharkov National University
Kharkov, Ukraine
Co-Smith@yandex.ru

Kovalenko I.F.
Institute for Problems of Cryobiology and Cryomedicine of the National Academy of Sciences of Ukraine
Kharkov, Ukraine
ikovalenki@rambler.ru

Abstract— Changes in JC-1 fluorescence indicating mitochondrial activity and Ca^{2+} content were investigated in human buccal epithelium cells. "Trigger" effects of microwave radiation and magnetic field JC-1 red fluorescence in mitochondria were detected. The redistribution of Ca^{2+} between cell nucleus and cytoplasm was reveled after microwaves and magnetic field exposure.
Keywords— electromagnetic field; static magnetic field; calcium ions; mitochondrial activity

I. INTRODUCTION

The biological effects of microwave radiation and magnetic field on cell are intensively explored in recent years [1]. Some investigations show decrease of mitochondrial energy metabolismafter microwave exposure [2]. The decrease of intracellular calcium is also shown [1, 3].

II. METHODS

Human buccal epithelium cells of 26 years old donor were used as an experimental object. Cells were collected before experiment and stored in 3.03mM phosphate buffer solution supplemented with 2.89 mM $CaCl_2$ [2]. Cells were exposed to microwave radiation (MW, 36.64 GHz, power densities 0.1 and 1 W/m^2, exposure time – 30 seconds) and to static magnetic field (MF), with magnetic induction 25 mT, exposure time – 5 minutes). Cells were exposed in10 µl of cell suspension placed on the preparation slide (~0.1 mm layer). After 1 hour of exposure cells were stained with mitochondrial membrane potential probe JC-1 (10µg/ml) or calcium probe Fluo-3 (10µg/ml). Stained cell samples were examined with lased fluorescent microscope LSM 510 META for red and green fluorescence, for JC-1 and Fluo-3, respectively (Figure 1 and Figure 2).

III. RESULTS

According to the results of experiments the most distinctivechanges in cells occurred under exposure to microwave radiation of 1 W/m^2 surface power density.This exposure caused both the increase in mitochondrial activity (more than 2 times comparing to control values) and removal of Ca^{2+} from cytoplasm and transport of calcium into nucleus. The 0.1 W/m^2 MW also reduced the Ca^{2+} content in cytoplasm butlowered the intensity of mitochondrial functioning at the same time.

The magnetic field stimulated mitochondrial fluorescence and had almost the same effect on Ca^{2+} redistribution as 0.1
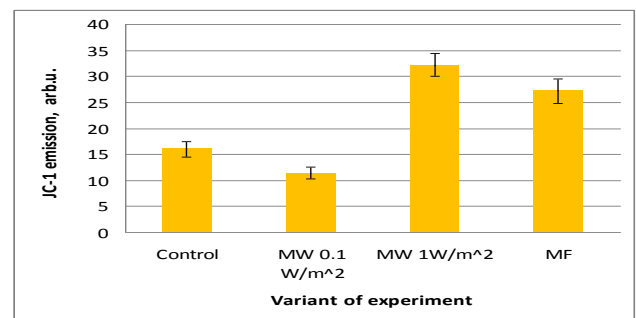

Figure 1. Rate of mitochondrial potential in human buccal epithelium cells
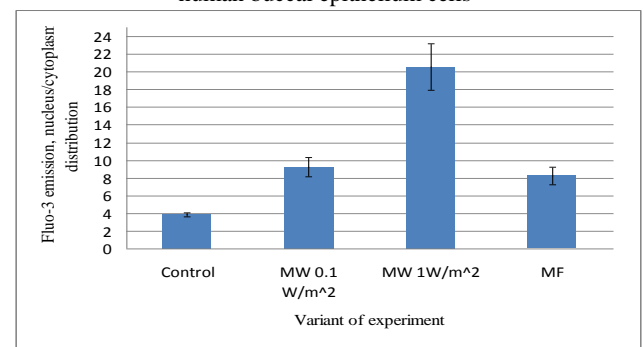

Figure 2. Calcium distribution in human buccal epithelium cells

W/m^2 MW. Thus, the results of the present investigation show the redistribution of calcium in cell, and also mitochondria activation induced by microwaves and magnetic field. The absence of pronounced microwave–induced inhibition of mitochondria activity in our experiments may be connected with low MW energies and exposure time in our experiments.

REFERENCES
[1]Yan-HuiHao, Li Zhao, Rui-Yun Peng Effects of microwave radiation on brain energy metabolism and related mechanisms. Military Medical Research (2015) 2:4; DOI 10.1186/s40779-015-0033-6.
[2] Y.G.Shckorbatov, V.G.Shakhbazov, A.M. Bogoslavsky, A.O.Rudenko.On age-related changes of cell membrane permeability in human buccal epithelium cells. / // Mech. Ageing Develop. (1995) 83: 87–90.
[3] Shckorbatov Y.G., Pasiuga O.S., Kovalenko I.F., Ryabukha S.S., Kolchigin N.N. Effect of microwave irradiaton of low intensity and magnetic fields on the Ca^{2+} contents in pea root cells.[23rd] Int. Crimean Conference "Microwave & Tele-communication Technology" (CriMiCo'2013). 9—13 September, Sevastopol, Crimea, Ukraine.(2013): 1101-1102.

Indian Initiatives on Development of Gyrotron

S. N. Joshi
CSIR - Central Electronics Engineering Research Institute
Pilani (Rajasthan) 333031 India
snj@ceeri.er.in   snjoshi_15@yahoo.com

Abstract - Gyro devices particularly Gyrotron came into prominence for last several decades and efforts are being made around the globe for further improving their performances.

Keywords-Gyrotron, Gyro devices, fast wave devices, ITER, energy, multi institutional approach

I. INTRODUCTION

 In the Indian context, due to several reasons the research and development in this area could not be initiated. Now, due to the support of Department of Science and Technology, New Delhi, a major multi-institutional project was initiated for design and development of 42 GHz, 200 kW (long pulse) Gyrotron. CSIR - Central Electronics Engineering Research Institute (CEERI) is the Nodal laboratory with IIT (R), Roorkee, IIT (BHU), Varanasi, SAMEER, Mumbai and IPR, Gandhinagar as other participating Laboratories. This Gyrotron has been successfully integrated and mounted in the system developed by Institute for Plasma Research (IPR), Gandhinagar. At present the developed Gyrotron is being characterized at IPR. In addition, CSIR-CEERI has successfully designed and developed 170 GHz, 100 kW (short pulse) Gyrotron, ultimately aiming for 170 GHz, 100 MW(CW) Gyrotron for ITER application. This 170 GHz Gyrotron is awaiting for the required testing infrastructure for its evaluation. CSIR-CEERI has developed a strong design base in the country for taking up challenging tasks in future.

II. GYROTRON DEVELOPMENT

After this initiative of CSIR-CEERI, other organizations like Microwave Tube Research & Development Centre (MTRDC), Bangalore has also initiated a major programme for design and development of a specific Gyrotron. IIT(R), Roorkee has also developed a strong design base particularly in collaboration with KIT, Germany and has also been actively participating in other design programme with CSIR-CEERI and MTRDC, Bangalore. SAMEER, Mumbai have also taken initiatives in design and development of 28 GHz Gyrotron. IIT (BHU), Varanasi has also been participating actively in this area in addition of working on other Gyro devices like Gyro Klystrons, Gyro TWTs, MILOs etc.,

Around the globe also, lot of initiatives are being taken to develop Gyrotrons, as they find multiple applications in the area of energy, health, cloud monitoring, deep space communication, mm-wave Radars, Imaging etc. In India also efforts are being made by various organizations in this advanced area having lot of application up to the THz range of rf spectrum. This paper gives an overview of all these advancements.

Overview of X-band Relativistic Triaxial Klystron Amplifier Research at the National University of Defense Technology

Jinchuan Ju, Wei Zhang, Xingjun Ge, Lishan Zhao, Huihuang Zhong, and Jun Zhang
College of Optoelectronic Science and Engineering, National University of Defense Technology, Changsha 410073, Hunan Province, China.
jujinchuan@nudt.edu.cn

Figure 1.   Typical experimental results of the X-band TKA.

Abstract— High power microwave (HPM), owing to its broad potential applications in scientific and civil fields, has become a hotspot of research in the field of relativistic vacuum electronics. The state-of-the-art HPM generators are capable of producing gigawatt-class radiations in the frequencies ranging from P-band to Ku-band, whereas further increase of the output power of a single HPM generator is essentially restricted by the issue of radio-frequency (RF) breakdown. Coherent power combining of multi-HPM generators thus provides an alternative scheme to overcome the RF breakdown limit, which would lead to the realization of equivalent output powers in the level of hundreds of GWs, and provides opportunities to explore microwave related physics at extremes.

The relativistic triaxial klystron amplifier (TKA) has attractive merit of high power capacity in high-frequency bands, which is a promising candidate for coherent power combining of HPMs. However, the development of TKA was significantly by the issue of parasitic mode excitation. In this work, we present a review on the recent research of an X-band TKA carried out at the National University of Defense Technology (NUDT) in China.

The proposed TKA consists of a reentrant input cavity, a three-gap buncher cavity, and a double-gap output cavity. In order to simplify the seed microwave input system, we develop a transverse injection scheme, which divides the seed microwave signal by half/half into two branches and then injects into the input cavity through two rectangular waveguides. In this case, a solenoid with two sections is employed to guide the electron beam. The electrons are modulated by the coaxial TM_{011} mode excited in the input cavity gap. The modulation is then strengthened by the three-gap buncher cavity operating at the coaxial TM_{013} mode. Furthermore, the structure of the buncher cavity was carefully optimized to achieve low TEM mode leakage. In the output cavity, the well-bunched electron beam transfers its kinetic energy to electromagnetic field, giving rise to HPM radiation. In order to generate GW-class long pulse radiation in X-band, the output cavity is designed with two gaps to reduce the maximum electric field strength on the cavity surface, so power capacity can be enhanced. In addition, parasitic modes (TEM mode and high order asymmetric TE mode) were suppressed by adopting specially designed coaxial reflectors together with microwave attenuation materials.

After optimization by particle-in-cell (PIC) simulation, the proposed TKA was examined in experiment. Typically
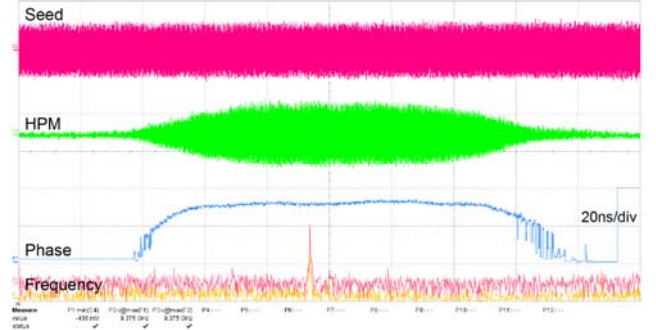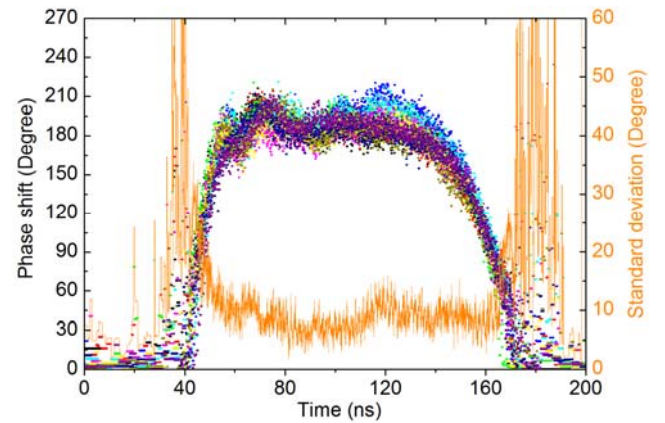

Figure 2. Phase shifts between the input and output microwaves for ten consecutive shots in experiment.

in PIC simulation, HPMs with power of 1.1 GW at the frequency of 9.375 GHz can be generated by the TKA when the diode voltage and current are 570 kV and 6.5 kA, respectively. The corresponding efficiency is about 30%, and the gain is 42.6 dB. Recently, phase-locked GW-level long pulse HPM radiations have been demonstrated in our experiments, which show a peak power of 1.1 GW with pulse durations in excess of 100 ns. Particularly as shown in Fig. 2, the shot-to-shot phase shift deviation between the input and the output microwaves is around 10 degree [1].

The presented results pave the way to accomplish coherent power combining of X-band HPMs in the near future. Moreover as a forward step, an improved high-gain and high-efficiency TKA is being studied, and the associated results will be reported.

Keywords-High power microwave; triaxial klystron amplifier; X-band; phase-locking; long pulse

REFERENCES
[1] J. C. Ju, J. Zhang, Z. M. Qi, J. H. Yang, T. Shu, J. D. Zhang, and H. H. Zhong, "Towards coherent combining of X-band high power microwaves: phase-locked long pulse radiations by a relativistic triaxial klystron amplifier," Sci. Rep., vol. 6, pp. 30657, August 2016.

Investigation of a compact mesoband high power microwave source

Yuwei Wang, Dongqun Chen, Jiande Zhang, Jinchuan Ju, Xingjun Ge and Lishan Zhao
College of Optoelectronic Science and Engineering
National University of Defense Technology
Changsha, Hunan, P. R. China
ywei_wang@163.com

Abstract − A compact high power mesoband microwave source based on switch oscillator filled with transformer oil for insulation and electric-magnetic vibrator combined antenna is presented in this paper. By pumping the oil flowing through the spark gap and arranging a gas buffer at the top of the outer conductor, the breakdown production of carbide and bubbles between spark gap can be removed from the space with high intensity electric field. It ensures the switched oscillator can re-operate shortly after one shot. Simulation proves that the voltage capability could exceed -330 kV within a charging time of 15 ns and the energy conversation efficiency could reach up to 86% when the fall-time of the voltage across the spark gap is 0.6 ns. The electric-magnetic vibrator combined antenna was designed to be with a 200×200 mm^2 physical aperture and a coaxial feeding port. It is shown by simulation that in the frequency range from 300 MHz to 500 MHz, this antenna keeps good impedance characteristics and radiation patterns. Finally, the transient performance of this high power microwave source was investigated experimentally. The peak intensity of the electric field (E_p) at a distance (r) of 5 m is typically measured to be ~24.9 kV/m(Figure 1), while the central frequency is about 375 MHz with a 3dB bandwidth of 24%(Figure 2).

 Keywords- mesoband high power microwave; switched oscillator; electric-magnetic vibrator combined antenna; high voltage breakdown
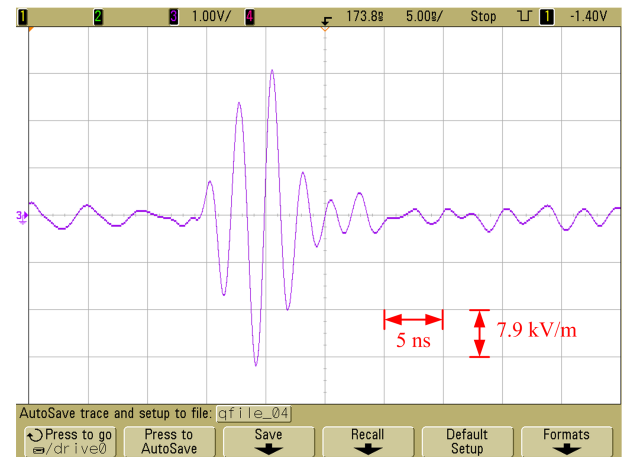
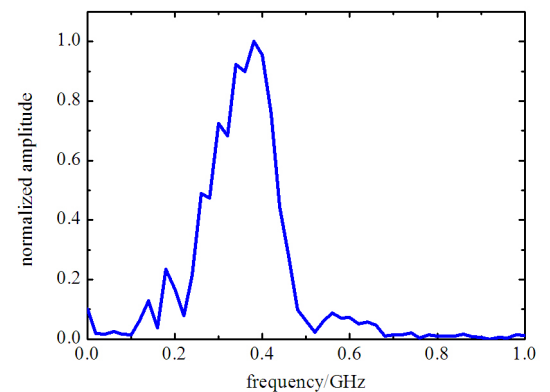Figure 1.Waveform of the radiated electric field at the distance of 5 m

Figure 2.Spectrum of the radiated electric field

A Gigawatt-class, Repetitively Pulsed, Vacuum-sealed High-power Microwave Source

Tao Xun, Han-wu Yang, Yu-wei Wang, Jian-de Zhang
College of Opto-electric Science and Engineering,
National University of Defense Technology,
Changsha, 410073, People's Republic of China
Corresponding author: xtao_0301@hotmail.com

Abstract—The majority of future high-power-microwave (HPM) applications will require compact, robust, and portable systems that are optimized for energy efficiency. However, current laboratory HPM sources typically require bulky external vacuum pumping systems to maintain the high-vacuum operating environment. The available literature on sealed-tube HPM source, such as a vicator, capable of operating at pulse repetition rate >100 Hz exists. However, the typical output power is MW level. Open reports on the vacuum-sealed, giga-watt class, repetitively pulsed high power tube are scanty up to now. In this work, a compact sealed-tube magnetically insulated transmission line oscillator (MILO) source has been developed at National University of Defense Technology (NUDT) that does not require bulky external vacuum pump for repetitive operations.

This hard-tube device with a ceramic insulated vacuum interface and a carbon-velvet high-current cathode has a base vacuum pressure in the low 10^{-8} Torr range. The housing is stainless steel tube sealed with all knife-edge copper gasket seals, and contains a commercially sourced glass window through which microwave radiation is extracted. Instead of the common plastic insulator, the sealed-tube utilizes a ceramic high-electric field vacuum interface. The ceramic disk is joined to stainless steel shell by brazing solder, and the vacuum interface can work stably with the hold-off voltage more than 600 kV. The cathode is comprised of carbon fiber array that have longer lifetime and lower pulse desorption. Due to the impact of high energy, high current density beam on the anode causing out-gassing, plasma, and even anode melting, the material selected for slow-wave-structure (SWS) and beam dump is off-the-shelf copper tungsten with high thermal conductivity and melting point compared to stainless steel.

In order to evaluate the gas evolution, a dynamic pumping model for the MILO device was proposed using DSMC method. In the free molecular flow that becomes Knudsen Number (Kn)>>1 for the non-dimensional parameter, the intermolecular collisions can be disregarded. It only has to track an individual sample particle that exists in the computational domain individually, and the speed change of each sample particle is caused when colliding with the boundary wall. In addition, the natural material out-gassing in the simulation is ignored. The only gas source is pulsed desorption load derived from the cathode surface.

In the 5 Hz repetition rate operation, using a 600 kV diode voltage and 48 kA beam current, the average radiated microwave power is about 3.4 GW in 45 ns FWHM at 1.575 GHz. The equilibrium pressure for 25 pulses is below 4.5×10^{-4} Torr. Pulse shortening limitations at this vacuum level have not been observed. Characteristic voltage, current, microwave waveforms in conjunction with pressure burst data for 25 pulse at 5 Hz, respectively, are presented. This sealed-tube MILO device is useful for compact and portable HPM applications.
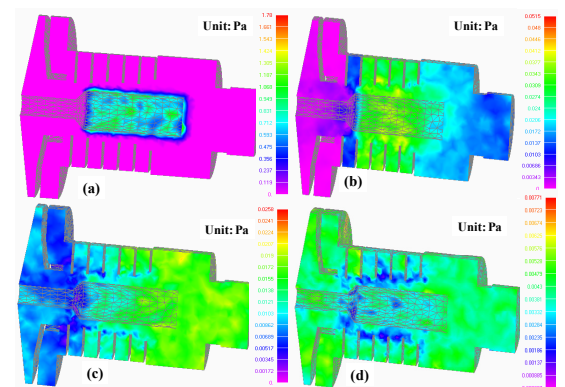

Fig.1 Time- and space- resolved pressure distribution in the sealed- tube MILO after a discharge pulse: (a) 100 ns, (b) 1 ms, (c) 100 ms, and (d) 200 ms.

Keywords- high-power microwaves (HPMs); hard-tube MILO; repetitive operation; pulse desorption; Monte-Carlo simulation; dynamic pumping

REFERENCE
[1]. T. Xun, J. D. Zhang, H. W. Yang, and Z. C. Zhang, J. Appl. Phys. 113, 164505 (2013).
[2]. Y. W. Fan, H. H. Zhong, J. D. Zhang, T. Shu, and J. L. Liu, Rev. Sci. Instrum. 85, 053512, (2014).
[3]. T. Xun, H. W. Yang, and J. D. Zhang, IEEE Trans. Plasma. Sci. 43, 4130 (2015).

A High-efficiency Long-pulse Relativistic Backward-wave Oscillator with Coaxial Extractor

Xingjun Ge, Jinchuan Ju, Lishan Zhao, Jun Zhang, Jianhua Yang
College of Optoelectronic Science and Engineering
National University of Defense Technology
Changsha (Hunan), People's Republic of China
gexingjun230230@aliyun.com

Abstract— The physical idea, the specific structure and the main testing results of a high-efficiency long-pulse relativistic backward-wave oscillator (RBWO) with a coaxial extractor are presented. The central features of the device include: (1) dual resonant cavities replacing the cutoff neck of a typical RBWO are used to enhance the efficiency and to reduce the electric field; (2) non-uniform slow wave structures (SWSs) are introduced in the device to enhance the efficiency; (3) a well-designed coaxial extractor is utilized to achieve longitudinal mode selection, which can enhance the beam-wave conversion efficiency and stabilize the microwave frequency; (4) the diode and the collector are reasonably designed to reduce the influence of cathode and collector plasmas. In simulation, driven by an 840 kV, 9 kA electron beam, microwaves at frequency of 3.77 GHz are generated with power of 3.3 GW and beam-wave conversion efficiency of 43%. However, the pulse duration of the device does not exceed 70 ns owing to the pulse shortening phenomenon in initial experiments. It was found that the plasma caused by an intense radio frequency electric field on the surface of the coaxial extractor played a main role in pulse shortening. To restrain the pulse shortening phenomenon, special attentions are paid on two aspects. One is to optimize the electrodynamic structures to decrease the electric field on the surfaces of the coaxial extractor while maintaining high beam-wave conversion efficiency. The other is to improve the smoothness and cleanness on the surfaces of the SWSs and improve the vacuum level thereby elevating the breakdown threshold. In the experiments after these measures are taken, microwave at frequency of 3.752 GHz are generated with power of 2 GW, beam-wave conversion efficiency of 36%, repetition rate of 20 Hz and pulse duration above 110 ns.

Keywords-high power microwave (HPM), relativistic backward-wave oscillator (RBWO), pulse shortening, long pulse, high efficiency

I. INTRODUCTION

Relativistic backward wave oscillators (RBWOs) are one type of devices that are promising for producing high power microwaves (HPMs) and are extensively investigated because, for example, they have compact structure, high efficiency, and good stability.[1–4] In L-, S-, C-, and X-bands, RBWOs have achieved output power of 2-6.5 GW, efficiency of 20%-36%, and repetition rate of 20-100 Hz.[5–9] However, the pulse duration of RBWOs usually does not exceed 20-30 ns owing to the "pulse shortening" phenomena.[10–13]

Recently, many studies have been carried on with regard to restraining pulse shortening, trying to prolong the microwave pulse duration. In 2008, researchers from the Institute of High Current Electronics, Russian Academy of Sciences reported that their S-band RBWO achieved 3 GW output power and 90 ns pulse duration in the experiments.[14] Compared with the diode voltage pulse width (300 ns), there occurred serious pulse shortening phenomena. No repetition rate experiment results are reported in their study.

In 2011, researchers of the National University of Defense Technology in China reported recent advances in long-pulse HPM sources with repetitive operation in S-, C-, and X-Bands.[15] In experiments, when driven by a repetitive long-pulse accelerator (the diode voltage pulse width is about 160 ns), the S-band source operated stably with output power of 1.2 GW and pulse duration of about 100 ns, in 20 Hz repetition mode. The X-band source band source produced similar results. The C-band source generated HPMs with power of about 2 GW and pulse duration of about 100 ns in single-shot mode. It was suggested that explosive emissions on surfaces of the eletrodynamic structures of the devices designed there restrained pulse duration and operation stability. But the beam-wave conversion efficiencies of the above HPM sources are all below 25%.

Although great progress has been made on the research of long-pulse RBWOs, there are some shortages, for example, as follows: (a) the pulse shortening phenomenon is obvious, which makes the pulse width difficult to exceed 100 ns, and (b) the beam-wave conversion efficiencies is low, which is generally below 30%. As is known, HPM sources with high-efficiency and long-pulse have great prospects in both industrial and defense fields. Therefore, the work presented in this study on RBWOs that can simultaneously achieve long pulse duration and high efficiency is of both theoretical and practical significance.

II. DEVICE DESIGN AND PHYSICAL ANALYSIS

The structure of the device is shown in Fig. 1. The device consists of a circular cathode, dual resonant cavities, nonuniform slow-wave structures (SWSs), a taper waveguide, a collector, a coaxial extractor and a coil.
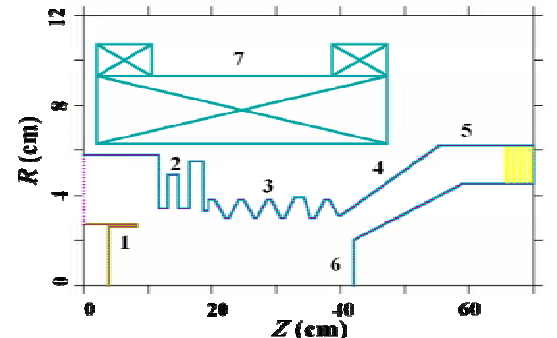

Figure 1. Schematic of the high-efficient long-pulse RBWO: 1 circular cathode, 2 dual resonant cavities, 3 nonuniform SWSs, 4 taper waveguide, 5 collector, 6 coaxial extractor, and 7 coil.

The nonuniform SWSs applied to improve the efficiency. Moreover, the guiding-magnetic field distribution within the tube is adjusted to make the downstream electron beam closer to the SWSs surface. Thus, the coupling impedance between the slow space charge wave on the electron beam and the surface harmonic of the backward TM_{01} mode can be enhanced. The central features are presented as follows.

A. Functions of the dual resonant cavities

The dual resonant cavities replacing the cutoff neck are used to enhance the efficiency and to decrease the electric field. Electron beams can be pre-modulated through the dual resonant cavities, which is beneficial to beam-wave interaction.

Moreover, the dual resonant cavities can completely reflect the microwave (the TM_{01} mode) transmitted from the SWSs to the diode. In addition, the radial distance between the cathode and the dual resonant cavities is about 5 mm, which is contributive to avoiding electrons scraping the cavity surfaces and to reducing the RF field.

B. Functions of the coaxial extractor

In our previous work,[16] the S-parameter method is employed to investigate the longitudinal resonant characteristics of the finite-length SWSs. Using the S-parameter method, we are able to conduct a comparative investigation on the five-period non-uniform SWSs with a coaxial extractor and those without the coaxial extractor in Fig. 2. Let us excite the structures by a smooth wall waveguide TM_{01} mode that runs from the left end to the right end. It is supposed that there is a perfect matching in the input and output cross-sections of the two structures. It is convenient to characterize their resonance properties by the transmission coefficient T, which is defined as

$$T(f) = S_{out}^{+} / S_{in}^{+} \tag{1}$$

where S_{out}^{+} and S_{in}^{+} are the electromagnetic power fluxes for the direct waves through the input and the output cross-section of a structure, respectively.
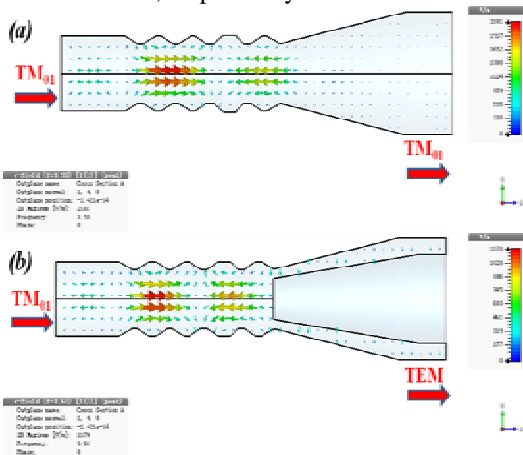

Figure 2. Electric field distribution in: (a) five-period non-uniform SWSs and (b) five-period non-uniform SWSs with a coaxial extractor.

Figure 2 also shows the electric field distributions of the $2\pi/5$ mode of the TM_{01} mode in the above two structures. Figure 3 shows the transmission coefficient as a function of frequency. The solid and dashed curves stand for the resonance properties of the five-period non-uniform SWS with a coaxial extractor and those without the coaxial extractor, respectively. Each peak in Fig.3 represents a longitudinal mode of TM_{01} wave. It is clearly found that,

the general transmission coefficient of the $2/5\pi$ mode of the TM_{01} mode in the former (point "A") is higher than that in the latter (point "B"), which means the power of the former is less difficult to be extracted. Furthermore, it has been revealed that the occurrence of other longitudinal modes (point "C") in the latter, whose frequency is in the range of 3.5–3.8GHz, will result in mode competition as the diode voltage value fluctuates. Thus, the structure of five-period non-uniform SWSs with a coaxial extractor is more beneficial to high efficiency and frequency stability.
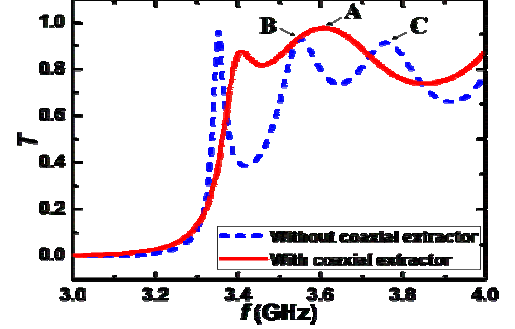

Figure 3. Transmission coefficients dependence on the frequency of the TM_{01} mode for the five-period non-uniform SWSs with and without a coaxial extractor.

In simulation, the microwave power of the device with a coaxial extractor is larger than that without the coaxial extractor by 1.3GW, and the beam-wave conversion efficiency of the former exceed than that of the latter by 21%.
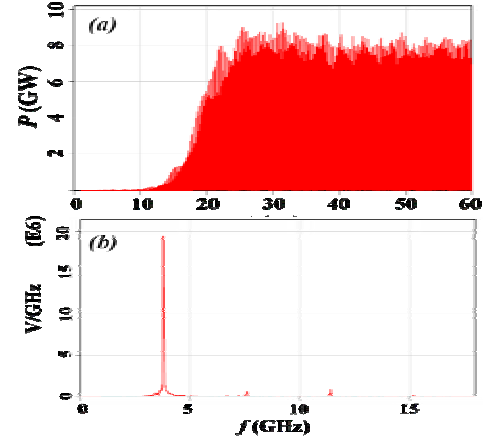

Figure 4. Typical simulation results: (a) spectrum of output power and (b) output power versus time.

To validate the theoretical analysis, a high-efficiency long-pulse RBWO with a coaxial extractor is investigated and optimized in detail with particle-in-cell (PIC) methods. During simulation, the diode voltage is 840 kV, the current is 9 kA, and the guiding-magnetic field is 1.6 T. Typical simulation results are shown in Fig. 4. Figure 4(a) shows that the HPM oscillation starts at 10 ns and reaches saturation at 22 ns. After saturation, the amplitude is stable and the average power is about 3.3 GW, while the power conversion efficiency is about 43%. Figure 4(b) shows that the output microwave spectrum is pure, whose center frequency is 3.77 GHz, and the frequency-doubling and the high order mode are suppressed effectively.

III. PRELIMINARY EXPERIMENTAL RESULTS AND PULSE SHORTENING REASONS ANALYSES

To verify the theoretical analysis and simulation results, we designed and fabricated an S-band high-efficiency long-pulse RBWO with coaxial extractor and investigated its performance preliminarily. The initial experiment is carried out on a long-pulse accelerator

capable of producing a 160 ns duration electron beam with a voltage range of 0.5-1 MV. The repetition rate of the accelerator varies from 1 Hz to 20 Hz.

In the experiment, the diode voltage is 800 kV, the current is 8.1 kA and the guiding-magnetic field is 1.6 T. Figure 8 shows the microwave signal and the corresponding FFT. Notably, the generated microwave frequency remains approximately 3.764 GHz, which belongs to the S-band. The radiated microwave is generated with power of 2 GW and pulse duration of about 65 ns, as shown in Fig. 5. The power conversion efficiency is 31%. Notably, the microwave pulse width (65 ns) is much shorter than the diode voltage pulse width (160 ns) owing to the pulse shortening phenomenon.
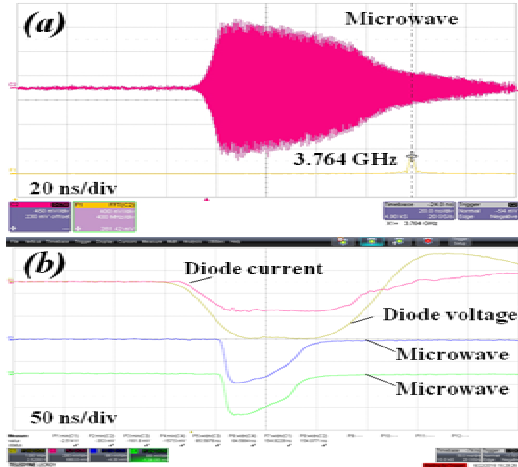

Figure 5. Typical experimental results: (a) the microwave and its spectrum and (b) diode voltage, beam current, and microwave power.

After the experiment, many traces of emission spots are found on the surface of the coaxial extractor, which is shown in Fig. 6. Referring to the simulation results of the distribution of electric field in the device as is illustrated in Figure 7 (a), it is clear that the position of the highest electric field is on the surface of the coaxial extractor, where the peak value reaches 900 kV/cm. It is shown that the plasma formed by an intense radio frequency electric field on the surface of the coaxial extractor apparently plays a main role in pulse shortening.

Figure 6. The photo of the surface of the coaxial extractor after the experiment.

IV. IMPROVEMENT MEASURES AND LONG PULSE EXPERIMENTAL RESULTS

To restrain the pulse shortening phenomenon, special attentions are paid on two aspects.

A. Optimize the electrodynamic structures to decrease the electric field

One aspect on which the attention is paid is to optimize the electrodynamic structures to decrease the electric field on the surfaces of coaxial extractor while maintaining high beam-wave conversion efficiency. In simulation the shape of the coaxial extractor is changed to decrease the electric field shown in Fig. 7 (b). The peak value of the electric field on the surfaces of coaxial extractor can be reduced to 500 kV/cm with the structure parameters optimizing.
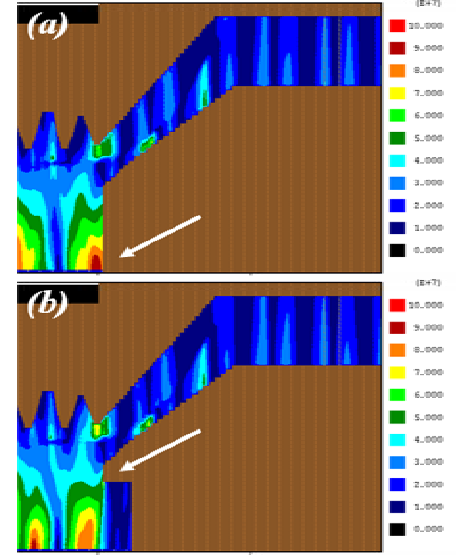

Figure 7. The electric field contour obtained in PIC simulation: (a) before parameters optimizing, and (b) after parameters optimizing.

B. Increase the smoothness and cleanness on the surfaces of SWSs

The other aspect of efforts taken to overcome pulse shortening was to increase the smoothness and cleanness on the surfaces of SWSs and improve the vacuum level to elevate the breakdown threshold.Measures such as treating SWSs surfaces with electroplating and introducing new metallic materials with low electron emission rate, have been taken to improve the pulse duration and the operation stability. The photos of the SWSs with different technologies and materials are shown in Fig. 8.

Figure 8. The photo of the SWSs with different technologies and materials.
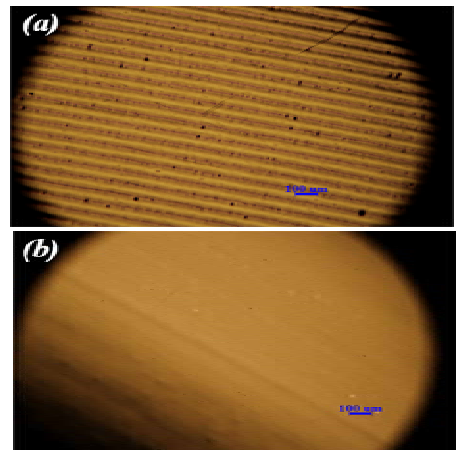

Figure 9. The micro-mechanisms of the SWS: (a) before electroplating, and (b) after electroplating.

Furthermore, the micro-mechanisms of the SWS are observed by the optical microscope as shown in Fig. 9. Figure 9(a) shows the micromechanism of the stainless steel SWS before electroplating. There are obvious grains

made by the mechanical turnery. Figure 9(b) gives the micromechanism of the stainless steel SWS after electroplating. The surface is much smoother as the surface is plated by the metal foil.

C.   *The long-pulse experimental results*
In the experiment, the diode voltage is 700 kV, the current is 8 kA and the guiding-magnetic field is 1.6 T. The accelerator is operated under a repetition rate of 20 Hz. Figure 10 (a) shows the microwave signal and the corresponding FFT. Notably, the generated microwave frequency remains approximately 3.752 GHz, which belongs to the S-band. The radiated microwave with power of 2 GW and pulse duration above 110 ns is generated, as shown in Fig. 10 (b). The power conversion efficiency is 36%. The experimental results show that the S-band long-pulse RBWO is steady and has a good overlapping of 20 pulses. The experimental results show that the pulse shortening phenomenon is restrained effectively and the beam-wave conversion efficiency is enhanced significantly.
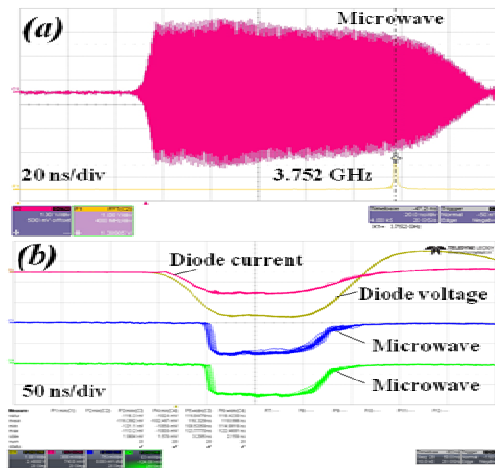

Figure 10. Typical experimental results: (a) microwave and its spectrum and (b) diode voltage, beam current, and microwave power under repetition rate of 20 Hz.

V.   SUMMARY AND CONCLUSION
This paper presents the physical idea, the specific structure and main testing results of a high-efficient long-pulse RBWO with coaxial extractor. First, the central features of the device are analyzed. In addition, the preliminary experimental results and pulse shortening reasons are presented. In the initial experiment, the microwave pulse width is much shorter than the diode voltage pulse width owing to the pulse shortening phenomenon. It is shown that the plasma formed by an intense radio frequency electric field on the surface of the coaxial extractor apparently plays a main role in pulse shortening. Moreover, the improvement measures and long pulse experimental results are introduced. The experimental results show that the pulse shortening phenomenon is restrained effectively and the beam-wave conversion efficiency is enhanced significantly.

By analyzing the experimental phenomenon, we come to the conclusion that the explosive emission on the surface of the electrodynamics structure in intense RF field mainly leads to the earlier unexpected termination of microwave output. Further investigations, such as optimal design of diode and collector, application of cathode material with low expansion velocity, and treating SWSs surfaces with new technology, will be done to improve pulse duration and operation stability.

REFERENCES
[1] J. A. Nation, "On the coupling of a high-current relativistic electron beam to a slow wave structure," Appl. Phys. Lett., vol. 17, pp. 491-494, December 1970.
[2] J. A. Swegle, J. W. Poukey, and G. T. Leifeste, "Backward wave oscillators with rippled wall resonators: analytic theory and numerical simulation," Phys. Fluids., vol. 28, pp.2882-2294, June 1985.
[3] G. S. Nusinovich and Yu. P. Bliokh, "Mode interaction in backward-wave oscillators with strong end reflections," Phys. Plasmas., vol. 7, pp.1294-1301, November 2000.
[4] A. V. Gunin, A. I. Klimov, S. D. Korovin, I. K. Kurkan, I. V. Pegel, and S. D. Polevin, "Relativistic X-Band BWO with 3-GW Output Power," IEEE Trans. Plasma Sci., vol. 26, 326-330, June 1998.
[5] C. Chen, G. Liu, W. Huang, Z. Song, J. Fan, and H. Wang, "A repetitive X-band relativistic backward-wave oscillator," IEEE Trans. Plasma Sci., vol. 30, pp. 1108–1111, June 2002.
[6] J. Zhang, H. H. Zhong, Z. Jin, T. Shu, S. Cao, and S. Zhou, "Studies on efficient operation of an X-band oversized slow-wave HPM generator in low magnetic field," IEEE Trans. Plasma Sci., vol. 37, pp. 1552–1557, August 2009.
[7] A. I. Klimov, I. K. Kurkan, S. D. Polevin, V. V. Rostov, and E. M. Totmeninov, "A multigigawatt X-band relativistic backward wave oscillator with a modulating resonant reflector," Tech. Phys. Lett., vol. 34, pp. 235–237, March 2008.
[8] R. Z. Xiao, X. W. Zhang, L. J. Zhang, X. Z. Li, L. G. Zhang, W. Song, Y. M. Hu, J. Sun, S. F. Huo, C. H. Chen, Q. Y. Zhang, and G. Z. Liu, "Efficient generation of multi-gigawatt power by a klystron-like relativistic backward wave oscillator," Laser Part. Beams, vol. 28, pp. 505–511, 2010.
[9] X. J. Ge, H. H. Zhang, B. L. Qian, J. Zhang, L. Gao, Z. X. Jin, Y. W. Fan, and J. H. Yang, "An L-band coaxial relativistic backward wave oscillator with mechanical frequency tenability," Appl. Phys. Lett., vol. 97, pp. 101503, 2010.
[10] K. Hahn and E. Schamiloglu, "Long-pulse relativistic BWO operation utilizing a disk cathode," IEEE Trans. Plasma Sci., vol. 30, pp. 235–239, June 2002.
[11] S. D. Korovin, G. A. Mesyats, I. V. Pegel, S. D. Polevin, and V. P. Tarakanov, "Pulsed width limitation in the relativistic backward wave oscillator," IEEE Trans. Plasma Sci., vol. 28, pp. 485–495, June 2000.
[12] F. J. Agee, "Evolution of pulse shortening research in narrow band, high power microwave sources," IEEE Trans. Plasma Sci., vol. 26, pp. 235–245, June 1998.
[13] A. V. Gunin, V. F. Landl, S. D. Korovin, G. A. Mesyats, I. V. Pegel, and V. V. Rostov, "Experimental studies of long-lifetime cold cathodes for high-power microwave oscillators," IEEE Trans. Plasma Sci., vol. 28, pp. 537–541, June 2000.
[14] S.D. Polevin, S.D. Korovin, B.M. Kovalchuk, K.V. Karlik, I.K. Kurkan, G.E. Ozur, I.V. Pegel, D.I. Proskurovsky, M.Yu. Sukhov, and S.N. Volkov, "Pulse Lengthening of S-band resonant relativistic BWO," 13th International Symposium on High Current Electronics. Tomsk, pp. 246-249, 2004.
[15] J. Zhang, Z. X. Jin, J.H. Yang, H. H. Zhong, T. Shu, J. D. Zhang, B. L. Qian, C. W. Yuan, Z. Q. Li, Y. W. Fan, S.Y. Zhou, and L. R. Xu, "Recent Advance in Long-Pulse HPM Sources With Repetitive Operation in S-, C-, and X-Bands," IEEE Trans. Plasma Sci., vol. 39, pp. 1438–1445, June 2011.
[16] X. J. Ge, H. H. Zhong, B. L. Qian, L. Liu, Y. G. Liu, L. M. Li, T. Shu, and J. D. Zhang, "Transversal and longitudinal mode selections in double-corrugation coaxial slow-wave devices," Phys. Plasmas, vol.16, pp.063107, June 2009.

Experimental investigation of S-band magnetically insulated transmission line oscillator (MILO)

V Nallasamy, C Narasimhamurthy, U Shanmuganathan, Saket Khandekar, Srinivas Nekkanti,
B Vijay Kumar and SUM Reddy
Microwave Tube Research and Development Centre, DRDO, Bangalore-560013, INDIA.
Email: nallasamy@mtrdc.drdo.in

Abstract- Experimental investigation of S-band MILO has been carried out for generation of microwaves with the Megawatts power. As a first experiment in India, a compact MILO composed of 3-Slow Wave Structure (SWS) cavities and 2-choke cavities and one coupling cavity with improved axial power extraction. In this preliminary experiment, the RF output power of 4.0MW has been measured at a frequency of 3.26GHz for the beam voltage of 485kV and the current of 48.5kA with the Full width Half Maximum (FWHM) pulse duration of 130nsec is generated by high voltage and high current Marx generator.

Index Terms- Magnetically insulated line oscillator (MILO), Dispersion relation, Cross field device, Slow-wave structure.

I. INTRODUCTION

The MILO is a crossed-field device that generates gigawatts-level of high-power microwaves (HPM). This device is compact because it generates the magnetic field by itself. The physical structure resembles the co-axial linear magnetron without a magnet. In the early stage of researches on MILO, the generated power at interaction cavities has been extracted via top of the cavities like conventional magnetrons. However, the radial power extraction breaks the axial symmetry and causes mode competition between TM and TE mode resulting in poor efficiency. In this experiment, the power was axially extracted through matched section.

II. EXPERIMENTAL INVESTIGATION

The Fig.1 shows the experimental test set-up of S-band MILO which is connected to high voltage and high current Marx generator of MTRDC. A preliminary hot test has been carried out and the RF power is measured through D-dot probe which is kept at far field. The measured power is 4MW with 50ns duration as shown in Fig. 2(a) and FFT of output signal is shown in Fig.2(b). The beam voltage and current used in this preliminary experiment are 485kV and 48.4kA, respectively as shown in Fig.3. The applied voltage pulse has a rise time of 9ns and a flat top of about 80ns.
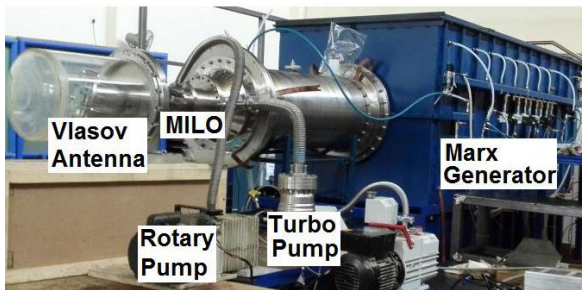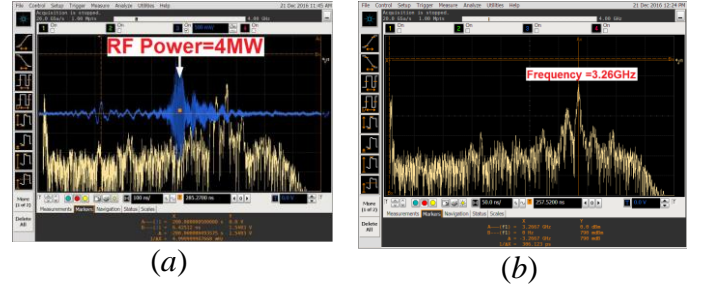

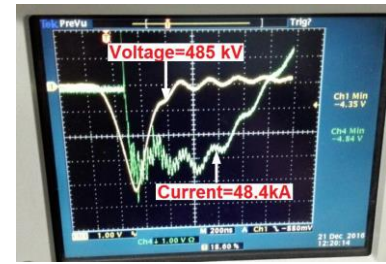Figure 2. (*a*) RF output power   (*b*) FFT of output signal

Figure 3. Experimental result of applied beam voltage and current

A Vlasov antenna as shown in Fig.1 has been designed as a mode convertor for measuring the RF power in TE_{11} mode as well as to test MILO device in the laboratory environment and also an anechoic chamber has been prepared for radiated power and pattern measurement. Still the hot test is underway.

III. CONCLUSION

A compact S-band MILO with 2-choke, 3-SWS cavities and one coupling cavity has been experimented and the RF output power of 4.0MW at a frequency of 3.26GHz for the beam voltage of 485kV and the current of 48.4kA has been obtained.

REFERENCES

[1] M.Collins Clark, Barry M. Marder, and Larry D. Bacon, Appl. Phys. Lett. **52**, 78, 1988.

[2] V. Nallasamy, S. K. Datta, SUM Reddy, and P. K. Jain, "Efficiency enhancement of an S-band magnetically insulated line oscillator," International Journal of Microwave and Optical Technology, vol.11, No.5, pp. 324-331, Sept 2016.

[3] Y. W. Fan, H. H. Zhong, T. Shu, and Z. Q. Li, "Theoretical investigation of the fundamental mode frequency of the magnetically insulated transmission line oscillator," Physics of Plasmas, vol. 15, pp. 123504(1-5), 2008.

Figure 1. Experimental test set-up of S-band MILO

Challenges Associated with the Development and Operation of a High Power Reverberation Chamber

G D M Barber
QinetiQ Ltd. Farnborough, Hampshire, UK
gdbarber@qinetiq.com

T Hague
ARUK, Milton Keynes, UK
THague@ARWorld.US

Abstract— Over the past 2 years QinetiQ have developed a reverberation chamber and associated amplifier/antenna system for performing high level E-field susceptibility testing of equipment and missile systems. The reverberation chamber has specifically been developed for testing from 200 MHz to 18 GHz and utilizes high power solid state and TWT based amplifiers. The chamber can be operated in mode stirred or mode tuned operation, dependent upon the specific test standard requirements. Amplifier Research (AR) solid state amplifiers provide the high RF power input to this chamber over the low frequency range 200 MHz to 4.2 GHz. This paper addresses some of the main technical challenges associated with driving high RF powers into reverberation chambers.

Keywords-component; Reverberation, mode tuned, mode stirred, RF, Amplifier, TWT, Paddle, Tuner, VSW, Solid State, Circulators

I. INTRODUCTION

Reverberation chambers have been operated for many years and are commonly used by test facilities to generate high level E-fields required for the susceptibility testing of commercial aircraft systems, military systems and small platform (missiles, UAVs), over the frequency range 100 MHz to 18 GHz, dependent upon the chambers dimensions and performance. Many standards include the use of the reverberation chamber as an alternative approach to conventional radiated test methods. The main advantages of the reverberation chamber being (1) thorough test method, as equipment can be illuminated at multiple aspect angles and polarizations (2) efficient in terms of the RF power required to generate the E-Field and (3) able to accommodate large systems or multiple devices within a single test. The use of mode stirred and mode tuned methods is also discussed and addresses some of the pros and cons of employing these methods.

Currently the QinetiQ reverberation chamber, Figure 1, is used to perform testing to RTCA DO-160F/G [1], Military Standard 461F/G [2] and Defence Standard 59-411, Part 3 [3].

Some 'bespoke' requirements also require testing to be performed to E-field levels in excess of 10kV/m, to meet specific peak RF Environments. The requirements for Rotorcraft as detailed within RTCA DO-160F/G, requires pulsed E-fields over the frequency range of 2-6 GHz of between 6000 - 7200 V/m.

These E-field levels would be extremely challenging to meet using conventional radiated susceptibility methods, even using relatively high power amplifiers and high gain transmit antennas. A more efficient method is to use moderately rated amplifiers and efficient transmit antennas within a reverberation chamber test environment.

Figure 1. QinetiQ Reverberation Chamber

II. TECHNICAL CHALLENGES

This paper describes in detail technical challenges related to operating high power CW and Pulsed amplifiers within the reverberation chamber, employing both mode tuned and mode stirred techniques, covering:-

1. Heating Issues - cables, connectors and EUT
2. Poor VSWR
3. Use of circulators
4. Use of CW based Vs Solid State amplifiers
5. Solid State amplifiers with fold-back protection

REFERENCES
[1] RTCA DO-160G, Environmental Conditions and Test Procedure for Airborne Equipment, dated Dec 2010.
[2] Military Standard 461G, Requirement for the control of Electromagnetic Interference Characteristics of Sub Systems and equipment, dated 11 Dec 2015.
[3] Defence Standard 59-411, Part 3, Test Methods & Limits for Equipment & Sub Systems, Issue 2.0, dated 31 March 2014.
[4] Challenges of Meeting the HIRF Testing Requirements of RTCA DO-160, G Barber, EMCUK 2010.

Research on HPEM in High Power Laser Facility

MengCui[1,2], Jin Han Bing[1,2] , Xu Zhiqian[1,2], Yang Chao[1,2], Zheng Wanguo[3]

1 Department of Engineering Physics, Tsinghua University, Beijing, China, 100084
2 Key Laboratory of Particle & Radiation Imaging, Ministry of Education, Beijing, China, 100084
Beijing, China
3 Laser Fusion Research Center, China Academy of Engineering Physics, Miangyang 621900, China

Abstract

The EMC problem of the high power laser facility is very serious. Many kind of electromagnetic pulse are generated after the high power laser interact with the target. A 2.5D time bias FDTD –PIC(finite difference in time domain and particle-in-cell) code is developed to simulate the process that the escape hot electrons radiate high power electromagnetic pulse in the chamber and to simulate SGEMP.Three kind electromagnetic sensors are developed to measure the electromagnetic environment in the target bay.

Keywords: high power laser ,electromagnetic pulse, PIC, hot electron ，SGEMP

1 INTRODUCTION

Electromagnetic pulse (EMP) has been found during the interaction of laser pulses and solid targets, which may cause electromagnetic interference problems, such as interfering or damaging electronic equipment and diagnostics.

For example, in experiments of Titan short-pulse laser facility, researchers observed high-level EMP with a broad frequency up to GHz[1]. Energetic electrons are produced in laser p lasma interaction, and a small fraction of these electrons escape the target. It is believed that escaping electrons are the main source of EMP [1,2,3], and the photon electrons made by the Xray in a metal cavity will radiate system generated electromagnetic pulse(SGEMP). To research the HPEM in high power laser facility is important for EMC design.

2 NUMERICAL SIMULATION WITH PIC

2.1 Simulation of Laser-Plasma Interaction Producing Hot Electrons

The high-intensity laser pulse interaction with plasma is modeled in a two-dimension geometry. Charged particles, mainly electrons, are accelerated by electromagnetic fields. Simulated domain is a rectangle of $10\mu m \times 10\mu m$. A p-polarized laser pulse is injected horizontally from the left side and propagates through vacuum and homogeneous copper plasma, with the wavelength at $1.06\mu m$, the intensity at $10^{19}W/cm^2$, and the duration at the half maximum 50fs. The laser intensity presents a Gaussian shape profile along y axis as well as in time domain. Assume that the plasma density is $1.6 \times 10^{21}/cm^3$. Lindman absorption boundary condition is used in the left boundary.

We vary the laser intensity from 0.2×10^{19} to $10^{19}W/cm^2$ and the duration remains 50fs. The simulation results indicate that the temperature of hot electrons depend essentially on the laser intensity.

2.2 Simulation of Escaping Electrons Emission

2D cylindrical coordinates are used and variables are simplified into toroidal symmetry. The solid target is in the center of the chamber. The escaping electrons is produced in a 2mm-high，10mm-diam cylinder. The electromagnetic field at an appropriate position is recorded and the electric field as a function of time with a peak filed of order 100kV/m is obtained, and the peak field of magnetic is about 4×10^{-4}T. EMP has a broad frequency extending up to5GHz.

3 MEASUREMENT

We developed E-field, B-Dot, and D-Dot time-domain electromagnetic field sensors, performed theoretical analyses of the sensors' performance indicators, and experimentally calibrated the sensors. The electromagnetic environments of different areas within the facility were also successfully determined using these sensor systems.

4 CONCLUSION

The EMP environment is accordance with the format of the power density of high power laser, the target and the interaction format of the laser-target kind. the amplitude of electric field in target chamber is about 10kV/m ,SGEMP may be 10^6V/m. The amplitude of electric field in target room is about kV/m when there is window on the chamber. All electric equipment in these areas must be designed specially in order to increase the EMC level.

References

[1] C. G. Brown, E. Bond, T. Clancy, S. Dangi, D. C. Eder, W. Ferguson, etal., "Assessment and Mitigation of Electromagnetic Pulse (EMP) Impacts at Short-pulse Laser Facilities," Sixth International Conference on Inertial Fusion Sciences and Applications, Parts 1-4, vol. 244, p. 4,2010.

[2] J. L. Dubois, F. Lubrano-Lavaderci, D. Raffestin, J. Ribolzi, J. Gazave, A. C. L. Fontaine, et al., "Target charging in short-pulse-laser–plasma experiments," Physical Review E, vol. 89, 2014.

[3] Meng Cui,Yang Chao,Li Xin, Development of electromagnetic environment research of high power laser facility, Journal of Terahertz Science and Electronic Information Technology, Vol.15,No.1,Feb.2017,P825-830